Extended Donor and Acceptor Molecules for Organic Electronics

Dissertation zur Erlangung des Grades

“Doktor der Naturwissenschaften”

am Fachbereich Chemie, Pharmazie und Geowissenschaften

der Johannes Gutenberg-Universität Mainz

Ralph Rieger

geboren in Bad Neuenahr-Ahrweiler

Mainz im Jahr 2009

Die vorliegende Arbeit wurde in der Zeit von Juli 2006 bis Juli 2009 im Max-Planck-Institut für Polymerforschung in Mainz unter Anleitung von Prof. Dr. Müllen durchgeführt.

Ich danke Prof. Dr. K. Müllen für seine wissenschaftliche und persönliche Unterstützung sowie für seine fortwährende Diskussionsbereitschaft.

Contents

Index of Abbreviations

2D-WAXS	two-dimensional wide-angle X-ray scattering
AcOH	acidic acid
BEDT-TTF	bisethylene-dithio-tetrathiafulvalene
CPU	central processor unit
d	doublet (NMR)
DBU	1,8-Diazabicyclo[5,4,0]undec-7-en
DCM	dichloromethane
DFT	density functional theory
DMF	N,N-dimethylformamide
DSC	differential scanning calorimetry
EI	electron impact
Et	ethyl
F4TCNQ	tetrafluoro-tetracyanoquino-dimethane
FD	field desorption
FET	field-effect transistor
FF	fill factor
GPC	gel permeation chromatography
h	hour
HBC	hexa-*peri*-hexabenzocoronene
HOMO	highest occupied molecular orbital
HOPG	highly ordered pyrolytic graphite

HPLC	high performance liquid chromatography
iPr	iso-propyl
LDA	lithium diisopropylamide
LED	light emitting diode
LUMO	lowest unoccupied molecular orbital
m	multiplett (NMR)
MALDI-TOF	matrix-assisted laser desorption/ionization time-of-flight
Me	methyl
min	minute
MS	mass spectrometry
NMP	N-methylpyrolidinone
NMR	nuclear magnetic resonance
NOE	nuclear OVERHAUSER effect
NOESY	nuclear OVERHAUSER enhancement spectroscopy
NTCDI	naphtalene-tetracarboxylic-diimide
OAc	acetate
oDCB	1,2-dichlorobenzene
OPV	organic photovoltaics
OSC	organic semiconductor
P3HT	poly(3-hexylthiophene)
PAH	polycyclic aromatic hydrocarbon
PCBM	phenyl-C61-methylbutyrate
[70]PCBM	phenyl-C71-methylbutyrate
PCC	pyridiniumchlorochromate
PEDOT-PSS	poly(ethylenedioxythiophene)-poly(styrenesulfonate)
PEN	polyethylene naphthalate

PET	polyethylene terephthalate
Ph	phenyl
PL	photoluminescence
PLE	photoluminescence excitation
POM	polarization optical microscopy
ppm	parts per million
PS	polystyrene
PTCDI	perylene-tetracarboxylicdimide
PTFE	poly-tetra-fluoro-ethylene
q	quartet (NMR)
quin	quintuplet (NMR)
RFID	radio frequency identification tag
RT	room temperature
s	singlet (NMR)
SEM	scanning electron microscopy
STM	scanning tunneling microscopy
STS	scanning tunneling spectroscopy
t	triplet (NMR)
TBAF	tetra-iso-butyl ammonium fluoride
tBu	tert-butyl
TCB	1,2,4-trichlorobenzene
TCNQ	7,7,8,8-tetracyanoquinodimethane
TEM	transmission electron microscopy
TES	triethylsilane
THF	tetrahydrofuran
TGA	thermo-gravimetry analysis
TLC	thin layer chromatography

TMEDA	N,N,N',N'-tetramethylethylene-diamine
TMS	trimethylsilyl-
TOF	time-of-flight
tt	triplet of triplets (NMR)
TTF	tetrathiafulvalene
TTN	tetrathianaphthalene
UPS	ultra violet photoemission spectroscopy
UV-vis	ultraviolet-visible absorption spectroscopy
XPS	X-ray photoemission spectroscopy

1 Introduction

For a long time, it was believed that only metals and inorganic composites could conduct electricity. Organic molecules were believed to be insulators due to their large intermolecular distances and lack of suitable charge carriers. In 1954, it was reported that bromine-doped perylene (**I-1**) was electrically conductive.[1] The scientific community, however, attributed the conductivity to the bromine rather than the perylene. Ten years later, a report about electrically conductive polypyrrole was published.[2] The authors have pyrolized tetraiodopyrrole obtaining an iodine-doped polypyrrole (**I-2**) with a conductivity of 1 S/cm. Little attention was paid to this discovery. It was not before 1972 that people started to believe in this phenomenon, when the group of Alan J. Heeger published the conductivity of a fully organic charge-transfer complex.[3] It consisted of *N*-methyl-phenazine (NMP) and tetracyanoquino-dimethane (TCNQ) (**I-4**). One year later, the same group discovered superconductivity in a charge-transfer complex of tetrathiafulvalene (TTF) and TCNQ (**I-5**).[4] The first organic semiconductor was discovered by McGinness et. al. in 1974.[5] They could switch the conductivity of melanine, the skin pigment isolated from biological tissue, by applying a certain threshold voltage. In 1977, Shirakawa, MacDiarmid and Heeger reported electrical conductivity in iodine-doped polyacetylene (**I-3**).[6, 7] For this discovery they received the Nobel Prize for Chemistry in 2000.

In the last decades, many new organic (semi-)conductors have been developed and incorporated into devices, such as transistors,[8] diodes,[9, 10] photovoltaic

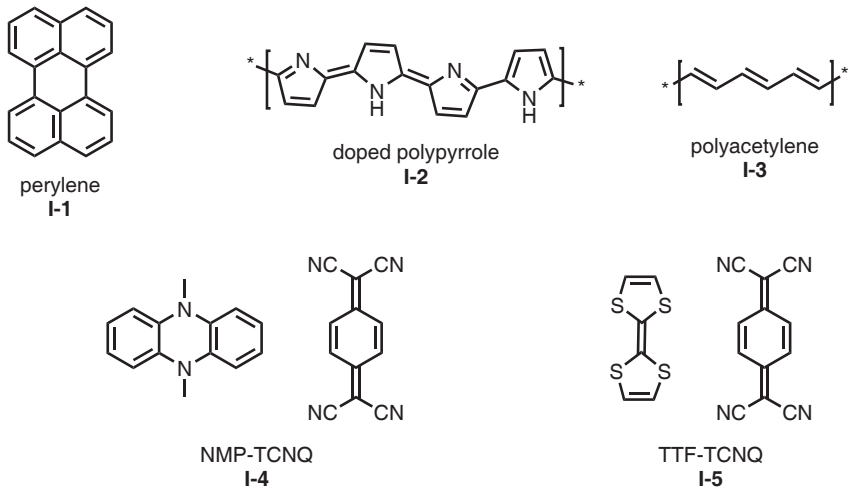

Figure 1.1: Chemical structure of the first conductive materials.

cells,[11] and sensors.[12] A stage has been reached at which commercial applications are about to be launched, so people in industry have joined academic researchers in enhancing the possiblities of organic semiconductors. Experts predict a hugh demand for new devices in the low-cost segment, such as radio-frequency identification tags (RFID).[13, 14] Some enthusiasts even see silicon semiconductors being totally replaced by organic materials in the future. This is very unlikely to happen, but it is worth having a closer look at where strengths of inorganic semiconductors remain and where organic ones will play a role.

1.1 Comparison of Organic and Inorganic Semiconductors

Modern life heavily depends on inorganic semiconductors. No electronic device is conceivable without them, predominantely silicon-based materials.[15] More than one hundred years of research and development has been focused on silicon.[16] It is, therefore, no surprise that the performance is still superior to any organic material. Its high environmental stability allows device lifetimes of more than 25 years.[17] Also, its high charge-carrier mobility is unreached.[18] The thermal and

mechanical stability make it very likely that inorganics will play a very important role in semiconductor technologies in the future.

Despite its undisputed advantages, inorganic semiconductors are brittle materials. New applications, such as "intelligent" clothing, paper-like displays, or flexible sensors, require lightweight materials, which can withstand mechanical deformation. This is where organic semiconductors come into play.[19] Especially polymers are intrinsically more flexible as adjacent chains can easily slip along each other.[20] Devices made out of organic semiconductors are, furthermore, expected to be inexpensive. Only very thin films, i.e. low amounts of material, are needed. The possiblity of processing the semiconductors at moderate temperatures from solution decreases the energy demand and consequently lowers the costs. Silicon, in contrast, needs processing temperatures above 600 °C.[21]

The versatility of organic synthesis allows the fine-tuning of material properties to find the ideal solution for each application. For inorganic molecules, the possiblities to control properties are much more restricted. Furthermore, the device size can, in principle, be down-sized to single molecules.[22, 23] Semiconductor properties in inorganic materials break down at a certain size limiting future miniaturization.[24]

1.2 Charge Transport in Organic Materials

The classical theory of charge transport describes semiconductors with the aid of the band transport model.[25] Energy levels of single sites, such as silicon atoms, are strongly coupled to neighboring sites. In this way, an energy continuum is formed in which charges can move by thermal excitation. In organic semiconductors, however, the coupling between adjacent molecules is too weak, so that the band theory is not applicable.[26]

Much better descriptions are obtained when using a hopping model in which charges are assumed to hop between localized states.[27] The energy for a hopping

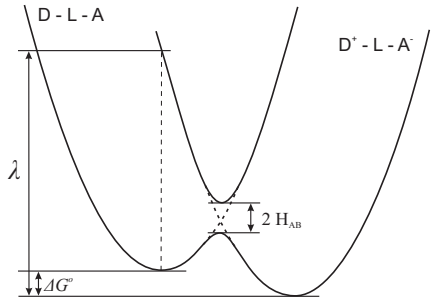

Figure 1.2: Energy profile of charge hopping between two molecules according to the Marcus theory.

event is provided by lattice vibrations, a process typically referred to as phonon-assisted hopping.[28] The mathematical description makes use of the Marcus theory, originally used by Richard A. Marcus to model redox processes.[29] For this theory he was awarded the Nobel Prize for Chemistry in 1992. The rate of hopping of a charge carrier from one site to the next is described by the formula

$$k_{et} = \frac{2\pi}{\hbar} |H_{AB}|^2 \frac{1}{\sqrt{4\pi\lambda k_b T}} \exp\left(\frac{-\left(\lambda + \Delta G^0\right)^2}{4\lambda k_b T}\right)$$

where k_{et} is the rate of electron transfer (i.e. hopping rate), $|H_{AB}|$ is the electronic coupling between the initial and final states, λ is the reorganization energy, ΔG^0 is the total Gibbs free energy change for the electron transfer reaction, and k_b the Boltzmann constant. The corresponding potential diagram including the physical parameters is depicted in Figure 1.2.

High hopping rates, i.e. high charge-carrier mobilities, need an effective electronic coupling (H_{AB}) between adjacent hopping sites. High polarizability of the molecules is beneficial, as found in extended π systems constituting most organic semiconductors.[30] Diffuse orbitals, especially in the periphery of the molecules, contribute to a strong electronic coupling. Sulfur and selenium atoms in a conjugated π system form the basis of many good semiconductors.[31]

The reorganization energy λ should be small for high hopping rates. λ increases with the distance between the two hopping sites. Consequently, the molecules

should pack as densely as possible to allow high mobilities.[32] Finally, ΔG^0 should have the maximum negative value. In a perfectly uniform material, ΔG^0 represents the potential difference between two molecules induced by the electric field. If, however, the material is inhomogeneous, ΔG^0 can be positive, hindering the charge to hop to the next site. This phenomenom is called trapping and can be caused by impurities, grain boundaries, or structural defects to mention just a few. For high mobilities, it is, therefore, absolutely necessary to use very pure materials and avoid any inhomogeneities.[33]

1.3 Organic Semiconductors as Active Materials in Devices

Semiconductors are used in many different devices that make up modern life. Field-effect transistors and solar cells are important examples. As they play a central role in the present work, their operation principles and common materials are presented in the following part.

1.3.1 Organic Field-Effect Transistors

In a field-effect transistor, the conductivity between a source and a drain electrode is modulated by an additional electrical field.[34] The result is a switch operated by an electrical voltage, hence no mechanical operation takes place. By combining several of these switches it is possible to build up logic circuits. A central processing unit (CPU) in a computer consists of millions of individual transistors, so the development of transistor performance has a direct impact on computer power.[35]

Fundamental Device Architecture

In a classical organic field-effect transistor setup, a silicon wafer with an oxide layer is used. Gold electrodes are placed on top followed by the semiconductor.

The gold electrodes are connected to a voltage supply and work as source and drain. Independently, a voltage is applied to the silicon to create an electric field to switch the transistor, the so called gate voltage. The insultor, in this case the silicon dioxide, is crucial to prevent current from flowing between the silicon and the drain electrode, the so called leakage current.[36]

To obtain the charge-carrier mobility, one records the source-drain current I_{SD} as a function of the source-drain voltage V_{SD} at a given gate voltage V_G. A theoretical treatment gives the following relation:[37]

$$I_{SD} = \frac{W}{L}\mu_{FE}C_i\left[(V_G - V_{th})V_{SD} - \frac{1}{2}V_{SD}^2\right]$$

where W and L are the width and the length of the channel, respecively, μ_{FE} is the charge-carrier mobility, C_i the capacitance of the insulator, and V_{th} the threshold voltage, i.e. the gate voltage at which significant current flow begins. As the latter value is often hard to determine, it is better to resort to the derivative:

$$\frac{dI_{SD}}{dV_G} = \frac{W}{L}\mu_{FE}C_iV_{SD}$$

The above described device setup is called bottom-contact bottom-gate (compare Figure 1.3a). It is possible to change to different geometries. In the case of all polymeric devices, using e.g. polyethylene terephthalate (PET) as substrate, it has turned out that a top-contact top-gate is much more effective.[38] The polymer is deposited on the PET substrate, electrodes are evaporated on top, on which a dielectric such as polystyrene with a contact metal are deposited on top as depicted in Figure 1.3b. This geometry encapsulates the active material, increasing device lifetime in ambient conditions considerably.

There are two operation modes for transistors, depending on the nature of the charge carrier: hole and electron conduction. If a negative gate voltage is applied,

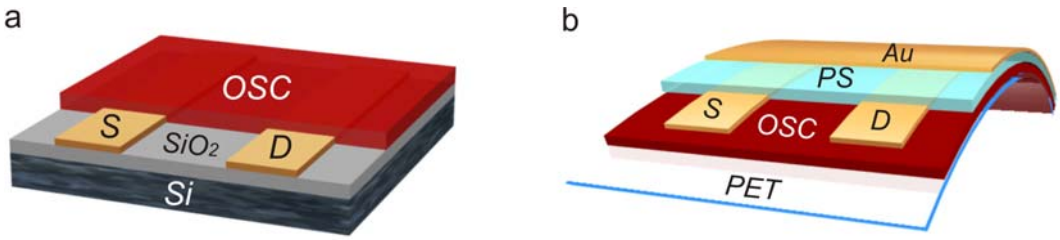

Figure 1.3: FET geometries: **a.** bottom-contact bottom-gate on silicon wafer; **b.** top-contact top-gate on flexible PET film; OSC: organic semiconductor, S: source electrode, D: drain electrode, Si: silicon electrode, SiO_2: silicon dioxide dielectric, PET: polyethylene terephthalate substrate, PS: polystyrene dielectric, Au: gold gate electrode.

positively charged holes, i.e. vacant places for electrons which do not compensate the positive charge of the atomic nucleus, accumulate at the interface. Charge transport takes place by filling the vacant place with an electron of a neighboring site where a new vacant place is created. By a series of such events, it looks as if the hole moved along the electric field. If, on the other hand, a positive gate voltage is applied, electrons accumulate at the interface which move along the electric field. Depending on the nature of the semiconductor, it is more facile to accumulate holes (p-type semiconductors) or electrons (n-type semiconductors). Electron rich compounds are typically p-type semiconductors, electron poor materials are n-type semiconductors. If both electrons and holes can be generated in one material, it is called an ambipolar semiconductor.[39]

Common Materials

The active materials currently used for organic field-effect transistors can be divided into four groups:

- small, typically insoluble molecules which are evaporated on the substrate,
- single crystals,
- small, soluble molecules processed from solution,
- polymers processed from solution.

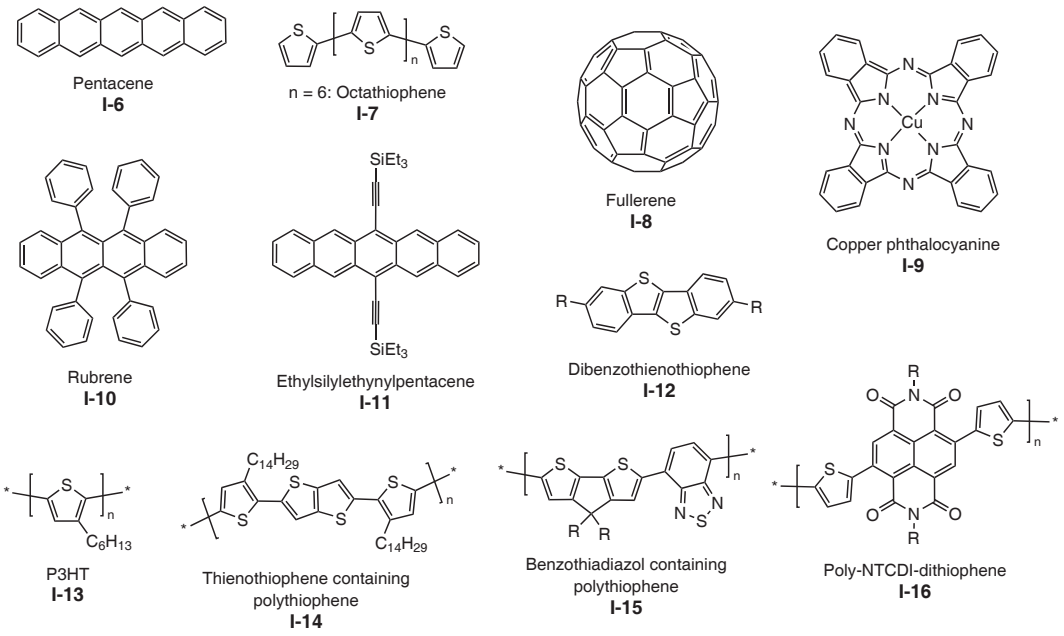

Figure 1.4: Common materials used in organic field-effect transistors.

The most famous molecule out of the first group is pentacene (**I-6**). It is sparingly soluble and, therefore, typically processed by evaporation. Field-effect mobilities of 2.2 $cm^2V^{-1}s^{-1}$can be obtained when using ultra-pure material.[40] Oligothiophenes are another class of insoluble, vapor deposited molecules. For octathiophene (**I-7**) a mobility of 0.33 $cm^2V^{-1}s^{-1}$has been reported.[41] Copper-phthalocyanine (**I-9**) represents the class of disc-like polycyclic aromatic hydrocarbons (PAH). It is preferentially used in flexible devices and exhibits a good mobility (0.01 $cm^2V^{-1}s^{-1}$).[42] A typical n-type material processed from the gas phase is fullerene (C_{60}, **I-8**) with an electron mobility up to 4.9 $cm^2V^{-1}s^{-1}$when deposited on a pentacene film.[43]

By far the highest charge-carrier mobilities are reached in single crystals. Their structural perfection reveals the intrinsic values which the mobility can reach in organic materials. Rubrene (**I-10**) and pentacene (**I-6**) exhibit mobilities up to 15 $cm^2V^{-1}s^{-1}$upon contacting single crystals in a certain orientation on a PDMS stamp as dielectric.[44, 45]

In order to be able to process the organic semiconductor from solution, soluble derivatives of the above mentioned materials have been prepared. By attach-

ing trialkylsilylethynyl groups to pentacene (**I-11**), highly conductive molecules were obtained (μ = 0.4 $cm^2V^{-1}s^{-1}$).[46] Oligothiophene, especially with fused rings bearing alkyl chains, show high mobilities when processed from solution. Alkyl substituted dibenzothienothiophene (**I-12**) was reported to exhibit a mobility of 2.8 $cm^2V^{-1}s^{-1}$.[47]

Among the polymers, poly-(3-hexylthiophene) (P3HT, **I-13**) is the most intensively studied one.[48] Many derivatives of this polymer have been developed with remarkable mobilities and processing characteristics.[49] For a long time, a polythiophene incorporating thienothiophene (**I-14**) was the benchmark with regard to mobility of a polymer (μ = 0.6 $cm^2V^{-1}s^{-1}$).[50] Recently, a polythiophene containing benzothiadiazole units (**I-15**) was reported to exhibit a mobility as high as 1.4 $cm^2V^{-1}s^{-1}$.[51] Remarkable electron conductivity in a polymer was discovered when naphthalene-tetracarboxylic-diimide (NTCDI) was copolymerized with dithiophene (**I-16**). The electron mobility reached values up to 0.85 $cm^2V^{-1}s^{-1}$.[52]

Morphology Investigation

The morphology of an organic semiconductor film plays a crucial role with regard to field-effect mobility. The higher the molecular order the fewer potential trapping sites are present (compare section 1.2). To get a good insight into the morphology of a system of interest, X-ray diffraction is the most powerful technique.[53] The fundamental relationship to appreciate diffraction patterns is Bragg's law:[54]

$$n\lambda = 2d \cdot \sin\theta$$

where n is the order of reflexion, λ the wave length of the radiation, d the distance between lattice planes, and θ the angle between the incident ray and the scattering planes.

Three important X-ray diffraction experiments are used in this work:

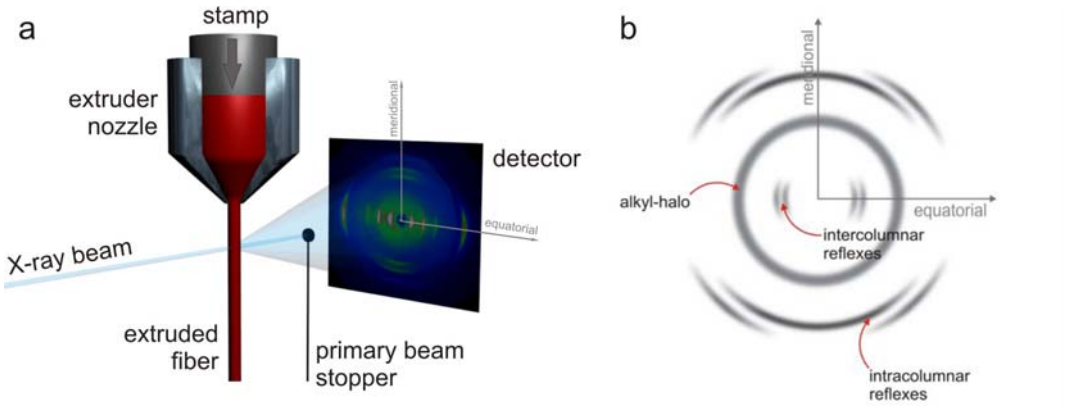

Figure 1.5: Two dimentional fiber wide angle X-ray diffraction. **a.** experimental setup. **b.** diffraction pattern obtained by a discotic liquid crystal.

- Single crystal analysis,
- Film diffraction,
- 2D WAXD.

In case one can grow a single crystal, very sharp reflections are recorded with which crystal planes can be calculated according to Bragg's law. The beam hits the crystal from many different directions giving many diffraction patterns. After a complicated mathematical treatment, the crystal structure can be obtained revealing all positions of the atoms allowing the determinatioin of bond length, bond distances, and intermolecular distances.[55]

Unfortunately, single crystals of only very few substances can be grown. Especially for polymers, it is not possible at all. Some information can still be elucidated by film diffraction.[56, 57] A thin film is deposited on a silicon wafer or a glass substrate. The film is hit by an X-ray beam and the diffracted beam is plotted against the diffraction angle. Using Bragg's law, one is able to calculate the corresponding lattice distances in the substance.

Even better insight is gained when a fiber is extruded as depicted in Figure 1.5a.[58] The beam hits the fiber and is detected by a two dimensional CCD camera. Reflections in the fiber direction (meridional) and perpendicular to the fiber direction (equatorial) are recorded. This methode is referred to as two-dimensional

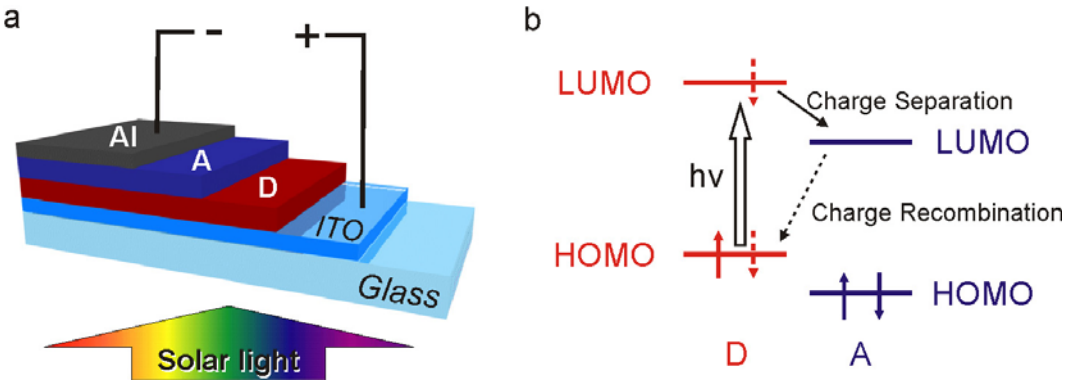

Figure 1.6: Principal of a solar cell. **a.** Setup of a solar cell, Al: aluminium cathode, A: electron acceptor material, D: electron donor material, ITO: indium tin oxide anode **b.** energy level diagram of a bulk heterojunction.

wide angle X-ray diffraction (2D-WAXD). A typical diffraction pattern can be seen in Figure 1.5b.[59] The interpretation of results from 2D WAXD has to take into account that sheer forces during the extrusion process significantly affect the crystallinity and the orientation of the crystal planes.

1.3.2 Organic Solar Cells

In a solar cell light is converted to electrical power, a technology with high potential to significantly contribute to energy supply in the future.[60] When light is absorbed in the active material of the solar cell, excitons are produced. If the exciton binding energy can be overcome, the holes move to the cathode and the electrons to the anode in an electric field. In this way, a voltage is created which can be used to drive an electric current.[61]

In order to overcome the exciton binding energy for efficient charge separation, a bulk heterojunction is beneficial.[62] An electron donor and an acceptor are sandwiched between two electrodes as depicted in Figure 1.6a. The transition of the electron from the LUMO of the donor to the LUMO of the acceptor provides the energetic driving force to overcome the exciton binding energy (compare Figure 1.6b).[63] The energy difference between the HOMO of the donor and the

LUMO of the acceptor equals the maximum voltage a solar cell can produce.[64] The latter is called open circuit voltage, V_{OC}, as the maximum voltage can only build up when the electrical circuit is open and no current flows. The maximum current, on the other hand, can be measured when connecting the anode and the cathode without resistance, hence shorting the circuit. Consequently, the maximum current is called short circuit current, I_{SC}. One might suggest that the power conversion is the product of V_{OC} and I_{SC}. In real systems, however, the maximum power is a fraction of this value. This fraction is called the fill factor (FF), another important parameter of a solar cell.

The solar cell parameter of highest interest is the total power efficiency η, i.e. the electrical energy obtained by the solar cell divided by the energy of the incident photons. Values of around 5 % can be reached with organic solar cells at the moment.[65] For comparison, silicon based solar cells reach efficiencies of 25 %.[66] Lower production costs may, nevertheless, compensate this efficiency gap.[67]

The most commonly used materials are poly(3-hexylthiophene) (P3HT) as the donor in combination with a fullerene derivative (PCBM) as the acceptor.[68] Copper-phthalocyanine with fullerene also gives satisfying efficiencies.[69] Solar cells consisting of only disc-like molecules have been prepared using perylene-tetracarboxylic-dimide (PTCDI) together with hexaphenyl-hexa-*peri*-hexabenzocoronene (HBC).[70]

1.4 Organic Molecules as Auxiliary Materials in Devices

The applicability of organic molecules goes well beyond the function as active material. An electronic device is a complex composite of different materials with many interfaces. Organic molecules can assist charge injection by forming interlayers or can increase charge conduction by doping.

1.4.1 Electrode Work Function Manipulation by Organic Molecules

In an ideal device, the Fermi level of a metal electrode equals the HOMO level of the semiconductor for hole injection or the LUMO level for electron injection.[71] Especially in the latter case, it is very hard to find suitable materials. LUMO levels of organic molecules are relatively high, so only very reactive materials, such as calcium or barium, possess a high enough Fermi energy level.[72] In the case of hole injection, on the other hand, Fermi levels are often too high. Many device scientists apply an interlayer of poly(ethylenedioxythiophene) which is doped with poly(styrenesulfonate) (PEDOT-PSS, **I-17**) to reduce the injection barrier.[73] The high acidity of PSS, nevertheless, is very unfavorable with regard to device lifetime as it degrades many organic semiconductors.[74]

An alternative approach to tune the work function (i.e. the difference between Fermi level and vacuum level) of a metal is the deposition of a single layer of organic molecules. The electron clouds of the metal are pushed into the metal. This so called push-back effect decreases the work function of a metal and is independent of the nature of the deposited molecule.[75, 76]

When a strong electron acceptor is applied, the LUMO levels of the acceptor are partially filled, leaving the metal with fewer electrons.[77] The Fermi level is decreased, so the work function is increased. The opposite effect applies when the metal is coated by strong donor molecules. The electron density of the metal is increased, the work function, therefore, is decreased.

By appropriate choice of molecules, the Fermi levels of the metals can be adjusted to the used semiconductor. Furthermore, if the work function can be decreased strongly enough, coinage metals such as copper or silver can be used to inject electrons.[78] In this case, it is not necessary to use materials which are not stable in ambient conditions.

To reach the above described goals, many materials have been tested. In-

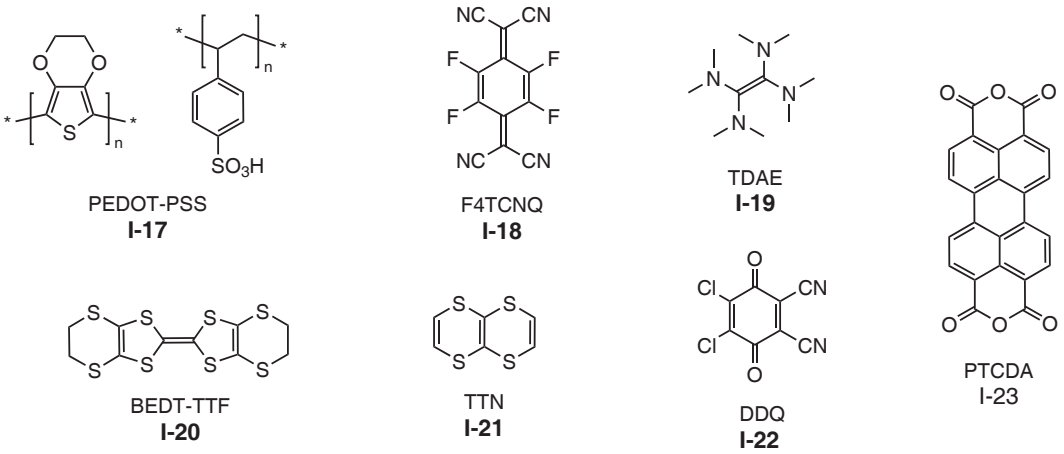

Figure 1.7: Donor and acceptor materials for organic electronics used for work function manipulation and doping.

tensive studies have been performed with tetrafluoro-tetracyanoquino-dimethane (F4TCNQ, **I-18**), a very strong acceptor which significantly increases the work function.[79] Also, perylene-tetracarboxylic-dianhydride (PTCDA, **I-23**) has successfully been used.[80] A work function reduction of a cathode was achieved using tetrakis(dimethylamino)ethene (TDAE, **I-19**).[81]

To analyze the effect of molecules on metals, photoemission spectroscopy is frequently used. It is a powerful surface analysis technique.[82] Due to its significance for this work, it is briefly described below.

Photoemission Spectroscopy

In a photoemission spectroscopy experiment, a sample is irradiated with a beam of photons in vacuum which generates free electrons, the so-called photoelectrons. Their kinetic energy is measured by an analyzer (see Figure 1.8a). By subtracting this energy from the energy of the incident photons, the binding energy of the corresponding electron in the sample is accessible. Only electrons near the surface can reach the detector, others are reabsorbed by the sample.[83, 84] A typical spectrum can be seen in Figure 1.8b.

Depending on the nature of the photons, two experiments are distinguished: UPS

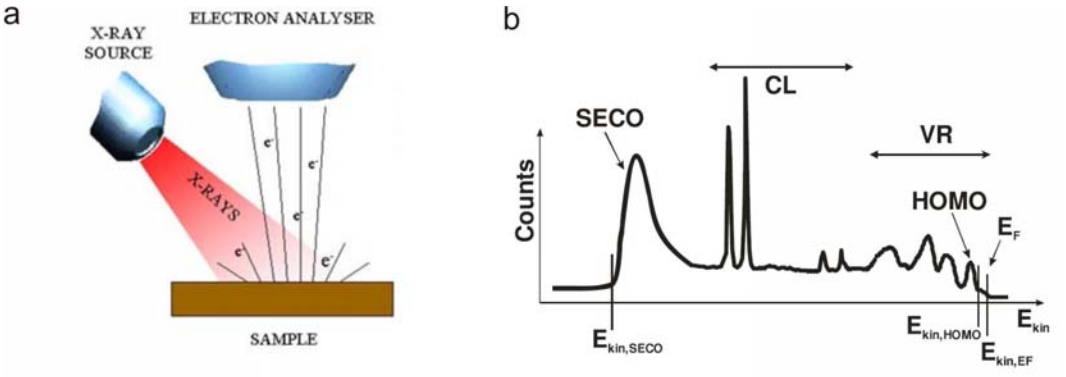

Figure 1.8: Photoelectron spectroscopy: **a.** principle setup, **b.** typical spectrum, SECO: secondary electron cut-off, CL: core level (strongly bound elecrons), VL: valence level (loosely bound electrons), E_{kin} kinetic energy, E_F: Fermi energy.

and XPS. If one is only interested in loosely bound electrons, such as valence electrons or those near the Fermi edge of a metal, ultraviolet irradiation is used to create the photoelectrons. The method is refered to as ultraviolet photoemission spectroscopy (UPS).[85] The electrons more strongly bound to the atoms are accessible when using X-rays instead of ultraviolet irradiation. Consequently, this method is called X-ray photoemission spectroscopy (XPS).[86]

1.4.2 Doping

Many of the issues discussed in the previous section can be addressed as well by introducing strong donors or acceptors into the semiconductor layer of a device.[87] The donors transfer negative charge to the semiconductor, increasing its energy level. Acceptors remove electrons from the semiconductors, decreasing its energy level. This phenomenom is called doping. It is well known in the inorganic semiconductor technology, but can be equally well applied to organic semiconductors.[88]

By appropriate doping, the energy level can be adjusted to the electrode materials to reduce Ohmic losses at the interface and ease charge injection. Also, the conductivity is increased, because free charges are generated and/or trapping states

are filled. By doping, it is even possible to turn a p-type semiconductor to an n-type one. In this way, p-n-homojunctions can be realized.[89]

Common materials for doping are tetrafluoro-tetracyanoquino-dimethane (F4TCNQ, **I-18**) and dichloro-dicyanobenzoquinone (DDQ, **I-22**) for p-doping.[90, 91] For n-doping, people have used bisethylene-dithio-tetrathiafulvalene (BEDT-TTF, **I-20**) or tetrathianaphthalene (TTN, **I-21**).[92, 93]

For all previously described investigations, the energy levels of the molecules are needed. Cyclic voltammetry is a powerful analytical technique to obtain these values.[94] Its working principle is layed out briefly due to its significance for this work.

Cyclic voltammetry

In a cyclic voltammetry experiment the electric potential is determined which is needed to oxidize or reduce a molecule under investigation.[95] For this purpose, a working electrode and a counter electrode are immersed into a solution of the analyte. Between these electrodes a voltage is linearly ramped while measuring the current flow (compare Figure 1.9). When the oxidation/reduction potential (depending of the sign of the voltage) is reached, a strong increase in current flow is observed which later on decreases again as the electroactive substance in the proximity of the electrode is depleted. At a set voltage, the ramp is reversed to reduce/oxidize the substance back. One notices a current increase at a slightly shifted voltage in comparison to the forward ramp due to kinetic phenomena. If the oxidized or reduced species is not stable, one does not observe current peaks in the backscan.

The accuracy of the measurement is ensured by using an additional reference electrode which is connected to a standard cell, e.g. a calomel electrode.[96] To increase electric conductivity of the analyte solution and reduce interface charging

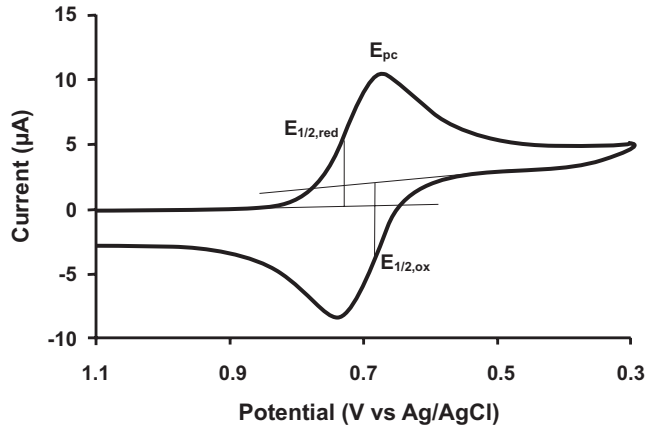

Figure 1.9: Typical cyclic voltagram.

an electrolyte is added.[97] In organic solvents, tetrabutylammonium salts are often used. It is crucial for the measurements in organic solvents to avoid moisture and oxygen.[98] The latter frequently reacts with radicals formed after charging the molecule. If water is electrolyzed in the cell, the superimposed signal makes elucidation of redox potentials of the molecule impossible.

For data analysis, the half-step potential $E_{1/2}$ is determined.[99] The LUMO energy level is calculated according to

$$E_{\mathrm{HOMO}} = -4.8\,V + E_{1/2,\mathrm{red}} \quad \text{and} \quad E_{\mathrm{LUMO}} = -4.8\,V - E_{1/2,\mathrm{ox}}$$

For good comparability, it is good practice to add some ferrocene as internal standard.[100] Ferrocene is a very stable redox active compound. Its very low oxidation potential makes it unlikely to interfere with other redox potentials.

1.5 Bibliography

[1] Akamatu, H.; Inokuchi, H.; Matsunaga, Y. *Nature* **1954**, *173*, 168–169.

[2] Mcneill, R.; Weiss, D. E.; Wardlaw, J. H.; Siudak, R. *Aust. J. Chem.* **1963**, *16*, 1056–1057.

[3] Epstein, A. J.; Etemad, S.; Garito, A. F.; Heeger, A. J. *Phys. Rev. B* **1972**, *5*, 952–977.

[4] Coleman, L. B.; Cohen, M. J.; Sandman, D. J.; Yamagish.Fg,; Garito, A. F.; Heeger, A. J. *Solid State Comm.* **1973**, *12*, 1125–1132.

[5] Mcginnes.J,; Corry, P.; Proctor, P. *Science* **1974**, *183*, 853–855.

[6] Shirakawa, H.; Louis, E. J.; Macdiarmid, A. G.; Chiang, C. K.; Heeger, A. J. *J. Chem. Soc.-Chem. Comm.* **1977**, 578–580.

[7] Chiang, C. K.; Fincher, C. R.; Park, Y. W.; Heeger, A. J.; Shirakawa, H.; Louis, E. J.; Gau, S. C.; Macdiarmid, A. G. *Phys. Rev. Lett.* **1977**, *39*, 1098–1101.

[8] Sirringhaus, H.; Ando, M. *MRS Bull.* **2008**, *33*, 676–682.

[9] Sirringhaus, H.; Tessler, N.; Friend, R. H. *Science* **1998**, *280*, 1741–1744.

[10] Friend, R. H.; Gymer, R. W.; Holmes, A. B.; Burroughes, J. H.; Marks, R. N.; Taliani, C.; Bradley, D. D. C.; Dos Santos, D. A.; Bredas, J. L.; Logdlund, M.; Salaneck, W. R. *Nature* **1999**, *397*, 121–128.

[11] Thompson, B. C.; Frechet, J. M. J. *Angew. Chem. Int. Ed.* **2008**, *47*, 58–77.

[12] Someya, T.; Pal, B.; Huang, J.; Katz, H. E. *MRS Bull.* **2008**, *33*, 690–696.

[13] IDTechEx, *RFID Forecasts, Players and Opportunities 2008-2018*; 2008.

[14] Steudel, S.; Myny, K.; Arkhipov, V.; Deibel, C.; De Vusser, S.; Genoe, J.; Heremans, P. *Nat. Mater.* **2005**, *4*, 597–600.

[15] Sze, S. M. *Physics of Semiconductor Devices*; Wiley and Sons, 1982.

[16] Yu, P. Y.; M., C. *Fundamentals of Semiconductors. Physics and Materials Properties*; Springer, 2001.

[17] Banerjee, S. K.; Streetman, B. G. *Solid State Electronic Devices*; Pentice Hall, 2005.

[18] Chan, K. Y.; Knipp, D.; Carius, R.; Stiebig, H. *MRS Bull.* **2008**, *1066*, 293–298.

[19] Hush, N. S. *Ann. N.Y. Acad. Sci.* **2003**, *1006*, 1–20.

[20] Allegra, G.; Meille, S. V. *Macromol.* **2004**, *37*, 3487–3496.

[21] O'Mara, W. C.; Hunt, L. P.; Herring, R. B. *Handbook of Semiconductor Silicon Technology*; Noyes Publications, 1990.

[22] Nitzan, A.; Ratner, M. A. *Science* **2003**, *300*, 1384–1389.

[23] Jäckel, F.; Watson, M. D.; Müllen, K.; Rabe, J. P. *Phys. Rev. Lett.* **2004**, *92*, 188303.

[24] Soloviev, V. N.; Eichhofer, A.; Fenske, D.; Banin, U. *J. Am. Chem. Soc* **2000**, *122*, 2673–2674.

[25] Bonilla, L. L. *J. Phys.-Condes. Matter* **2002**, *14*, R341–R381.

[26] Coropceanu, V.; Cornil, J.; da Silva, D. A.; Olivier, Y.; Silbey, R.; Bredas, J. L. *Chem. Rev.* **2007**, *107*, 2165–2165.

[27] Jaiswal, M.; Menon, R. *Polym. Int.* **2006**, *55*, 1371–1384.

[28] Emin, D. *Adv. Phys.* **1975**, *24*, 305–348.

[29] Marcus, R. A. *J. Chem. Phys.* **1956**, *24*, 966–978.

[30] Heeger, A. J. *Rev. Mod. Phys.* **2001**, *73*, 681–700.

[31] Kelley, T. W.; Baude, P. F.; Gerlach, C.; Ender, D. E.; Muyres, D.; Haase, M. A.; Vogel, D. E.; Theiss, S. D. *Chem. Mater.* **2004**, *16*, 4413–4422.

[32] Heeger, A. J. *Faraday Discuss. Chem. Soc.* **1989**, 203–211.

[33] Chabinyc, M. L.; Jimison, L. H.; Rivnay, J.; Salleo, A. *MRS Bull.* **2008**, *33*, 683–689.

[34] Bao, Z.; J., L. *Organic Field-Effect Transistors*; CRC, 2007.

[35] Brey, B. B. *Intel Microprocessors*, 8th ed.; Prentice Hall, 2008.

[36] Facchetti, A.; Yoon, M. H.; Marks, T. J. *Adv. Mater.* **2005**, *17*, 1705–1725.

[37] Singh, T. B.; Sariciftci, N. S. *Ann. Rev. Mater. Res.* **2006**, *36*, 199–230.

[38] Backlund, T. G.; Sandberg, H. G. O.; Osterbacka, R.; Stubb, H.; Makela, T.; Jussila, S. *Synth. Met.* **2005**, *148*, 87–91.

[39] Cornil, J.; Bredas, J. L.; Zaumseil, J.; Sirringhaus, H. *Adv. Mater.* **2007**, *19*, 1791–1799.

[40] Roberson, L. B.; Kowalik, J.; Tolbert, L. M.; Kloc, C.; Zeis, R.; Chi, X. L.; Fleming, R.; Wilkins, C. *J. Am. Chem. Soc.* **2005**, *127*, 3069–3075.

[41] Hajlaoui, M. E.; Garnier, F.; Hassine, L.; Kouki, F.; Bouchriha, H. *Synthetic Metals* **2002**, *129*, 215–220.

[42] Someya, T.; Kato, Y.; Sekitani, T.; Iba, S.; Noguchi, Y.; Murase, Y.; Kawaguchi, H.; Sakurai, T. *Proc. Natl. Acad. Sci. USA* **2005**, *102*, 12321–12325.

[43] Itaka, K.; Yamashiro, M.; Yamaguchi, J.; Haemori, M.; Yaginuma, S.; Matsumoto, Y.; Kondo, M.; Koinuma, H. *Adv. Mater.* **2006**, *18*, 1713–+.

[44] Sundar, V. C.; Zaumseil, J.; Podzorov, V.; Menard, E.; Willett, R. L.; Someya, T.; Gershenson, M. E.; Rogers, J. A. *Science* **2004**, *303*, 1644–1646.

[45] Jurchescu, O. D.; Popinciuc, M.; van Wees, B. J.; Palstra, T. T. M. *Adv. Mater.* **2007**, *19*, 688–692.

[46] Sheraw, C. D.; Jackson, T. N.; Eaton, D. L.; Anthony, J. E. *Adv. Mater.* **2003**, *15*, 2009–2011.

[47] Ebata, H.; Izawa, T.; Miyazaki, E.; Takimiya, K.; Ikeda, M.; Kuwabara, H.; Yui, T. *J. Am. Chem. Soc.* **2007**, *129*, 15732–15733.

[48] Sirringhaus, H.; Brown, P. J.; Friend, R. H.; Nielsen, M. M.; Bechgaard, K.; Langeveld-Voss, B. M. W.; Spiering, A. J. H.; Janssen, R. A. J.; Meijer, E. W.; Herwig, P.; de Leeuw, D. M. *Nature* **1999**, *401*, 685–688.

[49] Ong, B. S.; Wu, Y. L.; Li, Y. N.; Liu, P.; Pan, H. L. *Chem. Eur. J.* **2008**, *14*, 4766–4778.

[50] McCulloch, I.; Heeney, M.; Bailey, C.; Genevicius, K.; Macdonald, I.; Shkunov, M.; Sparrowe, D.; Tierney, S.; Wagner, R.; Zhang, W. M.; Chabinyc, M. L.; Kline, R. J.; McGehee, M. D.; Toney, M. F. *Nat. Mater.* **2006**, *5*, 328–333.

[51] Tsao, H. N.; Cho, D.; Andreasen, J. W.; Rouhanipour, A.; Breiby, D. W.; Pisula, W.; Müllen, K. *Adv. Mater.* **2009**, *21*, 209–212.

[52] Yan, H.; Chen, Z. H.; Zheng, Y.; Newman, C.; Quinn, J. R.; Dötz, F.; Kastler, M.; Facchetti, A. *Nature* **2009**, *457*, 679–688.

[53] Roe, R.-J. *Methods of X-Ray and Neutron Scattering in Polymer Science*; Oxford University Press, 2000.

[54] Bragg, W. L. *Proceeding of the Cambridge Philosophical Society* **1913**, *17*, 43–57.

[55] Clegg, W. *Crystal Structure Determination*; Oxford University Press, 1998.

[56] Aggarwal, S. L.; Sweeting, O. J.; Tilley, G. P. *J. Polym. Sci.* **1961**, *51*, 551–568.

[57] Prosa, T. J.; Winokur, M. J.; Moulton, J.; Smith, P.; Heeger, A. J. *Macromol.* **1992**, *25*, 4364–4372.

[58] Tashiro, K.; Sasaki, S. *Prog. Polym. Sci.* **2003**, *28*, 451–519.

[59] Pisula, W.; Tomovic, Z.; Simpson, C.; Kastler, M.; Pakula, T.; Müllen, K. *Chem. Mater.* **2005**, *17*, 4296–4303.

[60] Brabec, C. J.; Durrant, J. R. *MRS Bull.* **2008**, *33*, 670–675.

[61] Würfel, P.; Würfel, U. *Physics of Solar Cells: From Basic Principles to Advanced Concepts*; Wiley-Vch, 2009; Vol. 2nd.

[62] Dennler, G.; Scharber, M. C.; Brabec, C. J. *Adv. Mater.* **2009**, *21*, 1323–1338.

[63] Scholes, G. D.; Rumbles, G. *Nat. Mater.* **2006**, *5*, 683–696.

[64] Shrotriya, V.; Li, G.; Yao, Y.; Moriarty, T.; Emery, K.; Yang, Y. *Adv. Funct. Mater.* **2006**, *16*, 2016–2023.

[65] Kim, J. Y.; Kim, S. H.; Lee, H. H.; Lee, K.; Ma, W. L.; Gong, X.; Heeger, A. J. *Adv. Mater.* **2006**, *18*, 572–576.

[66] Green, M. A.; Emery, K.; Hishikawa, Y.; Warta, W. *Prog. Photovolt. Res. Appl.* **2009**, *17*, 85–94.

[67] Brabec, C. J.; Scherf, U.; Dyankonov, V. *Organic Photovoltaics: Materials, Device Physics, and Manufacturing Technologies*, 1st ed.; Wiley-VCH, 2008.

[68] Irwin, M. D.; Buchholz, B.; Hains, A. W.; Chang, R. P. H.; Marks, T. J. *Proc. Natl. Acad. Sci. USA* **2008**, *105*, 2783–2787.

[69] Xue, J. G.; Rand, B. P.; Uchida, S.; Forrest, S. R. *Adv. Mater.* **2005**, *17*, 66–71.

[70] Schmidt-Mende, L.; Fechtenkötter, A.; Müllen, K.; Moons, E.; Friend, R. H.; MacKenzie, J. D. *Science* **2001**, *293*, 1119–1122.

[71] Shen, Y. L.; Hosseini, A. R.; Wong, M. H.; Malliaras, G. G. *ChemPhysChem* **2004**, *5*, 16–25.

[72] Parker, I. D. *J. Appl. Phys.* **1994**, *75*, 1656–1666.

[73] Groenendaal, B. L.; Jonas, F.; Freitag, D.; Pielartzik, H.; Reynolds, J. R. *Adv. Mater.* **2000**, *12*, 481–494.

[74] Chia, P. J.; Chua, L. L.; Sivaramakrishnan, S.; Zhuo, J. M.; Zhao, L. H.; Sim, W. S.; Yeo, Y. C.; Ho, P. K. H. *Advanced Materials* **2007**, *19*, 4202–4207.

[75] Bagus, P. S.; Staemmler, V.; Wöll, C. *Phys. Rev. Lett.* **2002**, *89*, 96104.

[76] Lüth, H. *Solid Surfaces, Interfaces and Thin Films*, 4th ed.; Springer: Berlin, 2001.

[77] Koch, N. *Chem. Phys. Chem.* **2007**, *8*, 1438–1455.

[78] Bröker, B.; Blum, R. P.; Frisch, J.; Vollmer, A.; Hofmann, O. T.; Rieger, R.; Müllen, K.; Rabe, J. P.; Zojer, E.; Koch, N. *App. Phys. Lett.* **2008**, *93*, 243303.

[79] Koch, N.; Duhm, S.; Rabe, J. P.; Vollmer, A.; Johnson, R. L. *Phys. Rev. Lett.* **2005**, *95*, 237601.

[80] Duhm, S.; Gerlach, A.; Salzmann, I.; Bröker, B.; Johnson, R. L.; Schreiber, F.; Koch, N. *Org. Electron.* **2008**, *9*, 111–118.

[81] Osikowicz, W.; Crispin, X.; Tengstedt, C.; Lindell, L.; Kugler, T.; Salaneck, W. R. *Appl. Phys. Lett.* **2004**, *85*, 1616–1618.

[82] Schattke, W.; van Hove, M. A. *Solid-State Photoemission and Related Methods: Theory and Experiment*, 1st ed.; Wiley-VCH, 2003.

[83] Cahen, D.; Kahn, A. *Adv. Mater.* **2003**, *15*, 271–277.

[84] Salaneck, W. R.; Friend, R. H.; Bredas, J. L. *Phys. Rep.* **1999**, *319*, 232–251.

[85] Ishii, H.; Sugiyama, K.; Ito, E.; Seki, K. *Adv. Mater.* **1999**, *11*, 972–972.

[86] Castle, J. E. *J. Vac. Sci. Technol., A* **2007**, *25*, 1–27.

[87] Walzer, K.; Maennig, B.; Pfeiffer, M.; Leo, K. *Chem. Rev.* **2007**, *107*, 1233–1271.

[88] Levy, R. A. *Microelectronic Materials and Processes*, 1st ed.; Kluwer Academic Publisher, 1989.

[89] Harada, K.; Werner, A. G.; Pfeiffer, M.; Bloom, C. J.; Elliott, C. M.; Leo, K. *Phys. Rev. Lett.* **2005**, *94*, 36601.

[90] Maennig, B.; Pfeiffer, M.; Nollau, A.; Zhou, X.; Leo, K.; Simon, P. *Phys. Rev. B* **2001**, *64*, 195208.

[91] Maitrot, M.; Guillaud, G.; Boudjema, B.; Andre, J. J.; Simon, J. *J. Appl. Phys.* **1986**, *60*, 2396–2400.

[92] Nollau, A.; Pfeiffer, M.; Fritz, T.; Leo, K. *J. Appl. Phys.* **2000**, *87*, 4340–4343.

[93] Tanaka, S.; Kanai, K.; Kawabe, E.; Iwahashi, T.; Nishi, T.; Ouchi, Y.; Seki, K. *Jpn. J. Appl. Phys.* **2005**, *44*, 3760–3763.

[94] Bard, A. J.; R., F. L. *Electrochemical Methods. Fundamentals and Applications*, 2nd ed.; Wiley and Sons, 2001.

[95] Heinze, J. *Angew. Chem. Int. Ed.* **1984**, *23*, 831–847.

[96] Bond, A. M. *Modern Polarographic Methods in Analytical Chemistry*; Marcel Dekker Inc., 1980.

[97] Eberson, L. *Adv. Phys. Org. Chem.* **1981**, *18*, 79.

[98] Hammeric.O,; Parker, V. D. *Electrochim. Acta* **1973**, *18*, 537–541.

[99] Parker, V. D. *Electroanal. Chem.* **1986**, *14*, 1–111.

[100] Seiwert, B.; Karst, U. *Anal. Bioanal. Chem.* **2008**, *390*, 181–200.

2 Objectives and Motivation

Organic molecules constitute highly promising materials towards flexible, lightweight, large-area, and cost-effective semiconductor devices. Experts predict a wide variety of new applications which cannot be realized with traditional inorganic semiconductors. Many materials have been found to work well in field-effect transistors,[1–4] solar cells,[5–9] light-emitting diodes,[10–13], sensors,[14, 15] and memories.[16] Nevertheless, silicon is still unreached with respect to charge-carrier mobility and long-term stability. A lot of research is still to be done to improve the performance of organic materials and address open issues in the processing of devices.

Two approaches are common to optimize device performances: working on the device physics and the processing of the material or making new molecules with better performance. The former strategy includes varying electrode materials, surface treatments, interlayers, formulations, and so on.[17–19] As many parameters can be changed, an incredible number of possible device setups are conceivable. When changing one paramter it is never clear if other parameters are implicitely changed as well.

Even the best device optimization, however, cannot satisfy all requirements for applications. This is where synthesis comes into play. It can provide specialized materials for a desired purpose making tedious device optimization less important.[20] Functionality can be introduced into existing structures to fine-tune materials properties, or completely new systems can be built up to possibly generate completely

new materials properties. An aspect of particular relevance is the electronic structure, i.e. the energy levels of a molecule. It can be lowered by introducing certain functions rendering electron acceptors. Electron donors are accessible by the appropriate choice of functional groups as well. Donor and acceptor molecules are crucial as auxiliary molecules for organic electronics as they can help charge injection in a device which is often the limiting factor for performance (compare section 1.4 on page 22).[21] Furthermore, the directed design of the electronic levels of an organic semiconductor is useful to facilitate hole or electron transport.

Small molecules are advantageous with respect to processing as they allow both solution deposition as well as sublimation.[22] Some molecules can even be crystallized into single crystals, giving a deep insight into the molecular packing. Polycyclic aromatic hydrocarbons are particularly important due to their rigid geometry, polarizability and strong affinity to surfaces.[23–26] When the molecules are used at interfaces for work function manipulation or doping, the size has to be considered carefully: too large molecules can barely be sublimed and often possess low solubility. Too small molecules, on the other hand, tend to diffuse into other layers which leads to instabilities during operation and significantly reduces lifetime and device performance.[27]

Considerable effort has been spent on triphenylene, producing a library of substances of different electronic levels.[28, 29] Good conductivity along the stacking axis of a discotic thiosubstituted triphenylene is measured.[30] The much more extended hexa-*peri*-hexabenzocoronene (HBC) has been investigated in great detail as well.[23, 31] Coronene represents a PAH of intermediate size. Although the parent compound is intensively studied by physicists and theoreticians,[32–34] functionalized derivatives are rarely mentioned in the literature, most likely due to its difficult synthesis.[35–37] However, coronene derivatives can be sublimed and crystallized, but the molecules should not diffuse too much in devices. Furthermore, there is an important difference between coronene on the one hand and triphenylene/HBC

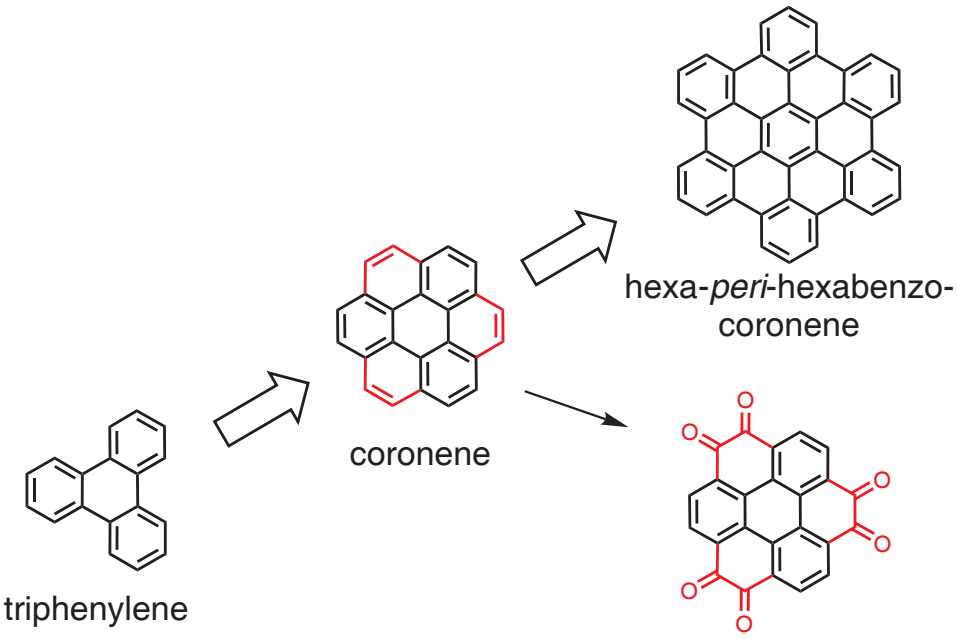

Figure 2.1: Polycyclic aromatic hydrocarbons with increasing size from triphenylene over coronene to HBC, the K-region is marked red.

on the other hand: it possesses a K-region which is the position of increased reactivity in the periphery of a PAH.[38–41] As a consequence, the molecule allows the introduction of up to three α-diketones as depicted in the lower right part of Figure 2.1. This molecule is a central target of this work. Phenanthrene and pyrene can be converted into the diketone and the tetraketone, respectively, by direct oxidation of the parent PAH, coronene only reacts once to form coronene-dione.[42–44] The more diketones are present in one molecule the stronger is the acceptor, leading to stronger interactions with metals and higher adsorption energies. In addition, diketones are a valuable synthetic platform for other structures: This moiety easily undergoes condensations with diamines, is converted to imidazoles, or benzothiadiazoles to mention just a few.[45–47]

Despite the electronic structure, the symmetry of a molecule plays a crucial role with regard to molecular packing, dipole moments, and chemisorption.[48, 49] A synthetic approach is especially valuable when different symmetries are accessible. In this case, one has multiple options at hand to build up complex structures without

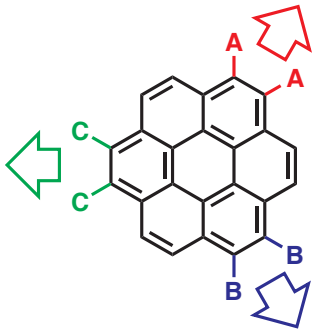

Figure 2.2: Threefold symmetry options on coronene.

changing the whole synthetic route. In Figure 2.2 one can see the various symmetry options when choosing A, B, and C. D_{3h} is established when all substituents are equal. Favorable crystallization tendency and regular two-dimensional lattice formation on surfaces are the consequences. Choosing different substituents renders molecules with permanent dipoles leading to different behavior in electric fields or different chemisorption.

Electron donors are particularly useful as active materials for organic electronics when incorporating thiophene. For low-cost production, processing from solution is highly desirable, especially by fast fabrication methods such as ink-jet, or mass printing technologies such as gravure printing or flexography.[50] Materials are needed which quickly pack into a highly ordered film, guaranteeing high charge-carrier mobility. Conjugated polymers are the most promising materials to fulfill these requirements.[51] Poly-(3-hexylthiophene) (P3HT) is the "fruit fly" amoung the conjugated polymers for organic field-effect transistors,[52, 53] guiding structural considerations for new improved materials.

Benzo[2,1-b;3,4-b']dithiophene has been chosen as the building block to improve device performance with regard to efficient processing. A polymer containing this moiety retains the structure of P3HT, but bridges the thiophenes by benzo annellation. This shall reduce the ionization potential for improved air stability and increase the intermolecular interactions for higher order.

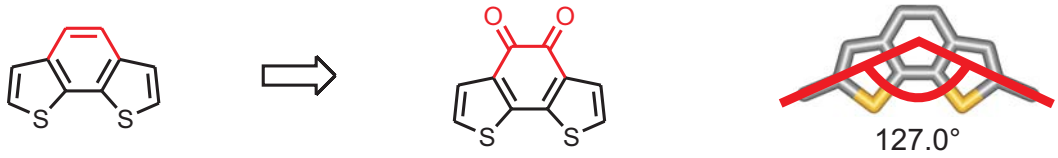

Figure 2.3: Benzo[2,1-b;3,4-b']dithiophene: structural similarity to coronene periphery and bond angle geometry.

A striking feature of this benzodithiophene is its non-linear bond geometry. When incorporated into a polythiophene polymer chain, it introduces a kink due to its bond angle of 127 °. This curvature effect in conjugated polymers has been investigated in this work. Previous developments almost exclusively rely on linear polymers. It is expected that higher solubility is combined with efficient packing of the extended π-system. Field-effect transistors and solar cells have been fabricated to explore if curvature in polymer chains really provides materials with better solution processing properties.

Benzodithiophene shows structural similarities to the coronene periphery: maximum aromaticity is retained upon conversion to the α-diketone as depicted in Figure 2.3. This molecule offers the possibility to make use of the geometric advantage of the kink in the acceptor chemistry as well. Donor-acceptor interactions including this molecule shall be investigated to gain a better understanding of the packing behavior and the electronic properties. These results shall guide future developments of new active materials based on conjugated donor-acceptor systems.

2.1 Bibliography

[1] Singh, T. B.; Sariciftci, N. S. *Ann. Rev. Mater. Res.* **2006**, *36*, 199–230.

[2] Facchetti, A. *Mater. Today* **2007**, *10*, 28–37.

[3] Allard, S.; Forster, M.; Souharce, B.; Thiem, H.; Scherf, U. *Angew. Chem. Int. Ed.* **2008**, *47*, 4070–4098.

[4] de Boer, B.; Facchetti, A. *Polym. Rev.* **2008**, *48*, 423–431.

[5] Dennler, G.; Scharber, M. C.; Brabec, C. J. *Adv. Mater.* **2009**, *21*, 1323–1338.

[6] Thompson, B. C.; Frechet, J. M. J. *Angew. Chem. Int. Ed.* **2008**, *47*, 58–77.

[7] Brabec, C. J.; Durrant, J. R. *MRS Bull.* **2008**, *33*, 670–675.

[8] Riede, M.; Mueller, T.; Tress, W.; Schueppel, R.; Leo, K. *Nanotechn.* **2008**, *19*, 424001.

[9] Goncalves, L. M.; Bermudez, V. D.; Ribeiro, H. A.; Mendes, A. M. *Energy Environ. Sci.* **2008**, *1*, 655–667.

[10] Friend, R. H.; Gymer, R. W.; Holmes, A. B.; Burroughes, J. H.; Marks, R. N.; Taliani, C.; Bradley, D. D. C.; Dos Santos, D. A.; Bredas, J. L.; Logdlund, M.; Salaneck, W. R. *Nature* **1999**, *397*, 121–128.

[11] Kulkarni, A. P.; Tonzola, C. J.; Babel, A.; Jenekhe, S. A. *Chem. Mater.* **2004**, *16*, 4556–4573.

[12] Hung, L. S.; Chen, C. H. *Mat. Sci. Eng. R.* **2002**, *39*, 143–222.

[13] Veinot, J. G. C.; Marks, T. J. *Acc. Chem. Res.* **2005**, *38*, 632–643.

[14] Rahman, M. A.; Kumar, P.; Park, D. S.; Shim, Y. B. *Sensors* **2008**, *8*, 118–141.

[15] Thomas, S. W.; Joly, G. D.; Swager, T. M. *Chem. Rev.* **2007**, *107*, 1339–1386.

[16] Chen, Q.; Bai, H.; Shi, G. Q. *Chin. Sci. Bull.* **2007**, *52*, 2017–2023.

[17] Facchetti, A.; Yoon, M. H.; Marks, T. J. *Adv. Mater.* **2005**, *17*, 1705–1725.

[18] Cornil, J.; Bredas, J. L.; Zaumseil, J.; Sirringhaus, H. *Adv. Mater.* **2007**, *19*, 1791–1799.

[19] Rhee, S. W.; Yun, D. J. *J. Mater. Chem.* **2008**, *18*, 5437–5444.

[20] Anthony, J. E.; Heeney, M.; Ong, B. S. *MRS Bull.* **2008**, *33*, 698–705.

[21] Malliaras, G. G.; Scott, J. C. *J. Appl. Phys.* **1998**, *83*, 5399–5403.

[22] Anthony, J. E. *Chem. Rev.* **2006**, *106*, 5028–5048.

[23] Watson, M. D.; Fechtenkötter, A.; Müllen, K. *Chem. Rev.* **2001**, *101*, 1267–1300.

[24] Müllen, K.; Rabe, J. P. *Acc. Chem. Res.* **2008**, *41*, 511–520.

[25] Grimsdale, A. C.; Müllen, K. *Angew. Chem. Int. Ed.* **2005**, *44*, 5592–5629.

[26] Ruffieux, P.; Gröning, O.; Fasel, R.; Kastler, M.; Wasserfallen, D.; Müllen, K.; Gröning, P. *J. Phys. Chem. B* **2006**, *110*, 11253–11258.

[27] Walzer, K.; Maennig, B.; Pfeiffer, M.; Leo, K. *Chem. Rev.* **2007**, *107*, 1233–1271.

[28] Kumar, S. *Liq. Cryst.* **2005**, *32*, 1089–1113.

[29] Laschat, S.; Baro, A.; Steinke, N.; Giesselmann, F.; Hagele, C.; Scalia, G.; Judele, R.; Kapatsina, E.; Sauer, S.; Schreivogel, A.; Tosoni, M. *Angew. Chem. Int. Ed.* **2007**, *46*, 4832–4887.

[30] Adam, D.; Schuhmacher, P.; Simmerer, J.; Haussling, L.; Siemensmeyer, K.; Etzbach, K. H.; Ringsdorf, H.; Haarer, D. *Nature* **1994**, *371*, 141–143.

[31] Wu, J. S.; Pisula, W.; Müllen, K. *Chem. Rev.* **2007**, *107*, 718–747.

[32] Grimme, S. *J. Comput. Chem.* **2004**, *25*, 1463–1473.

[33] Langhoff, S. R. *J. Phys. Chem.* **1996**, *100*, 2819–2841.

[34] Jeloaica, L.; Sidis, V. *Chem. Phys. Lett.* **1999**, *300*, 157–162.

[35] Shen, H. C.; Tang, J. M.; Chang, H. K.; Yang, C. W.; Liu, R. S. *J. Org. Chem.* **2005**, *70*, 10113–10116.

[36] Alibert-Fouet, S.; Seguy, I.; Bobo, J. F.; Destruel, P.; Bock, H. *Chem. Eur. J.* **2007**, *13*, 1746–1753.

[37] Rohr, U.; Schlichting, P.; Bohm, A.; Gross, M.; Meerholz, K.; Bräuchle, C.; Müllen, K. *Angew. Chem. Int. Ed.* **1998**, *37*, 1434–1437.

[38] Clar, E. *The Aromatic Sextet*; Wiley: London, 1972.

[39] Maksic, Z. B.; Baric, D.; Müller, T. *J. Phys. Chem. A* **2006**, *110*, 10135–10147.

[40] Clar, E.; Zander, M. *Chem. Ber.* **1956**, *89*, 749–762.

[41] Goh, S. H.; Harvey, R. G. *J. Am. Chem. Soc.* **1973**, *95*, 242–243.

[42] Wendland, R.; Lalonde, J. *Org. Synth.* **1954**, *34*, 76–78.

[43] Hu, J.; Zhang, D.; Harris, F. W. *J. Org. Chem.* **2005**, *70*, 707–708.

[44] Zinke, A.; Ott, R.; Sobotka, M.; Kretz, R. *Monatsh. Chem.* **1952**, *83*, 546–548.

[45] Gao, B.; Wang, M.; Cheng, Y.; Wang, L.; Jing, X.; Wang, F. *J. Am. Chem. Soc* **2008**, *130*, 8297–8306.

[46] Steck, E. A.; Day, A. R. *J. Am. Chem. Soc.* **1946**, *68*, 771–772.

[47] Conte, G.; Bortoluzzi, A. J.; Gallardo, H. *Synthesis* **2006**, 3945–3947.

[48] Ruiz-Morales, Y. *J. Phys. Chem. A* **2002**, *106*, 11283–11308.

[49] Ashkenasy, G.; Cahen, D.; Cohen, R.; Shanzer, A.; Vilan, A. *Acc. Chem. Res.* **2002**, *35*, 121–128.

[50] Gamota, D. R.; P., B.; Kalyanasundaram, K.; Zhang, J. *Printed Organic and Molecular Electronics*; Kluwer Academic, 2004.

[51] Sirringhaus, H.; Ando, M. *MRS Bull.* **2008**, *33*, 676–682.

[52] Sirringhaus, H.; Brown, P. J.; Friend, R. H.; Nielsen, M. M.; Bechgaard, K.; Langeveld-Voss, B. M. W.; Spiering, A. J. H.; Janssen, R. A. J.; Meijer, E. W.; Herwig, P.; de Leeuw, D. M. *Nature* **1999**, *401*, 685–688.

[53] Kline, R. J.; McGehee, M. D.; Kadnikova, E. N.; Liu, J. S.; Frechet, J. M. J. *Adv. Mater.* **2003**, *15*, 1519–1522.

3 Coronene Chemistry

3.1 Introduction

Generations of chemists have been working on the synthesis of various polycyclic aromatic hydrocarbons.[1–3] Already in the 1950s Clar published routes to make PAHs, mostly by extending smaller ones by Diels-Alder reactions with maleic anhydride.[4–6] In 1912 Scholl reported the aromatic bond formation between non-activated arenes upon treatment with aluminum(III) chloride.[7] This discovery was later on used to convert oligophenylene molecules into PAHs, a method which remains to be very popular for the synthesis of PAHs. The reaction has been optimized in the Müllen group such that even huge PAHs are accessible.[8–10] The mechanism, however, is still subject to discussions.[11–13] The use of an oxidant and a strong acid restricts the synthesis to fully aromatic precursors forming exclusively all-benzoid PAHs. Triphenylene and hexa-*peri*-hexabenzocoronene are well accessible with this method.[14, 15]

Despite all the work that has been performed on the synthesis of PAHs, functionalized coronenes are almost unknown. Nevertheless, coronene possesses a special role among the PAHs: its high symmetry and low band gap for a PAH of this size make it a highly promising molecule for further investigations.[16–18] Most of the more extended PAHs which research has focused on so far are fully benzenoid. In contrast, coronene possesses a full zig-zag periphery with many important consequences for the reactivity, such as K-region oxidation to α-diketones without loss of

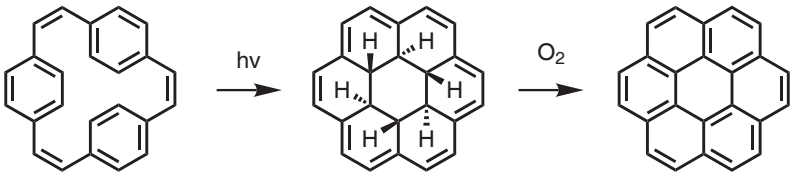

1 **2** **3**

Figure 3.1: Photochemical cyclization of [2.2.2]paracyclophane-triene (**1**) and accidental dehydrogenation to coronene.

aromaticity.[19, 20] The reason why there are so few functionalized coronenes is its difficult synthesis. Very few routes have been published, none of which are versatile enough to produce both electron rich and electron poor systems.[21–23] Also, there is no way of influencing the symmetry freely so far.

The strategy chosen to flexibly make substituted coronenes is derived from early work by the group of Boekelheide.[24] They irradiated [2.2.2]paracyclophane-triene (**1**) to obtain hexahydrocoronene (**2**). When oxygen was not excluded carefully enough, they obtained coronene as a side product. Substituted coronenes are thus accessible if the appropriate cyclophanes are irradiated in the presence of an oxidant.

If the functional groups are electron donating, extended donors are obtained. Electron withdrawing substituents render large acceptors. Ideally, the functionalities can be altered easily to tune the electronic level without starting the synthesis from the very beginning. Halogen atoms usually provide a versatile platform for modifications in late stages of the synthetic route, but halogenated PAHs are usually extremely insoluble hindering subsequent reactions substantially. Other strategies providing intermediates of better solubility appear more promising.

3.2 Cyclophane Synthesis

In the search for donor and acceptor substituted coronenes, methoxy substituents were chosen. They are electron donating and very tolerant to various reaction conditions.[25] Later on, the ether can be cleaved to form alcohols which undergo facile oxidation to ketones. In this way, a donor is switched to a strong acceptor in a single step.

3.2.1 Synthetic Procedures

The cyclophane is built up by a double Z-selective Wittig reaction of terephthalic dialdehyde (**9**) and *p*-xylene-bis(triphenylphosphonium) bromide (**12**) followed by a McMurry ring closure (compare Figure 3.2), a procedure which is derived from the literature.[26] The Z-selectivity of the Wittig reaction is crucial for the ring closure. Molecules containing E double bonds cannot be closed as the formed ring would be too strained.

The synthesis of methoxy substituted cyclophanes requires 2,3-dimethoxyterephthalic dialdehyde (**5**) (compare Figure 3.2). According to the literature, it is made by double lithiation of veratrol and subsequent treatment with DMF.[27] However, vanishingly small amounts are obtained using this method; mostly the single aldehyde is formed. Satisfying yields can be obtained when changing the reaction conditions as follows. Veratrol is singly lithiated first, then DMF is added. The lithium aminolate is formed which is stable as long as acidic protons are absent. The negative charge in this species is moved away from the aromatic center. Subsequent treatment with butyl lithium efficiently abstracts another proton due to decreased Coulomb repulsion. When again treated with DMF and worked up in acidic conditions, the dialdehyde **5** is formed.

This aldehyde is converted into the Wittig reagent **8** in three steps. Firstly, it is reduced to the dibenzylalcohol (**6**) with sodium borohydride in isopropanol. Hy-

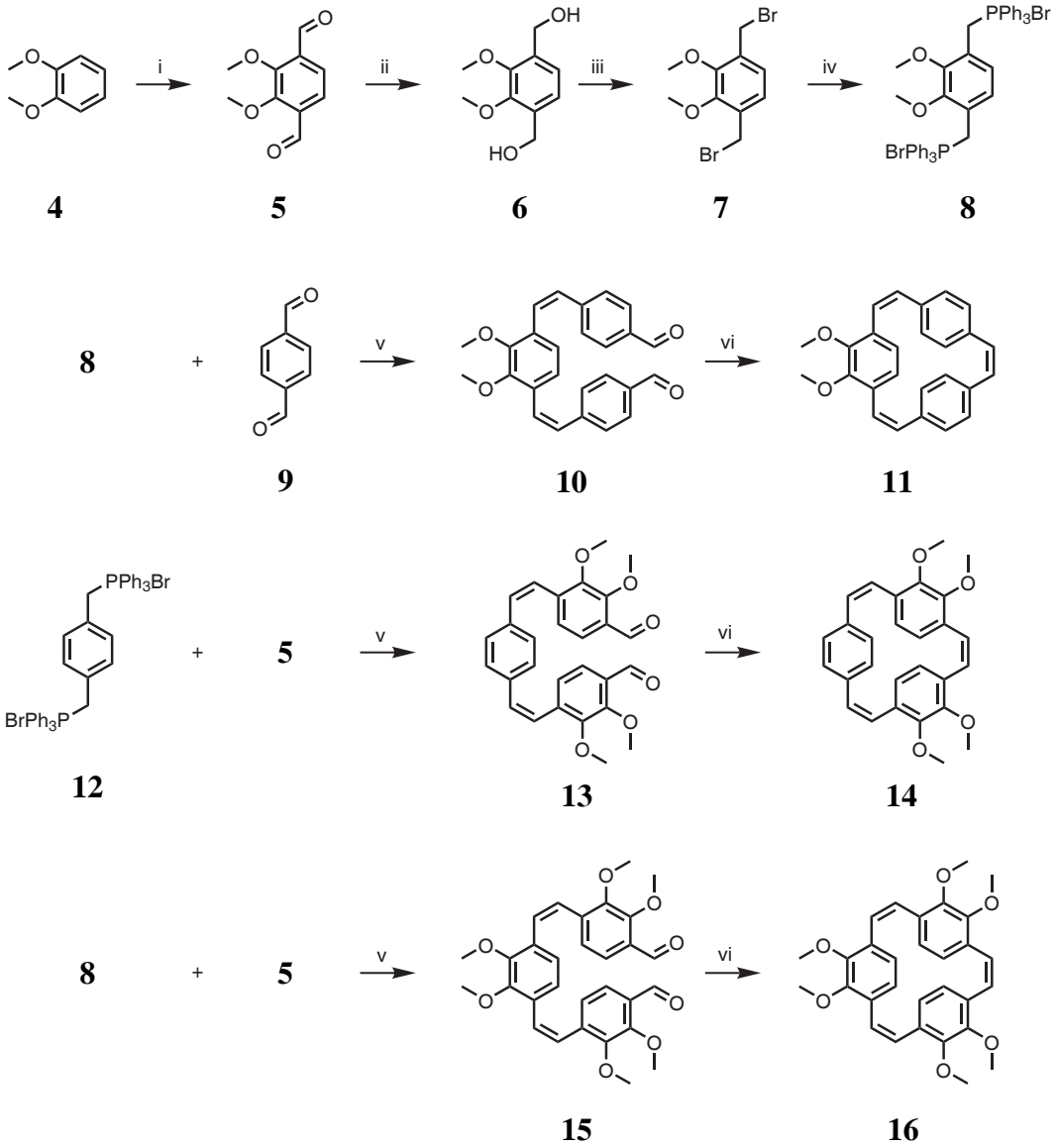

Figure 3.2: Synthesis of the cyclophanes. Conditions: *i* 1. n-BuLi, TMEDA, diethylether, RT 2. DMF, 3. n-BuLi, 4. DMF, 35 %; *ii* $NaBH_4$, isopropanol, RT, quantitative; *iii* HBr, dichloromethane, RT, quantitative; *iv* PPh_3, dichloromethane, RT, quantitative; *v* LiOEt, dichloromethane, ethanol, -40 °C, 21-46 %; *vi* $TiCl_4$, Zn, THF, reflux, 27-48 %.

drobromic acid converts the alcohol to the dibenzylbromide (**7**) in an S_N1 reaction. Finally, triphenylphosphine nucleophilically replaces the bromides to form the Wittig reagent **8**. All reaction conversions are quantitative as confirmed by NMR spectroscopy.

In the following Wittig reaction, it is possible to choose the number of methoxy

groups in the final cyclophane. Reacting the dimethoxy Wittig reagent (**8**) with terephthalic dialdehyde gives a cyclophane bearing two methoxy groups (**11**). Four methoxy groups are attached by reacting *p*-xylene-bis(triphenylphosphonium bromide) (**12**) with dimethoxy terephthalic dialdehyde (**5**). The combination of compounds **8** and **5**, finally, allow the introduction of six methoxy groups.

In order to obtain the highest possible Z-selectivity in the Wittig reaction, the reaction conditions needed to be optimized carefully. The temperature should be as low as possible to favor Z-olefin formation.[28–30] A temperature of -40 °C was found to be the lowest possible as the reaction does not take place any more at even lower temperatures. In addition, the solvent choice is crucial for the reaction to succeed. A mixture of dichloromethane and ethanol works best in this case. The former guarantees solubility, the latter stabilizes the transition state. Freshly prepared lithium ethanolate, made by butyl lithium and ethanol, was used as base to initiate the reaction.

The aldehyde function of the products (**10**, **13**, **15**) can react further with remaining phosphonium reagent in the reaction mixture. In fact, higher oligomers can be detected. A large excess of dialdehyde, however, does not reduce the formation of oligomers, but hinders the purification. Therefore, only small excesses are used. Yields of 40 % to 50 % are obtained which is a good value considering the difficulties of these reactions.

The rings are closed in a McMurry reaction.[31–33] Titanium(IV) chloride is reduced by zinc dust. The reduction time has a strong effect on the yield of the ring formation. One hour is ideal, longer reaction times lead to aggregation of the titanium particles and shorter reaction times yield more aldehyde reduction, probably due to residual zinc metal. A dilute solution of the dialdehyde (**10**, **13**, or **15**) is slowly added to the low-valent titanium suspension. This shall favor intramolecular reaction and thus suppress oligomerization. The molecules are expected to react more quickly than new molecules are added, a so-called pseudo dilution reaction.

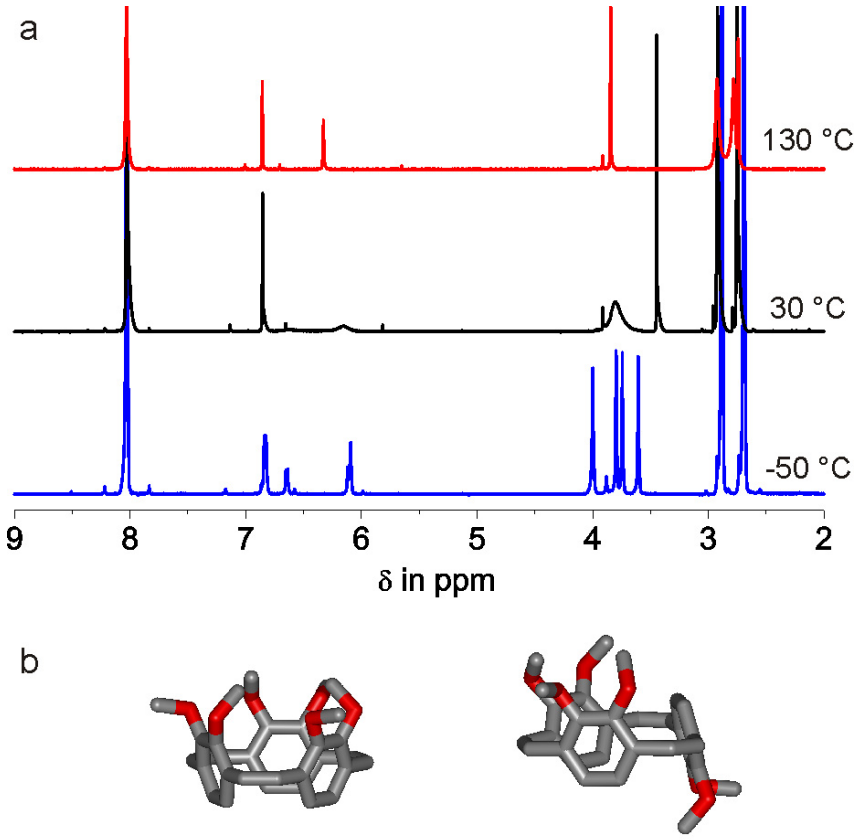

Figure 3.3: Coalescence of ^{1}H-NMR peaks of cyclophane **16**. **a.** ^{1}H-spectra in DMF$-d_7$ at various temperatures **b.** force-field optimized rotamers.

Yields of close to 50 % are obtained, a relatively good value for rings of intermediate size.[34] Despite the high dilution, the success of the ring closure reaction critically depends on the purity of the dialdehydes. If the product of the Wittig reaction is only roughly purified leaving residual E-isomers which is formed as side product, the McMurry ring closure does not afford satisfying product quantities.

3.2.2 NMR Analysis

The proton signals in the NMR spectrum of the cyclophane rings show expressed coalescence (see Figure 3.3a). The benzene units are twisted out of the cyclophane ring plane, their rotation is hindered by steric repulsion among each other. Two rotamers can be formed with different chemical environments giving rise to NMR signal groups for the methoxy protons, the olefinic protons, and the aromatic protons

respectively as depicted in Figure 3.3b. Depending on the relative position of the methoxy groups, their NMR signals are different. At room temperature, the interconversion of these two rotamers takes place within the NMR timescale (a few seconds), the peaks are broadened.

When cooling the solution to -50 °C, thermal energy does not suffice any more for a quick enough interconversion, the thermodynamically more stable rotamer is fixed with regard to the NMR timescale. The methyl protons give rise to three distinct peaks between 3.5 and 4 ppm. They arise from the trans rotamer (the lower one in Figure 3.3b) which is energetically favored. The fourth peak at about 4 ppm is caused by the water protons. It strongly shifts upfield on heating, *i.e.* from 4 ppm at -50 °C to 2.6 ppm at 130 °C.

At 130 °C, the interconversion of the two rotamers is so fast, that the NMR spectrum only shows one peak at the average chemical shift of the methoxy protons. The signals have merged to three singlets, one for the aromatic, one for the olefinic and one for the methoxy protons.

The wide temperature range from -50 °C to +130 °C limits the solvent choice. DMF was selected as it is liquid in the whole range. At higher temperatures, its methyl proton signals start to coalesce as well, but there are no other solvents available to meet the requirements.

A quantitative analysis of the ring interconversion was performed by peak line fitting.[35] For this purpose, the DNMR module of the Topspin© software package by Bruker® was used. The line width parameter of the peaks at the lowest temperature (-50 °C) was assumed to be unchanged, so the line broadening was solely attributed to the exchange reaction. An Arrhenius plot is made using the thus obtained exchange reactions constants (k) (Figure 3.4). According to the Arrhenius

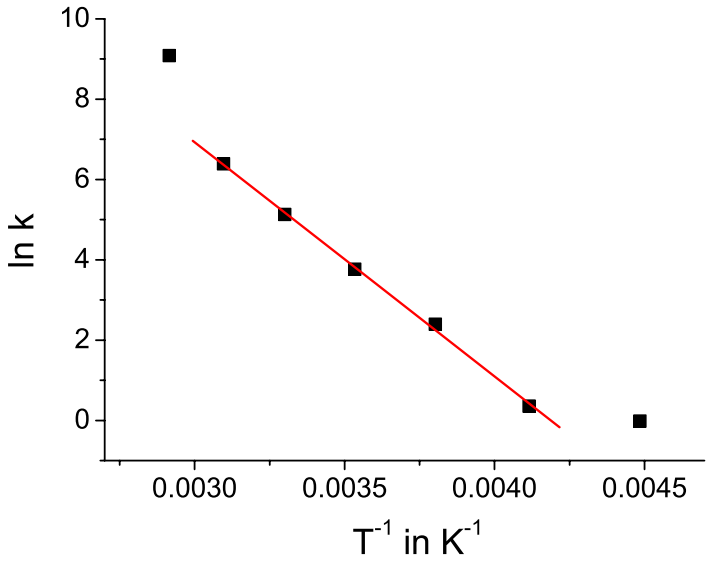

Figure 3.4: Arrhenius plot of the exchange rates (k) of the ring inversion in cyclophane **16** between -50 °C and 70 °C.

theory, the reaction rates are related to the activation energy (E_A) by the following equation.[36]

$$\ln(k) = -\frac{E_A}{RT} + \ln(A)$$

where R is the universal gas constant and A the frequency factor of the reaction. The activation energy can then be obtained according to

$$E_A = -R\left(\frac{\partial \ln(k)}{\partial\left(\frac{1}{T}\right)}\right)_P$$

i.e. the negative slope of the plot times the universal gas constant. The linear fit has only been performed for the values between -30 °C and 50 °C. At higher and lower temperatures, the peaks are about as narrow as the solvent peaks, thus no useful rate constant can be extracted.

The activation energy (E_A) is related to the enthalpy of activation by

$$\Delta H^{\neq} = E_A - RT$$

The entropy can be obtained by the relation

$$\Delta S^{\neq} = R\left[\ln\left(\frac{hA}{\kappa k_B T}\right) - 1\right]$$

where k_B is the Boltzmann constant, h the Planck constant, and κ the so-called transmission coefficient, which is usually set equal to 1. Finally, the free enthalpy of activation is given by

$$\Delta G^{\neq} = \Delta H^{\neq} - T\Delta S^{\neq}$$

The values obtained by this analysis are $\Delta H^{\neq}$ = 46 kJ mol^{-1}, $\Delta S^{\neq}$ = 5.6 J K^{-1}mol^{-1}, and $\Delta G^{\neq}$ = 44 kJ mol^{-1}, which indicate a relatively high rotational barrier.[37] Very similar values are measured in [6]paracyclophanes.[38] The structurally related calixarenes, on the contrary, exhibit much lower interconversion barriers in the order of 10 kJ mol^{-1}, which is a consequence of the bigger ring diameter.[39]

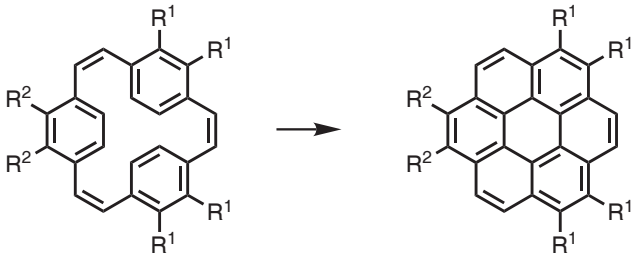

R^1 = H, R^2 = OMe: **11** R^1 = H, R^2 = OMe: **17**

R^1 = OMe, R^2 = H: **14** R^1 = OMe, R^2 = H: **18**

R^1 = OMe, R^2 = OMe: **16** R^1 = OMe, R^2 = OMe: **19**

Figure 3.5: Photochemical cyclodehydrogenation of methoxy substituted cyclophanes, conditions: 300 nm (40 W), cyclohexane, I_2, 70-85 %.

3.3 Photochemical Cyclodehydrogenation

In order to obtain the desired coronene derivatives, the cyclophanes described in the previous section need to be cyclodehydrogenated. Classical methods, such as treatment with iron(III) chloride, are excluded as the olefinic double bonds are oxidized before cyclodehydrogenation occurs. A much better method is a photochemically induced cyclodehydrogenation in the presence of a mild oxidant.[40]

Cyclophanes **11**, **14**, and **16** are respectively dissolved in cyclohexane at a low concentration, *i.e.* 1 mg/ml, to avoid intermolecular [2+2]cycloaddition.[41] Iodine is added to this solution as an oxidant and propylene oxide is included to scavenge the developing hydroiodic acid. In this way, ether cleavage by hydroiodic acid is suppressed. The solution is irradiated with UV light of 300 nm wavelength and a power of 40 W overnight. The wavelength is chosen such that the reagent absorbs the UV light in order to induce a reaction. Too short wavelengths, on the other hand, can lead to undesireable side reactions.[42, 43] A wavelength of 300 nm is just long enough that only the π system absorb the irradiation, the σ system is unaffected.

Cyclohexane was expected to be a non-solvent for the product, which should precipitate as it is formed and thus be hindered to undergo further photoreactions. It turns out that the methoxy groups increase the solubility so strongly, that no

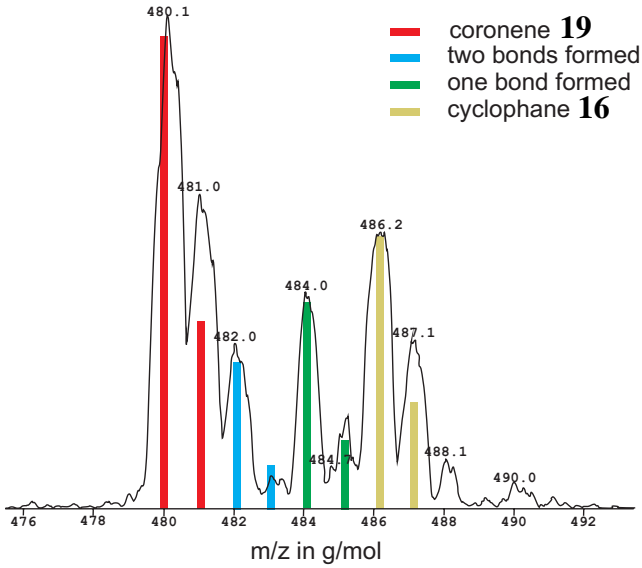

Figure 3.6: Field-desorption mass spectrum of cyclodehydrogenation reaction in progress with bars indicating the masses of calculated intermediates.

precipitation is observed. Nevertheless, the products are sufficiently stable, they can be obtained in good yields (75-80 %). In comparable stilbene systems, the loss of methoxy groups has been reported.[44] In the present case, only little amounts (< 5 %) are lost due to this elimination. The formed side products can be removed by preparative chromatography.

To get a better insight into this spectacular reaction, hexamethoxycyclophane (**16**) is irradiated for only two hours. In the mass spectrum (Figure 3.6), peaks can be found which correspond to intermediates with one and two bonds closed, respectively. On the TLC, one can see two additional spots with R_f values between those of the reagent and the product. The spot closer to the reagent can be isolated and subjected to NMR analysis. It clearly turns out that it is an intermediate with one bond formed, *i.e.* a phenanthrene cyclophane. The second intermediate is so unstable that it cannot be clearly identified. When it is separated by chromatography and analyzed, only hexamethoxycoronene (**19**) is found. It appears that this intermediate can thermally dehydrogenate to form the final product and thus escaping from structural analysis.

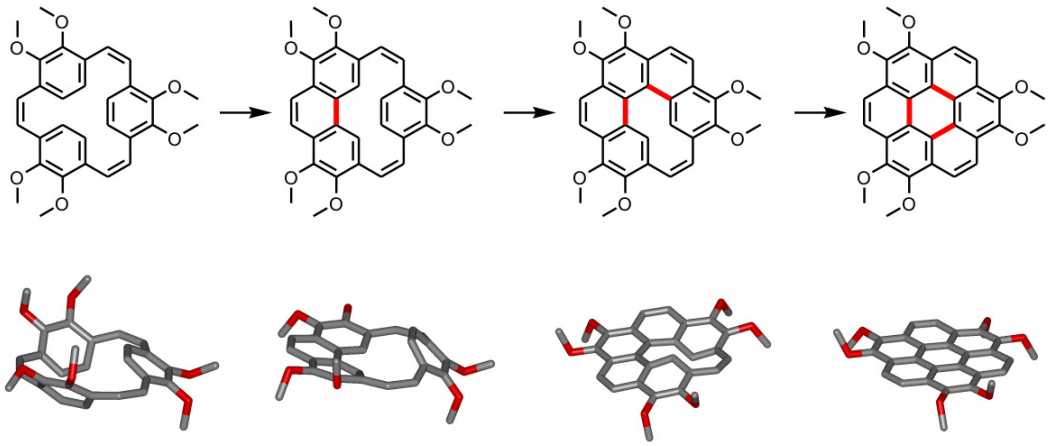

Figure 3.7: Step-wise cyclodehydrogenation of cyclophane **16** to coronene **19**, on the bottom force-field optimized structures are shown.

It can be concluded that the cyclodehydrogenation proceeds stepwise as depicted in Figure 3.7. When the first bond is formed, no strain is built up yet, the phenanthrene finds enough space in the cyclophane plane and the benzene ring can rotate out of this plane. After formation of the second bond, however, considerable strain is accrued and the aromatic system is distorted by the remaining hydrogen atoms strongly interfering with each other. The strain is released upon oxidation of the last bond facilitating product formation. The instability of this intermediate may even enable a thermally induced dehydrogenation reaction, so it cannot be isolated. Instead, only hexamethoxycoronene (**19**) is found when analyzed.

3.3.1 Surface Assisted Cyclodehydrogenation Process

In collaboration with Prof. R. Fasel at EMPA in Zürich, Switzerland, the cyclodehydrogenation process was investigated on the surface by scanning tunneling microscopy (STM). This method is very powerful to visualize chemical structures up to atomic resolution and follow chemical reactions.[45–47] A cyclodehydrogenation process has previously been observed for a hexa-*peri*-hexabenzocoronene derivative on a copper surface.[48]

As the instrumental setup does not allow UV irradiation, thermal treatment was

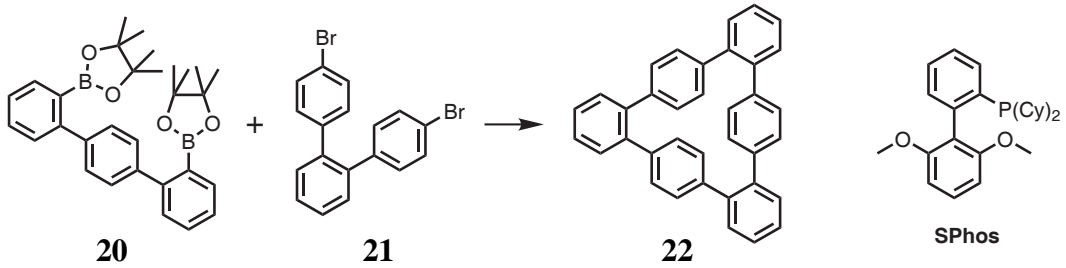

20 **21** **22**

Figure 3.8: Synthesis of *o*-*p*-*o*-*p*-*o*-*p*-cyclohexaphenylene (**22**), conditions: $Pd(OAc)_2$, **SPhos**, K_3PO_4, toluene, 100 °C, 32 %.

applied to supply the activation energy for the process. The molecules are sublimed on a surface, heated for a certain time, and visualized by scanning tunneling microscopy. The whole process is run in ultra-high vacuum.

For the sake of better visualization, higher thermal stability, and lower desorption probability, the tribenzo derivative of cyclophane **1**, *i.e.* *o*-*p*-*o*-*p*-*o*-*p*-cyclohexaphenylene (**22**), is synthesized. Two terphenyls are merged in a Suzuki coupling reaction utilizing the SPhos ligand developed by the Buchwald group.[49, 50] The dipinacolboronate functionalized *p*-terphenyl (**20**) is reacted with dibromo-*o*-terphenyl **21** in the presence of SPhos and $Pd(OAc)_2$ as a palladium source with potassium phosphate as base. Cyclohexaphenylene **22** is obtained in moderate yield (32 %).

It has been shown in the literature that this molecule undergoes cyclodehydrogenation under UV irradiation to form [a,g,m]-tribenzocoronene.[51, 52] The reaction mechanism is expected to proceed in a similar way to [2.2.2]paracyclophane-triene (paracyclophantriene), *i.e.* electrocyclic addition followed by oxidative hydrogen extrusion. The hydrogen is most likely dissolved in the underlying metal, a process known for many metals.[53]

Molecule **22** is sublimed in ultra-high vacuum onto a copper (111) surface where it forms a densely packed monolayer. The surface is heated in vacuum, cooled down again and visualized by STM. The result is depicted in Figure 3.9.

The triangular shape of the molecule is apparent, the size of the objects is consis-

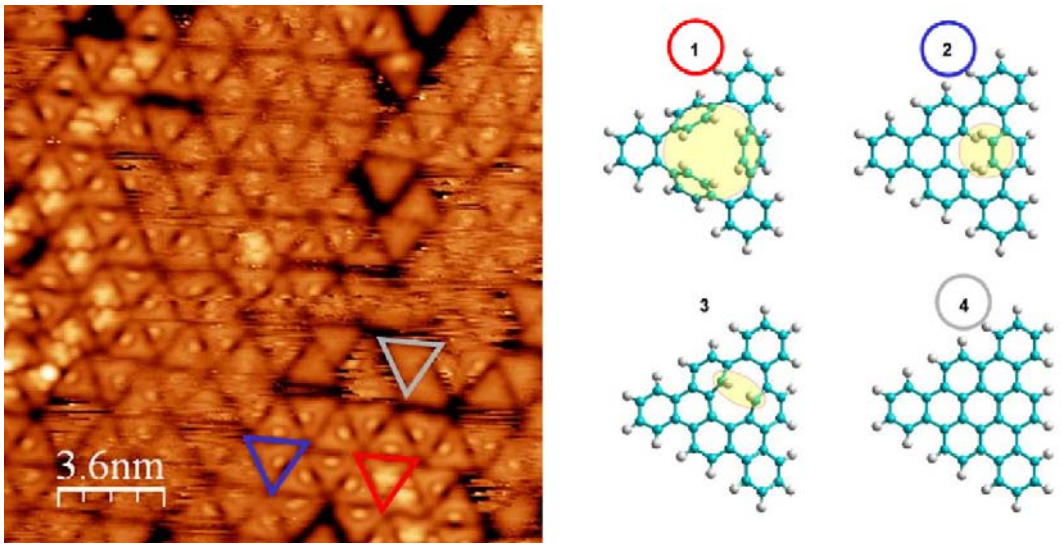

Figure 3.9: Scanning tunneling image of cyclohexaphenylene on a Cu(111) surface after heating.

tent with calculated models (about 1 nm). The dense packing is slightly disturbed, probably due to the heating process. The interesting feature revealed by the image is the presence of three different triangular molecules. Some molecules like the one marked in red are unchanged in comparison to the molecules before heating, their non-planarity gives rise to the bright spots. On the other hand, some molecules are fully planarized to tribenzocoronene like the one marked in gray.

Most of the molecules, however, are only partially planarized, they show one bright spot on the side of the triangle as the one marked in blue. A comparison to theoretical calculations reveals that one bond is closed in these molecules but the remaining two are still open. The benzene ring can rotate out of the molecular plane giving rise to the increased tunneling current.

Consistent with the solution based process, no structure is found in which only one bond remains open while two are closed. This highly strained molecule is too reactive, so it further planarizes and cannot be observed. Quantum mechanical calculations modelling this dehydrogenation process corrobrate the relative stability of the first intermediate, having one bond closed and the high unstability of the second intermediate having two bonds closed.

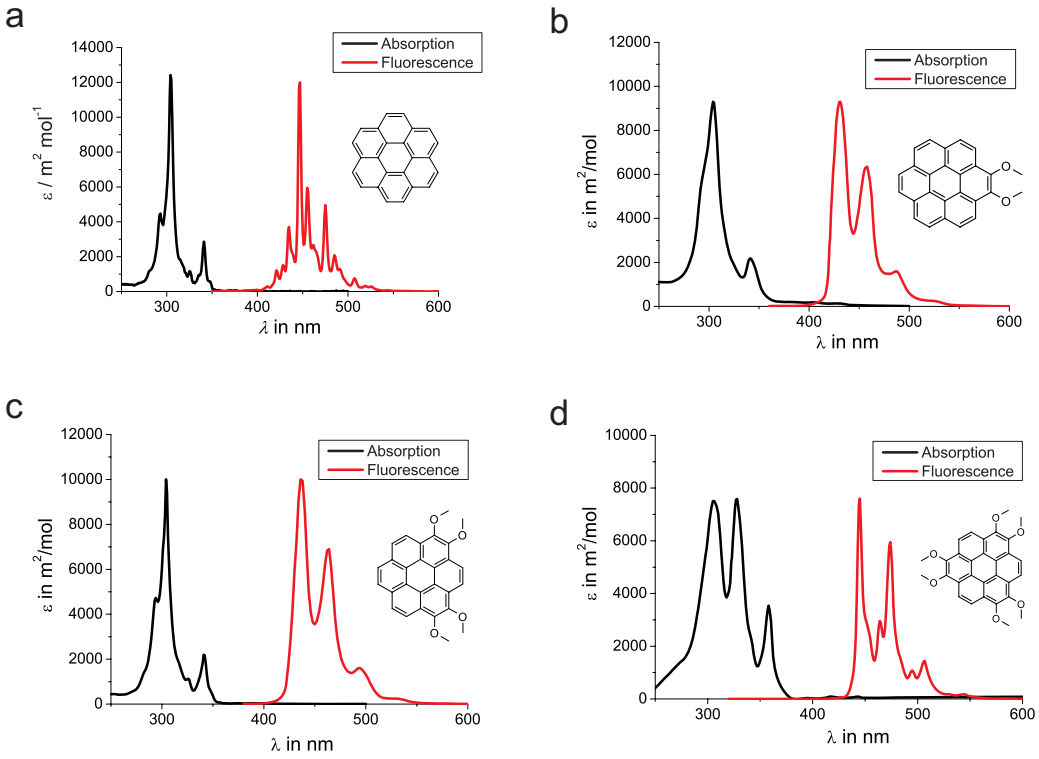

Figure 3.10: Absorption and photoluminescence spectra of the methoxy substituted coronenes and unsubstituted coronene for comparison, all compounds are measured in cyclohexane at a concentration of 10^5 M.

3.4 Optical Spectroscopy

To study the effect of the methoxy substitution on the electronic properties of coronene, UV-vis absorption and photoluminescence spectra are recorded for **17**, **18**, and **19** (see Figure 3.10). The substances are dissolved in cyclohexane at a concentration of 10^{-5} mol/l.

The position of both absorption and photoluminescence peaks are practically unchanged. All compounds absorb strongly around 300 nm which accounts for the fact that all compounds have a light yellow appearance. Photoluminescence is strongest at 450 nm, so all molecules are blue emitters. This means that the electronic structure is not significantly influenced by the presence of methoxy groups. The conjugation of the free electron pairs of the oxygen atoms is weak. This could be attributed to the motion of the methyl groups. However, triphenylene is signifi-

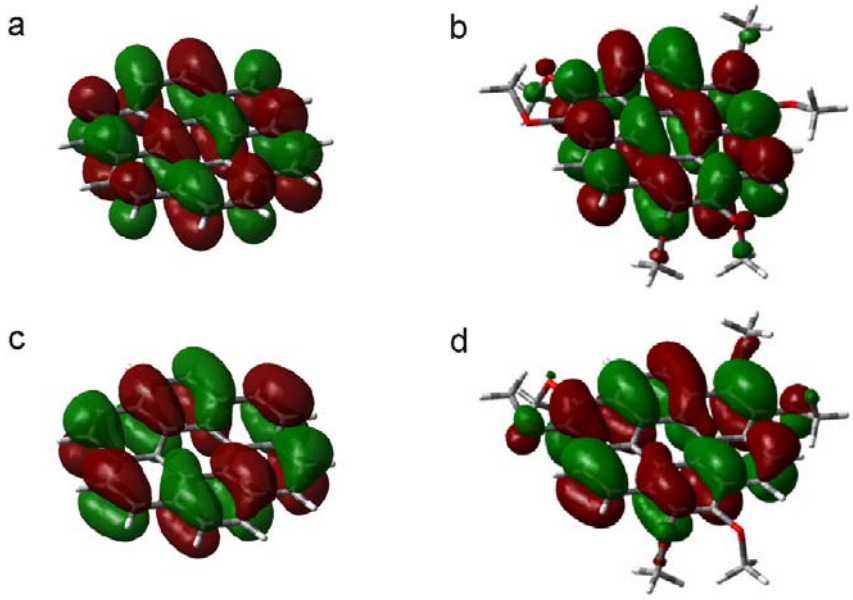

Figure 3.11: Orbital surfaces of coronene (left) and hexamethoxycoronene (right), **a** and **b** show LUMOs, **c** and **d** the HOMOs as calculated by density functional theory (B3LYP method, 6-31G basis).

cantly influenced by methoxy substitution shifting the absorption bathochromically by 50 nm.[54] The weak effect on coronene is more likely due to low orbital coefficients at the substitution position of the coronene. A similar effect has been observed for amino substituted HBC.[55]

Density functional theory calculations have been run to resolve the question why the UV-vis spectra are almost unchanged. Figure 3.11 shows the orbital surfaces for coronene and hexamethoxycoronene (**19**). It is obvious that these frontier orbitals are not perturbed by the presence of methoxy groups. The conjugation of the free electron pairs to the aromatic core is poor, they hardly contribute to the frontier orbitals. As a consequence, the optical absorption spectra do not change upon substitution.

The relative intensity of the absorption peaks of hexamethoxycoronene **19** is, nevertheless, significantly changed. The extinction coefficient of the two peaks at 300 nm and 350 nm, respectively, has increased by about a factor of two, while the peak at 320 nm is basically unchanged.

When looking at the fine structure of the absorption and in particular the photoluminescence bands pronounced differences are visible. Unsubstituted coronene shows many resolved peaks. Its high symmetry (D_{6h}) gives rise to many quantum mechanically not-allowed transitions, leaving only a few sharp peaks.[56] Lowering the symmetry makes more transitions allowed, less fine structure is the consequence.

Hexamethoxycoronene (**19**) being of D_{3h} symmetry, shows less fine structure in comparison to coronene. Even less fine structure is observed in the case of dimethoxycoronene (**17**) and tetramethoxycoronene (**18**) as they are of C_{2v} symmetry. A very similar trend has been observed in a series of bay functionalized HBC derivatives.[57] In addition to the symmetry, the rotation of the methoxy groups should contribute to line broadening as well. The vibronic and rotatoric states of these couple with the energy levels of the core in broad peaks in the spectrum.

On the first glance on the absorption-emission spectra of Figure 3.10 one might suggest large Stokes shifts of the molecules.[58, 59] Upon closer inspection, there are absorption peaks present at the position of the emission cut-off (0-0 transitions). For coronene, they are hardly visible, but for the methoxy substituted derivatives, low intensity peaks arise around 400 nm. These are quantum mechanically not allowed, the disturbance of the methoxy groups makes the transition slightly more allowed.

The fluorescence quantum yield (ϕ_T) of coronene is low (2.8 %).[60] Hexamethoxycoronene (**19**) possesses a value of 10 % as determined by a comparing the emission to diphenylanthracene.[61] This higher value in comparison to coronene can be attributed to the more allowed transition, favoring fluorescence over non-radiative decay processes.

3.5 Crystal Structure Analysis

Materials properties crucially depend on the intermolecular arrangement of the molecules in the solid state. Particularly when studying charge transport phenomena, the knowledge of intermolecular distances and orientation is of fundamental interest.[62, 63] Most of this information is gained when the crystal structure is known. Single crystals of sufficient quality and size need to be grown. The X-ray diffraction pattern finally enables one to solve the crystal structure.

In the present case, it was possible to grow single crystals for all methoxy substituted coronene derivatives. Hexamethoxycoronene (**19**) possesses the highest crystallization propensity due to the high symmetry and the good solubility. Large crystals of good quality can be easily grown by slow evaporation of the solvent. Tetramethoxycoronene (**18**) and in particular dimethoxycoronene (**17**) are much more difficult to crystallize. The latter forms thin needles which tend to break along their needle axis.

Figure 3.12 shows the unit cells of the three methoxy substituted coronene derivatives as well as that of unsubstituted coronene. The latter structure is shown for the sake of comparison, it has already been known for a long time.[64] All molecules form sandwich herringbone structures, a typical motif for polycyclic aromatic hydrocarbons.[65] Two discs are aligned parallel to each other, the next disc is turned such that its edge points towards the surface of the next disc. This behavior can be attributed to quadrupolar interactions of the negatively charged π electron cloud and the positively charged σ-system.[66, 67]

The methoxy groups have a significant influence on the interplanar distances. While unsubstituted coronene has a $\pi - \pi$ distance of 3.3 Å, it increases in the case of dimethoxycoronene (**17**) and tetramethoxycoronene (**18**) to 3.4 Å. In hexamethoxycoronene (**19**) it has widened to even 3.6 Å. The increased solubility of the compounds with increased number of methoxy groups is a consequence. More than

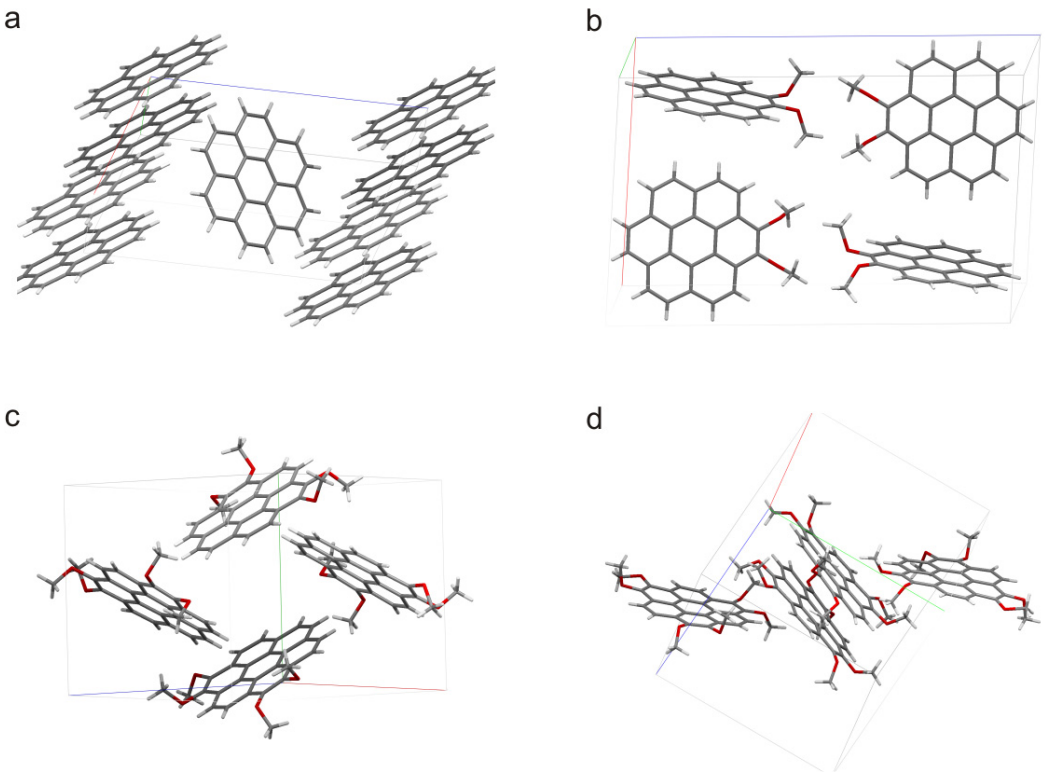

Figure 3.12: Crystal structures of the coronene derivatives. **a.** unsubstituted coronene for comparison; **b.** dimethoxycoronene (**17**); **c.** tetramethoxycoronene (**18**); **d.** hexamethoxycoronene (**19**).

50 mg of hexamethoxycoronene (**19**) dissolve in one milliliter of dichloromethane. Lower intermolecular interactions due to larger distances decrease the lattice energy which needs to be overcome upon dissolving.[68]

Furthermore, the methoxy groups reduce the intermolecular Coulomb interactions. The partial negative charge of the oxygen atoms reduces the attractive forces between the positive backbone and the negative π electron cloud of the aromatic disc. It is obvious that the molecules tend to avoid these contacts. In all cases, the unsubstituted part of the molecule edge is close to the face of the next molecule. The more methoxy groups are present in the molecule, the less Coulomb stabilization is gained. This contributes to the solubility trend as well.

The methoxy groups of adjacent molecules stand in close contact to each other. This is likely to be a consequence of microphase separation, *i.e.* the alkyl part of

the molecule avoids contact to the aromatic part. In the case of dimethoxycoronene (**17**), the methoxy groups line up in a plane. Low attraction forces within this plane explains the high tendency of the crystals to break apart.

Interestingly, the density of the crystal is almost unaffected by the different lattice energies. The values vary between 1.42 and 1.44 g/cm^3. When methoxy groups are attached to HBC, the density drops from 1.544 g/cm^3 for the unsubstituted molecule to 1.505 g/cm^3.[69, 70]

Much more drastic changes in the series are observed when comparing the angles of adjacent molecules to each other. Dimethoxycoronene (**17**) arranges almost perpendicularly (85°), just as unsubstituted coronene does. The value goes down to 68° for tetramethoxycoronene (**18**) and to even 38° for hexamethoxycoronene (**19**). Weakened quadrupolar Coulomb interactions due to the presence of methoxy groups are likely to cause this change. The free electron pairs of the methoxy groups shield the positive charge of the aromatic backbone reducing Coulombic attraction of adjacent molecules. This effect contributes to the solubility trend in addition to the increase of intermolecular distances.

3.6 Coroneneketones

The synthesized methoxy substituted coronene derivatives are reasonably strong donor molecules. Corresponding acceptors are also desirable for the study of charge-transfer complexes, interfacial behavior, or redox phenomena. One may start over from the very beginning by synthesizing acceptor substituted terephthalic dialdehydes and go through all the steps (see Figure 3.2 and Figure 3.5). A much more effective way to obtain acceptors is the conversion of the donors to acceptors. In the present case, the methyl groups need to be cleaved leaving hydroxy groups which undergo oxidation to α-diketons, a very strong electron acceptor functionality.[71]

3.6.1 Synthesis

The critical issue about these reactions, especially in the case of hexamethoxycoronene (**19**), is network formation of the intermediates while cleaving the ether and obtaining the hydroxy groups. Hydroxy groups form hydrogen bonds with the developing ketones as it is well known from quinhydrone.[72–74] These interactions are accompanied by a complex redox behavior.[75–77]

In order to cleave the ether, boron tribromide is used. When added to a solution of the methoxycoronenes, immediate precipitation occurs, no product can later be obtained. Alternatively, a solution of the methoxycoronenes is added to a ten-fold excess of boron tribromide solution in dichloromethane. Precipitation of the adduct sets in a few seconds after addition. It turns out that this time is sufficient for complete conversion. The low solubility of the boron tribromide adduct may be explained by intermolecular crosslinking by the boronbromide, since this molecule can react three times with ethers. In Figure 3.14 a possible intermediate of the boron tribromide addition to hexamethoxycoronene (**19**) is shown (**26**). Cyclic adducts of the catechol (marked in red on **26**) is likely to occur due to the spatial proximity of the two methoxy groups. Bridging to neighboring molecules can happen when the

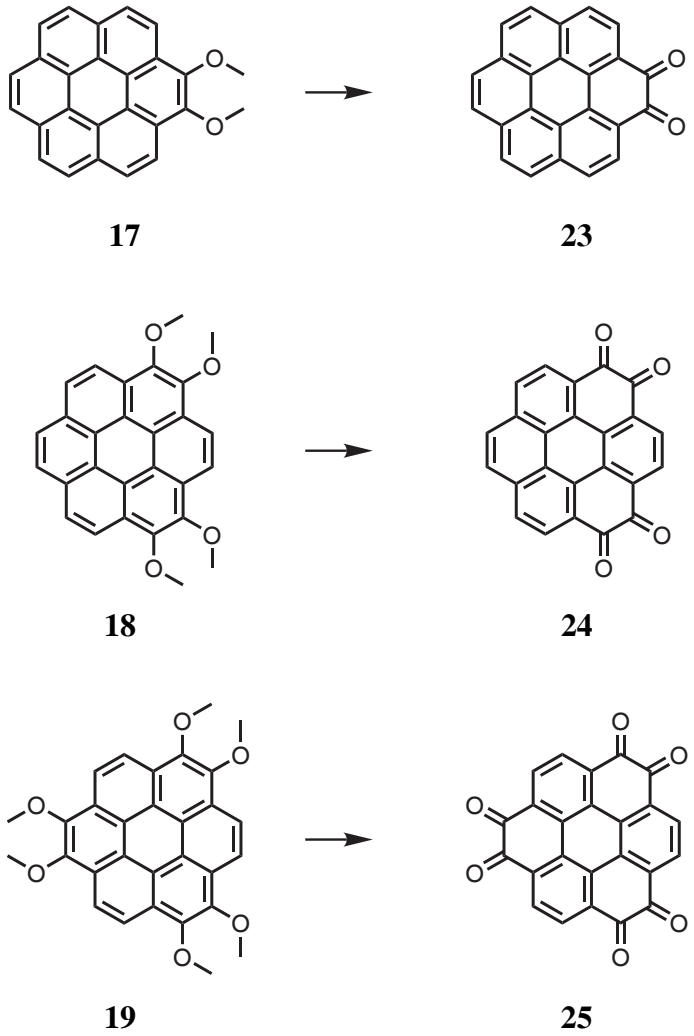

Figure 3.13: Ether cleavage and oxidation to form coroneneketones, conditions: 1. BBr_3, dichloromethane, RT, 2. HNO_3, RT, 65-85 %.

BBr_2 fragments react further with ethers (highlighted in yellow). Larger excesses of boron tribromide, however, does not render a soluble intermediate. Coronene bearing six $OBBr_2$ groups may possess very low solubility. More likely is the formation of exclusively cyclic BBr_3 adducts leading to completely planar discs of very poor solubility. A similar, but much weaker solubility trend was observed in the case of 4,5,9,10-tetramethoxypyrene which is converted to 4,5,9,10-pyrene-tetraone.[78]

A mild acidic hydrolysis of the boron tribromide adduct such as treatement with dilute hydrochloric acid like most examples reported in the literature only yields a

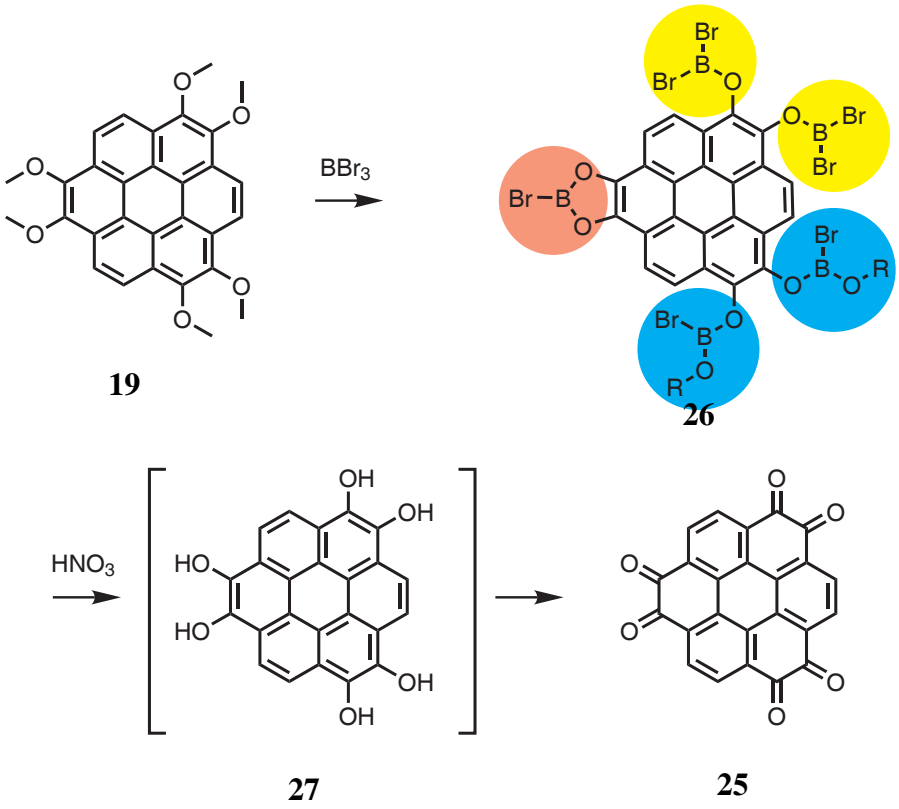

Figure 3.14: Reaction intermediates of the ether cleavage of hexamethoxycoronene (**19**).

tar-like black product of intractable substances. Instead, excess boron tribromide is removed in high vacuum leaving a yellow solid which is treated with concentrated nitric acid. Following this procedure, the hydrolyzed hydroxy intermediate (such as **27**) is oxidized in situ to the product. The reaction proceeds heterogeneously, both reagent and product do not dissolve in nitric acid. After diluting with water the product can be conveniently isolated by filtration.

All three methoxy substituted coronenes can be converted into their corresponding α-diketones (Figure 3.13). In this way, it is possible to switch electron donor molecules to strong acceptors in one single step. Particularly in the case of hexamethoxycoronene (**19**) this is a remarkable shift in orbital energies.

The solubility of all coroneneketones is rather low. Coronene-dione, which has been made by direct oxidation of coronene before, only dissolves in hot nitrobenzene.[79] The more ketone groups that are present, the lower the solubility in

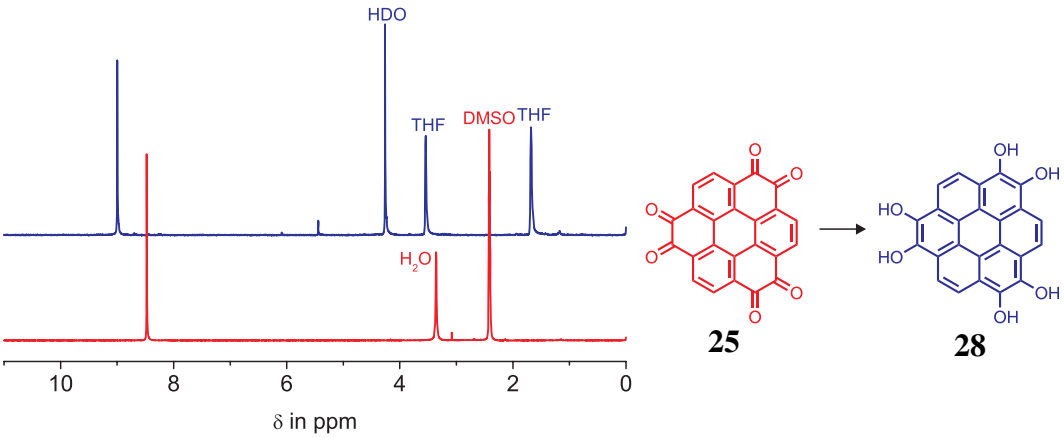

Figure 3.15: ^{1}H-NMR spectrum (250 MHz, RT) of coronene-hexaone (**25**) in DMSO—d_6 and the reduced hexahydroxycoronene (**28**) in a mixture of THF—d_8 and D_2O with $Na_2S_2O_4$.

solvents of low polarity. On the other hand, highly polar solvents such as dimethylsulfoxide (DMSO) dissolve coronene-hexaone (**25**) to a reasonable extent, *i.e.* about 1 mg/ml. Coronene-tetraone (**24**) dissolves to a slightly less amount in DMSO. The highly polar ketones favor contact to DMSO, whereas the aromatic core does not, less polar aromatic or chlorinated solvents are favorable. As coronene-diketone (**23**) possesses the strong dipole inducing diketone group on the one side and an unsubstituted coronene disc on the other side, its low solubility in almost all solvents is not surprising.

Coronene-hexaone (**25**) can be sufficiently dissolved in deuterated DMSO to record a proton NMR. Figure 3.15 shows the corresponding spectrum (red line). One peak in the aromatic region is observed at 8.5 ppm. Hexamethoxycoronene (**19**) exhibits its aromatic proton at a chemical shift of 9.1 ppm. This is a consequence of the reduced ring current of the aromatic system magnetically deshilding the protons. The coronene core is effectively reduced to a triphenylene system in coronene-hexaone (**25**). In fact, triphenylene shows a peak in the ^{1}H-NMR spectrum at 8.5 ppm.[80]

α-Diketones can be reductively alkylated to aromatic 1,2-dialkoxy compounds.[81, 82] This reactions is effectively the reversal of the oxidative ether

cleavage towards coronene-hexaone (**25**). According to the published procedures, sodium dithionate in water is added to a solution of the diketone in THF to form the catechol. After a while, the alkylating reagent and a base are added.

When coronene-hexaone (**25**) is exposed to these conditions, a black tar of intractable products is formed. In order to investigate if the reduction or the alkylation fails, an NMR tube is charged with coronene-hexaone (**25**) suspended in deuterated THF and sodium dithionate in D_2O. The solution is shaken until the organic phase is bright yellow and homogeneous. The proton NMR spectrum of this mixture is depicted in Figure 3.15 (blue curve). One singlet at 9.0 ppm is observed which is in good agreement with the structure of hexahydroxycoronene (**28**). This compound has regained the full ring current of coronene, thus exhibits a similar shift as hexamethoxycoronene (**19**). The hydroxy protons are visible at 5.4 ppm. As these protons exchange with deuterons of D_2O, the integral is much smaller than that of the aromatic region.

It can be concluded that the reduction of the diketones works very well. According to the NMR spectrum, no side products are formed. This means that the alkylation process does not work properly. Upon addition of a base, the hydroxy protons are abstracted leaving an anion which may be extremely susceptible to oxidation. Careful exclusion of oxygen does not improve the reaction, so maybe even the alkylation reagent acts as an oxidant.

Nevertheless, hexahydroxycoronene (**28**) can be reoxidized to coronene-hexaone (**25**). If only exposed to air in the absence of a reducing agent, a black tar-like substance is formed, very similar to the first attempts of the oxidative cleavage of the methoxy groups in hexamethoxycoronene (**19**) described above. It can be derived that this substance consists of partially oxidized hexahydroxycoronene (**28**) possessing both ketones and hydroxy groups which interact to form a network via hydrogen bonding. This interaction has been shown in the literature with phenanthrenequinone and dihydroxyphenanthrene which does not form a network, so a

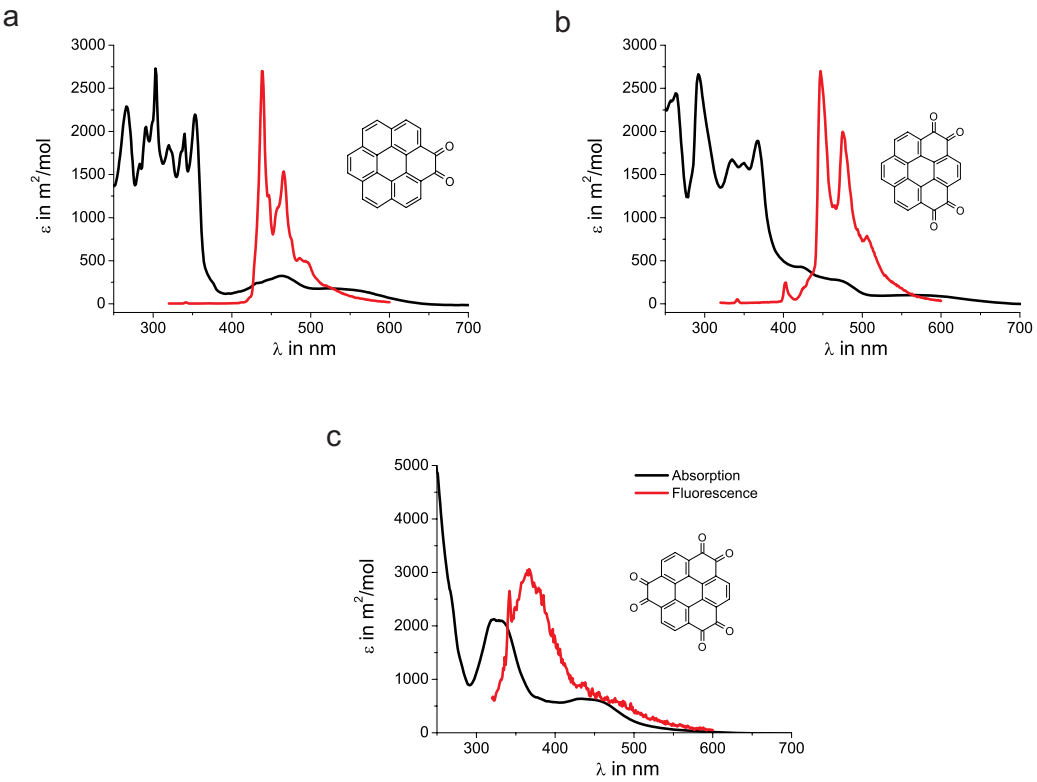

Figure 3.16: UV-vis absorption and photoemission spectra of the coroneneketones: **a.** coronene-dione (**23**); **b.** coronene-tetraone (**24**); **c.** coronene-hexaone (**25**).

crystal structure could be obtained.[83] Concentrated nitric acid is capable of cleaving this network and oxidizing the substance back to coronene-hexaone (**25**).

3.6.2 Electronic Structure

The electronic structure of the synthesized strong acceptors is of special importance. Energy levels need to be known when bringing in contact with other materials, such as electron rich organic molecules in charge-transfer complexes or metals in an organic-metal interface.

UV-vis absorption and photoluminescence spectra of coroneneketones **23**, **24**, and **25** are measured. Due to the low solubility of the compounds, only THF could be used as solvent. Its affinity to polar groups may induce a solvochromic effect, hindering comparisons to quantum mechanical calculations which are normally

only possible for molecules in the gas phase.[84] The results of the measurement are depicted in Figure 3.16.

The extinction coefficients are significantly lower than for the methoxy substituted coronenes. The presence of the ketones obviously leads to significantly different orbital shapes of the HOMO in contrast to the LUMO resulting low Frank-Condon factors.[85, 86] The effect is even more obvious in the fluorescence spectra. The intensities are very low, particularly in the case of coronene-hexaone (**25**) for which the fluorescence intensity is hardly detectable.

Additionally, the ketone groups broaden the absorption peaks. Coronene-dione (**23**) shows a spectrum with a high degree of fine structure. The peaks become broader as more ketones are present. For coronene-hexaone (**25**), basically one broad band can be observed around 300 nm. As mentioned above, the strong solvation of the ketone units by the highly polar solvent THF may account for this trend.

At shorter wavelengths, less fine structure is measured as more ketones are attached to the molecule. In the case of coronene-tetraone (**24**), absorption up to 700 nm is observed. n-π^*-transitions cause these bands as was intensively studied for phenanthrenequinone.[87] Coronene-hexaone (**25**) does not absorb light of as long wave length as the other coroneneketones. Most likely, the higher symmetry makes the transitions at long wave length symmetry forbidden.

Density functional theory calculations have been performed for hexamethoxycoronene (**19**) and coronene-hexaone (**25**) as the interconversion of these two molecules induces the strongest shift of the energy levels. Figure 3.17 shows the outcome of this calculation. The LUMO energy is dramatically lowered by almost 3 eV, an extremely high value for a single synthetic step. Also, the HOMO energy is decreased by more than 2 eV, but less than the LUMO. Consequently, the HOMO-LUMO gap goes down from 3.85 eV in hexamethoxycoronene (**19**) to 3.10 eV in coronene-hexaone (**25**). These values are in good agreement to UV-vis absorption,

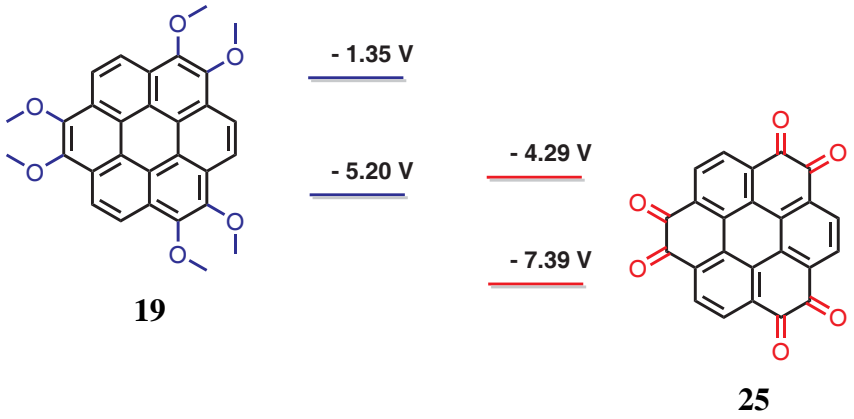

Figure 3.17: Orbital energies before and after ether cleavage as calculated by DFT (B3LYP method, 6-31G* basis set).

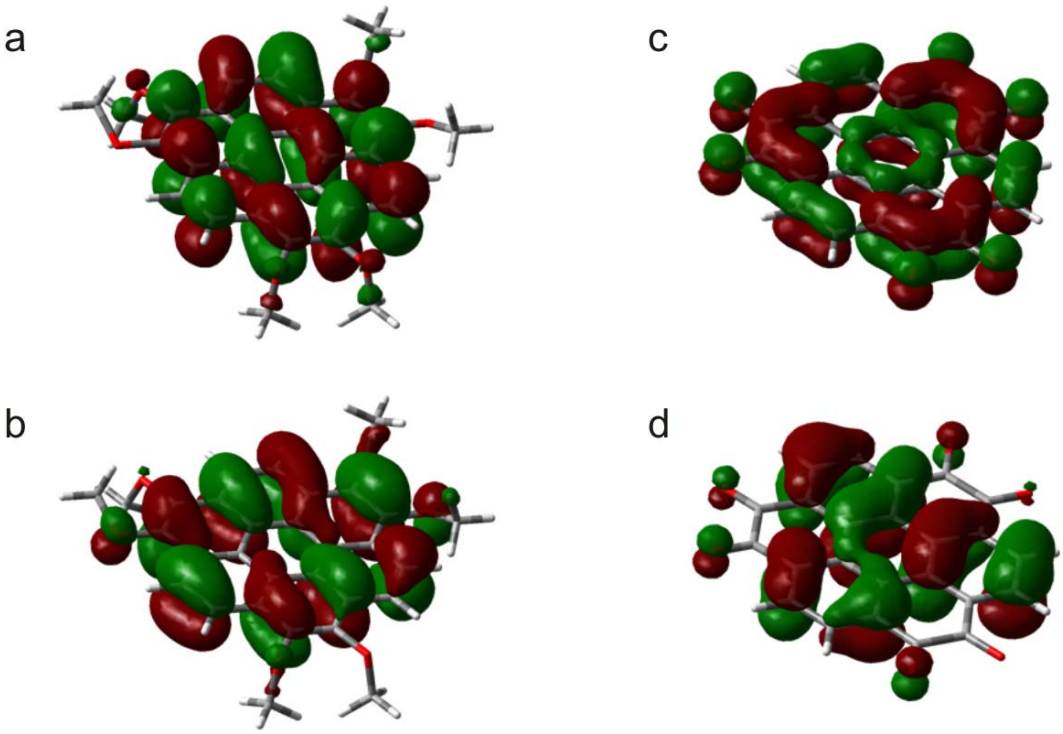

Figure 3.18: Orbital surfaces as obtained by DFT calculations. **a.** LUMO and **b.** HOMO of hexamethoxycoronene (**19**); **c.** LUMO and **d.** HOMO of coronene-hexaone (**25**).

n-π^* transitions as discussed above can be made responsible for the lower HOMO-LUMO gap.

The orbital surfaces (90 % of the electron spatial probability density) obtained by the calculations are depicted in Figure 3.18. The dramatic change from the donor hexamethoxycoronene (**19**) to the strong acceptor coronene-hexaone (**25**) is

obvious. While the former roughly resembles unsubstitued coronene, in line with the absorption spectra (Figure 3.10 on page 55), the latter is dominated by the ketone function. The carbonyl carbon atoms represent orbital nodes in the HOMO. In the LUMO, they are the place of high orbital coefficients.

The differences between the HOMO and the LUMO of hexamethoxycoronene (**19**) are very low, whereas the differences in the case of coronene-hexaone (**25**) are quite expressed. The low extinction coefficients of the UV-vis absorption are a consequence of the mismatch of electron distribution upon excitation of the molecule.

3.6.3 Cyclic Voltammetry

In order to further investigate the electronic levels, especially the reduction potential, cyclic voltammetry is employed.[88] The analyte is dissolved in anhydrous DMF at a 1 mM concentration. A solution of 0.1 M tetrabutylammonium perchlorate serves as electrolyte, and ferrocene is added as a reference compound due to its outstanding electrochemical properties.[89] The solution is degassed before a platinum working and counter electrode as well as a silver quasi reference electrode are immersed. A voltage is ramped at 50 mV/s while the current flow is measured.

The result is shown in Figure 3.19. The big peak arises from the ferrocene. Due to the low solubility of coronene-hexaone (**25**), the peaks of the material are relatively weak. Nevertheless, the reduction properties can be elucidated. The first reduction occurs at -0.47 V against ferrocene, which corresponds to 0.16 V against the normal hydrogen electrode. The LUMO energy level is determined to -4.3 eV, which is a low level, thus coronene-hexaone (**25**) is a very strong acceptor, only about 0.3 eV above 7,7,8,8-tetracyanoquinodimethane (TCNQ), one of the strongest organic acceptors known.[90] Considering the size of coronene-hexaone (**25**), this a notable result.

One can further see that three distinct reduction steps exist. The second is only

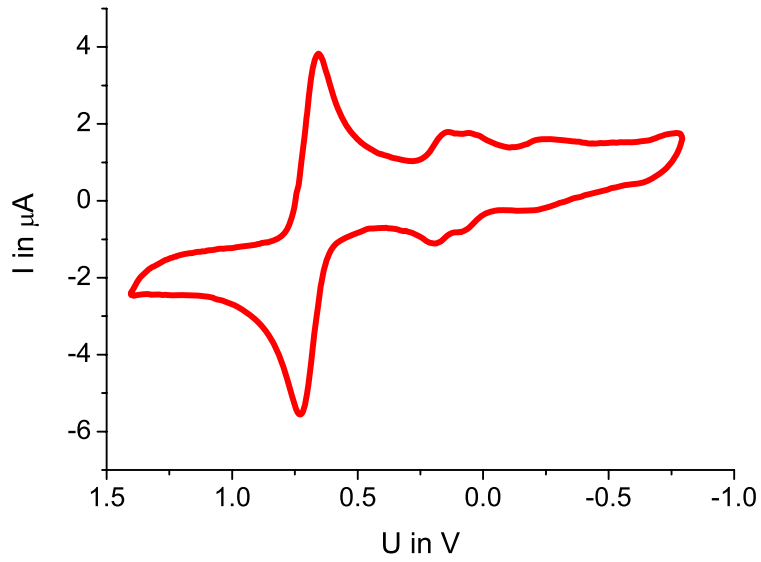

Figure 3.19: Cyclovoltagram of coronene-hexaone (**25**) with ferrocene as reference, the voltage is set against the normal hydrogen electrode (NHE).

at 0.1 V more negative voltages, the third about 0.5 V. A peak fit can give the information if the peak corresponds to a one or a two electron transfer process.[91] The low intensity and the peak overlap, however, make the shape analysis very difficult and unreliable. Due to this reason, it has not been performed.

In order to put the results into perspective, a comparative cyclic voltammetry study has been performed using quinoid structures. The results are summarized in Figure 3.20. All measurements were performed under indentical conditions for maximum comparability, *i.e.* DMF as solvent, Bu_4NClO_4 as electrolyte, and ferrocene as internal reference.

The highest structural similarity to coronen-hexaone (**25**) can be found in pyrene-tetraone (**32**) and phenanthrenequinone (**37**) which both are accessible by direct oxidation of pyrene and phenanthrene, respectively.[19, 92]

It is not surprising that the molecules become more electron deficient as the number of carbonyl groups increases. Nevertheless, the differences of the LUMO energy levels of the molecules in this series are not intuitive. The LUMO level

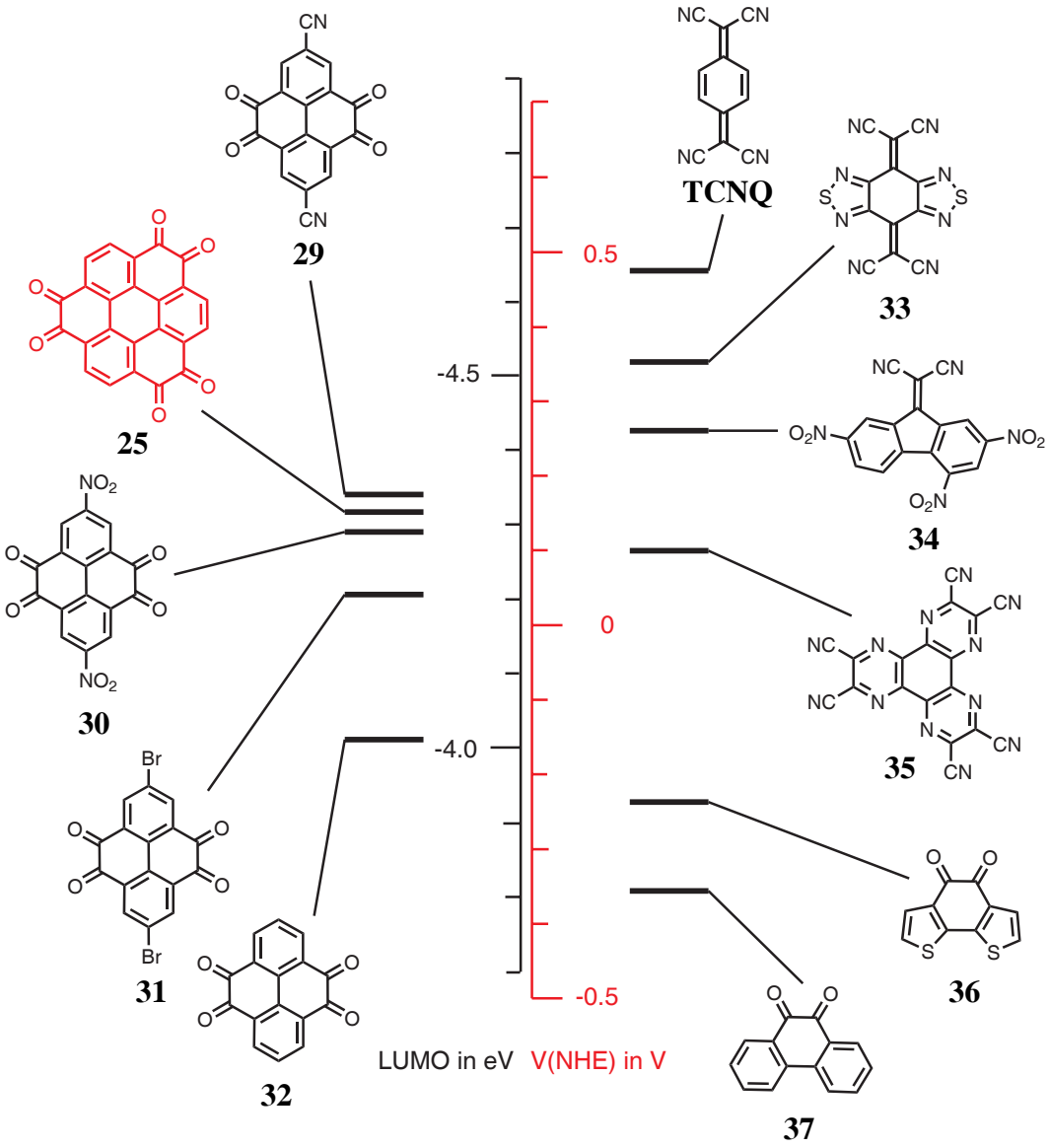

Figure 3.20: Reduction potentials of quinoid molecules as determined by cyclic voltammetry under identical conditions.

of pyrene-tetraone (**32**) is 0.19 eV lower than that of phenanthrenequinone (**37**), but 0.33 eV higher than the one of coronene-hexaone (**25**). This gap is even more surprising when considering the fact that the ratio of carbon atoms per carbonyl group is the same for pyrene-tetraone (**32**) and coronene-hexaone (**25**). In the latter case, the electron withdrawing effect of the carbonyl oxygen seems to be particularly effective.

Pyrene-tetraone (**32**) has been substituted with various electron withdrawing

functional groups in collaboration with Shinishiro Kawano who synthesized bromo and cyano functionalized pyrene-tetraones (**31** and **30**). Two bromine atoms lower the LUMO energy by 0.2 eV, two nitro groups by 0.3 eV. Still, the acceptor character of coronene-hexaone (**25**) is not reached. Only two highly electron withdrawing cyano groups make pyrene-tetraone (**32**) a stronger acceptor than coronene-hexaone (**25**).

In addition to these α-diketone functionalized polycyclic aromatic compounds, some well-known strong acceptors have been measured. Tetracyanoquinodimethane (TCNQ) is on the top of the present list being an extremely strong acceptor. Its four cyano groups in combination with a quinodized structure lower the LUMO energy to an extreme level. Benzothiadiazole is a typical acceptor which finds widespread use in materials for organic electronics.[93, 94] It was expected that the annellation of thiadiazole to TCNQ could even lower its LUMO. The corresponding molecule (**33**) was synthesized in a four-step procedure starting from chloranil according to the literature.[95] It turns out that the LUMO level of **33** is not lower but even 0.15 eV higher than that of TCNQ. The thiadiazole units, therefore, serve as donors in this particular case.

9-Dicyanomethylene-2,4,7-trinitrofluorene (**34**) combines the dicyanoquinoid structure found in TCNQ with the strongly electron accepting nitro groups. Its high tendency to form charge-transfer complexes with donors and to yield crystals suitable for crystal structure analysis make it a popular molecule.[96, 97] It is not as strong an acceptor as TCNQ, but its LUMO level is energetically lower than that of coronene-hexaone (**25**).

Hexaazatriphenylene-hexacarbonitrile (HATCN, **35**) is an easily accessible strong acceptor which has been used in various charge-transfer crystals and has further been derivatized to form discotics.[98, 99] Its six cyano groups in combination with the electron poor aza functions reduce its LUMO energy level significantly. It is, however, not as strong an acceptor as coronene-hexaone (**25**).

This result is surprising as cyano groups are typically stronger acceptor functions than ketone groups. As both molecules possess the same symmetry (D_{3h}) they are ideal for comparison. Later on, this symmetry match has been exploited by making charge-transfer salts.

An interesting feature in donor-acceptor chemistry is revealed by benzodithiophene-dione (**36**):[100] thiophene usually operates as a donor due to the high electron density at the sulfur atom.[101] When comparing the reduction potential of benzodithiophene-dione (**36**) with phenanthrenequinone (**37**), one can clearly see that the thiophene units lower the LUMO energy level by about 0.1 eV. This makes benzodithiophene-dione (**36**) an interesting molecular building block for organic electronics as it combines high electron affinity with the intermolecular interaction induced by sulfur atoms. This finding shall be used in the next chapter.

3.6.4 Surface Interactions

Strong acceptor molecules can interact with metal surfaces such that they extract electrons out of it. The thus formed surface dipole increases the work function of the metal.[102] Charge injection barriers in organic devices can be reduced by adjusting the metal's work function with an interlayer of a strong acceptor.[103] In this way, the efficiency of devices can be optimized without changing the metal which is often difficult in the fabrication process.

Coronene-hexaone (**25**) is particularly interesting in this sense as it is a strong acceptor bearing ketone groups which are expected to strongly interact with the metal surface. Furthermore, its size is a good compromise: it is large enough to decrease diffusion into other layers, but not too large to sublime the molecule.

In the context of the project ICONTROL, which is funded by the European Commission (NMP-3-CT-2006-033197), measurements are performed in collaboration with Norbert Koch and Benjamin Bröker at the Humboldt University Berlin.

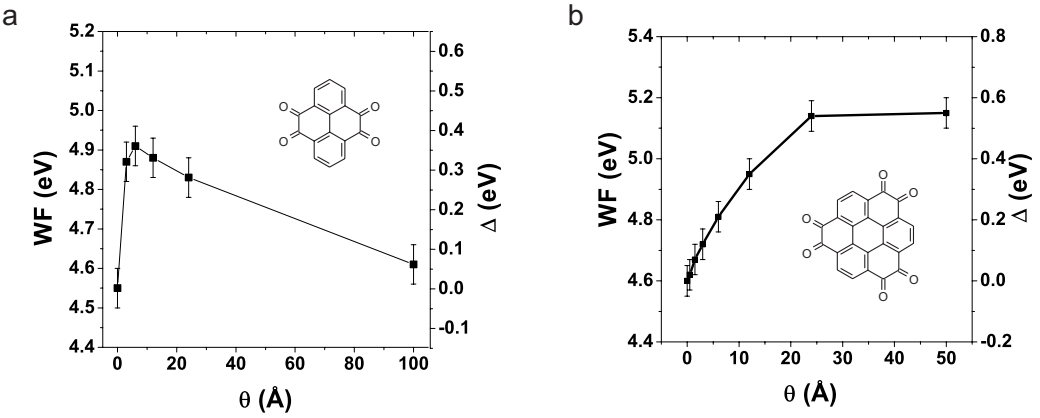

Figure 3.21: Workfunction manipulation of a Ag(111) surface. **a.** Pyrene-tetraon (**32**) **b.** Coronene-hexaone (**25**), θ: layer thickness.

Coronene-hexaone (**25**) was sublimed in ultra high vacuum onto different metal surfaces. Ultraviolet photoelectron spectroscopy (UPS) was measured at a synchrotron to follow the work function while subliming the molecule.

Figure 3.21 shows the changes of the work function of a Ag(111) surface when subliming pyrene-tetraone (**32**) as reference and coronene-hexaone (**25**). The layer thickness is calculated from the mass increase as determined by a quartz micro balance.[104] In both cases the work function is increased immediately upon deposition. This is remarkable as organic molecules tend to decrease the work function of a metal due to the push-back effect.[105]

Pyrene-tetraone (**32**) increases the work function up to a layer thickness of about 10 Å with a maximum change of 0.35 eV. With thicker layers the work function decreases again, most likely due to electronic relaxation of the molecules in bulk.[106] Coronene-hexaone, in contrast, increases the work function by 0.55 eV with no decrease when going to thicker layers. The highest change measured so far in the literature is 1.2 eV with the extremely strong tetrafluoro-TCNQ.[107] Considering the push-back effect, which is always present and accounts for 0.4 eV, the present result is quite remarkable. Also, the density of acceptor molecules in a monolayer is higher for the smaller tetrafluoro-TCNQ. On a unit area, there are fewer coronene-

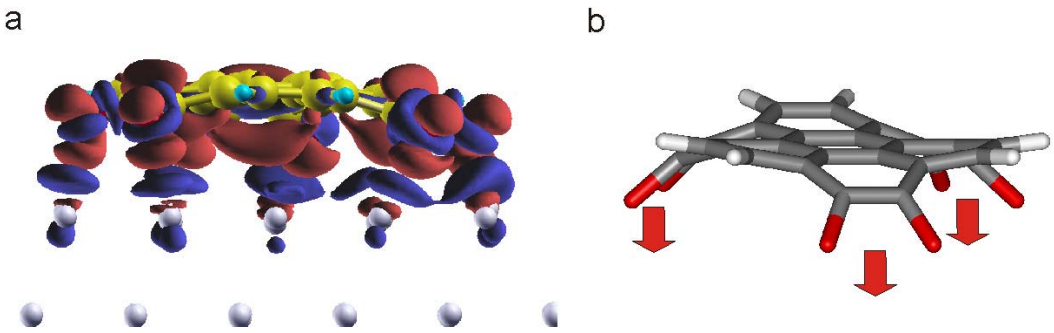

Figure 3.22: a. Semi-empirical calculation of the charge redistribution of coronen-hexaone (**25**) on a Ag(111) surface, blue stands for decreased, red for increased charge density; **b.** model of the contorted molecule.

hexaone molecules present causing the work function shift which means that the effect per molecule is roughly the same as for tetrafluoro-TCNQ.

To get a better understanding of the metal molecule interaction, semi-empirical calculations have been performed in collaboration with Prof. Egbert Zojer and Oliver Hofmann at the Technical University Graz, Austria. The coronene-hexaone molecule (**25**) has been modeled on a silver lattice, the geometry of the molecule is relaxed to find the structure and the orientation with regard to the metal surface which has an important influence on the organic-metal interface.[108] Figure 3.22 shows the charge redistribution in the system. The blue zones indicate decreased charge density. They are predominantly located in the first metal layer leading to an electron deficiency and consequently to a higher work function. The charge has moved onto the molecule as indicated by the red regions.

The molecule on the surface is clearly bent out of planarity. The carbonyl oxygen atoms are closer to the surface than the rest of the molecule. This creates a dipole perpendicular to the surface enhancing the charge extraction out of the metal. Also, the π^* orbital of the carbonyl bond can better interact with the metal leading to a charge decrease on the metal atom. In the literature it is reported that standing wave X-ray measurements evidence the bending of carbonyl groups in perylene-tetracarboxylic-dianhydride (PTCDA).[109]

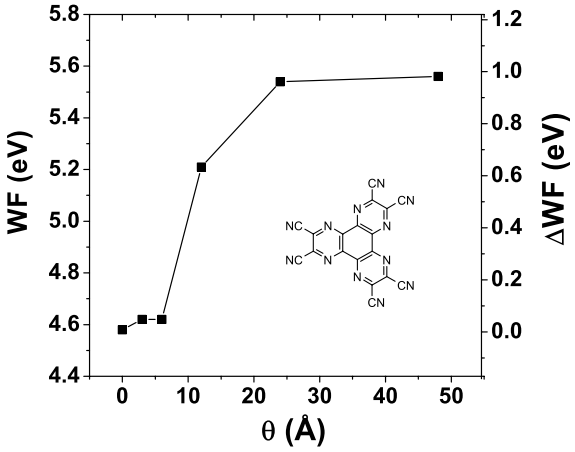

Figure 3.23: Change of the workfunction of a silver (111) surface upon covering with HATCN (**35**) as determined by UPS, θ: layer thickness.

Due to the structural similarity, hexaaza-triphenylene-hexacarbonitrils (HATCN, **35**) have been included into the measurements. It has been sublimed on various coinage metals while its workfunction is measured by UPS. For a silver (111) surface, the work function and its change is plotted against the thickness of the organic layer in Figure 3.23. At the very beginning of the sublimation process, the work function is almost unchanged. The push-back effect obviously compensates the electron extraction by the acceptor. Beginning from a layer thickness of about 6 Å, the work function increases very strongly up to 1 eV. A plateau is reached at a thickness of 25 Å, diminishment with a thicker layer is not observed in contrast to pyrene-tetraone (**32**).

Quantum mechanical calculations show that HATCN (**35**) is non-planar on the surface similar to coronene-hexaone (**25**): the cyano groups are bent towards the metal surface, the rest of the molecule is slightly bent away from it. A strong interaction of the π^* orbitals of the cyano group is revealed. It extracts electrons out of the metal even more effectively than coronene-hexaone (**25**), thus the stronger increase in the work function of the silver, although the electron affinities are about the same (compare cyclic voltammetry in the previous section).

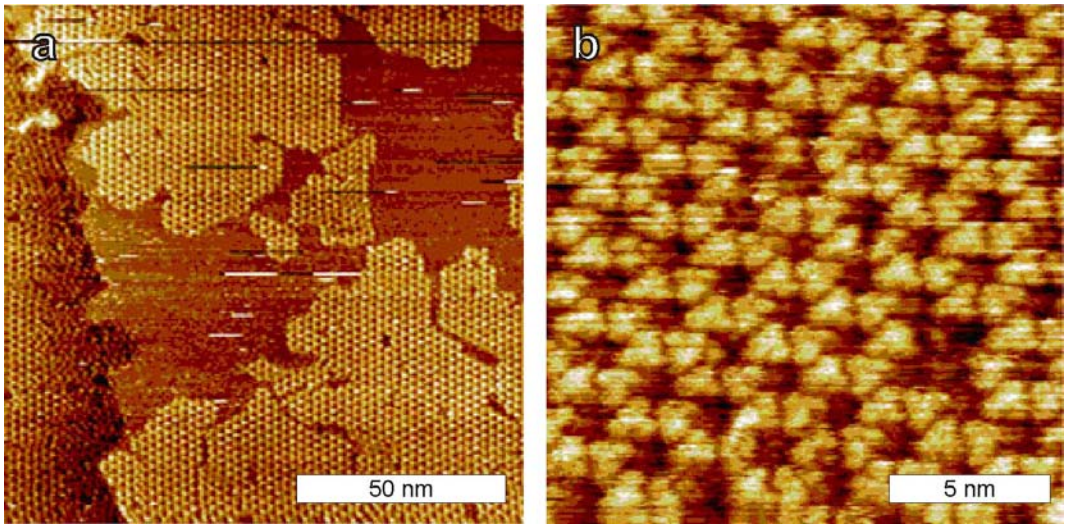

Figure 3.24: Scanning tunneling microscopy of a submonolayer of HATCN on Ag(111) **a.** 123 $\times$ 123 nm^2 (U=-1.2 V, I=0.2 nA), **b.** 16 $\times$ 16 nm^2 (U=-1.0 V, I=0.3 nA).

A very important aspect with regard to work function manipulation by organic molecules is the growth mode on the surfaces.[110] A low effect is expected when the acceptor forms islands upon deposition on the surface, the so-called Volmer-Weber growth mode.[111] Better interactions are present if the molecules form a closely packed monolayer first. This growth mode is often refered to as the Stranski-Krastanov mode.[112]

Figure 3.24 shows the scanning tunneling microscopy images of HATCN sublimed onto the Ag(111) at about half a monolayer. It is obvious that the molecule forms a monolayer first, no island growth can be observed. The interactions with the surface are, therefore, stronger than the interactions of the molecules among each other. HATCN forms an hexagonal pattern as it is frequently observed for molecules of D_{3h} symmetry.[113]

3.7 Charge-Transfer Complexes

Charge-transfer complexes are composed of an electron donor and an electron acceptor which attract each other due to a partial transfer of negative charge from the donor to the acceptor.[114, 115] Conductivity or even superconductivity can be the consequence of this phenomenon given a strong intermolecular coupling and a transfer of electrons to create partially filled bands.[116–118] Having a set of donors and acceptors at hand, it is obvious to go for these charge-transfer complexes, especially with the large, polarizable molecules like hexamethoxycoronene (**19**).

3.7.1 Hexamethoxycoronene (19) - TCNQ

Hexamethoxycoronene (**19**) has been dissolved in THF and added to an equimolar solution of TCNQ in THF. Upon slow evaporation of the solvent, crystals grow suitable for X-ray structure analysis. They need to be handled with care due to destruction upon solvent loss, which means that the solvent must not evaporate until dryness during the crystallization process.

Figure 3.25 shows the crystal structure of this charge-transfer complex. The unit cell is very complicated, therefore only the essential part showing the stacking behavior is presented. TCNQ is sandwiched by two coronene discs, an arrangement in which most charge-transfer complexes crystallize. Unsubstituted coronene has been co-crystallized with TCNQ as well in the literature.[119] Its crystal structure is very similar, coronene and TCNQ form alternating stacks.

The $\pi - \pi$ distance of two neighboring coronene discs in a stack is 3.9 Å in the case of hexamethoxycoronene (**19**). In the case of unsubstituted coronene, in contrast, this distance accounts for only 3.3 Å. The significantly increased distance in the presence of methoxy groups may be due to the space demand by the methoxy groups as was already observed in the crystal structure of the pristine substance. As TCNQ is not very big and the distance increase is much weaker in the crystal of

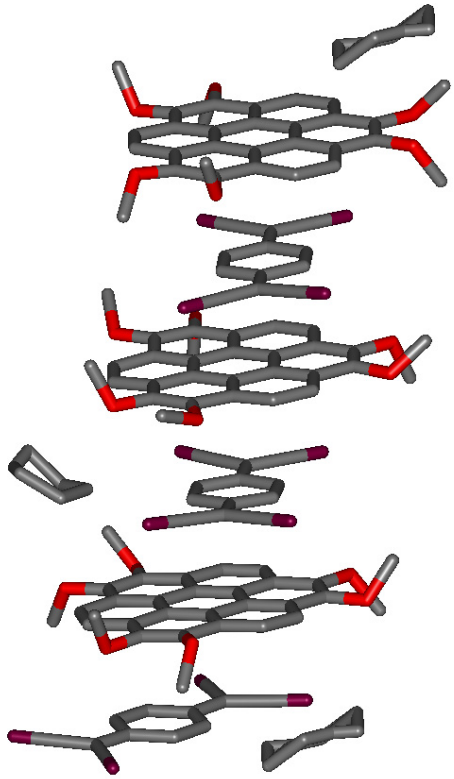

Figure 3.25: Crystal structure of the charge-transfer complex hexamethoxycoronene (**19**) - TCNQ.

pristine hexamethoxycoronene, this contribution should be small. The THF solvate may contribute to the increased distance since it fills space which is left between two coronene discs and not filled by TCNQ. Electronic reasons, however, are most likely, meaning that the orbital overlap of TCNQ with hexamethoxycoronene (**19**) is not effective enough for a strong charge transfer, leading to small $\pi - \pi$ distances. The symmetry mismatch between hexamethoxycoronene (D_{3h}) and TCNQ (D_{2h}) probably leads to the weak interaction.[120]

The degree of charge transfer is determined by infrared spectroscopy. The charge-transfer complex is measured in the evanescence field of an FT-IR spectrometer, TCNQ is measured as reference. The CN bond stretch vibration band shifts by 3 cm^{-1} as depicted in Figure 3.26. In the literature, it has been shown that this band shifts linearly in relation to the percentage of charge transfer.[121] The TCNQ

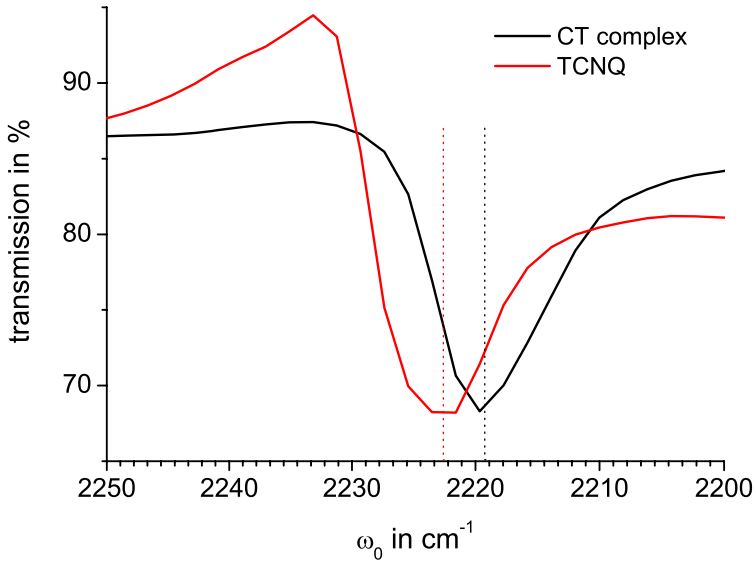

Figure 3.26: Infrared spectroscopy of the CN stretch vibration of TCNQ in the charge-transfer crystal with hexamethoxycoronene (**19**) in reference to pristine TCNQ.

anion exhibits a shift of 44 cm^{-1} relative to pristine TCNQ. Several other complexes of known degree of charge transfer fit into this linear relationship. Following this evaluation, the charge transfer in the complex of hexamethoxycoronene (**19**) and TCNQ is less than 10 %. For comparison, TTF transfers 59 % of a charge to TCNQ in a co-crystal.[122] Lower degrees of charge transfer are observed for tetramethyltetraselenofulvalene (21 %). The methyl groups and the bigger size of the selenium atoms increase the intermolecular distances, thus reduce the electron transfer. The same seems to be true in the present case where the intermolecular distances are relatively high.

The low degree of charge transfer resulting from the large intermolecular distances have discouraged conductivity measurements. Contacting single crystals is experimentally very demanding and no good results are expected in this case.

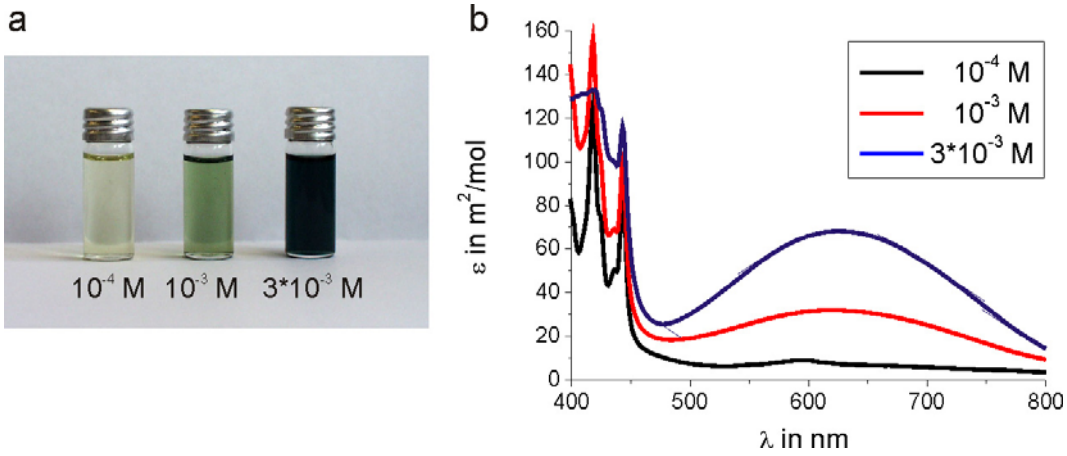

Figure 3.27: Charge-transfer complex of hexamethoxycoronene (**19**) and HATCN (**35**): **a.** photographs of THF solutions at different concentrations, **b.** corresponding UV-vis absorption spectra.

3.7.2 Hexamethoxycoronene (19) - HATCN (35)

Hexamethoxycoronene (**19**) and hexaazatriphenylene-hexacarbonitrile (HATCN, **35**) both possess D_{3h} symmetry, and therefore fit well to form close contacts. A solution containing both compounds turns deep green, indicating a charge-transfer complex formation.

Figure 3.27a depicts the strongly colored solutions of the charge-transfer complex. The UV-vis absorption spectra (Figure 3.27b) show a broad band between 500 and 800 nm which vanishes at low concentration, a typical behavior for charge-transfer complexes.[123] At low concentration the entropy drives the loosely bound molecules apart. At concentrations above 3×10^{-3} M the complex precipiates, although the pristine substances possess higher solubility.

Figure 3.28 explains the additional bands arising upon charge-transfer complex formation. The donor partially transfers electrons from its HOMO to the LUMO of the acceptor. Electrons from the HOMO-1 level of the donor can now be excited to the vacant position in the HOMO. The energy difference is normally lower than the HOMO-LUMO gap giving rise to absorption bands at longer wavelengths. The electron occupying the LUMO of the acceptor can be excited to the LUMO+1 level

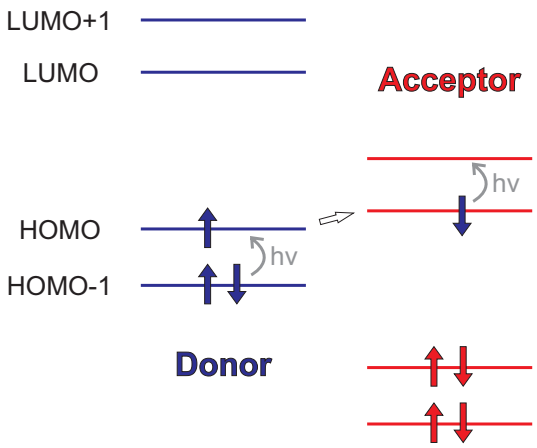

Figure 3.28: Energy scheme of a charge-transfer complex explaining the additional optical transitions.

which is energetically closer to the LUMO level than the HOMO-LUMO gap. The low intensity of the charge-transfer absorption band accounts for the fact that only small amounts of electrons are actually transfered from the donor to the acceptor.

Crystallization was tried by several methods, *i.e.* slow evaporation of the solvent, slow cooling of a hot solution, diffusion of a non-solvent into a solution. In all cases fine needles with a diameter below 5 µm are obtained which do not allow X-ray analysis. These crystals are even too small for analysis with a synchrotron X-ray beam to disclose the molecular packing.

3.7.3 Hexamethoxycoronene (19) - coronene-hexaone (25)

A charge-transfer complex out of hexamethoxycoronene (**19**) and coronene-hexaone (**25**) is particularly interesting due to their structural similarity. They share the same aromatic backbone, namely coronene, and are interconvertible by one synthetic step. Their almost equal size does not leave any empty space in the crystal, therefore optimum interaction is granted. Due to the poor solubility of coronene-hexaone (**25**) it was not possible to grow crystals from these two substances. The solution does not show charge-transfer bands as only the highly polar solvent DMSO which strongly solvates the diketones and thus reduces CT

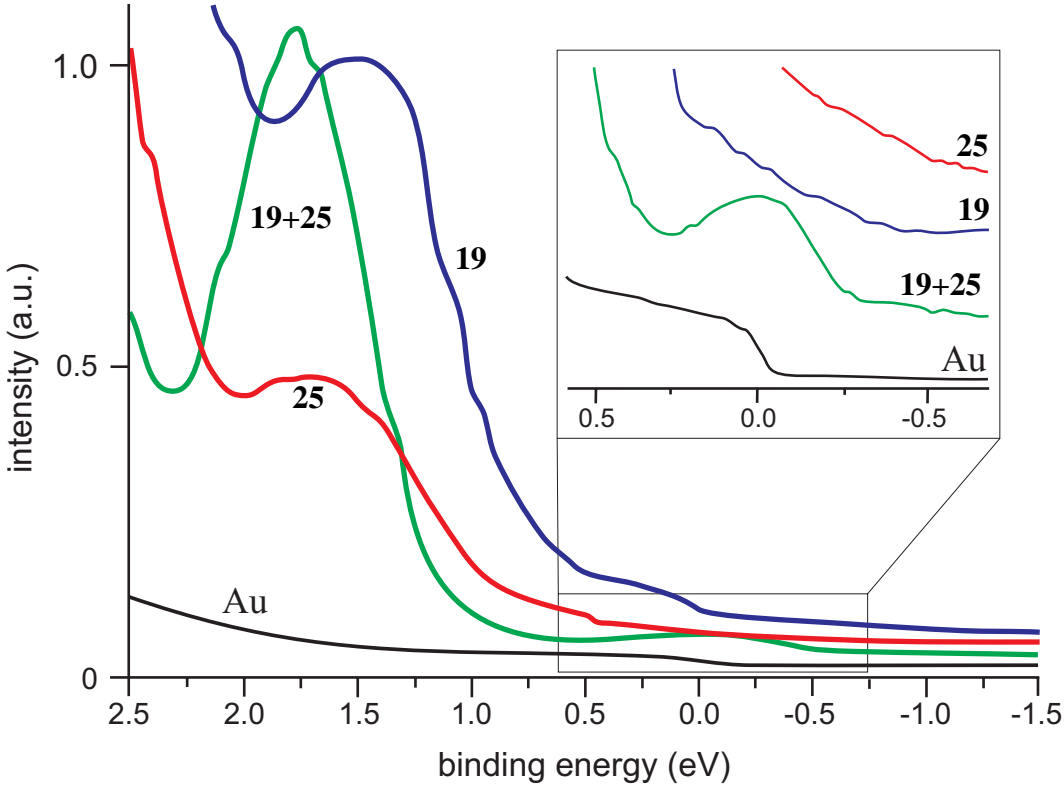

Figure 3.29: Ultraviolet photoemission spectra of the charge-transfer complex out of hexamethoxycoronene (**19**) and coronene-hexaone (**25**) on a gold substrate.

formation can be employed. Also, the concentration is rather low due to solubility issues.

In collaboration with the group of Prof. Schönhense at the Physical Department of the University of Mainz in the context of the transregio SFB TR49, a charge-transfer complex was made from the gas phase. Alternating single layers are evaporated successively onto a gold substrate. The substrate is gently heated to 80°C to allow interdiffusion to facilitate CT complex formation on the surface without solvent in vacuum.[124]

Figure 3.29 shows the ultraviolet photoemission spectroscopy (UPS) results. The clean gold substrate has a Fermi edge at -0.1 eV, so photoelectrons originating from more weakly bound states definitely arise from the organic molecules. Hexamethoxycoronene (**19**) and coronene-hexaone (**25**) have been sublimed separately on the gold for reference purposes. When codepositing both substances, it is obvi-

ous that the spectra do not simply add. The main peak at around 1.5 eV is slightly shifted to higher voltages, meaning the inner electrons are more strongly bound.

The striking feature of the UPS spectrum of the mixed layers is the peak arising at -0.2 eV. This peak is absent in both substances alone. Weakly bound electrons are very likely to originate from a charge-transfer state. Its electrons are less localized and possess lower binding energy. A charge-transfer complex made from the gas phase has not yet been described in the literature.

To further corroborate the assumption, that the low energy band is due to a charge transfer, more measurements are needed. Infrared spectroscopy can, for example, be used to quantify the charge transfer.[121] Furthermore, Kelvin probe force microscopy is a powerful tool to analyze the local energy states to get proof for a charge transfer.[125] These experiments are ongoing, results are not yet obtained.

3.8 Condensation Reactions

The α-diketone moiety is synthetically very interesting as it allows a variety of condensation reactions. The most important one is the quinoxaline formation with diamines.[126–128] This condensation reaction is typically accompanied by little to no side products which makes the reaction well suited for several reactions in one molecule. When aromatic diamines like phenylenediamine are used, extended π conjugated systems are accessible. Substituted with alkyl chains, discotic mesogens can be formed, an important class of molecules which find various applications.[129] The triangular shape may be advantageous for charge-carrier transport if the molecules stack on top of each other with a twist angle of 60°, a "magic angle" as recently reported.[130]

3.8.1 Synthesis

Two methods are conceivable to attach alkyl substituted phenylene-diamines to coronene-hexaone (**25**). Firstly, commercially available 4,5-dichlorophenylene-diamine can be reacted with coronene-hexaone (**25**) to form a six-fold chlorinated extended disc. In a second step, the chlorine atoms can be replaced by alkylthiolates in an aromatic nucleophilic substitution reaction. This route has been used in the literature for pyrene-tetraone (**32**).[131] Due to the extremely low solubility of the reagent, intermediates, and the product of the first reaction, this route was not followed. Instead, the reaction of alkylated phenylene-diamines with coronene-hexaone (**25**) seemed more promising as the intermediates and the product should dissolve and allow the reaction to come to completion. Nevertheless, alkylated phenylene-diamines afford more synthetic steps.

Figure 3.30 shows the route to obtain the desired alkylated phenylenediamines. Commercial 1,2-dinitrobenzene (**38**) is iodinated by iodine in oleum at elevated temperatures.[132] This allows a subsequent Hagihara reaction to form alkynyl-

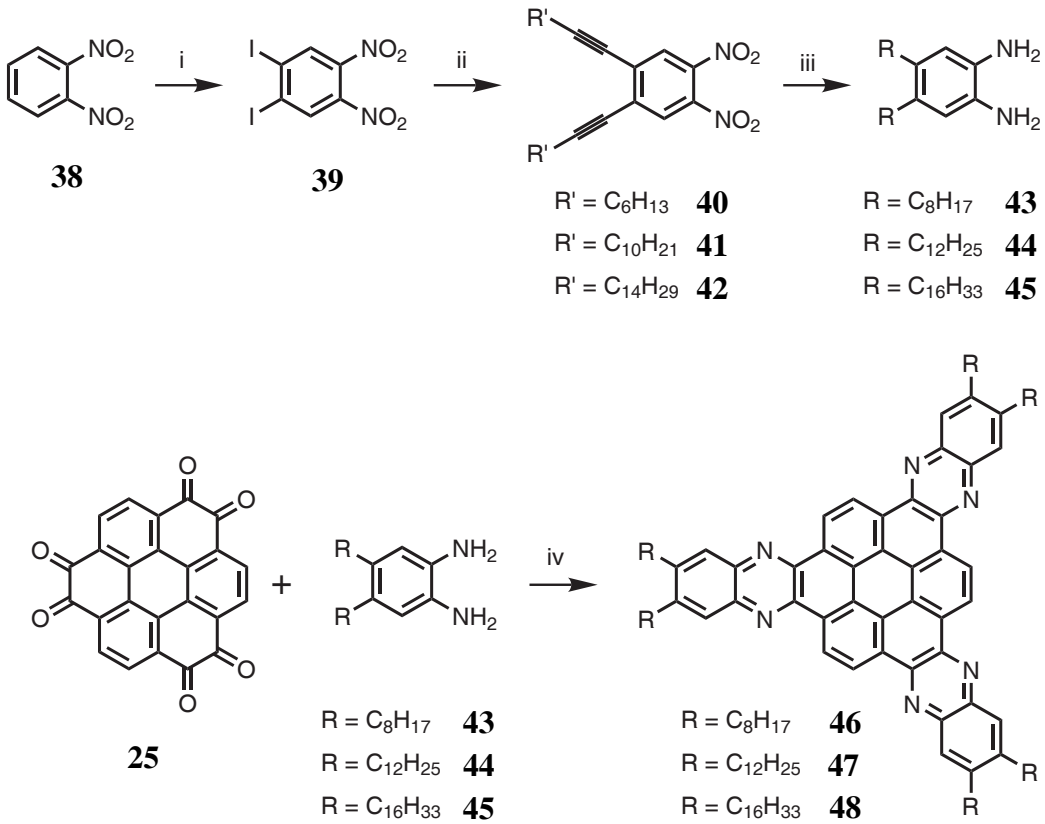

Figure 3.30: Phenylene diamine derivative condensations of coronene-hexaone (**25**), conditions: *i.* I_2, $H_2SO_4 \cdot SO_3$, 80 °C, 57 %; *ii.* alkylethyne, $Pd(PPh_3)_2Cl_2$, NEt_3, toluene, RT, 85 %; *iii.* Et_3SiH, Pd/C, methanol, RT, 75 %; *iv.* chlorobenzene - acetic acid 1:1 v/v, reflux, 85 %.

dinitrobenzenes (**40**-**42**). The reduction to the desired dialkylphenylenediamines (**43**-**45**) is most effective when using the McMurray method.[133] The dinitro compound is suspended in methanol, palladium on active charcoal, and finally triethylsilane are added. The reaction is finished within a few minutes affording the diamines in almost quantitative yields. Conventional hydrogenation with hydrogen gas is unreliable for these compounds as it sometimes leaves considerable amounts of nitroamino intermediates. Using the triethylsilane method greatly facilitates the purification process.

The condensation reaction of the alkylated phenylenediames (**43** - **45**) with coronene-hexaone (**25**) is performed in a 1:1 mixture of chlorobenzene and acetic acid. The latter is needed to catalyze the reaction, the former is needed to solubilize

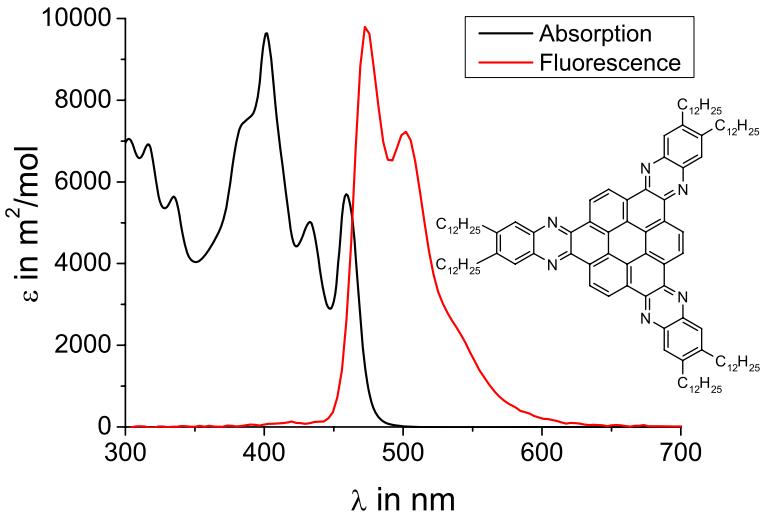

Figure 3.31: UV-vis absorption and photoluminescence spectra of compound **47** in *o*-dichlorobenzene at 10^{-5} M.

the product. Coronene-hexaone (**25**) is practically insoluble under these conditions, but as the reaction proceeds, the intermediates and the product dissolve, driving the reaction to completion. High yields and good purity are obtained after reprecipitation of the products (**46**-**48**).

The compounds are all poorly soluble at room temperature in common organic solvents, but very well soluble at slightly elevated temperatures (40 °C to 50 °C). The UV-vis absorption and photoluminescence spectra of the C12 derivative (**47**) are depicted in Figure 3.31. The high degree of fine structure indicates high symmetry due to a variety of symmetry-forbidden transitions.[134] This is consistent with the flat core of the molecule, giving rise to D_{3h} symmetry. The absorption and photoluminescence is shifted bathochromically by about 150 nm with regard to coronene accounting for the extended π system. The extinction coefficients and the photoluminescence intensities are much higher than those of coronene-hexaone, the reagent. The disappearance of the α-diketones increases the transition probability to a level comparable to the coronene derivatives (compare Figure 3.10 on page 55).

The quinoxaline derivatives are much less electron accepting than the reagent

coronene-hexaone (**25**). Compound **44** has been subjected to cyclic voltammetry. However, no reduction peak can be recorded before the solvent decomposition sets in. The LUMO level has, therefore, increased by more than 1 eV during the reaction with the diamine.

3.8.2 Aggregation in Solution

The atypical solubility behavior of the coronene quinoxaline derivatives **46**-**48**, *i.e.* almost no solubility ($< 10^{-4}$ M) at room temperature, but good solubility (> 0.1 M) at slightly elevated temperaturs (40 °C), gave motivation to investigate the solution aggregation properties in more detail. Concentration dependent NMR experiments have turned out to be an effective method, which allows the elucidation of the association constant.[135] The theory is based on the observation that the chemical shift of a particular proton in a stack is different from that of the single molecule. In polycyclic aromatic hydrocarbons the aromatic protons experience the ring current of the next disc in a stack leading to strong resonance shifts.

The NMR chemical shifts of the two protons in the C16 quinoxaline compound (**48**) are plotted in Figure 3.32. The measurement has been performed at 50 °C due to the poor solubility of the compound at room temperature. The typical sigmoidal shape of the fit curve is clearly visible. For the analysis, it was assumed that the association follows an attenuated K model, which means that the association constant i-mer formation equals

$$K_i = \frac{1}{i} K_A$$

where K_A is a constant association constant for the system.[136] Two equations need to be solved iteratively to obtain K_A

$$L = x(1 + \tau(e^x - 1))$$

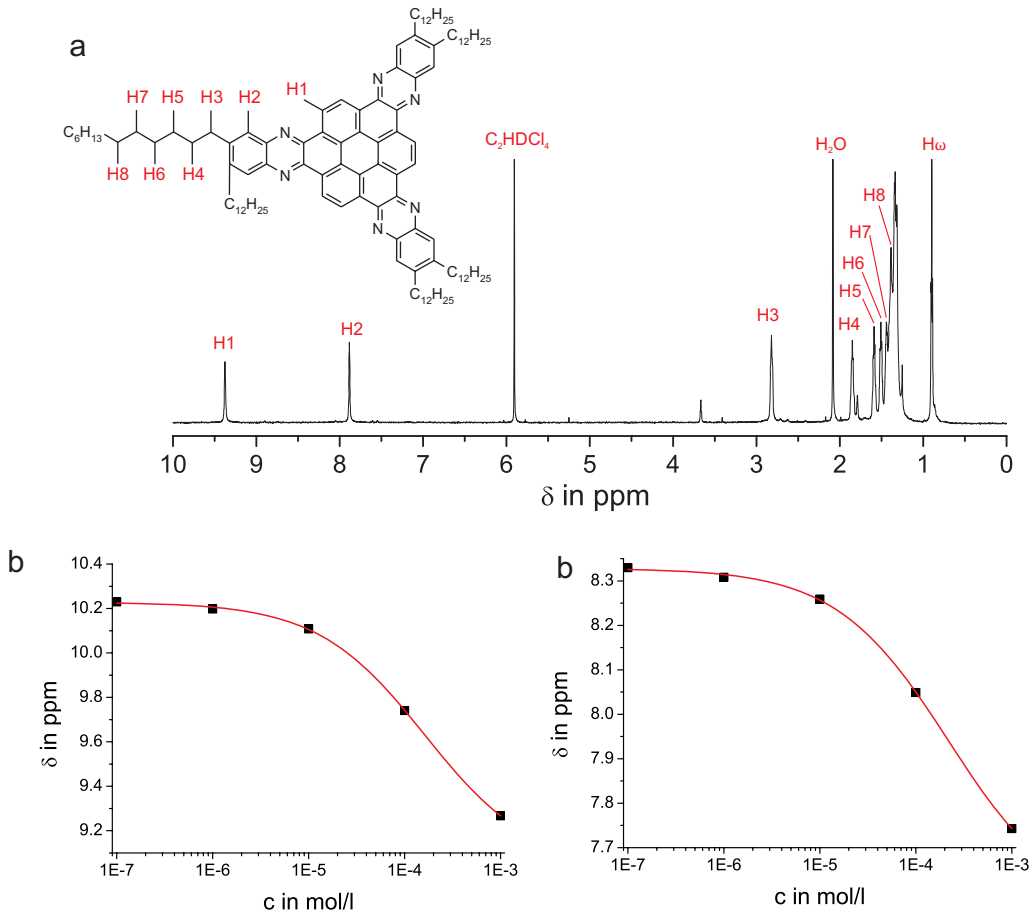

Figure 3.32: Concentration dependend NMR spectra of the coronene quinoxaline derivative **48**. **a.** ^{1}H-NMR spectrum in $C_2D_2Cl_4$ at 100 °C (500 MHz) **b.** concentration dependence of H1 **c.** concentration dependence of H2.

$$\alpha = \frac{1}{1+\tau(e^x-1)}$$
$$\text{with } x = K_A\,[A] \text{ and } L = K_A C_T$$

where $[A]$ is the concentration of the monomeric molecules, C_T the total concentration of the molecule, and τ is the preference for a dimer over higher oligomers. The analysis is performed in collaboration with Lei Dou at the Technical University Darmstadt. Separate peak fittings are performed for both proton signals independently yielding equal results within the standard deviation.

For K_A a value of 590 l/mol is obtained. HBC with C12 chains exhibits a value of K_A=457 l/mol, so the association of the coronene quinoxaline (**48**) is stronger

than for a comparable HBC derivative.[137] Even much weaker association constants have been measured for a variety of phenylene-ethynylene macrocycles exhibiting a similar shape and size as the the coronene-quinoxalines **46**-**48**. In chlorinated solvents, values between 20 and 50 l/mol have been determined.[138]

Surprisingly, the proton NMR signals of the coronene quinoxaline derivatives are exactly the same for all compounds (**46**-**48**). That means, the alkyl chains do not have an influence on the aggregation behavior in solution. For HBC derivatives, a strong dependence of the type of alkyl chains on the aggregation behavior has been measured.[139] In the present case, the geometry of the aromatic core may lead to this effect. The alkyl chains are located far from the center leaving space in the bay, such that the association of the aromatic discs is not affected by the alkyl chains.

3.8.3 Surface Deposition

The deposition of planar molecules on metal surfaces enables the visualization of the molecules by scanning tunneling microscopy (STM).[140] Information about the interfacial assembly and the mode of 2D network formation is gained.[141–143] In some cases, it is even possible to run reactions at the surface and follow the progress by STM.[48, 144]

In collaboration with the group of Prof. De Feyter at Katholieke Universiteit Leuven, Belgium, solution STM investigations are performed. Compound **47** is assembled onto HOPG by putting a droplet of a 1,2,4-trichlorobenzene solution on top. The tip of an STM is brought into the solution close to the surface. Figure 3.33 shows the images thus obtained.

The triangular shape of the molecule can be seen clearly. The substance forms honeycomb patterns spanned by six molecules with void space in the center. This is a typical behavior for molecules of triangular shape.[145–147] There are several defects in the structure, which means that the tendency to form stable and densely

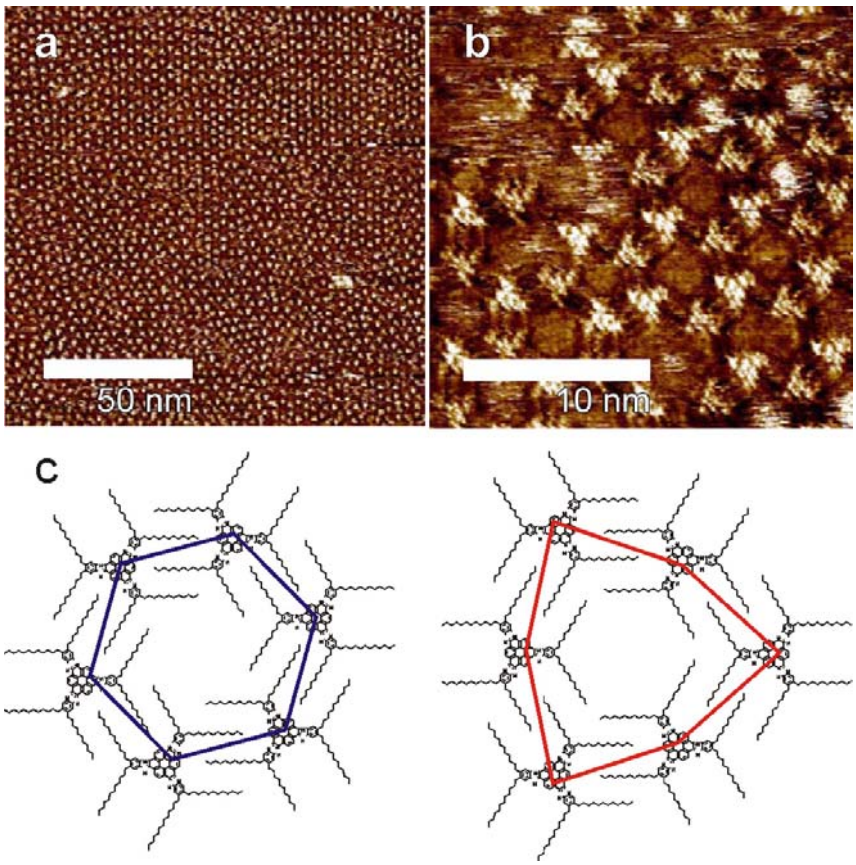

Figure 3.33: Scanning tunneling microscopy images of coronene-quinoxaline derivative **47** on HOPG surface in a drop of 1,2,4-trichlorobenzene **a.** 127.3 · 127.3 nm^2 (53 pA, -784 mV) **b.** 22.8 · 22.8 nm^2 (24 pA, 743 mV) **c.** two possible arrangements of the molecules.

packed monolayers is not very expressed. In Figure 3.33b one can see that a pattern of five molecules in a circle can be formed as well, so no clear preference for a particular assembly is observed.

In Figure 3.33c two possible arrangements of the molecule leading to a honeycomb pattern are depicted. The left structure possesses C_6 symmetry, the right one C_3. By carefully comparing the position of the aromatic discs relative to each other one can disclose that both cases are actually formed. The C_6 cell is a regular hexagon, the C_3 cell resembles almost a triangle. This difference induces mismatches in the lattice leading to the relatively low degree of order.

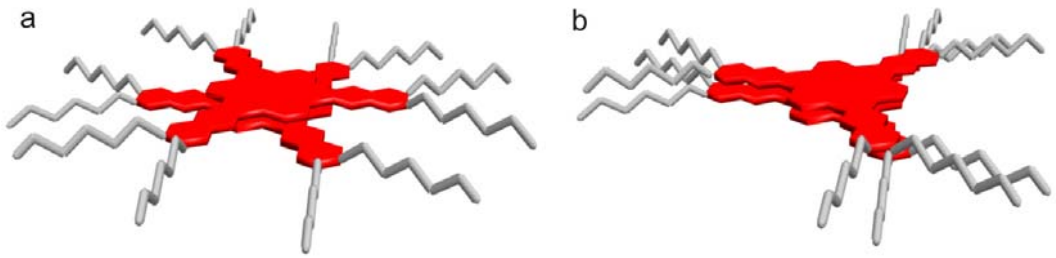

Figure 3.34: Two possible intermolecular arrangements of the coronene quinoxaline derivatives: **a.** staggered **b.** eclipsed.

3.8.4 Bulk Properties

The morphology in the bulk material is of primary interest when dealing with discotic molecules. The intermolecular assembly strongly influences the properties of the materials, especially with regard to charge-carrier mobility.[148] It crucially depend on the distance between adjacent molecules.[149]

The shape of the aromatic disc in the quinoxaline derivatives **46**-**48** is particularly interesting with regard to the intermolecular arrangement. If two adjacent molecules are rotated against each other by 60 °, they can fully avoid steric hindrance of the alkyl chains as depicted in Figure 3.34a. This arrangement shall be called staggered considering the similarity of the rotational barrier of ethane. In such a situation, the aromatic discs can get as close to each other as in unsubstituted PAHs, or even graphite. An eclipsed arrangement (Figure 3.34b), in contrast, does not allow this close packing as the steric repulsion of the alkyl chains of adjacent discs drives the discs apart. The overlap of the aromatic cores, however, is maximized in this case, so it is worthwhile to investigate the packing in detail.

Differential scanning calorimetry (DSC) is measured first for the three derivatives to see if phase transitions exist. Only melting points can be observed for the three compounds. The C16 derivative (**48**) melts at 85° C, the lowest one due to the long alkyl chains. A temperature of 116° C is measured for the C12 derivative (**47**) and 205° C for the C8 derivative (**46**). The trend is not surprising as the entropy

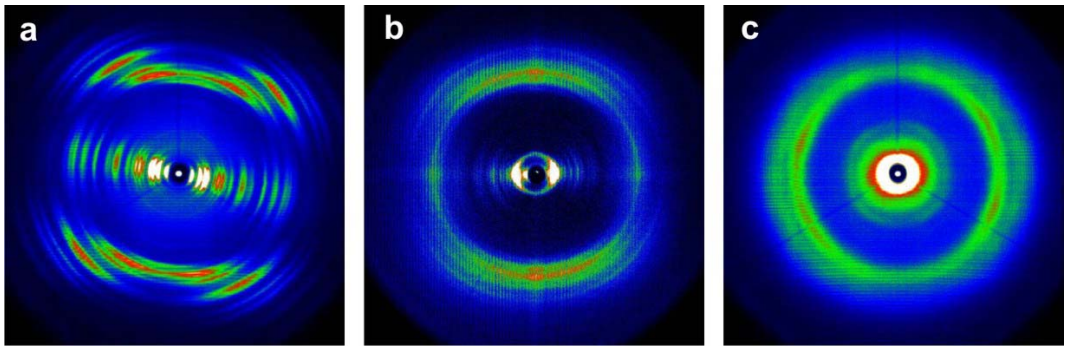

Figure 3.35: Fiber X-ray diffraction patterns of the coronene quinoxaline derivatives. **a.** C8 derivative (**46**), **b.** C12 derivative (**47**), **c.** C16 derivative (**48**).

gain upon melting becomes bigger with increasing alkyl chain length. This trend is known for triphenylene systems as well.[150]

In collaboration with Wojciech Pisula and Alexey Mavrinskiy X-ray diffraction has been measured to investigate the morphology. The material is extruded as a fiber and exposed to an X-ray beam. The diffraction pattern in transmission mode is recorded while blocking the primary beam. These patterns are depicted for all compounds in Figure 3.35. In all cases the molecules form crystalline phases at room temperature. At high scattering angles, four peaks are present at the maximum angle which arise from the $\pi - \pi$ stacking of tilted columns as typically found in crystalline phases of discotics.[151]

The degree of order is highest for the C8 derivative and decreases when going to the longer alkyl chains. The higher flexibility of the long chains gives rise to lower order for entropic reasons. This result is in line with the decreasing melting points when increasing the alkyl chain length. The distance between stacks increases with the length of the alkyl chain as they need to fit into this space. Due to their high mechanical flexibility, the interaction forces between the columns become lower the longer the distance is, which consequently leads to a lower degree of order.

The inter disc distance for the three molecules is determined to be 3.4 to 3.5 Å. This value is comparable to the distance in unsubstituted HBC (3.44 Å),[69] but larger than in graphite (3.35 Å).[152] Interplanar distances of this order have also

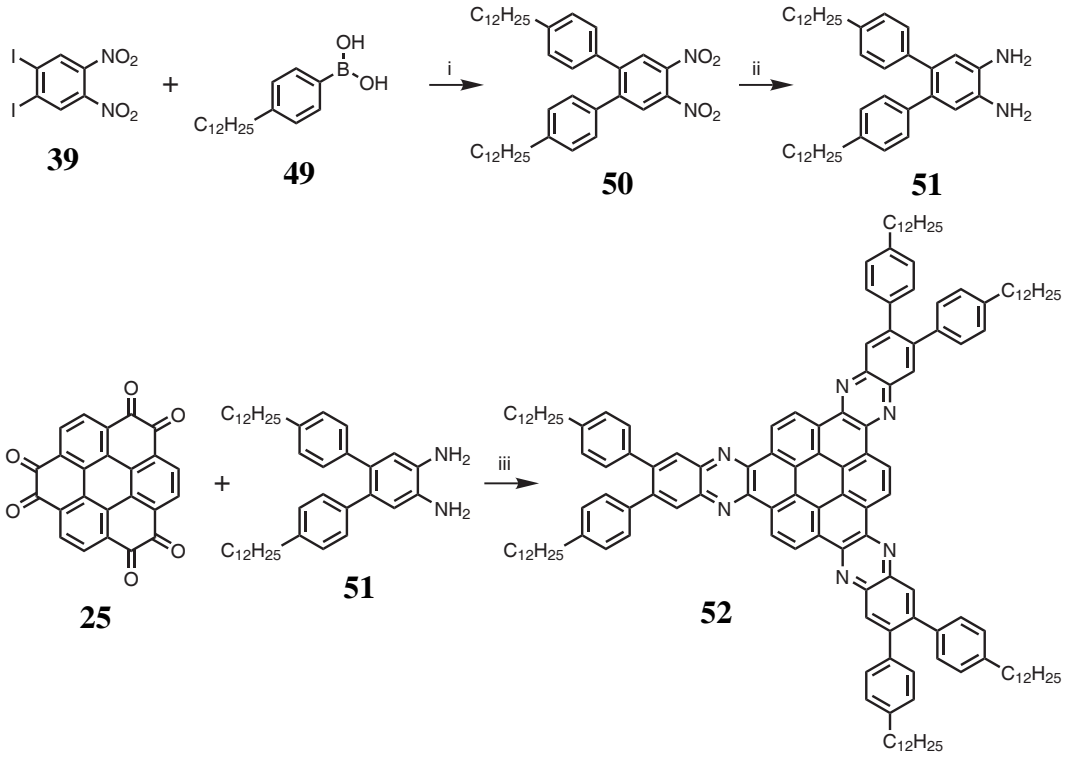

Figure 3.36: Preparation of a phenyl substutituted coronene quinoxaline derivative, conditions: *i.* K_2CO_3 $Pd(PPh_3)_4$, ethanol, toluene, 90 °C, 65 %; *ii.* Et_3SiH, Pd/C, methanol, RT, 82 %; *iii.* chlorobenzene - acetic acid 1:1 v/v, reflux, 80 %.

been measured in alkylated HBC derivatives.[153] The lowest value so far measured in discotic materials is 3.18 Å in triphenylene where the assembly is assisted by hydrogen bonding.[99]

No hint for order along the stacking axis can be obtained from the X-ray diffraction patterns. It is, therefore, unlikely that the discs stack preferentially in a staggered or eclipsed conformation as depicted in Figure 3.34 on page 92. It seems likely, that the discs possess high enough thermal energy to overcome the small rotation potential. If the discs do not rotate, which they usually only do in liquid crystalline phases, the low potential differences may still lead to little preference for the molecule for a certain relative position to each other. They may just aribrarily be stacked on top of each other.

In order to increase the rotational barrier and thus enhance the order of the molecule, additional phenyl units have been introduced to the system. The corre-

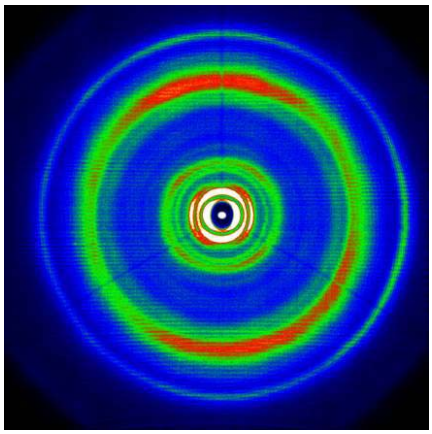

Figure 3.37: 2D wide angle X-ray diffraction pattern of an extruded fiber of **52**.

sponding synthesis is depicted in Figure 3.36. Diiodo-dinitrobenzene (**39**) is subject to a Suzuki coupling with dodecylphenylboronic acid (**49**) followed by a reduction to yield bis(dodecylphenyl)phenylenediamine (**51**). This diamine is condensed with coronene-hexaone (**25**) in the same way as before to give the final molecule **52**.

With the additional phenyl rings, the molecule does not melt up to 350 °C, where it decomposes under ambient conditions. An increased intermolecular interaction arising from phenyl-phenyl attraction should be responsible for this effect. The DSC curve discloses a phase transition at 150 °C, which is definitely no melting point as for the purely alkyl substituted derivatives (**46**-**48**).

The wide angle X-ray diffraction pattern of an extruded fiber is shown in Figure 3.37. The increased order is obvious from the highly resolved peaks. The molecule forms a liquid crystalline phase which can be concluded from the presence of only two peaks at the widest diffraction angle. The $\pi - \pi$ distance is unchanged at 3.4 Å, so no unfavorable steric interactions disturb the packing in comparison to the structures without phenyl spacers.

The diffraction pattern at a lower angle indicates helical packing. The phenyl rings have obviously increased the rotational barrier so much that the molecule cannot rotate any more around the stacking axis. This is remarkable for the liquid crys-

talline phase, where molecular motion is typically high. A quite similar behavior has been reported for hexaphenyl subsituted HBC.[154]

3.8.5 Three-Center Metal Organic Complex

A further impressive demonstration of the synthetic possibilities which are offered by coronene-hexaone (**25**) is a condensation reaction with ruthenium(II)-bipyridine ligands. Ruthenium complexes have gained considerable intrest due to their high stability, their redox and absorption behavior spanning almost the entire visible range.[155] Especially the latter has made ruthenium complexes attractive for use as dyes in dye-sensitized solar cells.[156–158]

This condensation is once more based on the very efficient reaction between α-diketones and 1,2-phenylene-diamines. For pyrene-tetraone (**32**) the analogous condensation leading to a two-centered ruthenium complex has been reported in the literature.[159] Figure 3.38 on page 97 shows the synthetic route.

To obtain the required diamino complex **57** 5-nitrophenthroline (**53**) is aminated by reacting with hydroxylamine under basic conditions.[160, 161] The practically insoluble 5-amino-6-nitrophenanthroline (**54**) is complexed by cis-dichlorobis-(2,2'-bipyridin)-ruthenium(II) (**55**) to obtain complex **56** which is soluble in highly polar solvents. This enables a catalytic reduction to the diamine complex **57** with palladium on charcoal and elemental hydrogen gas.[162]

The condensation reaction with coronene-hexaone (**25**) does not proceed as effectively as for the substituted phenylene-diamines in the previous section. The polarity of the solvents employed to dissolve the ruthenium complex seems to be incompatible with the need to dissolve coronene-hexaone (**25**). Nevertheless, complex **58** containing three ruthenium centers could be obtained after several attempts. It is purified by an anion exchange reaction. Therefore, complex **58** is dissolved in

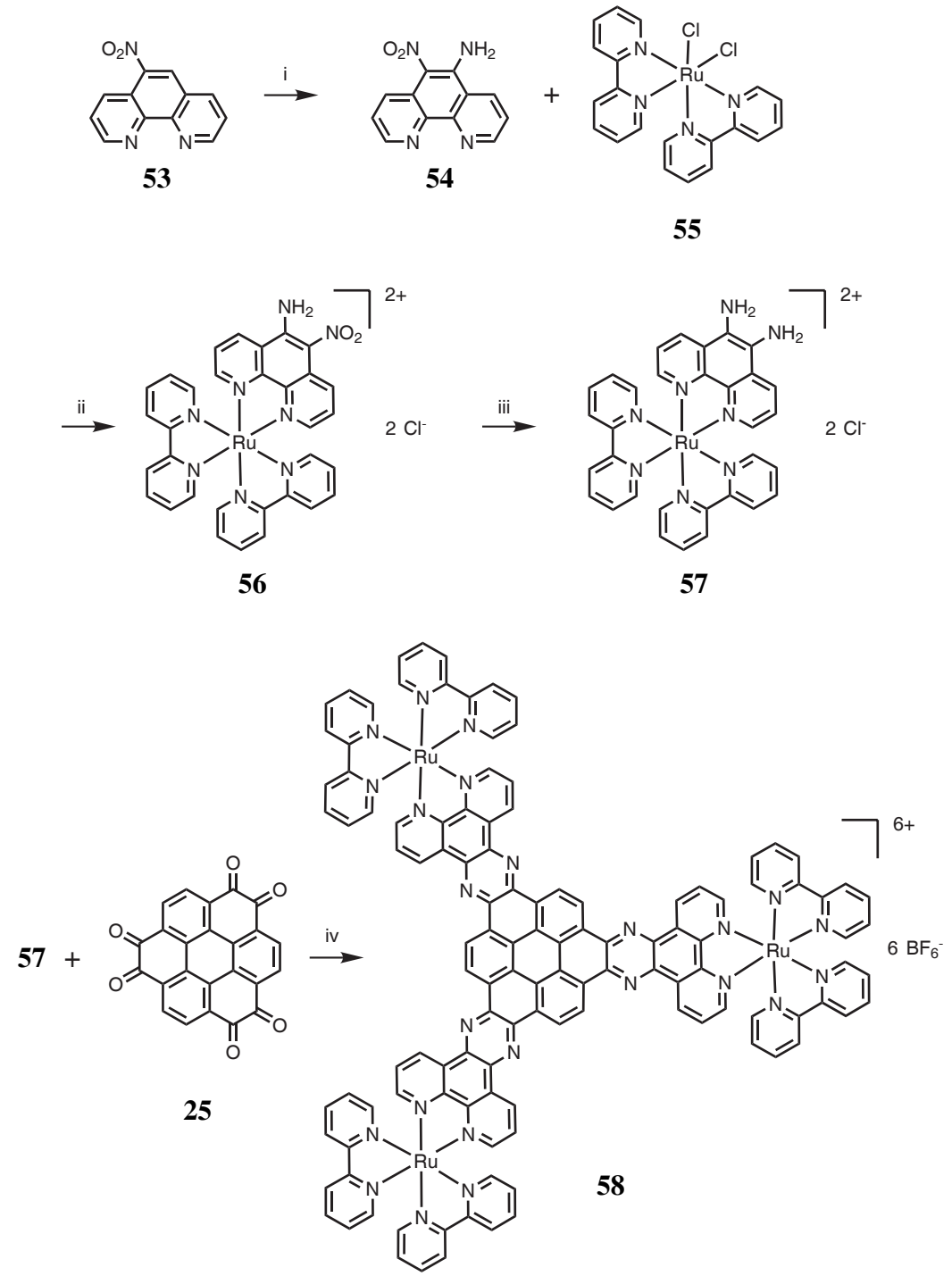

Figure 3.38: Synthesis of three-center ruthenium complex by a condensation reaction with coronene-hexaone (**25**). Conditions: *i* $H_2NOH \cdot HCl$, KOH, EtOH, reflux, 49 %; *ii* EtOH, reflux, quantitative; *iii* H_2, Pd/C, EtOH, RT, quantitative; *iv* 1. CH_3CN, MeOH, HOAc 20:15:1, 90 °C 2. NH_4PF_6, H_2O, 90 %.

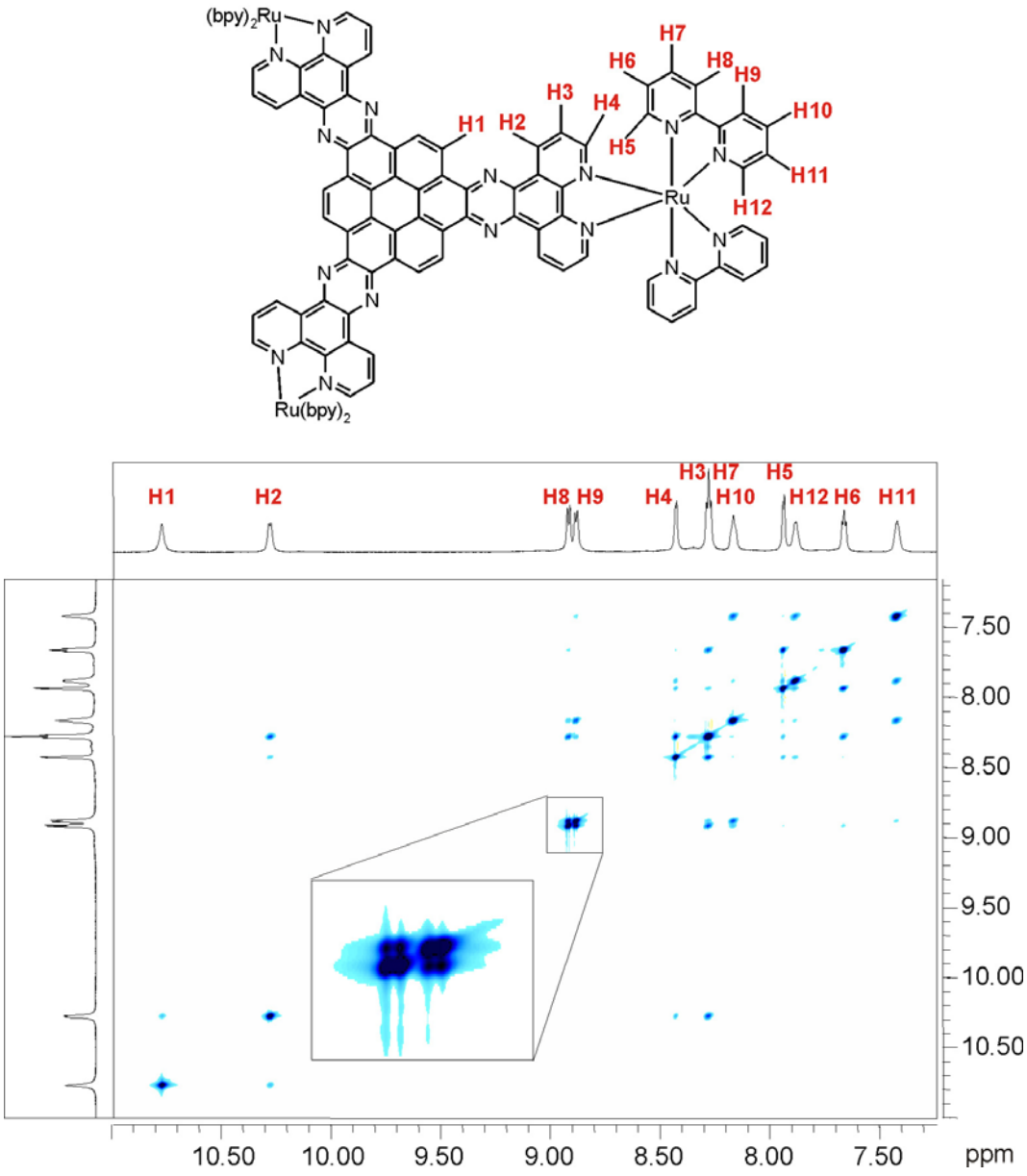

Figure 3.39: NOESY spectrum of three-centered ruthenium complex **58**.

water and precipitated by the addition of an ammonium-hexafluorophosphate solution.

Figure 3.39 shows the H-H NOE spectrum measured in deuterated DMSO at room temperature on a 700 MHz spectrometer. Only the aromatic region between 7 and 11 ppm is shown as there are no aliphatic protons present in this molecule. The peak at 10.7 ppm can be clearly assigned to the proton at the coronene core. It is strongly deshielded by the ring current of the big aromatic disc. The through-

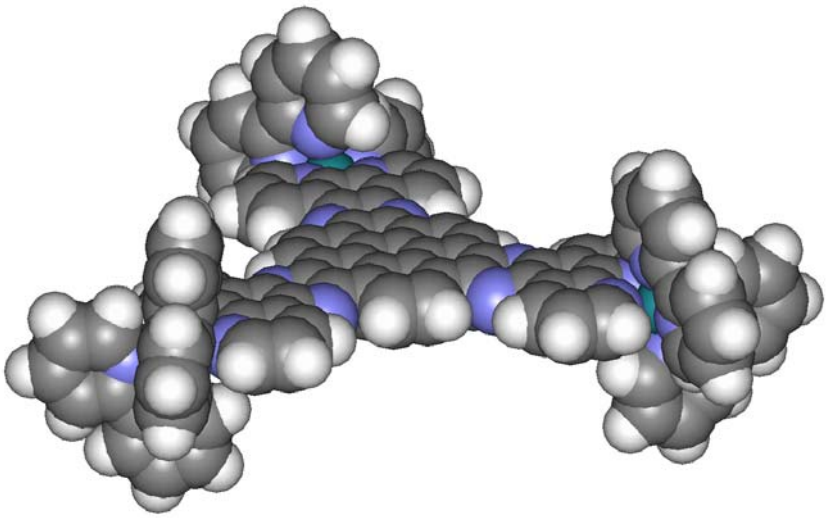

Figure 3.40: Space-filling model of three-centered ruthenium complex **58**.

space coupling identifies the peak at 10.3 ppm to arise from the proton of the fused phenanthroline unit pointing towards the inner core (H2 in Figure 3.39).

Following the chain of coupling protons, all signals can be identified to belong to one molecule. The coupling patterns fit well to the structure of complex **58**. A point worth mentioning is the desymmetrization of the bipyridine ligand. In tris-(2,2'-bipyridin)-ruthenium(II), the pyridine subunits are symmetrically equivalent giving rise to one ABC spin system. In complex **58**, however, two ABC systems for the bipyridine ligand are found. The fact that both systems exhibit very similar chemical shifts and are in close spacial proximity as detected by their NOESY cross peaks (enlarged inset in Figure 3.39) strongly suggests a desymmetrized bipyridine ligand. In the octahedral coordination sphere of ruthenium, one nitrogen of the bipyridines occupies the trans position with regard to the nitrogen of the large disc and the other one the trans position to the second bypridine. These differences cause the desymmetrization of the bipyridine and explain the peak pattern of the NMR spectrum.

Considering the enormous size of the aromatic core, *i.e.* 102 carbon or nitrogen

atoms spanning the π-system, it is amazing that no aliphatic side chains are needed to ensure solubility. The complex does not show any aggregation phenoma in the NMR spectrum like aromatic discs of even much smaller size do. The space-filling model shown in Figure 3.40 gives the explanation. The bipyridine ligands on the ruthenium atoms stand out of the plane of the aromatic core. Any aggregation is effectively prohibited by the steric clash of these bipyridines. Repulsive Coloumb interactions between the positively charged ruthenium centeres drive the molecules apart. This suppresses aggregation and makes complex **58** even soluble in water when chloride is the counter ion.

3.9 Summary

In summary, it could be shown that the photochemically induced cyclodehydrogenation of [2.2.2]cyclophanes opens a versatile route to substituted coronenes. It turns out, that the dehydrogenation proceeds stepwise forming one bond after the other. Furthermore, it has been demonstrated that the symmetry can be easily influenced by the appropriate choice of reagents in the cyclophane synthesis.

As an example, three methoxy substituted coronene derivatives have been prepared. They are investigated by optical spectroscopy, revealing little influence of the functional groups on the electronic structure of coronene. It was possible to crystallize all derivatives and study the molecular superstructure within the crystal. The sandwich herringbone structural motif of coronene is retained, but intermolecular distances are increased by the methoxy groups.

Upon ether cleavage and subsequent oxidation, the electron donor molecules can be easily converted to strong acceptors bearing the chemically versatile α-diketone functions. These molecules are very strong acceptors according to the reduction potentials determined by cyclic voltammetry in comparison to other well-known acceptors and derivatives thereof.

Coronene-hexaone proves to be particularly useful to increase the work function of a metal, which can be used as interlayer to reduce contact resistances. The strong electron acceptor character of the molecule extracts electrons out of the metal, most effectively out of silver. In addition, the α-diketone moieties bend towards the metal surface creating a strong dipole which enhances the work function increase.

Having at hand a set of donor and acceptor molecules, various charge-transfer complexes have been realized. Hexamethoxycoronene could be co-crystallized with TCNQ to show alternative stacks. The former molecule shows strong charge transfer with HATCN, a strong acceptor of the same symmetry, as disclosed by concentration dependend UV-vis measurements. A charge-transfer complex of the chemi-

cally interconvertible molecules hexamethoxycoronene and coronene-hexaone have been prepared from the gas phase by cosublimation. UPS measurements show characteristic shifts at the Fermi edge.

Coronene-hexaone can be used as synthetic platform to build up larger structures. As an example, the quinoxaline condensation with alkylated phenylenediamines has been performed. Triangular PAHs are obtained which show increased order in the bulk the shorter their alkyl chains are. In contrast, the aggregation in solution is unaffected by the length of the alkyl chain. Close $\pi-\pi$ distances indicate low steric repulsion of adjacent substituents, a consequence of the triangular shape. When substituted solely by alkyl chains, a phase transition from the crystalline phase to the isotropic melt is observed. Additional phenyl rings in between the alkyl chains and the aromatic core stabilize intermolecular interactions giving rise to higher order in the crystalline phase with helical superstructure. At elevated temperature, the system forms a liquid crystalline phase.

An extended aromatic disc containing 102 carbon or nitrogen atoms is available by condensation with a diamino-functionalized bipyridine-ruthenium complex. This complex is highly soluble without any aliphatic alkyl chains. It possesses a sixfold positive charge allowing to change the molecules properties by exchanging the counter ion.

3.10 Bibliography

[1] Watson, M. D.; Fechtenkötter, A.; Müllen, K. *Chem. Rev.* **2001**, *101*, 1267–1300.

[2] Wu, J. S.; Pisula, W.; Müllen, K. *Chem. Rev.* **2007**, *107*, 718–747.

[3] Grimsdale, A. C.; Müllen, K. *Angew. Chem. Int. Ed.* **2005**, *44*, 5592–5629.

[4] Zander, M. *Polycycl. Aromat. Compd.* **1994**, *5*, 1–25.

[5] Clar, E. *The Aromatic Sextet*; Wiley: London, 1972.

[6] Hosoya, H. *Top. Curr. Chem.* **1990**, *153*, 255–272.

[7] Scholl, R.; Seer, C. *Justus Liebigs Annalen Der Chemie* **1912**, *394*, 111–177.

[8] Dötz, F.; Brand, J. D.; Ito, S.; Gherghel, L.; Müllen, K. *J. Am. Chem. Soc.* **2000**, *122*, 7707–7717.

[9] Wasserfallen, D.; Kastler, M.; Pisula, W.; Hofer, W. A.; Fogel, Y.; Wang, Z. H.; Müllen, K. *J. Am. Chem. Soc.* **2006**, *128*, 1334–1339.

[10] Tomovic, Z.; Watson, M. D.; Müllen, K. *Angew. Chem. Int. Ed.* **2004**, *43*, 755–758.

[11] Rempala, P.; Kroulik, J.; King, B. T. *J. Am. Chem. Soc.* **2004**, *126*, 15002–15003.

[12] King, B. T.; Kroulik, J.; Robertson, C. R.; Rempala, P.; Hilton, C. L.; Korinek, J. D.; Gortari, L. M. *J. Org. Chem.* **2007**, *72*, 2279–2288.

[13] Di Stefano, M.; Negri, F.; Carbone, P.; Müllen, K. *Chem. Phys.* **2005**, *314*, 85–99.

[14] Kumar, S.; Manickam, M. *Chem. Comm.* **1997**, 1615–1616.

[15] Stabel, A.; Herwig, P.; Müllen, K.; Rabe, J. P. *Angew. Chem. Int. Ed.* **1995**, *34*, 1609–1611.

[16] Deleuze, M. S. *J. Phys. Chem. A* **2004**, *108*, 9244–9259.

[17] Zhao, Y.; Truhlar, D. G. *J. Phys. Chem. C* **2008**, *112*, 4061–4067.

[18] Norinaga, K.; Deutschmann, O.; Huttinger, K. J. *Carbon* **2006**, *44*, 1790–1800.

[19] Hu, J.; Zhang, D.; Harris, F. W. *J. Org. Chem.* **2005**, *70*, 707–708.

[20] Fogel, Y.; Kastler, M.; Wang, Z. H.; Andrienko, D.; Bodwell, G. J.; Müllen, K. *J. Am. Chem. Soc.* **2007**, *129*, 11743–11749.

[21] Shen, H. C.; Tang, J. M.; Chang, H. K.; Yang, C. W.; Liu, R. S. *J. Org. Chem.* **2005**, *70*, 10113–10116.

[22] Alibert-Fouet, S.; Seguy, I.; Bobo, J. F.; Destruel, P.; Bock, H. *Chem. Eur. J.* **2007**, *13*, 1746–1753.

[23] Rohr, U.; Schlichting, P.; Bohm, A.; Gross, M.; Meerholz, K.; Bräuchle, C.; Müllen, K. *Angew. Chem. Int. Ed.* **1998**, *37*, 1434–1437.

[24] Otsubo, T.; Gray, R.; Boeckelheide, V. *J. Am. Chem. Soc.* **1978**, *100*, 2449–2454.

[25] Greene, T. W.; Wuts, P. G. M. *Protective Groups in Organic Synthesis*, 4th ed.; Wiley and Sons, 2006.

[26] Tanner, D.; Wennerström, O.; Norinder, U.; Müllen, K.; Trinks, R. *Tetrahedron* **1986**, *42*, 4499–4502.

[27] Kuhnert, N.; Rossignolo, G. M.; Lopez-Periago, A. *Org. Biomol. Chem.* **2003**, *1*, 1157–1170.

[28] Vedejs, E.; Peterson, M. J. *Top. Stereochem.* **1994**, *21*, 1–157.

[29] Vedejs, E.; Marth, C. F. *J. Am. Chem. Soc.* **1988**, *110*, 3948–3958.

[30] Vedejs, E.; Fleck, T. J. *J. Am. Chem. Soc.* **1989**, *111*, 5861–5871.

[31] McMurry, J. E. *Chem. Rev.* **1989**, *89*, 1513–1524.

[32] Furstner, A.; Bogdanovic, B. *Angew. Chem. Int. Ed.* **1996**, *35*, 2442–2469.

[33] Ephritikhine, M. *Chem. Comm.* **1998**, 2549–2554.

[34] Eliel, E. E.; Wilen, S. H. *Stereochemistry of Organic Compounds*; Wiley: New York, 1994.

[35] Günther, H. *NMR Spectroscopy*, 2nd ed.; Wiley, 1995.

[36] Atkins, P. W.; de Paula, J. *Atkins' Physical Chemistry*, 7th ed.; Oxford University Press, 2001.

[37] Ernst, L. *Prog. Nucl. Magn. Res. Spectrosc.* **2000**, *37*, 47–190.

[38] Günther, H.; Schmitt, P.; Fischer, H.; Tochtermann, W.; Liebe, J.; Wolff, C. *Helvetica Chimica Acta* **1985**, *68*, 801–812.

[39] Iwamoto, K.; Shinkai, S. *J. Org. Chem.* **1992**, *57*, 7066–7073.

[40] Mallory, F. B.; Mallory, C. W. *Org. React.* **1984**, *30*, 1–133.

[41] Ramamurthy, V.; Scaiano, J.; Turro, N. J. *Modern Molecular Photochemistry of Organic Molecules*; Palgrave Macmillan, 2009.

[42] Turro, N. J.; Scaiano, J. C.; Ramamurthy, V. *Principles of Molecular Photochemistry: An Introduction*; Palgrave Macmillan, 2009.

[43] Klan, P.; Wirz, J. *Photochemistry of Organic Compounds: From Concepts to Practice*, 1st ed.; Wiley and Sons, 2009.

[44] Mallory, F. B.; Rudolph, M. J.; Oh, S. M. *J. Org. Chem.* **1989**, *54*, 4619–4626.

[45] Witte, G.; Woll, C. *J. Mater. Res.* **2004**, *19*, 1889–1916.

[46] De Feyter, S.; De Schryver, F. C. *Chem. Soc. Rev.* **2003**, *32*, 139–150.

[47] Wolkow, R.; Avouris, P. *Phys. Rev. Lett.* **1988**, *60*, 1049–1052.

[48] Weiss, K.; Beernink, G.; Dötz, F.; Birkner, A.; Müllen, K.; Woll, C. H. *Angew. Chem. Int. Ed.* **1999**, *38*, 3748–3752.

[49] Walker, S. D.; Barder, T. E.; Martinelli, J. R.; Buchwald, S. L. *Angew. Chem. Int. Ed.* **2004**, *43*, 1871–1876.

[50] Barder, T. E.; Walker, S. D.; Martinelli, J. R.; Buchwald, S. L. *J. Am. Chem. Soc.* **2005**, *127*, 4685–4696.

[51] Fujioka, Y. *Bull. Chem. Soc. Jpn.* **1984**, *57*, 3494–3506.

[52] Fujioka, Y. *Bull. Chem. Soc. Jpn.* **1985**, *58*, 481–489.

[53] Termsuksawad, P.; Niyomsoan, S.; Goldfarb, R. B.; Kaydanov, V. I.; Olson, D. L.; Mishra, B.; Gavra, Z. *J. Alloys Compd.* **2004**, *373*, 86–95.

[54] Markovitsi, D.; Germain, A.; Millie, P.; Lecuyer, P.; Gallos, L. K.; Argyrakis, P.; Bengs, H.; Ringsdorf, H. *J. Phys. Chem.* **1995**, *99*, 1005–1017.

[55] Kastler, M. Ph.D. thesis, University of Mainz, 2002.

[56] Ruiz-Morales, Y. *J. Phys. Chem. A* **2002**, *106*, 11283–11308.

[57] Kastler, M.; Schmidt, J.; Pisula, W.; Sebastiani, D.; Müllen, K. *J. Am. Chem. Soc.* **2006**, *128*, 9526–9534.

[58] Maroncelli, M. *J. Mol. Liq.* **1993**, *57*, 1–37.

[59] Fleming, G. R.; Cho, M. H. *Ann. Rev. Phys. Chem.* **1996**, *47*, 109–134.

[60] Horrocks, A. R.; Wilkinso.F, *Proc. R. Soc. London, Ser. A* **1968**, *306*, 257–273.

[61] Hamai, S.; Hirayama, F. *J. Phys. Chem.* **1983**, *87*, 83–89.

[62] Grozema, F. C.; Siebbeles, L. D. A. *Int. Rev. Phys. Chem.* **2008**, *27*, 87–138.

[63] Kline, R. J.; McGehee, M. D. *Polym. Rev.* **2006**, *46*, 27–45.

[64] Robertson, J. M.; White, J. G. *J. Chem. Soc.* **1945**, 607–617.

[65] Desiraju, G.; Gavezzotti, A. *Acta Cryst. B* **1989**, *45*, 473.

[66] Hunter, C. A.; Sanders, J. K. M. *J. Am. Chem. Soc.* **1990**, *112*, 5525–5534.

[67] Hunter, C. A.; Lawson, K. R.; Perkins, J.; Urch, C. J. *J. Chem. Soc. Perkin Trans. 2* **2001**, 651–669.

[68] Skowronski, M.; DeYoreo, J. J.; Wang, C. A. *Perspectives on Inorganic, Organic, and Biological Crystal Growth: From Fundamentals to Applications*; Springer, 2007.

[69] Goddard, R.; Haenel, M. W.; Herndon, W. C.; Kruger, C.; Zander, M. *J. Am. Chem. Soc.* **1995**, *117*, 30–41.

[70] Wang, Z. H.; Dötz, F.; Enkelmann, V.; Müllen, K. *Angew. Chem. Int. Ed.* **2005**, *44*, 1247–1250.

[71] Speier, G. *J. Mol. Catal.* **1986**, *37*, 259–267.

[72] Kuhn, R. *Angew. Chem.* **1954**, *66*, 678–679.

[73] Sakurai, T. *Acta Crystallographica* **1965**, *19*, 320–325.

[74] Michaelis, L.; Granick, S. *J. Am. Chem. Soc.* **1944**, *66*, 1023–1030.

[75] Boden, B. N.; Jardine, K. J.; Leung, A. C. W.; MacLachlan, M. J. *Org. Lett.* **2006**, *8*, 1855–1858.

[76] Hanif, M.; Lu, P.; Li, M.; Zheng, Y.; Xie, Z. Q.; Ma, Y. G.; Li, D.; Li, J. H. *Polym. Int.* **2007**, *56*, 1507–1513.

[77] Speier, G.; Tyeklar, Z.; Toth, P.; Speier, E.; Tisza, S.; Rockenbauer, A.; Whalen, A. M.; Alkire, N.; Pierpont, C. G. *Inorg. Chem.* **2001**, *40*, 5653–5659.

[78] Yamato, T.; Fujimoto, M.; Miyazawa, A.; Matsuo, K. *J. Chem. Soc. Perkin 1* **1997**, 1201–1207.

[79] Zinke, A.; Ott, R.; Sobotka, M.; Kretz, R. *Monatsh. Chem.* **1952**, *83*, 546–548.

[80] Cooper, M. A.; Manatt, S. L. *J. Am. Chem. Soc.* **1969**, *91*, 6325–6333.

[81] Paruch, K.; Vyklicky, L.; Katz, T. J. *Org. Synth.* **2003**, *80*, 227–231.

[82] Paruch, K.; Vyklicky, L.; Wang, D. Z.; Katz, T. J.; Incarvito, C.; Zakharov, L.; Rheingold, A. L. *J. Org. Chem.* **2003**, *68*, 8539–8544.

[83] Calderazzo, F.; Forte, C.; Marchetti, F.; Pampaloni, G.; Pieretti, L. *Helv. Chim. Acta* **2004**, *87*, 781–789.

[84] Langhals, H. *New J. Chem.* **1981**, *5*, 97–99.

[85] Condon, E. *Phys. Rev.* **1926**, *28*, 1182–1201.

[86] Atkins, P. W.; Friedman, R. *Molecular Quantum Mechanics*, 4th ed.; Oxford University Press, 2004.

[87] Nicodem, D. E.; Silva, R. S.; Togashi, D. M.; da Cunha, M. F. V. *J. Photochem. Photobiol., A* **2005**, *175*, 154–158.

[88] Heinze, J. *Angew. Chem. Int. Ed.* **1984**, *23*, 831–847.

[89] Seiwert, B.; Karst, U. *Anal. Bioanal. Chem.* **2008**, *390*, 181–200.

[90] Bond, A. M.; Fletcher, S.; Symons, P. G. *Analyst* **1998**, *123*, 1891–1904.

[91] Bard, A. J.; R., F. L. *Electrochemical Methods. Fundamentals and Applications*, 2nd ed.; Wiley and Sons, 2001.

[92] Wendland, R.; Lalonde, J. *Org. Synth.* **1954**, *34*, 76–78.

[93] Tsao, H. N.; Cho, D.; Andreasen, J. W.; Rouhanipour, A.; Breiby, D. W.; Pisula, W.; Müllen, K. *Adv. Mater.* **2009**, *21*, 209–212.

[94] Soci, C.; Hwang, I. W.; Moses, D.; Zhu, Z.; Waller, D.; Gaudiana, R.; Brabec, C. J.; Heeger, A. J. *Adv. Funct. Mater.* **2007**, *17*, 632–636.

[95] Suzuki, T.; Fujii, H.; Yamashita, Y.; Kabuto, C.; Tanaka, S.; Harasawa, M.; Mukai, T.; Miyashi, T. *J. Am. Chem. Soc.* **1992**, *114*, 3034–3043.

[96] Mukherje.Tk,; Levasseu.La, *J. Org. Chem.* **1965**, *30*, 644–646.

[97] Silverma.J,; Krukonis, A. P.; Yannoni, N. F. *Acta Cryst.* **1967**, *23*, 1057–1063.

[98] Kanakarajan, K.; Czarnik, A. W. *J. Org. Chem.* **1986**, *51*, 5241–5243.

[99] Gearba, R. I.; Lehmann, M.; Levin, J.; Ivanov, D. A.; Koch, M. H. J.; Barbera, J.; Debije, M. G.; Piris, J.; Geerts, Y. H. *Adv. Mater.* **2003**, *15*, 1614–1618.

[100] Wynberg, H.; Sinnige, H. J. M. *Recl. Trav. Chim. Pays-Bas* **1969**, *88*, 1244–1245.

[101] Yamamoto, T.; Zhou, Z. H.; Kanbara, T.; Shimura, M.; Kizu, K.; Maruyama, T.; Nakamura, Y.; Fukuda, T.; Lee, B. L.; Ooba, N.; Tomaru, S.; Kurihara, T.; Kaino, T.; Kubota, K.; Sasaki, S. *J. Am. Chem. Soc.* **1996**, *118*, 10389–10399.

[102] Koch, N. *Chem. Phys. Chem.* **2007**, *8*, 1438–1455.

[103] Shen, Y. L.; Hosseini, A. R.; Wong, M. H.; Malliaras, G. G. *ChemPhysChem* **2004**, *5*, 16–25.

[104] Frubose, C.; Doblhofer, K.; Soares, D. M. *Phys. Chem. Chem. Phys.* **1993**, *97*, 475–478.

[105] Bagus, P. S.; Staemmler, V.; Wöll, C. *Phys. Rev. Lett.* **2002**, *89*, 96104.

[106] Koch, N. *J. Phys.-Condes. Matter* **2008**, *20*, year.

[107] Koch, N.; Duhm, S.; Rabe, J. P.; Vollmer, A.; Johnson, R. L. *Phys. Rev. Lett.* **2005**, *95*, 237601.

[108] Duhm, S.; Heimel, G.; Salzmann, I.; Glowatzki, H.; Johnson, R. L.; Vollmer, A.; Rabe, J. P.; Koch, N. *Nat. Mater.* **2008**, *7*, 326–332.

[109] Gerlach, A.; Sellner, S.; Schreiber, F.; Koch, N.; Zegenhagen, J. *Phys. Rev. B* **2007**, *75*, 45401.

[110] Venables, J. A. *Surf. Sci.* **1994**, *299*, 798–817.

[111] Floro, J. A.; Hearne, S. J.; Hunter, J. A.; Kotula, P.; Chason, E.; Seel, S. C.; Thompson, C. V. *J. Appl. Phys.* **2001**, *89*, 4886–4897.

[112] Mo, Y. W.; Savage, D. E.; Swartzentruber, B. S.; Lagally, M. G. *Phys. Rev. Lett.* **1990**, *65*, 1020–1023.

[113] Müllen, K.; Rabe, J. P. *Acc. Chem. Res.* **2008**, *41*, 511–520.

[114] Yamashita, Y.; Tomura, M. *J. Mater. Chem.* **1998**, *8*, 1933–1944.

[115] Torrance, J. B. *Acc. Chem. Res.* **1979**, *12*, 79–86.

[116] Horiuchi, S.; Yamochi, H.; Saito, G.; Sakaguchi, K.; Kusunoki, M. *J. Am. Chem. Soc.* **1996**, *118*, 8604–8622.

[117] Williams, J. M.; Schultz, A. J.; Geiser, U.; Carlson, K. D.; Kini, A. M.; Wang, H. H.; Kwok, W.-K.; Whangbo, M.-H.; Schirber, J. E. *Science* **1991**, *252*, 1501–1508.

[118] Powell, B. J.; McKenzie, R. H. *J. Phys.: Condens. Matter* **2006**, *18*, R827–R866.

[119] Chi, X.; Besnard, C.; Thorsmolle, V. K.; Butko, V. Y.; Taylor, A. J.; Siegrist, T.; Ramirez, A. P. *Chem. Mater.* **2004**, *16*, 5751–5755.

[120] Radhakrishnan, T. P. *Acc. Chem. Res.* **2008**, *41*, 367–376.

[121] Chappell, J. S.; Bloch, A. N.; Bryden, W. A.; Maxfield, M.; Poehler, T. O.; Cowan, D. O. *J. Am. Chem. Soc.* **1981**, *103*, 2442–2443.

[122] Comes, R. *Chemistry and Physics of One-Dimensional Metals*; Plenum Press: New York, 1977.

[123] Barbara, P. F.; Meyer, T. J.; Ratner, M. A. *J. Phys. Chem.* **1996**, *100*, 13148–13168.

[124] Bauer, E. *Z. Kristallogr.* **1958**, *110*, 372–394.

[125] Nonnenmacher, M.; O'Boyle, M. P.; Wickramasinghe, H. K. *App. Phys. Lett.* **1991**, *58*, 2921–2923.

[126] Foster, E. J.; Jones, R. B.; Lavigueur, C.; Williams, V. E. *J. Am. Chem. Soc.* **2006**, *128*, 8569–8574.

[127] Imai, K.; Kurihara, M.; Mathias, L.; Wittmann, J.; Alston, W. B.; Stille, J. K. *Macromol.* **1973**, *6*, 158–162.

[128] Gao, B.; Wang, M.; Cheng, Y.; Wang, L.; Jing, X.; Wang, F. *J. Am. Chem. Soc* **2008**, *130*, 8297–8306.

[129] Laschat, S.; Baro, A.; Steinke, N.; Giesselmann, F.; Hagele, C.; Scalia, G.; Judele, R.; Kapatsina, E.; Sauer, S.; Schreivogel, A.; Tosoni, M. *Angew. Chem. Int. Ed.* **2007**, *46*, 4832–4887.

[130] Feng, X. L.; Marcon, V.; Pisula, W.; Hansen, M. R.; Kirkpatrick, J.; Grozema, F.; Andrienko, D.; Kremer, K.; Müllen, K. *Nat. Mater.* **2009**, *8*, 421–426.

[131] Kaafarani, B. R.; Lucas, L. A.; Wex, B.; Jabbour, G. E. *Tetrahedron Lett.* **2007**, *48*, 5995–5998.

[132] Arotsky, J.; Butler, R.; Darby, A. C. *J. Chem. Soc. C* **1970**, 1480–1485.

[133] Mandal, P. K.; McMurray, J. S. *J. Org. Chem.* **2007**, *72*, 6599–6601.

[134] Dierksen, M.; Grimme, S. *J. Chem. Phys.* **2004**, *120*, 3544–3554.

[135] Martin, R. B. *Chem. Rev.* **1996**, *96*, 3043–3064.

[136] Heyn, M. P.; Bretz, R. *Biophys. Chem.* **1975**, *3*, 35–45.

[137] Wu, J. S.; Fechtenkötter, A.; Gauss, J.; Watson, M. D.; Kastler, M.; Fechtenkötter, C.; Wagner, M.; Müllen, K. *J. Am. Chem. Soc.* **2004**, *126*, 11311–11321.

[138] Zhao, D. H.; Moore, J. S. *Chem. Comm.* **2003**, 807–818.

[139] Kastler, M.; Pisula, W.; Wasserfallen, D.; Pakula, T.; Müllen, K. *J. Am. Chem. Soc.* **2005**, *127*, 4286–4296.

[140] Frommer, J. *Angew. Chem. Int. Ed.* **1992**, *31*, 1298–1328.

[141] Canas-Ventura, M. E.; Xiao, W.; Wasserfallen, D.; Müllen, K.; Brune, H.; Barth, J. V.; Fasel, R. *Angew. Chem. Int. Ed.* **2007**, *46*, 1814–1818.

[142] Ruffieux, P.; Gröning, O.; Fasel, R.; Kastler, M.; Wasserfallen, D.; Müllen, K.; Gröning, P. *J. Phys. Chem. B* **2006**, *110*, 11253–11258.

[143] Feng, X. L.; Wu, J. S.; Ai, M.; Pisula, W.; Zhi, L. J.; Rabe, J. P.; Müllen, K. *Angew. Chem. Int. Ed.* **2007**, *46*, 3033–3036.

[144] Weigelt, S.; Bombis, C.; Busse, C.; Knudsen, M. M.; Gothelf, K. V.; Laegsgaard, E.; Besenbacher, F.; Linderoth, T. R. *ACS Nano* **2008**, *2*, 651–660.

[145] Yatabe, T.; Harbison, M. A.; Brand, J. D.; Wagner, M.; Müllen, K.; Samori, P.; Rabe, J. P. *J. Mater. Chem.* **2000**, *10*, 1519–1525.

[146] Berner, S.; de Wild, M.; Ramoino, L.; Ivan, S.; Baratoff, A.; Guntherodt, H. J.; Suzuki, H.; Schlettwein, D.; Jung, T. A. *Phys. Rev. B* **2003**, *68*, 115410.

[147] Ma, X. J.; Li, Y. B.; Qiu, X. H.; Zhao, K. Q.; Yang, Y. L.; Wang, C. *J. Mater. Chem.* **2009**, *19*, 1490–1493.

[148] Chabinyc, M. L.; Jimison, L. H.; Rivnay, J.; Salleo, A. *MRS Bull.* **2008**, *33*, 683–689.

[149] Marcus, R. A. *J. Chem. Phys.* **1956**, *24*, 966–978.

[150] Stackhouse, P. J.; Hird, M. *Liq. Cryst.* **2008**, *35*, 597–607.

[151] Pisula, W.; Tomovic, Z.; Simpson, C.; Kastler, M.; Pakula, T.; Müllen, K. *Chem. Mater.* **2005**, *17*, 4296–4303.

[152] Delhaes, P. *Graphite and Precursors (World of Carbon)*; CRC Press, 2000.

[153] Jäckel, F.; Watson, M. D.; Müllen, K.; Rabe, J. P. *Phys. Rev. Lett.* **2004**, *92*, 188303.

[154] Pisula, W.; Tomovic, Z.; Watson, M. D.; Müllen, K.; Kussmann, J.; Ochsenfeld, C.; Metzroth, T.; Gauss, J. *J. Phys. Chem. B* **2007**, *111*, 7481–7487.

[155] Sauvage, J. P.; Collin, J. P.; Chambron, J. C.; Guillerez, S.; Coudret, C.; Balzani, V.; Barigelletti, F.; Decola, L.; Flamigni, L. *Chem. Rev.* **1994**, *94*, 993–1019.

[156] Oregan, B.; Grätzel, M. *Nature* **1991**, *353*, 737–740.

[157] Polo, A. S.; Itokazu, M. K.; Iha, N. Y. M. *Coord. Chem. Rev.* **2004**, *248*, 1343–1361.

[158] Grätzel, M. *Inorg. Chem.* **2005**, *44*, 6841–6851.

[159] Ishow, E.; Gourdon, A.; Launay, J. P. *Chem. Comm.* **1998**, 1909–1910.

[160] Nasielskihinkens, R.; Benedekvamos, M.; Maetens, D.; Nasielski, J. *J. Organomet. Chem.* **1981**, *217*, 179–182.

[161] Bolger, J.; Gourdon, A.; Ishow, E.; Launay, J. P. *Inorg. Chem.* **1996**, *35*, 2937–2944.

[162] Bodige, S.; MacDonnell, F. M. *Tetrahedron Lett.* **1997**, *38*, 8159–8160.

4 Donor-Acceptor Model Systems for Polythiophenes

4.1 Introduction

Conjugated donor-acceptor systems, in which an electron rich and an electron poor moiety are covalently linked within a π system, play a very important role in almost every field of materials research.[1–4] The low bandgap caused by the push-pull effect is the basis for dyes.[5–7] Many applications beyond coloration have emerged in the last years such as organic lasers, data storage, or switching to mention just a few.[8–10] Donor-acceptor substituted π systems, furthermore, interact with optical light non-linearly. Non-linear optics can be used in a variety of ways, for example optical information encoding and routing for telecommunication.[11, 12]

When both donors and acceptors are incorporated into conjugated polymers, low bandgap semiconductors are obtained.[13] These can serve to absorb a higher percentage of the solar spectrum than classical polymers in polymeric solar cells.[14–16] Ambipolar charge transport is often observed in low bandgap polymers enabling the fabrication of light-emitting transistors or CMOS circuits.[17–19]

A detailed understanding of the packing behavior and the electronic structure is of crucial importance for the development of new materials. The polymers themselves are very hard to study in detail as they are semicrystalline substances with low degree of long-range order. Molecular weight dispersity, undefined endgroups, and

occasional structural defects hinder an in-depth study to fully understand the underlying principles of inter- and intramolecular interactions. Defined small molecules resembling the molecular structure of polymers can serve as model systems to study the fundamental phenomena of interest.[20, 21] By extrapolating properties such as the optical gap of a series of oligomers, it is even possible to predict polymer properties.[22] The study of deviations of real polymers from the ideal infinite polymer as derived from oligomer extrapolation can give valuable information about the real system, e.g. the effective conjugation length.[23–25]

In the previous chapter, the efficiency of the α-diketone functionality as electron acceptor has been demonstrated on the coronene core. Furthermore, the comparison of the reduction potentials of phenanthrenequinone and benzo[2,1-b;3,4-b']dithiophene-5,6-dione (**36**), which have been measured by cyclic voltammetry under identical conditions, reveal that sulfur atoms increase the acceptor strength of the α-diketone functionlized molecule. This knowledge shall be used to design donor-acceptor systems and to investigate their packing behavior in detail. This is particularly relevant due to the fact that thiophene containing donor-acceptor polymers play an important role as active materials in organic electronics.[26–29] The benzodithiophene-dione (**36**) building block resembles a polythiophene chain if additional thiophene units are attached as donors such that a good conjugation between the donor and the acceptor is established.

The quinoid structure of **36** is quite similar to acceptors which have proven to be very effective for organic electronics. In particular, benzothiadiazole serves as an acceptor in conjugated polythiophenes showing high field-effect mobilities and good solar cell performances.[30, 31] α-Diketones can be converted into thiadiazoles, as well as a variety of other important structures.[32–34] The stable redox behavior and high crystallization tendency make **36** an attractive molecule for detailed investigations.

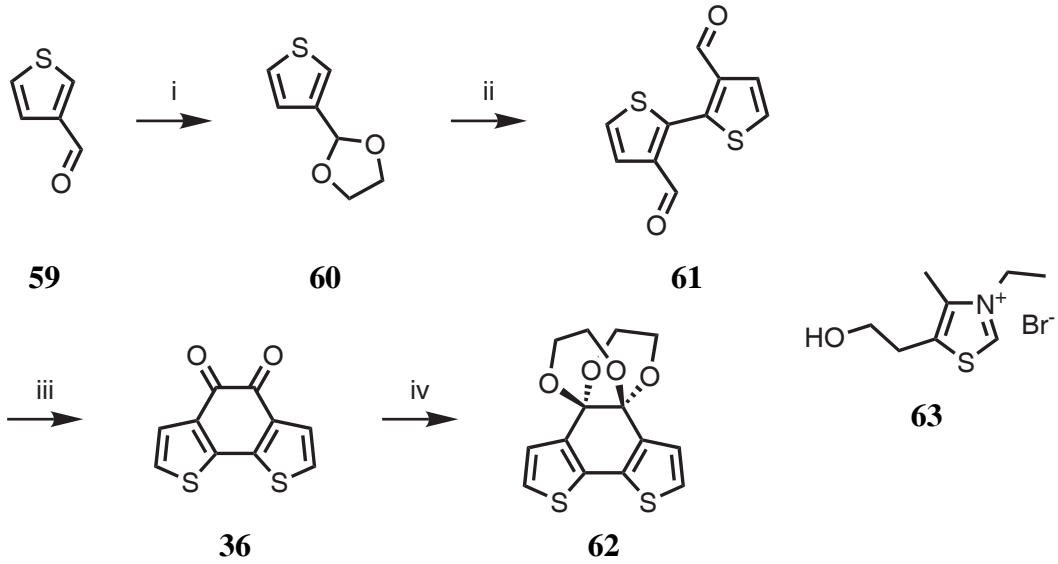

Figure 4.1: Synthesis of ethylene glycol proteced benzo[2,1-b;3,4-b']dithiophene-5,6-dione. Conditions: *i* ethylene glycol, toluene sulfonic acid, toluene, reflux, 90 %; *ii* 1. BuLi, THF, -78 °C 2. $CuCl_2$, -78 °C 3. HCl, RT, 53 %; *iii* 1. thiamine (**63**), DMF, triethylamine, 80 °C 2. O_2, RT, 85 %; *iv* ethylene glycol, trimethylchlorosilane, RT, 59 %.

4.2 Synthesis

4.2.1 Benzo[2,1-b;3,4-b']dithiophene-5,6-dione

For the synthesis of benzo[2,1-b;3,4-b']dithiophene-5,6-dione (**36**) the dithiophene-dialdehyde **61** is needed. It is accessible as described in the literature starting from 3-thiophenecarbaldeyhde (**59**).[35] After protection with ethylene glycol to allow lithiation, it is oxdiatively coupled by treating the lithiated species of **60** with anhydrous copper(II) chloride at -78 °C. Copper traces are difficult to remove from the product, but the aldehydes formed upon workup do not tolerate other methods such as iron(III) acetylacetonate.[36]

The conversion of dialdehyde **61** into **36** by an intramolecular benzoin condensation with subsequent oxidation of the benzoin to the diketone is described in the literature.[37] According to this experimental procedure, dialdehyde **61** is refluxed in ethanol in the presence of sodium cyanide and air. Only trace amounts of **36**

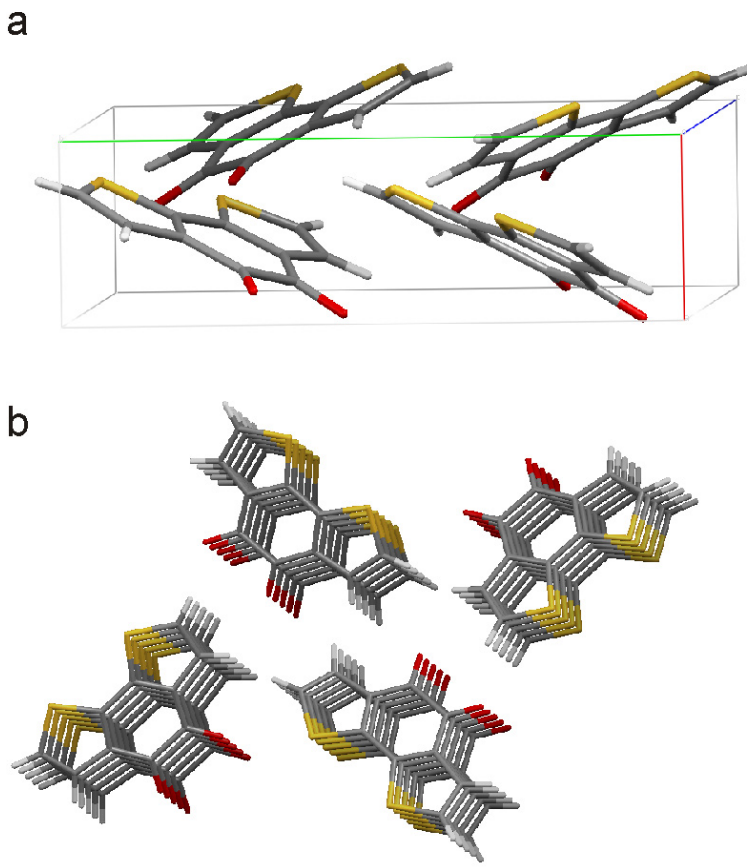

Figure 4.2: Crystal structure of benzo[2,1-b;3,4-b']dithiophene-5,6-dione (**36**), **a.** unit cell, **b.** view along the stacking axis showing five layers.

could be obtained in this way, the ^{1}H-NMR spectrum reveals the presence of many side products.

The group of Prof. W. You at the University of North Carolina has developed a better experimental procedure. Dithiophene-dialdehyde **61** is dissolved in anhydrous DMF under argon. Small amounts of thiamine (**63**) and triethylamine are added catalyzing the benzoin condensation at slightly elevated temperatures (80 °C).[38] Atmospheric oxygen is not allowed to come in contact with the substance before completion of the benzoin condensation. The solution is cooled down to room temperature and air is blown through, whereupon it turns red. After two hours, the product precipitates and can be collected by filtration. By this separation of benzoin condensation and oxidation, the reaction yield reaches 70 %.

Crystallization of **36** from THF affords single crystals suitable for X-ray analysis.

The crystal structure is depicted in Figure 4.2. The molecule forms stacks in which one molecule is positioned right on top of the other, which is surprising due to the unfavorable dipolar interactions of the diketone groups. The structurally similar pyrene-4,5-dione, in contrast, stacks antiparallel to the α-diketone function such that the dipoles exhibit attractive forces.[39] In the present case, the sulfur atoms can come in close contact which could be the reason for this assembly. The interlayer distance of two molecules is 3.45 Å, a typical distance in sulfur containing polycyclic aromatic hydrocarbons.[40–42]

Close contact between sulfur atoms can be found in this crystal between stacks as well. The stacks stand in contact to each other such that the sulfur atoms approach each other pairwise with an S-S distance of 3.4 Å. An increase in the lattice energy is the consequence leading to a high melting point (280 °C) and low solubility. Phenanthrenequinone, in comparison, already melts at 205 °C.[43] The molecular planes of neighboring stacks form an angle of 58°, a classical angle which is found in many polycyclic aromatic hydrocarbons.[44] The quadrupolar interactions are most likely to cause this tilt angle.[45]

For further chemical modifications in the α-position of the thiophene, the α-diketone function needs to be protected. Ethylene glycol is a stable protection group which does not need redox reactions. The typical reductive alkylation or silylation is often accompanied by side reactions upon cleavage.[46, 47] The protection works very well when **36** is treated with trimethylchlorosilane in anhydrous ethylene glycol.[48] The trimethylchlorosilane removes the water and thereby liberates hydrochloric acid which catalyzes the reaction. This method is so effective that the reaction runs at room temperature without side product formation.

The bisdioxane protected benzodithiophene **62** crystallizes very well, forming crystals of extended size in all three dimensions. For this reason, the crystal structure could be easily elucidated by X-ray diffraction analysis. Figure 4.3 shows the packing in the crystal. It can be clearly seen that the ethylene glycols bridge the

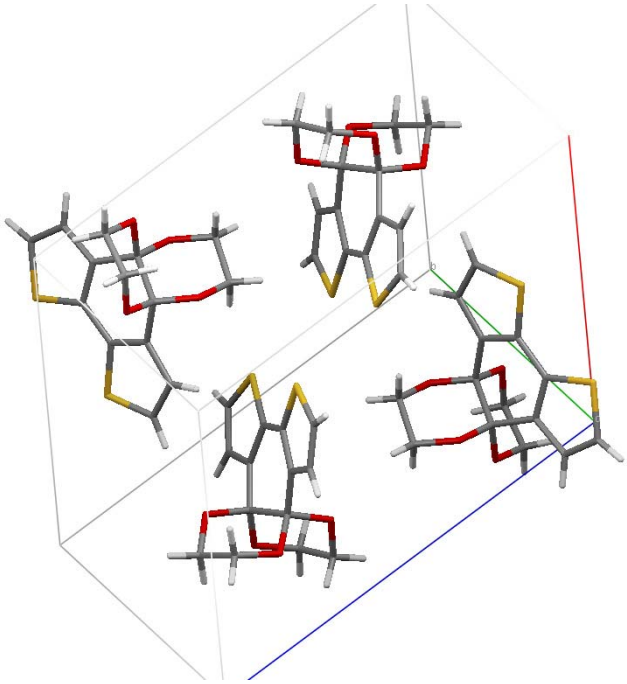

Figure 4.3: Crystal structure of the ethylene glycol protected benzodithiophene-dione **62**.

two diketones forming two six-membered rings. Occasionally, people draw structures with two five-membered rings formed by ethylene glycol reacting with both hydroxyl groups on one ketone.[49] This structure can clearly be ruled out in the present case.

The steric demand of the bis-dioxane moiety has a dramatic effect on the packing behavior. No stacks of parallel discs can be found anymore, reflecting the reduced tendency to form needles. In fact, the molecule readily forms crystals with about equal distances in all directions, the ideal case for crystal structure analysis. The aliphatic parts of the molecules are directed towards each other, the aromatic parts are as well. This is a typical case of microphase separation. The close contact of the sulfur atoms, however, is encountered once again. The two sulfur atoms of each molecule stand in contact with the two sulfur atoms of the neighboring molecule with a distance of 3.55 Å.

The absence of $\pi - \pi$ interactions due to the steric demand of the dioxane rings dramatically decreases the lattice energy of the crystal. A much higher solubility in

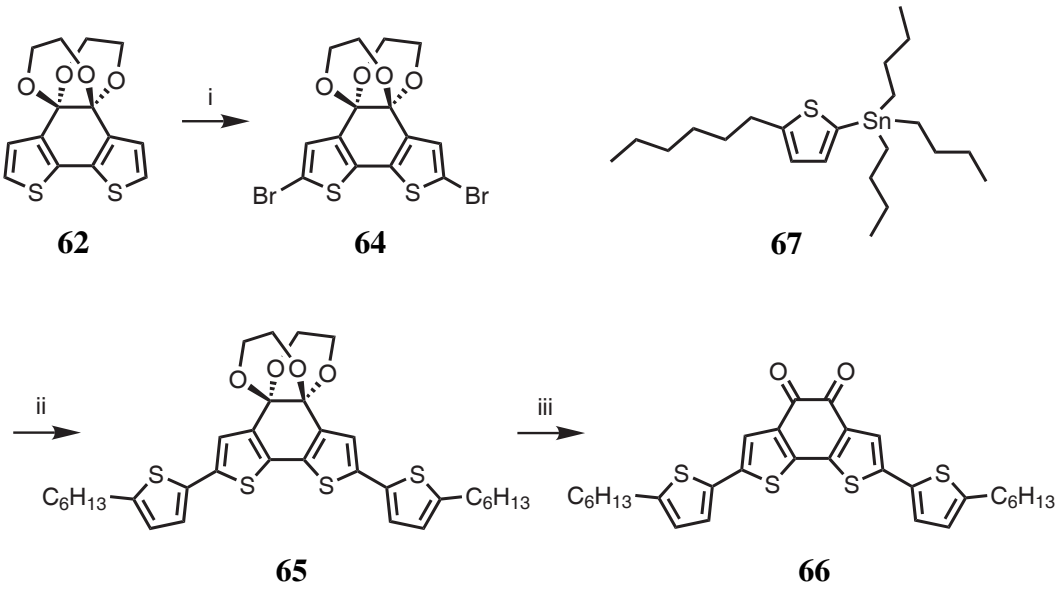

Figure 4.4: Attachment of thiophene and deprotection of the α-diketone. Conditions: *i* NBS, DMF, RT, 56 %; *ii* **67**, $Pd(PPh_3)_4$, DMF, 100 °C, 86 %; *iii* HBF_4, DCM-THF 2:1, RT, 82 %.

comparison to the unprotected benzodithiophene-dione (**36**) underlines this observation.

4.2.2 Attachment of Additional Thiophenes

For the attachment of an electron-rich thiophene unit, the two α positions need to be functionalized by bromine to make them accessible for coupling reactions. This can be done with N-bromosuccinicimide (NBS) in DMF at room temperature to yield the dibrominated molecule **64**. The reaction time and the concentration needed to be optimized to avoid decompositon of the molecule. Too long reaction times or too high concentrations reduce the reaction yields significantly.

Subsequently, a Stille reaction is performed on **64** with 2-hexyl-5-tributylstannyl-thiophene (**67**) to afford compound **65**. The hexyl chains are introduced to better resemble the donor-acceptor polymers which need the alkyl chains for solubility and to aid the assembly process. The reaction works best in DMF at 100 °C with

$Pd(PPh_3)_4$ as catalyst. Longer reaction times reduce the yields, most likely due to decomposition of the molecule under the reaction conditions.

To obtain the target compound (**66**), the protection group needs to be removed. For this purpose, perchloric acid or *p*-toluenesulfonic acid have been used in the literature.[48, 49] Nevertheless, the molecule decomposes under these conditions. The non-oxidizing trifluoroboronic acid, instead, removes the protective groups effectively. It is worth mentioning that the reaction only proceeds in a 2:1 mixture of dichloromethane-THF. The pristine solvents each leave the reagent (**65**) unaffected even after several days. This effect is definitely not a consequence of solubility because **65** dissolves well in both solvents and also in mixtures thereof.

A deep blue compound is obtained showing an efficient donor-acceptor character of the molecule by eye. It is well soluble in common solvents such as THF or dichloromethane. The compound can even be purified by preparative column chromatography which is rarely the case for molecules with α-diketones. The alkyl chains reduce the melting point by 130 °C compared to the unsubstituted benzo[2,1-b;3,4-b']dithiophene-5,6-dione (**36**) (i.e. from 280 °C to 150 °C).

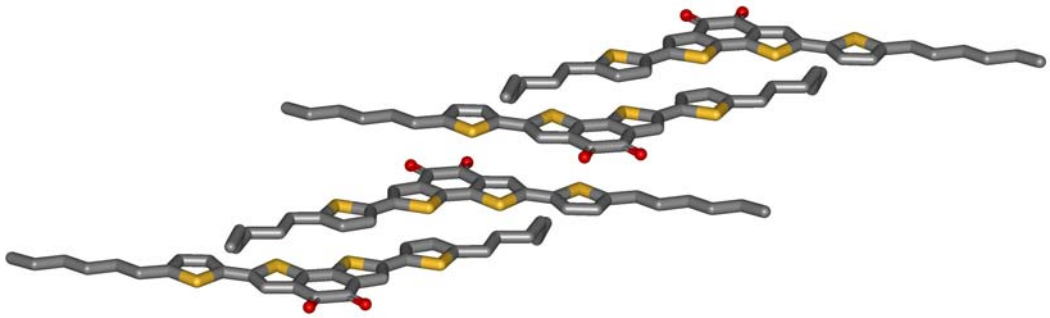

Figure 4.5: Crystal structure of bis(5-hexylthiophene-2-yl-)benzo[2,1-b;3,4-b']dithiophene-5,6-dione **66**.

4.3 Donor-Acceptor Interaction

4.3.1 Crystal Structure

The big advantage of small molecules over polymers is the possibility to get material of very high purity and to grow crystals for structure analysis. In-depth analysis of molecular arrangements and effects due to substitution can be done to gain a good understanding of intra- and intermolecular interactions of particular systems.[50–52]

Single crystals of compound **66** have been grown by slow evaporation of a dichloromethane solution. Small needles deposit on the glass which suffice for X-ray diffraction analysis. Figure 4.5 shows the corresponding crystal structure.

The striking feature of this structure is the fact that the electron poor benzodithiophene-dione unit is sandwiched by electron-rich thiophenes. This suggests that the crystallization process is dominated by intermolecular charge-transfer interactions. Four observations support this thesis:

1. No microphase separation. Normally, rod-like thiophene oligomers with pending alkyl chains prefer an arrangement in which the alkyl chains separate from the aromatic core to avoid unfavorable interactions.[53–55] Here, many contacts between alkyl chains and aromatic moieties are formed.

2. Unfavorable alkyl chain conformation. In the present case, half of the alkyl chains adopt a gauche conformation to allow the donor-acceptor interaction. In

most crystals, all-trans conformations are observed which is the energy minimum for the alkyl chain as no steric repulsions are present.[56]

3. Low $\pi - \pi$ distances. The planes including the aromatic system of a molecule are separated by 3.5 Å. This is a relatively low distance, most conjugated donor-acceptor polymer do not come closer than 3.7 Å.[57, 58] Coloumb attraction after the partial charge transfer brings the planes close together increasing the overlap integral of adjacent molecules.

4. No sulfur-sulfur contacts. The thiophene unit is located on top of the quinodized benzene ring, the sulfur-sulfur distances exceed the interplanar distances significantly. This can be regarded as further hint for a charge-transfer dominated structure formation. Also, between the depicted stacks, there are no close sulfur-sulfur contacts which is usually the case as described above. The thiophene rings are even close to an alkyl chain which is obviously the price for the donor-acceptor stacking.

These four arguments strongly support the thesis of a charge-transfer dominated crystallization. All of the observations above are energetically unfavorable thus a strong driving force for the packing is needed. The formation of a charge-transfer complex is likely to afford this energy.

4.3.2 Electronic Structure

Charge-transfer interactions can be best evidenced by UV-vis absorption spectra. If the donor partially transfers electron density to the acceptor, transitions at long wavelength occur due to transistions from the HOMO-1 to the partially depopulated HOMO in the donor or from the partially occupied LUMO to the LUMO+1 level in the acceptor.[59] The charge-transfer interactions in solution are concentration dependent. At low concentrations the tendency to form dimers is reduced for entropic reasons (compare section 3.7 on page 78).[60]

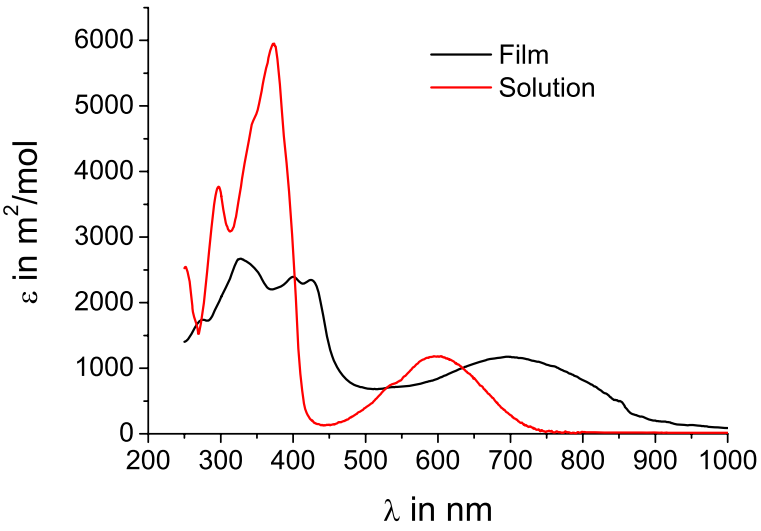

Figure 4.6: UV-vis absorption spectra of compound **66** in solution (cyclohexane, 10^{-5} M) and in film.

Figure 4.6 shows the UV-vis absorption spectrum of the hexylthienyl substituted benzodithiophene-dione (**66**). It has been recorded in solution at low concentrations (*i.e.* 10^{-5} M) in cyclohexane (red curve). A broad peak at about 600 nm is visible accounting for the blue color of the compound. The onset of this peak is located at 730 nm which demonstrates the potent intramolecular donor-acceptor character of this compound. No significant changes can be observed when changing the polarity of the solvent from cyclohexane over THF to acetone. Only chlorinated solvents such as dichloromethane or dichlorobenzene shift the band by 30 nm. Solvation effects of this order are not unusual.[61]

In the film absorption spectrum of **66** (black curve in Figure 4.6), a charge-transfer band appears at 700 nm with an onset beyond 900 nm. As the donor and the acceptor are in very close distance as revealed by the crystal structure, a charge-transfer complex formation is very likely. The bands at lower wavelengths have become broader, but are not shifted, so artifacts due to measurement mistakes can be excluded. Furthermore, the absorption band at long wavelengths in the film is more intense with regard to the short wavelength bands supporting the presence of

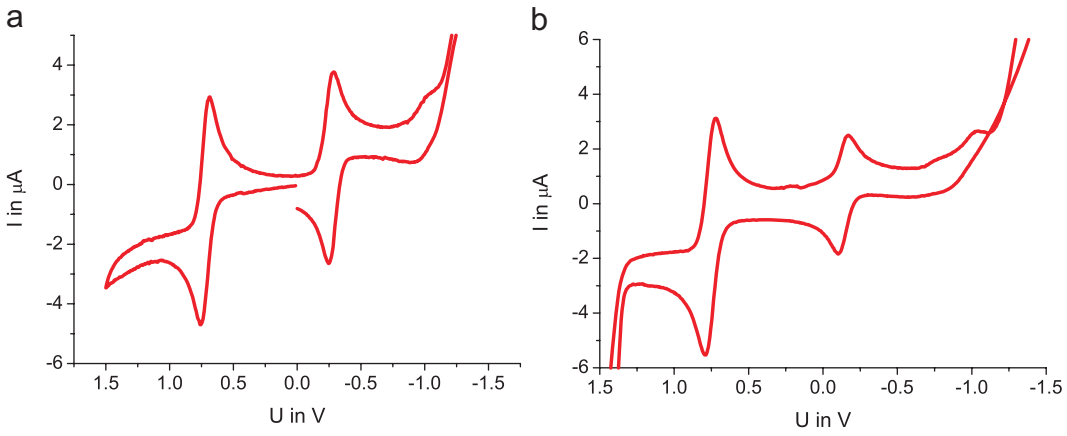

Figure 4.7: Cyclovoltagrames of **a.** benzodithiophene-dione (**36**) and **b.** hexylthiophene substituted benzodithiophene-dione **66**, both measured in DMF with Bu_4NClO_4 as electrolyte and ferrocene as internal standard, voltage plotted against NHE.

a charge transfer. This means that the assembly of molecule **66** is, in fact, driven by charge-transfer interactions rather than the typical microphase separation or the sulfur-sulfur interactions. Even more, the charge-transfer interaction overcompensate the latter two.

In order to better understand the intramolecular donor-acceptor interaction the electronic levels are explored by cyclovoltammetry. To compare the effect of the substitution, benzodithiophene-dione **36** is measured as reference. The substances are dissolved at 1 mM in DMF with Bu_4NClO_4 as electrolyte and ferrocene as internal standard. The results are depicted in Figure 4.7.

The first reduction peaks for both substances are practically identical at -0.85 V against ferrocene, translating to 0.22 V against the normal hydrogen electrode. This means that the LUMO level of benzodithophene-dione is unaffected by substitution with the electron rich thiophene, although it is conjugated and even coplanar in the solid.

The oxidation potential is not accessible in the cyclovoltammetry apparatus used because solvent oxidation sets in before. Ultra-dry conditions are needed to prevent this effect and access oxidation potentials beyond 1.5 V against NHE.[62, 63] Nevertheless, from the optical absorption spectrum, it can be concluded that the

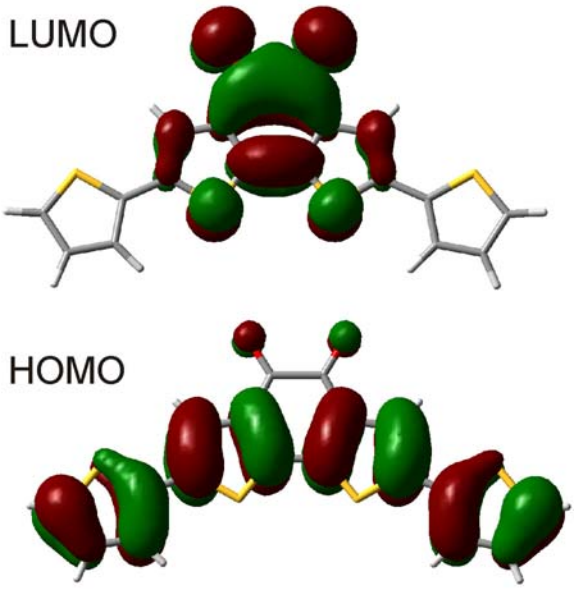

Figure 4.8: Electron density maps as calculated by DFT (B3LYP method, 6-31G basis).

HOMO level is strongly affected by the substitution. Benzodithiophene-dione **36** is a red compound, upon substitution to **66** it turns to a blue compound, so a strong intramolecular push-pull effect is obviously present.

Density functional theory calculations have been performed to resolve the question why the HOMO is so strongly affected by substitution, but the LUMO is not. The electron density surfaces of the corresponding orbitals are depicted in Figure 4.8. The hexyl chains are left out because they are not expected to significantly contribute to the electron density of the frontier orbitals which are typically located exclusively on the aromtatic backbone of the molecule.

It can be seen very clearly that the LUMO orbital is exclusively located on the central benzodithiophene-dione unit, and the thiophene does not contribute. The high electron affinity of the α-diketone dominates the LUMO, but the electron deficiency is restricted to the benzodithiophene. The further the carbon atoms are away from the carbonyl atoms, the lower the orbital coefficients on that particular atom. The smallest value is found at the connection to the electron rich thiophenes, which therefore does not contribute to the LUMO.

The contrary is true for the HOMO. Practically no contribution comes from the carbonyl atoms, but roughly equal coefficients are encountered for the remaining carbon atoms. The HOMO almost resembles a tetrathiophene with regard to the orbital coefficients at the carbon atoms. An interesting feature is found when comparing the orbital coefficints at the sulfur atoms. They are non-zero in the electron rich thiophenes, but zero in the electron poor benzodithiophene. This means that the sulfur acts as an electron acceptor rather than a donor which might be expected from the lone pair contributing to the aromatic ring, at least when only looking at the frontier orbitals.

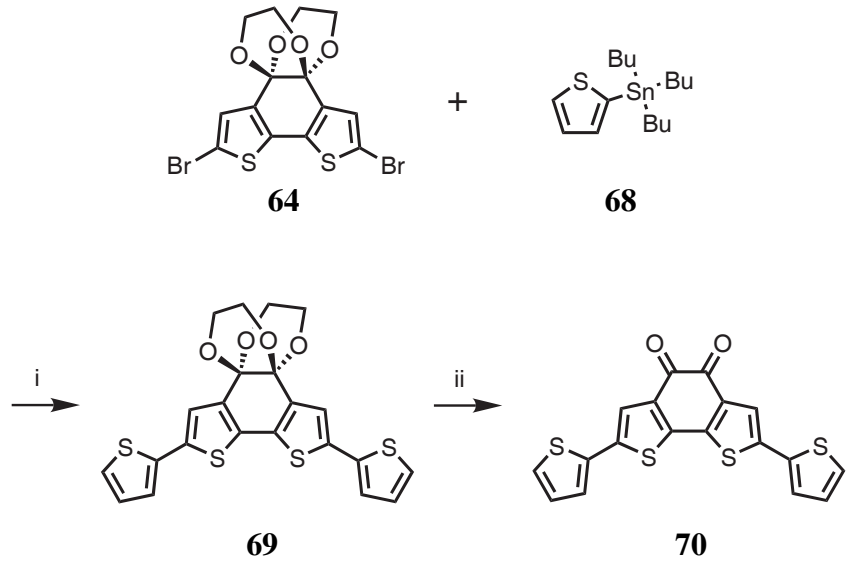

Figure 4.9: Synthesis of thiophene substituted benzodithiophene-dione without alkyl chains. Conditions: *i* $Pd(PPh_3)_4$, DMF, 100 °C, 59 %; *ii* HBF_4, DCM-THF 2:1, RT, 81 %.

4.4 Alkyl Chain Effect

A very important question for the donor-acceptor model system **66** is the influence of the alkyl chains. In the polymers they are needed for the solubility, but often the length and the type of chain (*i.e.* linear or branched) have a dramatic influence on device performances.[64–66] In the present case, the alkyl chain may also have a dominant influence on the molecular packing. To resolve this issue, a model compound without alkyl chains has been synthesized in analogy to compound **66** (see Figure 4.9). The ethylene glycol protected and bromine functionalized benzodithiophene-dione (**64**) is reacted in a Stille coupling reaction with tributylstannylthiophene to yield the dithienyl derivative **69**. Treatment with tetrafluoroboronic acid as for the alkylated analog **65** yields the thiophene substituted benzodithiophene-dione (**70**).

The compound is much less soluble than the alkylated one as expected. The electronic structure is unlikely to change, the deep blue color is again encountered. The melting point has gone up to 292 °C, but it is only gradually above the unsubstituted benzodithiophene-dione (**62**).

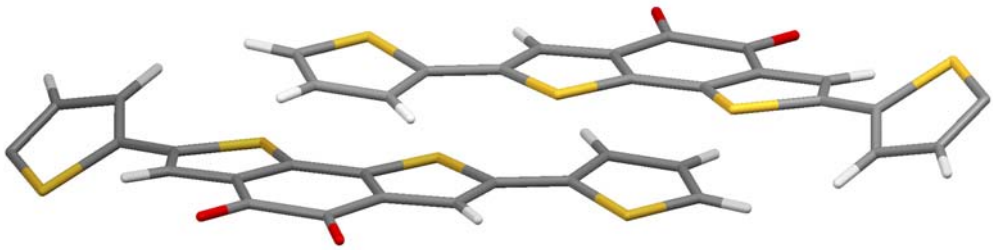

Figure 4.10: Crystal structure of thiophene substituted benzodithophene-dione (**69**).

Obtaining single crystals of compound **70** suitable for X-ray analysis is much harder. The molecule tends to form thin needles. Neverless, slow evaporation from a THF solution in a silanized glass tube yields a few crystals of sufficient quality to obtain the crystal structure, which is depicted in Figure 4.10.

The molecular assembly in this case is a bit more complex. Nevertheless, a clear preference of the donor-acceptor stacking is found again. The molecules stack pairwise such that the electron rich thiophene of the one molecule is placed on top of the electron-deficient benzodithiophene-dione of the next molecule and vice versa. Charge-transfer interactions are, therefore, present once again. In this crystal, the thiophene not involved in the charge-transfer interaction is rotated out of the aromatic plane of the rest of the molecule reducing the degree of conjugation. This is an unfavorable situation as the molecules in the crystal are less stabilized by electron delocalization in the π system. Once again, the dominating effect of the charge transfer on the crystal structure formation is demonstrated. Close sulfur-sulfur distances do not play a role in the present system similar to the alkylated molecule (**65**).

The distance between the planes including the aromatic systems of the two molecules stacking on top of each other is remarkably low. It is only 3.2 Å being even less than in graphite (3.3 Å).[67] In the alkylated analog (**66**) the distance

of adjacent molecules is 3.5 Å, so the alkyl chains significantly hinder the close contact of adjacent molecules. For a high charge-carrier mobility, a close distance of neighboring molecules is highly desirable.[68–70] In conjugated polymers, however, solubility goes down when the aromatic chains come in very close distance.

An optimal compromise between solubility and close contact has to be found. In donor-acceptor systems as the one presented here, the charge-transfer interactions bringing the molecular planes close together have to be included into the considerations. The alkyl chains drive this close packing apart, but the assembly is still closer than in systems built up of monomers of equal electron affinity. Special attention has to be paid to the positioning of these alkyl chains. The example presented here has a moderate effect on the interplanar distances, much larger effects can be observed when the steric demand further increases such as in fluorene where the alkyl chains spread out of the aromatic plane. $\pi - \pi$ distances exceeding 4 Å can be the consequence.[71, 72]

4.5 Bibliography

[1] Meier, H. *Angew. Chem. Int. Ed.* **2005**, *44*, 2482–2506.

[2] Reed, A. E.; Curtiss, L. A.; Weinhold, F. *Chem. Rev.* **1988**, *88*, 899–926.

[3] Braga, D.; Grepioni, F.; Desiraju, G. R. *Chem. Rev.* **1998**, *98*, 1375–1405.

[4] Shirota, Y. *J. Mater. Chem.* **2000**, *10*, 1–25.

[5] Zollinger, H. *Color Chemistry: Syntheses, Properties and Applications of Organic Dyes and Pigments*, 2nd ed.; Wiley-VCH, 1991.

[6] Herrmann, A.; Müllen, K. *Chem. Lett.* **2006**, *35*, 978–985.

[7] Mishra, A.; Behera, R. K.; Behera, P. K.; Mishra, B. K.; Behera, G. B. *Chem. Rev.* **2000**, *100*, 1973–2011.

[8] Rettig, W. *Angew. Chem. Int. Ed.* **1986**, *25*, 971–988.

[9] Mustroph, H.; Stollenwerk, M.; Bressau, V. *Angew. Chem. Int. Ed.* **2006**, *45*, 2016–2035.

[10] Petty, M. C.; Petty, M. *Molecular Electronics: From Principles to Practice*, 1st ed.; Wiley and Sons, 2007.

[11] Marder, S. R.; Kippelen, B.; Jen, A. K. Y.; Peyghambarian, N. *Nature* **1997**, *388*, 845–851.

[12] Segura, J. L.; Martin, N. *J. Mater. Chem.* **2000**, *10*, 2403–2435.

[13] Kroon, R.; Lenes, M.; Hummelen, J. C.; Blom, P. W. M.; De Boer, B. *Polym. Rev.* **2008**, *48*, 531–582.

[14] Thompson, B. C.; Frechet, J. M. J. *Angew. Chem. Int. Ed.* **2008**, *47*, 58–77.

[15] Brabec, C. J.; Durrant, J. R. *MRS Bull.* **2008**, *33*, 670–675.

[16] Dennler, G.; Scharber, M. C.; Brabec, C. J. *Adv. Mater.* **2009**, *21*, 1323–1338.

[17] Melzer, C.; von Seggern, H. *IT-Inf. Technol.* **2008**, *50*, 158–166.

[18] Cornil, J.; Bredas, J. L.; Zaumseil, J.; Sirringhaus, H. *Adv. Mater.* **2007**, *19*, 1791–1799.

[19] Zaumseil, J.; Sirringhaus, H. *Chem. Rev.* **2007**, *107*, 1296–1323.

[20] Martin, R. E.; Diederich, F. *Angew. Chem. Int. Ed.* **1999**, *38*, 1350–1377.

[21] van Hutten, P. F.; Krasnikov, V. V.; Hadziioannou, G. *Acc. Chem. Res.* **1999**, *32*, 257–265.

[22] Gierschner, J.; Cornil, J.; Egelhaaf, H. J. *Adv. Mater.* **2007**, *19*, 173–191.

[23] de Melo, J. S.; Silva, L. M.; Arnaut, L. G.; Becker, R. S. *J. Chem. Phys.* **1999**, *111*, 5427–5433.

[24] Chang, R.; Hsu, J. H.; Fann, W. S.; Liang, K. K.; Chiang, C. H.; Hayashi, M.; Yu, J.; Lin, S. H.; Chang, E. C.; Chuang, K. R.; Chen, S. A. *Chem. Phys. Lett.* **2000**, *317*, 142–152.

[25] Otto, P.; Gu, F. L.; Ladik, J. *J. Chem. Phys.* **1999**, *110*, 2717–2726.

[26] Facchetti, A. *Mater. Today* **2007**, *10*, 28–37.

[27] Ong, B. S.; Wu, Y. L.; Li, Y. N.; Liu, P.; Pan, H. L. *Chem. Eur. J.* **2008**, *14*, 4766–4778.

[28] Li, L. G.; Lu, G. H.; Yang, X. N.; Zhou, E. L. *Chin. Sci. Bull.* **2007**, *52*, 145–158.

[29] de Boer, B.; Facchetti, A. *Polym. Rev.* **2008**, *48*, 423–431.

[30] Zhang, M.; Tsao, H. N.; Pisula, W.; Yang, C. D.; Mishra, A. K.; Müllen, K. *J. Am. Chem. Soc.* **2007**, *129*, 3472–3473.

[31] Soci, C.; Hwang, I. W.; Moses, D.; Zhu, Z.; Waller, D.; Gaudiana, R.; Brabec, C. J.; Heeger, A. J. *Adv. Funct. Mater.* **2007**, *17*, 632–636.

[32] Conte, G.; Bortoluzzi, A. J.; Gallardo, H. *Synthesis* **2006**, 3945–3947.

[33] Schiedt, B. *J. Prakt. Chem.* **1941**, *157*, 203–224.

[34] Batanero, B.; Barba, F. *Org. Lett.* **2005**, *7*, 2567–2569.

[35] Gallazzi, M. C.; Toscano, F.; Paganuzzi, D.; Bertarelli, C.; Farina, A.; Zotti, G. *Macromol. Chem. Phys.* **2001**, *202*, 2074–2085.

[36] Nishide, Y.; Osuga, H.; Saito, M.; Aiba, T.; Inagaki, Y.; Doge, Y.; Tanaka, K. *J. Org. Chem.* **2007**, *72*, 9141–9151.

[37] Wynberg, H.; Sinnige, H. J. M. *Recl. Trav. Chim. Pays-Bas* **1969**, *88*, 1244–1245.

[38] Enders, D.; Balensiefer, T. *Acc. Chem. Res.* **2004**, *37*, 534–541.

[39] Wang, Z. H.; Enkelmann, V.; Negri, F.; Müllen, K. *Angew. Chem. Int. Ed.* **2004**, *43*, 1972–1975.

[40] Takimiya, K.; Ebata, H.; Sakamoto, K.; Izawa, T.; Otsubo, T.; Kunugi, Y. *J. Am. Chem. Soc.* **2006**, *128*, 12604–12605.

[41] Gao, J. H.; Li, L. Q.; Meng, Q.; Li, R. J.; Jiang, H.; Li, H. X.; Hu, W. P. *J. Mater. Chem.* **2007**, *17*, 1421–1426.

[42] Okamoto, T.; Kudoh, K.; Wakamiya, A.; Yamaguchi, S. *Chem. Eur. J.* **2007**, *13*, 548–556.

[43] Patrick, T. B.; Lefaivre, M. H.; Koertge, T. E. *J. Org. Chem.* **1976**, *41*, 3413–3415.

[44] Desiraju, G.; Gavezzotti, A. *Acta Cryst. B* **1989**, *45*, 473.

[45] Hunter, C. A.; Lawson, K. R.; Perkins, J.; Urch, C. J. *J. Chem. Soc. Perkin Trans. 2* **2001**, 651–669.

[46] Paruch, K.; Vyklicky, L.; Katz, T. J. *Org. Synth.* **2003**, *80*, 227–231.

[47] Ciszek, J. W.; Tour, J. M. *Tetrahedron Lett.* **2004**, *45*, 2801–2803.

[48] Kozaki, M.; Sugimura, K.; Ohnishi, H.; Okada, K. *Org. Lett.* **2006**, *8*, 5235–5238.

[49] Shirai, Y.; Osgood, A. J.; Zhao, Y. M.; Yao, Y. X.; Saudan, L.; Yang, H. B.; Chiu, Y. H.; Alemany, L. B.; Sasaki, T.; Morin, J. F.; Guerrero, J. M.; Kelly, K. F.; Tour, J. M. *J. Am. Chem. Soc.* **2006**, *128*, 4854–4864.

[50] Evans, O. R.; Lin, W. B. *Acc. Chem. Res.* **2002**, *35*, 511–522.

[51] Aakeroy, C. B. *Acta Cryst. B* **1997**, *53*, 569–586.

[52] Braga, D.; Brammer, L.; Champness, N. R. *CrystEngComm* **2005**, *7*, 1–19.

[53] Ebata, H.; Izawa, T.; Miyazaki, E.; Takimiya, K.; Ikeda, M.; Kuwabara, H.; Yui, T. *J. Am. Chem. Soc.* **2007**, *129*, 15732–15733.

[54] Garnier, F.; Yassar, A.; Hajlaoui, R.; Horowitz, G.; Deloffre, F.; Servet, B.; Ries, S.; Alnot, P. *J. Am. Chem. Soc.* **1993**, *115*, 8716–8721.

[55] Gao, P.; Beckmann, D.; Tsao, H. N.; Feng, X.; Enkelmann, V.; Baumgarten, M.; Pisula, W.; Müllen, K. *Adv. Mater.* **2008**, *21*, 213–216.

[56] Sozzani, P.; Bovey, F. A.; Schilling, F. C. *Macromol.* **1991**, *24*, 6764–6768.

[57] Yamamoto, T.; Zhou, Z. H.; Kanbara, T.; Shimura, M.; Kizu, K.; Maruyama, T.; Nakamura, Y.; Fukuda, T.; Lee, B. L.; Ooba, N.; Tomaru, S.; Kurihara, T.; Kaino, T.; Kubota, K.; Sasaki, S. *J. Am. Chem. Soc.* **1996**, *118*, 10389–10399.

[58] Tsao, H. N.; Cho, D.; Andreasen, J. W.; Rouhanipour, A.; Breiby, D. W.; Pisula, W.; Müllen, K. *Adv. Mater.* **2009**, *21*, 209–212.

[59] Barbara, P. F.; Meyer, T. J.; Ratner, M. A. *J. Phys. Chem.* **1996**, *100*, 13148–13168.

[60] Newton, M. *Electron Transfer in Chemistry*; Wiley-VCH: New York, 2001.

[61] Bayliss, N. S. *J. Chem. Phys.* **1950**, *18*, 292–296.

[62] Heinze, J. *Angew. Chem. Int. Ed.* **1984**, *23*, 831–847.

[63] Hammeric.O,; Parker, V. D. *Electrochim. Acta* **1973**, *18*, 537–541.

[64] Kaneto, K.; Lim, W. Y.; Takashima, W.; Endo, T.; Rikukawa, M. *Jpn. J. Appl. Phys.* **2000**, *39*, L872–L874.

[65] Kuo, C. T.; Weng, S. Z.; Huang, R. L. *Synth. Met.* **1997**, *88*, 101–107.

[66] Torsi, L.; Tanese, M. C.; Cioffi, N.; Gallazzi, M. C.; Sabbatini, L.; Zambonin, P. G.; Raos, G.; Meille, S. V.; Giangregorio, M. M. *J. Phys. Chem. B* **2003**, *107*, 7589–7594.

[67] Delhaes, P. *Graphite and Precursors (World of Carbon)*; CRC Press, 2000.

[68] Marcus, R. A. *J. Chem. Phys.* **1956**, *24*, 966–978.

[69] Vissenberg, M.; Matters, M. *Phys. Rev. B* **1998**, *57*, 12964–12967.

[70] Emin, D. *Adv. Phys.* **1975**, *24*, 305–348.

[71] Kim, J. S.; Ho, P. K. H.; Murphy, C. E.; Friend, R. H. *Macromol.* **2004**, *37*, 2861–2871.

[72] Donley, C. L.; Zaumseil, J.; Andreasen, J. W.; Nielsen, M. M.; Sirringhaus, H.; Friend, R. H.; Kim, J. S. *J. Am. Chem. Soc.* **2005**, *127*, 12890–12899.

5 Benzo[2,1-b;3,4-b']dithiophene Containing Polymers

5.1 Introduction

Polythiophenes are among the most successful semiconductor materials in organic electronic devices.[1–5] Their easy processability and reasonably high charge-carrier mobility make them highly promising for future applications.[6–10] Nevertheless, the known materials do not satisfy all necessary parameters simultaneously. These critical parameters are:

1. Good solution processability, ideally on different substrates.
2. No or only short annealing times at low temperatures.
3. High operational stability at ambient conditions.
4. High charge-carrier mobilities.
5. Easy synthesis which can be scaled up for production.

Poly(3-hexylthiophene) (P3HT) is the "fruit fly" of device physicists. When polymerized with high regioregularity it can reach good performances.[11–13] It is well soluble (if the regioregularity and molecular weight are not too high), but its operational stability is low and it is not easy to fabricate devices of good quality with high reproducibly.[14, 15]

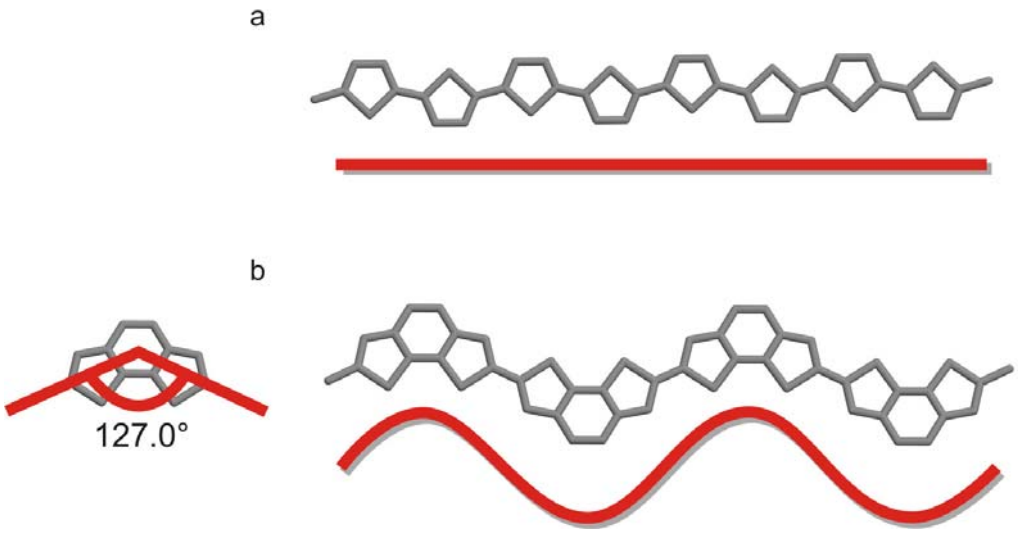

Figure 5.1: Different geometries of polythiophenes. **a.** linear backbone of P3HT **b.** curved backbone of the polymer incorporating benzo[2,1-b;3,4-b']dithiophene.

Various attempts have been made to improve these shortcomings of P3HT.[16] Changing the position of the alkyl chains for higher regioregularity and easier synthesis does not yield high enough charge carrier mobilities.[17] Incorporation of a linear benzo annellation to increase the ionization potential for higher air stability renders an almost insoluble polymer.[18] The incorporation of thiophene-derived monomers, in particular thienothiophene, is very advantageous for the mobility (up to 0.6 $cm^2V^{-1}s^{-1}$), but high annealing temperatures are needed ($>$ 180 °C), which is incompatible with inexpensive polymer substrates such as PET.[19]

A new strategy shall be investigated here by using a kinked monomer which introduces curvature into the polymer backbone. Hitherto, successful thiophene based polymers have only consisted of linear or very close to linear polymer backbones as depicted in Figure 5.1a using P3HT as example.

Benzo[2,1-b;3,4-b']dithiophene, in contrast, introduces a bond angle of 127 ° into the backbone of a conjugated polymer, rendering a curved chain as depicted in Figure 5.1b. The benzo annellation decreases the ionization potential of the polymer, thus increasing the stability against air and moisture.[20] The strong aggregation tendency of this moiety shall be moderated by the curvature which is expected

to increase the solubility due to entropic reasons. To obtain a high-performance polymer, the structure has to be optimized first, *i.e.* finding the best position for solubilizing alkyl chains and checking if additional thiophene units are needed.

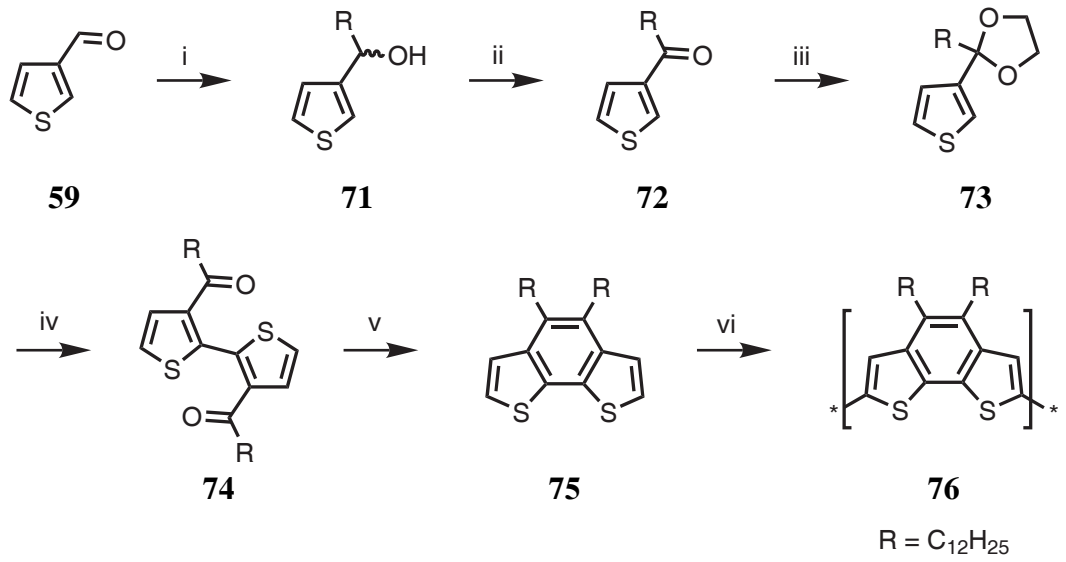

Figure 5.2: Synthesis of the homopolymer; conditions: *i* RMgBr, Et_2O, RT; *ii* PCC, CH_2Cl_2, RT, 67 % (for two steps); *iii* ethylene glycol, toluenesulfonic acid (cat.), toluene, reflux, quantitative; *iv* 1. *n*-butyllithium, THF, -78 °C 2. $Fe_2(acac)_3$ 3. HCl, 63 %; *v* $TiCl_4$, Zn, THF, reflux, 37 %; *vi* $FeCl_3$, *o*-dichlorobenzene, 60 °C, 85 %.

5.2 Structure Optimization

5.2.1 Homopolymer

The first approach towards a curved conjugated polymer is the homopolymerization of the benzo[2,1-b;3,4-b']dithiophene building block. Alkyl chains need to be attached to the molecule in order to solubilize the polymer and favor lamellar packing. If the alkyl chains were attached at the 4-position of the thiophene units, the polymer would be poorly conjugated due to steric congestion of the adjacent alkyl chains. Therefore, the alkyl chains need to be attached to the benzo units. Two such alkyl chains are needed to avoid regularity problems due to an unsymmetric monomer.

The synthesis of the polymer is derived from that of the unsubstituted benzodithiophene reported in the literature as depicted in Figure 5.2.[21, 22] Starting from thiophene-3-carboxylaldehyde (**59**) a Grignard reaction attaches a dodecyl chain. The thus obtained 3-(1-hydroxyalkyl)thiophene (**71**) is oxidized to 3-

alkanoylthiophene (**72**) using pyridiniumchlorochromate (PCC). This selective oxidant avoids unwanted oxidation on the sulfur atom of the thiophene ring.[23]

The oxidative dimerization needs a regioselectively lithiiated molecule. For this reason, the ketone group has to be protected such that lithiation is directed to the 2-position of the thiophene. Ethylene glycol as protection group serves this purpose as the free electron pairs of the oxygen atoms coordinate the lithium ion. Furthermore, this protection group is easy to attach, stable under basic conditions, and can be cleaved under mild conditions. After lithiation, oxolane **73** is oxidized by iron(III) acetylacetonate and hydrolyzed with hydrochloric acid whereupon the dialkanoyl-2,2'-dithiophene **74** is obtained. A McMurry ring closure reaction with titanium(IV) chloride reduced by zinc yields the dialkylated benzodithiophene **75**.

This monomer can be oxidatively polymerized with the aid of iron(III) chloride. To obtain high molecular weight, moisture has to be carefully excluded.[24, 25] Four equivalents of iron(III) chloride are added to the monomer in *o*-dichlorobenzene. The mixture is gently heated to 60 °C overnight to avoid gelation and to keep the polymer in solution. High concentrations ($>$ 50 mg/ml) are needed for the reaction for high molecular weight as usual for step-growth polymerization reactions.[26, 27] The thus obtained polymer is reprecipited from *o*-dichlorobenzene in methanol and consequently dedoped with hydrazine.

The polymer is well soluble in chlorinated benzenes. The molecular weight is determined by size exclusion chromatography in 1,3,4-trichlorobenzene at 135 °C using polystyrene as reference. A number average molecular weight of 18 kg/mol is obtained, a reasonable value for polythiophenes.[28, 29]

Good solubility in dichlorobenzene enables the polymer to be tested as the active material in a field-effect transistor (FET). The measurements are done in collaboration with Dirk Beckmann in the institute. A highly doped silicon wafer with a thermally grown oxide layer, silanized with HMDS is prepared as substrate.[30] The polymer is spin cast from a *o*-dichlorobenzene solution (5 mg/ml) and dried

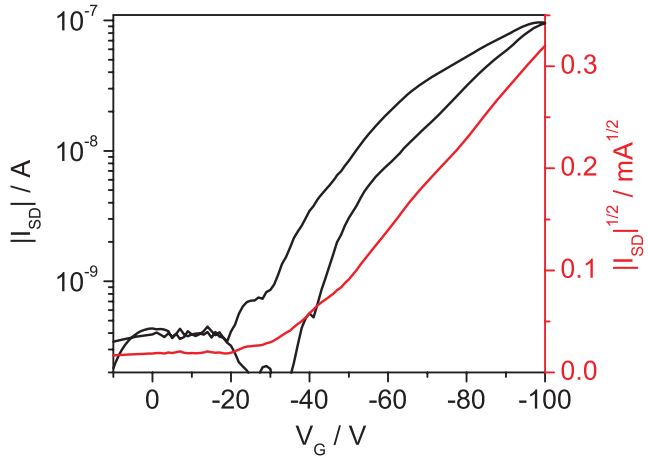

Figure 5.3: Transfer curve of polymer **76** on a silicon wafer.

at 100 °C for five minutes. Finally, top-contact gold electrodes are deposited by thermal evaporation.[31]

The transfer curve of this transistor is depicted in Figure 5.3. At higher voltages, the transistor reaches the space-charge limited regime as seen by the quadratic source-drain current dependence on the gate voltage, so there are no major injection barrier problems.[32–34] A threshold voltage of -30 V is observed, which is still reasonable for a polymer transistor. Low hysteresis is measured, the current at zero gate voltage goes back to a very low value (10^{-9} A). This means that the material is neither intrinsically doped, nor traps are created during operation. Nevertheless, the mobility is low, *i.e.* $\mu_{sat} = 1.4 \cdot 10^{-4}$ $cm^2V^{-1}s^{-1}$. Also, the on-off ratio ($I_{on}/I_{off} = 240$) is unsatisfactory as a result of the low on currents.

To analyze the reason for the low performance, X-ray diffraction has been measured. The reflection pattern (Figure 5.4a) of a drop cast film reveals very low order (the peak at $2\theta = 33$ ° is caused by the silicon lattice of the substrate). To get an even better insight into the polymer morphology, two-dimensional X-ray diffraction of an extruded fiber are recorded (Figure 5.4b). This is done in collaboration with Wojciech Pisula. Again, low order is indicated by very broad and weak peaks. In addition, the $\pi - \pi$ distance is determined to be 4.3 Å, a relatively high value in comparison to high-performance polymers reported in the literature. P3HT exhibits a

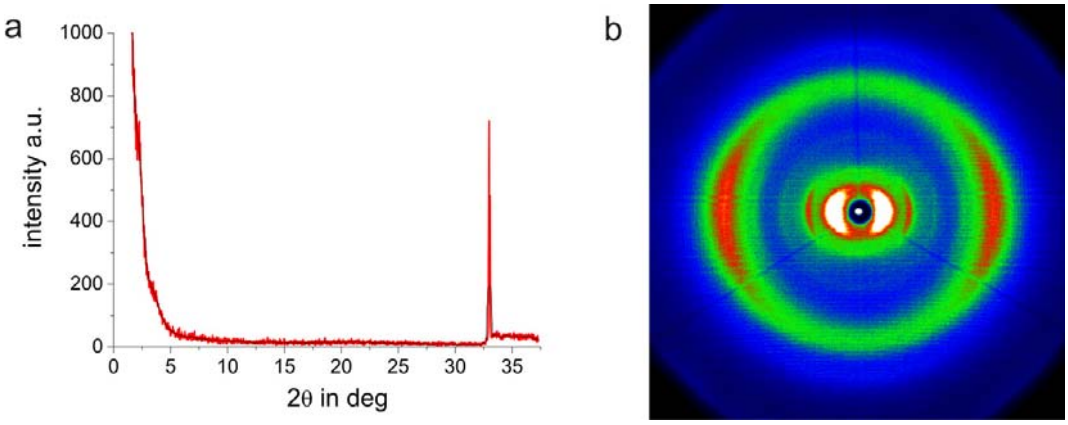

Figure 5.4: X-ray diffraction of polymer **76 a.** reflection of a drop cast film (the black line is the result of adjacent averaging to reduce the noise level) **b.** diffraction of an extruded fiber.

value of only 3.8 Å,[35] other polymers are in the same range.[19, 36] According to the hopping theory, large distances between the molecules decrease the mobility.[37, 38]

It seems as if the polymer is not flexible enough to form highly ordered films upon deposition. The repeat unit of the polymer backbone contains only one fused and thus stiff entity. Conformational changes, therefore, need a significant amount of activation energy. This makes the packing process too slow for spin casting. The result is an amorphous film. If there were smaller units in between the benzodithiophenes, the deposition process should be enhanced significantly.

5.2.2 Additional Dithiophenes

A common strategy to incorporate more flexibility into a polymer backbone is the copolymerization with dithiophene. The electronic structure of thiophene fits well to its derivative and good conjugation is retained. There are many examples in the literature where this strategy has successfully been applied.[18, 19, 39]

The synthetic procedure is shown in Figure 5.5. The dialkylbenzodithiophene (**75**) is brominated by NBS in DMF at the reactive 5- and 5'-positions, whereupon a Stille coupling with 2-tributylstannyl-3-alklythiophene yields the monomer **78** as an oil.

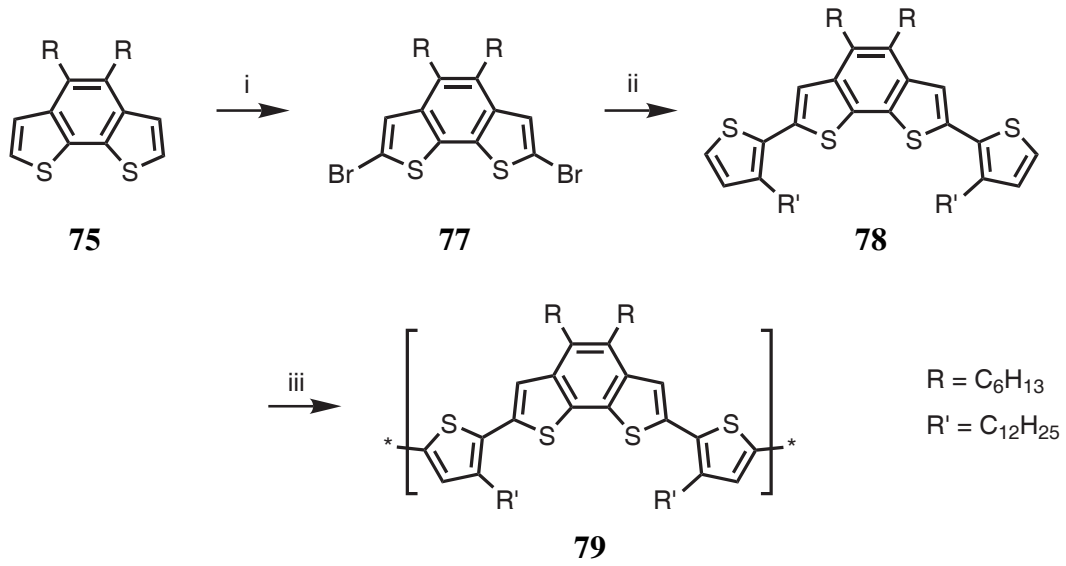

75 **77** **78**

79

Figure 5.5: Synthesis of a polymer incorporating additional dithiophene units; conditions: *i* NBS, DMF, RT, 71 %; *ii* 2-tributylstannyl-3-dodecylthiophene, DMF, $Pd(PPh_3)_4$, 100 °C, 70 %; *iii* $FeCl_3$, *o*-dichlorobenzene, 60 °C, 80 %.

By oxidative polymerization under similar conditions as previously described polymer **79** is obtained. After optimization of the reaction conditions, roughly the same molecular weight is obtained as for polymer **76**. Size exclusion chromatography in *o*-dichlorobenzene at 135 °C determines the number average molecular weight to 22 kg/mol against polystyrene as reference. Similar molecular weights enable better comparability of the polymers as the mobility can depend heavily on it.[40, 41]

The polymer is very well soluble in different solvents due to the presence of so many alkyl chains. To prepare field-effect transistors the same procedure as described above is followed for the reason of comparability. The result can be seen in Figure 5.6. The mobility has, in fact, increased by about one order of magnitude, namely $\mu_{sat} = 2.1 \cdot 10^{-3}$ $cm^2V^{-1}s^{-1}$. The on-off ratio also increases significantly to $I_{on}/I_{off} = 7.1 \cdot 10^3$.

The device characteristics have significantly improved: the threshold voltage is almost at 0 V, the hysteresis is much lower, and the transistor enters the space-charge limited regime already at around -30 V. The output curve, furthermore, indicates a

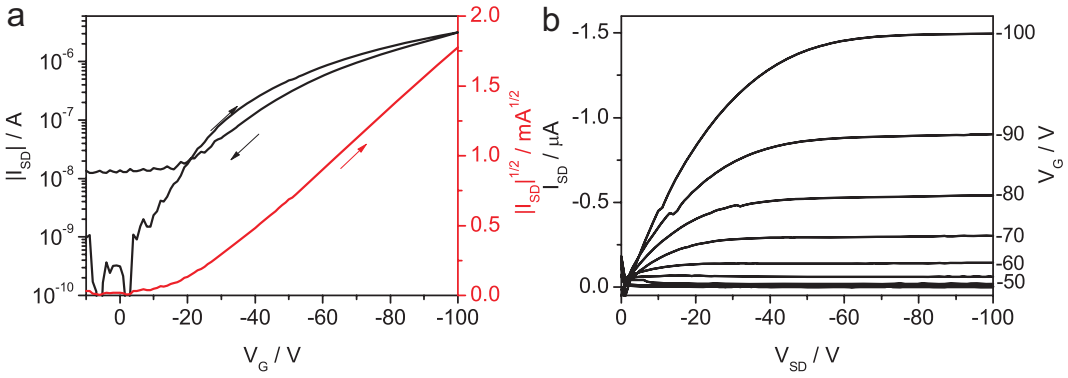

Figure 5.6: Field-effect transistor characteristics of polymer **79** on a silicon wafer prepared under standard conditions; **a.** transfer and **b.** output curves.

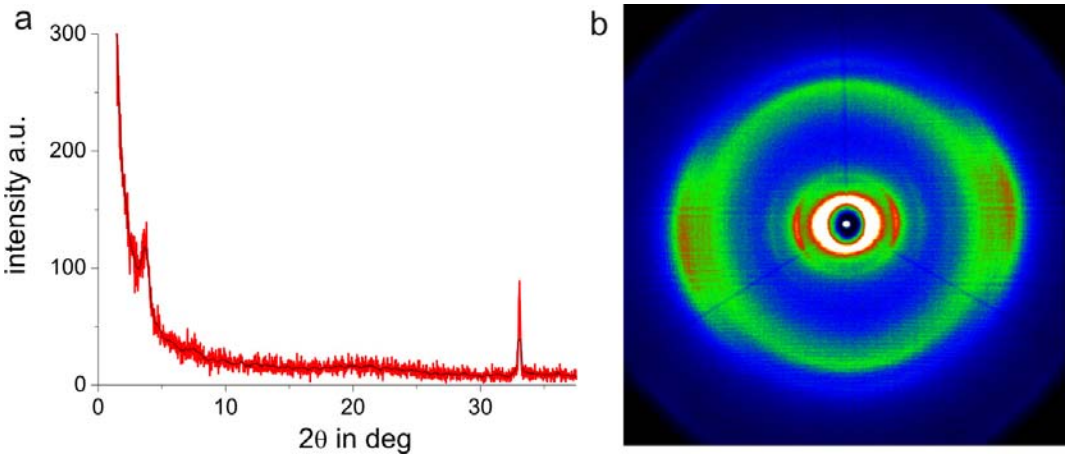

Figure 5.7: X-ray analysis of polymer **79** **a.** X-ray reflection **b.** X-ray diffraction of an extruded fiber.

well working transistor conducting current at very low source-drain voltages and reaching a plateau at higher voltages. This means that there are no contact problems nor leakage currents of notable extend.[42–44] However, the source-drain current remains above 10^{-8} A on the back sweep of the gate voltage which is two orders of magnitude higher than the voltage at the beginning. It seems as if leakage currents are the reason for this.

X-ray diffraction analysis has been carried out for polymer **79**, both as film on a silicon wafer in reflection mode (Figure 5.7a). Additionally, two-dimensional diffraction of an extruded fiber is recorded (Figure 5.7b). In the film diffraction pattern a peak can be seen at $2\theta = 3.7°$ which corresponds to the lamellar packing. It

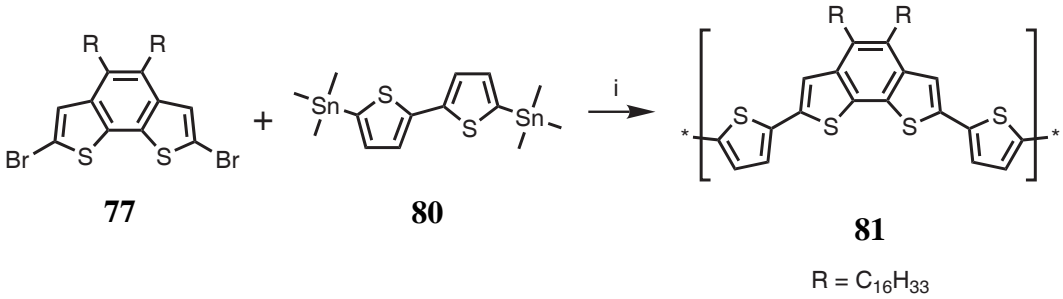

77 **80** **81**

R = $C_{16}H_{33}$

Figure 5.8: Synthesis of a polymer with fewer alkyl chains but the same backbone as **79**; conditions: P(*o*-tol)$_3$, $Pd_2(dba)_3$, *o*-dichlorobenzene, 140 °C, 3 days, 92 %.

translates to a lamellar distance of 2.4 nm and can be found as well on the equatorial axis of the two-dimensional fiber X-ray diffractogram. This indicates higher order than in the first case of polymer **76**, explaining the gain in mobility. In addition, the $\pi - \pi$ distance has decreased to 3.9 Å.

In conclusion, the strategy of adding dithiophene as a comonomer is successful. Nevertheless, more optimization is needed to obtain a mobility of at least 0.1 $cm^2V^{-1}s^{-1}$. The numerous alkyl chains may hinder efficient packing and "dilute" the active part of the polymer too much. Considering the high solubility of the polymer, fewer alkyl chains seem feasible.

5.2.3 Reduced Degree of Alkylation

A lower degree of alkylation can be achieved by leaving the additional thiophene units un-alkylated. Having already synthesized the dibrominated dialkylbenzodithiophene (**77**), the most straightforward way is the Stille polymerization reaction with the literature-known bis(trimethylstannyl)dithiophene (**80**) as a comonomer (see Figure 5.8).[45] The reaction conditions to obtain polymer **81** are derived from a published procedure for a similar polymer utilizing tri-*o*-tolylphosphine and tris(dibenzylideneacetone)-dipalladium(0) ($Pd_2(dba)_3$) in *o*-dichlorobenzene at 140 °C for three days.[46] The decreased number of alkyl chains

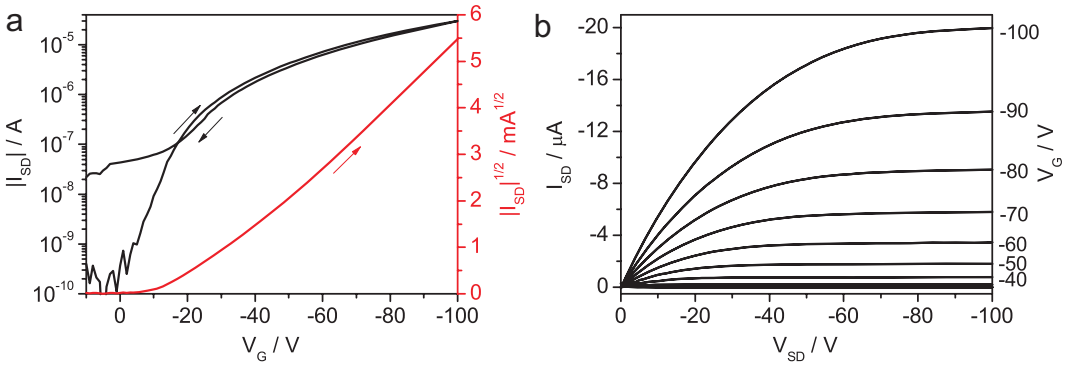

Figure 5.9: Field-effect transistor characteristics of polymer on silicon wafer prepared equal to other polymers **81 a.** transfer and **b.** output curves.

leads to drastically lower solubility. In order to be able to process the polymer from solution, hexadecyl chains are necessary.

The molecular weight is targeted again to the 20 kg/mol region. Size exclusion chromatography in trichlorobenzene at 135 °C against polystyrene standards determined the number average molecular weight to 21 kg/mol. So, good comparability is assured.

Field-effect transistors on silicon wafers are prepared in exactly the same way as for the other polymers. The transfer and output curves are shown in Figure 5.9. Good device characteristics are retained. Neglegible hysteresis, low contact resistance, and vanishing leakage current are observed. The mobility for this polymer reaches $\mu_{sat} = 2.3 \cdot 10^{-2}$ $cm^2V^{-1}s^{-1}$, the on-off ratio $I_{on}/I_{off} = 1.2 \cdot 10^4$. This means another improvement of one order of magnitude, so the goal is nearly attained.

X-ray diffraction analysis both as film and as extruded fiber is measured for polymer **81** as well. The results are presented in Figure 5.10. A further increase of the degree of order in comparison to polymers **76** and **79** can be observed. Sharp and intense peaks are seen, even higher order peaks of the lamellar packing on the equatorial axis are present.

The $\pi - \pi$ distance, however, is practically unchanged. It is determined to be 4.0 Å, even slightly larger than for polymer **79**. As mentioned above, very effective

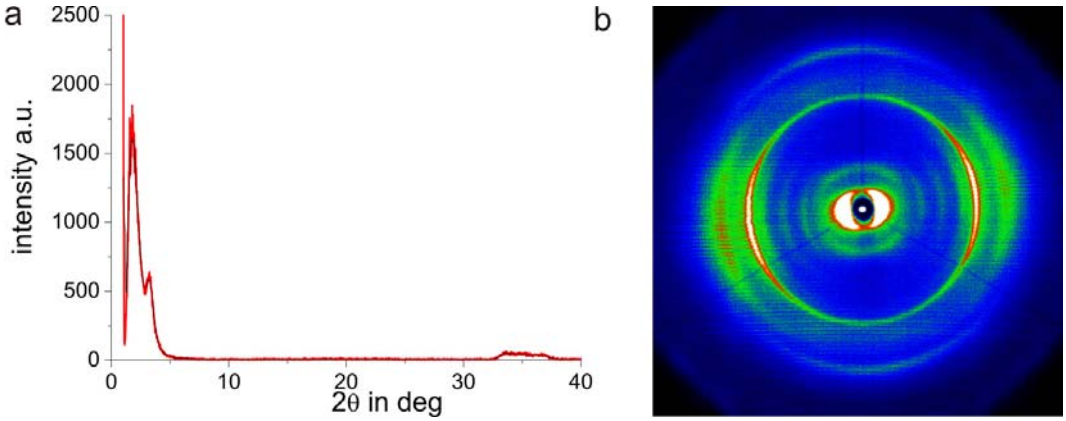

Figure 5.10: X-ray diffraction analysis of polymer **81** a. film reflection mode b. diffraction on an extruded fiber.

polymers pack with distances about 3.7 Å. If one assumes that the benzodithiophene unit is the dominant driving force for aggregation, it should be more effective to leave it unsubstituted for denser packing.

Furthermore, two adjacent alkyl chains are likely to mutually interfere. Their motion is thus correlated in the vicinity to the benzodithiophene moiety due to their spatial proximity, leading to a less effective solubilizing effect than two separate alkyl chains would have. A similar effect is observed in differently alkylated polythiophenes.[47] This motivated to make a polymer with unsubstituted benzodithiophene and attaching the alkyl chains solely to the thiophene units.

5.2.4 Unsubstituted Benzodithiophene

In order to obtain a polymer with unsubstituted benzodithiophene and alkylated thiophene units, a Stille polymerization between stannylated benzodithiophene and a dibromo-dialkyl-dithiophene is chosen. Benzo[2,1-b;3,4-b']dithiophene (**82**) is made according to a literature procedure.[21, 22]

The dialdehyde **61** previously prepared for the donor-acceptor model system in the previous chapter undergoes reductive coupling under McMurry conditions. $TiCl_4$ and zinc in anhydrous THF are employed affording benzodithiophene **82**. Its

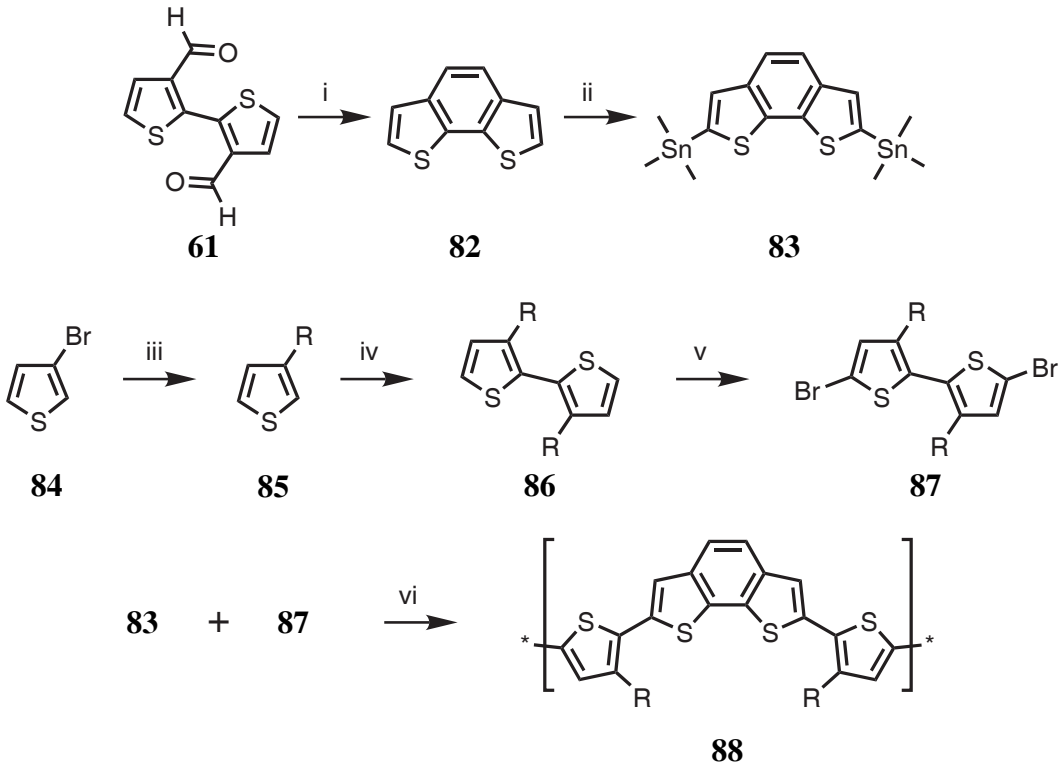

Figure 5.11: Synthesis of polymer **88** with unsubstituted benzodithiophene and alkylated dithiophene; conditions: *i* $TiCl_4$, Zn, THF, reflux, 53 %; *ii* 1. *t*-butyllithium, THF, -78 °C 2. Me_3SnCl 78 °C to RT, 44 %; *iii* RMgBr, $Ni(dppp)Cl_2$, diethylether, reflux, 85 %; *iv* 1. n-butyllithium, TMEDA, THF, RT, 2. $Fe_2(acac)_3$, RT, 59 %; *v* NBS, chloroform, RT, 68 %; *vi* $P(o\text{-tol})_3$, $Pd_2(dba)_3$, *o*-dichlorobenzene, 140 °C, 3 days, 87 %.

purity can be easily determined as it melts just above room temperature. If it is not pure, it remains an oil.

The preparation of the distannylated benzodithiophene (**83**) needed considerable optimization. The literature reports the use of *n*-butyllithium to deprotonate the α positions of thiophenes.[39, 48] Nevertheless, only the singly stannylated product is obtained. Neither the temperature nor the reaction time nor the amount of n-butyllithium helped to get the desired product. Only the application of the highly pyrophoric t-butyllithium is basic enough to doubly deprotonate benzodithiophene **82**. The product, however, does not crystallize directly after the workup. Also, it is not stable enough to submit it to column chromatography. Only reversed phase chromatography helps purifying the product sufficiently that it can be crystallized.

Octadecyl functionalized silica gel is used as stationary phase and acetonitrile as eluent. After crystallization, compound **83** can be obtained in high purity which is necessary for a step-growth polymerization.[49]

The dialkylated dibromo-dithiophene (**87**) is a well-known compound.[50] It is made by a Kumada reaction alkylating 3-bromothiophene (**84**). Lithiation deprotonates selectively the 5-position. Oxidative coupling with $Fe_2(acac)_3$ yields compound **86** which is brominated with N-bromosuccinimide to afford the comonomer **87**. It is very important to obtain the compound in high purity for a successful polymerization yielding high molecular weight. For this reason, the compound is recrystallized three times from ethyl acetate, a process in which about half of the material is sacrificed for the purity.

Both monomers (**83** and **87**) are copolymerized under Stille conditions as for polymer **81**: $Pd_2(dba)_3$ and P(*o*-tol)$_3$ are used as catalyst in a *o*-dichlorobenzene solution. The reaction is run for three days at 140 °C whereupon it is purified by precipitation. The polymer can be obtained with a number average molecular weight of 21 kg/mol as determined by size exclusion chromatography in trichlorobenzene at 135 °C in reference to polysytrene. This means good comparability to the previous polymers with regard to molecular weight.

An NMR spectrum can be recorded of the polymer in 1,2,4-trichlorobenzene-d_3 at 100 °C. To reduce the influence of the end groups in the spectrum, the polymer is subjected to Soxhlet extraction with chloroform in advance. The ^{1}H-NMR spectrum is depicted in Figure 5.12. In the aromatic region, three peaks can be seen which originate from the polymer. The peaks have been assigned by comparing the positions with polymer **79**, in which the peak at 7.8 ppm is absent, as well as the monomer of the latter polymer (**78**) showing two doubletts at 7.0 and 7.2 ppm.

The peak at 7.3 ppm partially overlaps with the solvent peak hindering integration. In the spectrum recorded in *o*-dichlorobenzene-d_4 it is completely hidden under the solvent signal. Using the peak fitting function of the MestReC© software,

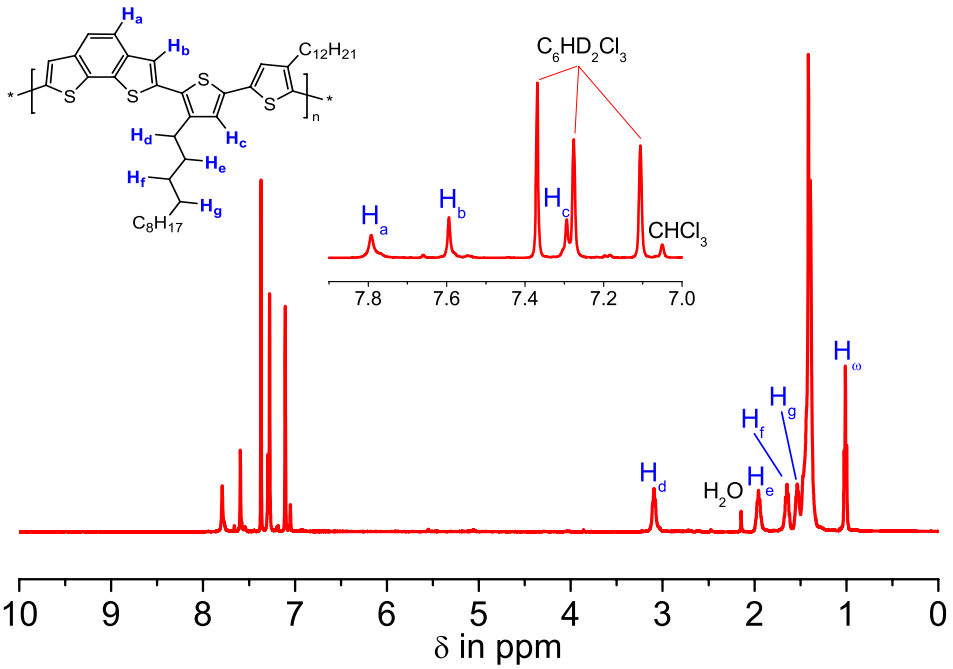

Figure 5.12: ^{1}H-NMR spectrum of polymer **88** in $C_6D_3Cl_3$ at 100 °C (500 MHz).

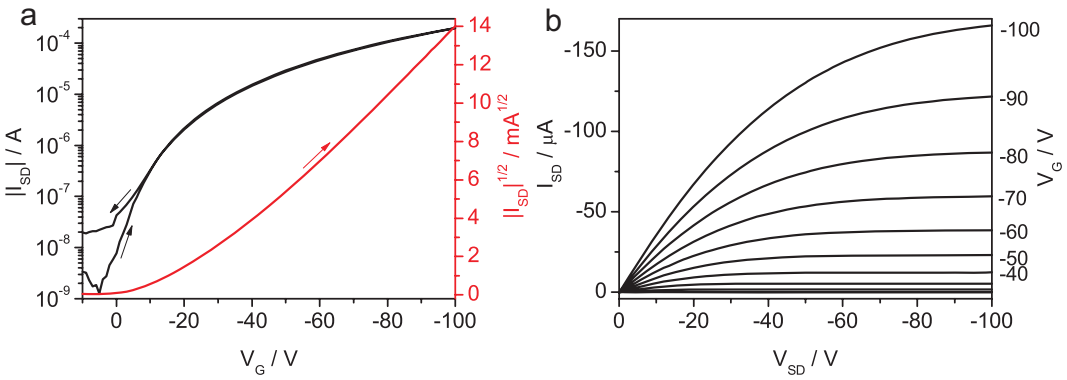

Figure 5.13: Field-effect transistor characteristics of polymer **88** on silicon wafer. **a.** transfer and **b.** output curve.

equal intensity of the three aromatic peaks can be determined. The aliphatic region also fits well to the structure of polymer **88**. The signals of the first four protons along the chain beginning at the thiophene are resolved. Their integrals equal four times those in the aromatic region as expected.

The transistor performance of this material is tested in the standard field-effect transistor setup using HMDS treated silicon wafers with top-contact gold electrodes.

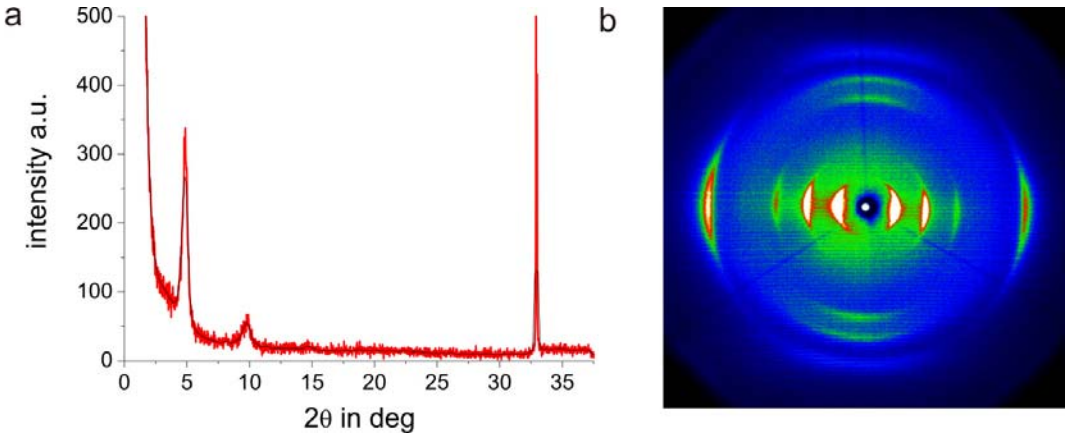

Figure 5.14: Morphology investigation of polymer **88**. **a.** film X-ray reflection diffraction, **b.** two-dimensional WAXD from an extruded fiber.

Figure 5.13 depicts the results. The transfer curve reveals practically absent hysteresis and a nicely linear relationship of the square-root of the current to the gate voltage. The output curves reach the space-charge limited current regime, so no contact resistances or leakage currents are detected.

The threshold voltage is shifted to slightly positive gate voltages, but the value is below +5 V, so uncritical for applications.[51] Worth mentioning is the low source-drain current on the back scan which goes down to values around 10^{-8} A, only one order of magnitude higher from where it has started.

The transistor exhibits a saturation mobility of $\mu_{sat} = 0.13$ $cm^2V^{-1}s^{-1}$with an on-off ratio of $I_{on}/I_{off} = 1.3 \cdot 10^5$. These excellent values are reached with high reproducibility, the standard deviation of five measurements is as low as 0.02 $cm^2V^{-1}s^{-1}$. This means that a material has been found with outstanding potential for applications.

The morphology investigations as depicted in Figure 5.14 reveal very high order of the polymer. The film X-ray reflection diffractogram shows peaks of the lamellar packing up to the third order which requires a large degree of crystallinity. This is corroborated by the two-dimensional wide-angle X-ray diffraction pattern. A

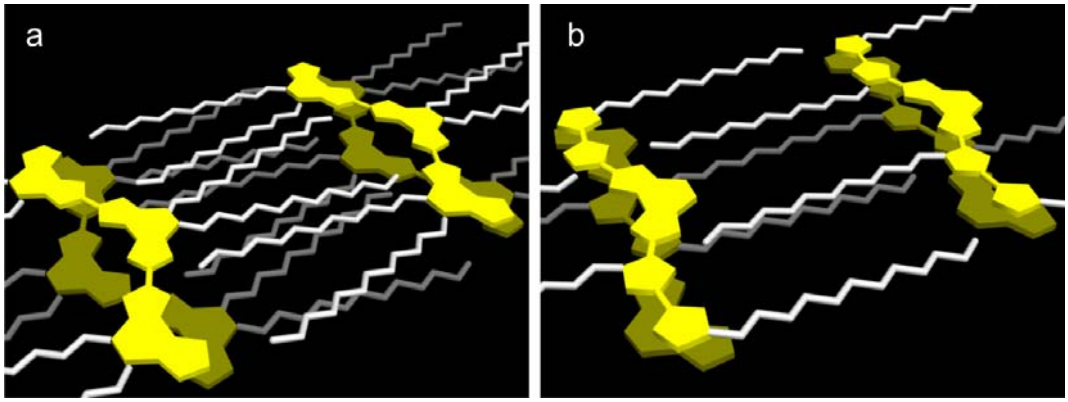

Figure 5.15: Cartoons of the morphology as determined by force-field optimization. **a.** polymer **76**, **b.** polymer **88**.

lamellar distance of 1.88 nm is elucidated, in good agreement with the length of a dodecyl chain plus the backbone diameter.

The $\pi-\pi$ distance can be determined from the latter to be 3.7 Å, a very low value leading to an efficient intermolecular interaction and, thus, low hopping barriers.[52] More peaks of interest can be seen in Figure 5.14b on the meridional axis. These originate from the crystalline alkyl chains being perpendicularly oriented to the polymer backbone. This emphasizes that the efficient packing and the high order lead to the good field-effect mobility.[53]

The huge morphological differences between the initial homo-polymer **76** and the finally optimized polymer **88** have been considered in more detail using a 3D-structure program to model the lameallar packing to get a better understanding of the structure-properties relationship. The polymers are optimized in terms of force field energy minimization (MMFF algorithm) and assembled such that they fit the X-ray data.

The proposed assembly of both polymers is shown in Figure 5.15. In the case of polymer **76**, it is not possible to superimpose two adjacent polymer chains such that the alkyl chains can pack effectively and a large π overlap of the backbone is formed. In many crystal structures of thiophene containing molecules, the sulfur atoms of adjacent molecules get in close contact.[54–56] In the present case, it is not

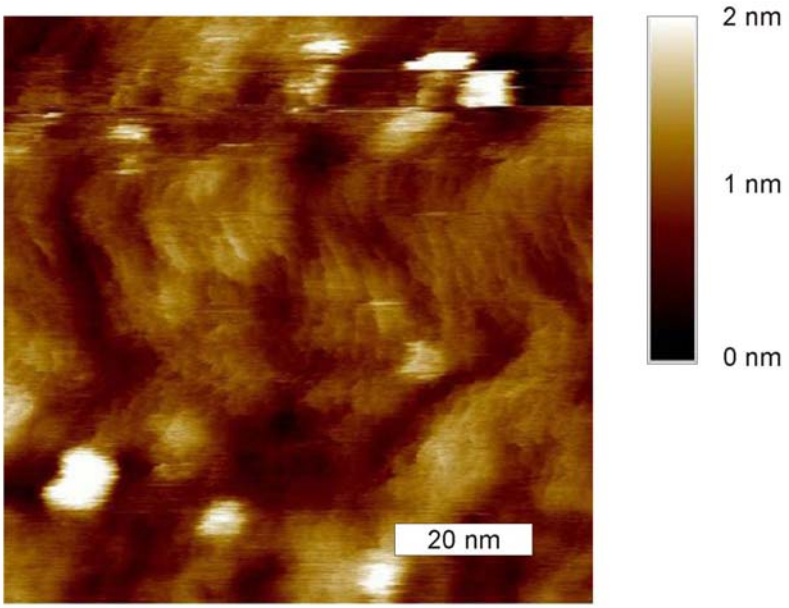

Figure 5.16: Atomic force microscopy image (tapping mode) spin-cast film of polymer **88**.

possible without significant steric strain caused by the alkyl chains. A large $\pi - \pi$ distance as determined by X-ray diffraction is the consequence leading to low lattice energy and finally to low order.

The opposite is true for polymer **88**. A good π overlap is reached when the sulfur atoms of adjacent polymer chains are in close contact. This is particularly favorable for charge conductivity due to the strong coupling of sulfur atoms which are in close proximity.[57] The alkyl chains can, furthermore, pack freely without creating steric strain, thus enabling close packing with a low $\pi - \pi$ distance. The distance of packed alkyl chains fit well to the X-ray data (see meridional peaks in Figure 5.14b). There are just enough alkyl chains to fill the space in between the lamellae, which means that the lamellar distance equals the length of the alkyl chain plus the diameter of the backbone. The X-ray data supports this close packing mode with a lamellar distance of 1.88 nm. Polymer **76**, instead, has too many alkyl chains leading to steric crowding and finally to an enlargement of the lamellae (2.19 nm).

Film formation properties can be visualized by atomic force microscopy (AFM). It has been shown for P3HT that the mesoscale morphology has an important influ-

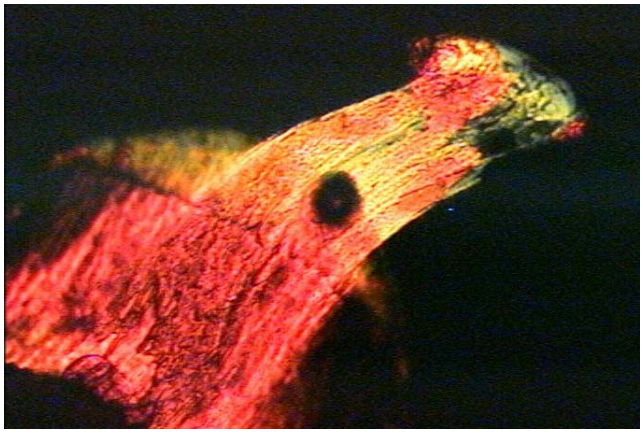

Figure 5.17: Polarized optical microscopy image of polymer **88** cooled from the melt under sheer forces.

ence on the field-effect mobility.[58] Polymer **88** is dissolved in *o*-dichlorobenzene and spin-cast on a silicon wafer following the procedure with which the transistors have been prepared.

The constant-high image recorded by AFM is depicted in Figure 5.16. The polymer forms a very smooth surface, the height differences fall within one nanometer. Grain boundaries are absent which lower the mobility significantly.[59] One can even see the steps induced by the lamellar packing of the molecule. The height difference (about 3 nm) corresponds well to the lamellar distance obtained by X-ray diffraction. The lamellar structures are visible practically everywhere underlining the high crystallinity of this polymer. The excellent film formation properties explain the good performance of the corresponding transistors.

When polymer **88** is heated to 200 °C, it starts to melt, and at 220 °C it is completely liquid. Melting polythiophenes have been reported before, but they are rare.[60, 61] This enables one to process the polymer from solution. In order to study the morphology of **88** upon cooling a liquid film, the material is sandwiched between two glass slides and heated to 220 °C. The cooling process is observed by optical microscopy using cross polarizers. No birefringence is observed when letting the polymer cool down slowly. If, however, the glass slides are moved against

Polymer	Alkyl Chain	M_n in kg/mol	μ_{sat} in $cm^2V^{-1}s^{-1}$	I_{on}/I_{off}
89	C10	13	0.070	$1.7 \cdot 10^5$
88	C12	21	0.106	$1.8 \cdot 10^5$
90	C14	20	0.094	$9.2 \cdot 10^5$
91	C16	16	0.066	$3.4 \cdot 10^5$

Table 5.1: Dependence of field-effect mobility on alkyl chain length of benzodithiophene-copolymers.

each other inducing a shear force, strong birefringence is detected. Figure 5.17 shows the corresponding image. This has important consequences as the material allows the preparation of films with preferred direction of the polymer chains potentially increasing the backbone current transport in the transistor leading to even better performance. The investigations are ongoing.

5.2.5 Variation of Alkyl Chain Length

The length of the solubilizing alkyl chains of conjugated polymers can have a strong effect on the field-effect mobility. Poly(3-alkylthiophene)s exhibit differences of four orders of magnitude between a hexyl and an octadecyl substituted derivative.[62] Other conjugated polymers show a similar behavior.[63, 64] The differences in conductivity are attributed to morphological differences. Very long alkyl chains usually lead to low order, very short to ineffective phase separation and poor solubility. That is why a compromise has to be found for each polymer backbone.

To investigate the influence of the alkyl chain on polymer **88**, three more polymers have been synthesized. Following the route outlined in Figure 5.11 on page 144, dibromo-dithiophenes (**87**) with different alkyl chains between ten and sixteen carbon atoms are used.

The field-effect mobilities of the polymers are measured in the standard setup. The results are summarized in Table 5.1. The mobility of the C12 and the C14 derivative (**88** and **90** respectively) are practically identical with the former being

Polymer	M_n/ kg·mol^{-1}	μ_{sat}/ cm^{2}V^{-1}s^{-1}	I_{on}/I_{off}	$d_{\pi-\pi}$/ nm	d_{lam}/ nm
76	18	$1.3 \cdot 10^{-4}$	$2.4 \cdot 10^{2}$	0.43	2.19
79	22	$2.1 \cdot 10^{-3}$	$7.1 \cdot 10^{3}$	0.39	2.38
81	21	$2.3 \cdot 10^{-2}$	$1.2 \cdot 10^{4}$	0.40	2.19
88	21	0.134	$1.8 \cdot 10^{5}$	0.37	1.83
P3HT	27	$1.1 \cdot 10^{-2}$	$1.7 \cdot 10^{2}$	0.38	1.65

Table 5.2: Overview of the field-effect performance and the morphology parameters of the polymer structure optimization process including P3HT as reference, d_{lam}: thickness of lamellae.

slightly higher. About 30 % lower mobilities are measured for the C10 and C16 derivatives (**89** and **91**, respectively). This is an insignificant difference considering the slightly different molecular weights. Also the on-off ratios are all of the same order of magnitude.

The practical independence of the mobility on the alkyl chain length is very advantageous in that the solubility can be tuned without affecting the transistor. For the polymer with C10 chain, it is easy to find orthogonal solvents in order to build up layered structures. The longer chains, on the other hand, offer the possiblity to process the device from non-chlorinated solvents. The solvent vapors can be burned without evolving hydrochloric acid, an important environmental aspect. In fact, polymer **91** with its C16 chain dissolves in toluene at 80 °C.

5.2.6 Summary

A summary of the optimization procedure is presented in Table 5.2. The homopolymer (**76**) with alkyl chains attached to the benzene unit shows low order and low mobility. The introduction of additional dithiophenes improves the performance of the FET in the case of the all-alkylated polymer (**79**) and even better for the polymer with the same backbone but less alkyl chains (**81**). The positioning of the alkyl chains away from the benzodithiophene to the thiophenes yields a polymer (**88**) with high order and good mobility, fullfilling all requirements needed for indus-

trial applications simultaneously: easy processablity from solution, short annealing times at low temperatures, high operational stability, high charge-carrier mobility, and easy synthesis.

Included is the well-known P3HT which has been tested under the same conditions as the other polymers. The mobility of $\mu_{sat} = 1.1 \cdot 10^{-2}$ $cm^2V^{-1}s^{-1}$is reasonable, values of $0.1 cm^2V^{-1}s^{-1}$are only reached in highly optimized setups.[11] The X-ray data for P3HT are taken from the literature.[65]

The trend of increasing mobility with decreasing $\pi - \pi$ distance is obvious for all polymers. The polymer obtained after optimization (**88**) packs even more closely than P3HT. Polymer **88** has a remarkably low lamellar distance in comparison to P3HT. In the latter case, only short hexyl chains need to find a place in between two polymer chains, whereas for **88** doubly long dodecyl chains need to fit. It seems as if they can pack so effectively that the end of the alkyl chain comes close to the next polymer backbone. No alkylation at the benzodithiophene unit leaves enough space for such an interdigitation.

The fact which has become very obvious is that the alkyl chains attached to the benzodithiophene unit have a very disadvantageous effect on the $\pi - \pi$ distances. The lowest value in this series is 0.39 nm which is far too much for high mobility. Close packing is undisturbed in the case of polymer **88** with an unsubstitued benzodithiophene unit leading to a strong interchain interaction.

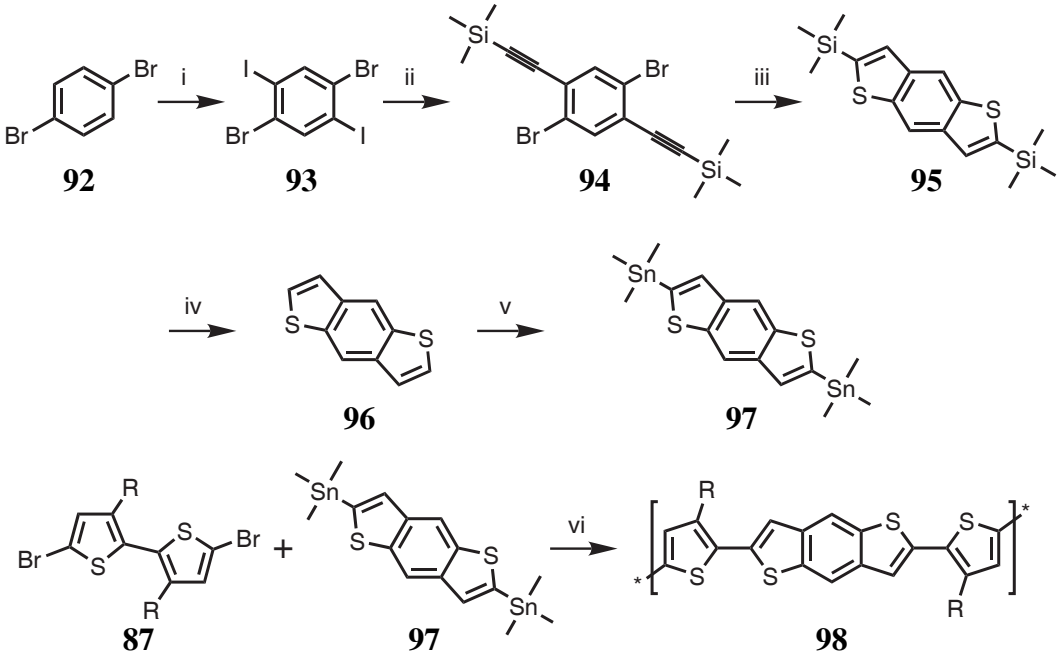

Figure 5.18: Synthetic route to the linear polymer, conditions: *i* I_2, H_2SO_4, 130 °C, 48 %; *ii* ethynyl-trimethylsilane, $Pd(PPh_3)_2Cl_2$, diisopropylamine, THF, RT, 91 %; *iii* 1. *t*-butyllithium, THF, -78 °C to RT 2. S_8, 3. ethanol, RT, 77 %; *iv* Bu_4NF, THF, RT, 96 %; *v* 1. *t*-butyllithium, THF, -78 °C, 2. Me_3SnCl, 59 %; *vi* $Pd_2(dba)_3$, P(*o*-tol)$_3$, *o*-dichlorobenzene, 140 °C, 94 %.

5.3 The Effect of Curvature

The striking feature about the benzo[2,1-b;3,4-b']dithiophene is the fact that it introduces curves into the polymer backbone (recall Figure 5.1 on page 133) in contrast to most successful polymers reported so far having a linear backbone. The curved polymer **88** exhibits a high charge-carrier mobility exceeding 0.1 $cm^2V^{-1}s^{-1}$and shows excellent device characteristics in combination with good processablity and high reproducibility. To examine the effect of the curvature in more detail, the linear isomer incorporating benzo[1,2-b;4,5-b']dithiophene (**96**) is prepared. Its electronic structure is expected to not significantly deviate from polymer **88**.

5.3.1 Isomeric Linear Polymer

The synthesis of benzo[1,2-b;4,5-b']dithiophene (**96**) is described in the literature.[66] Its key step is a double cycloaddition of a thiol to ethynyl moieties. Therefore, 1,4-dibromobenzene (**92**) is iodinated with iodine in sulfuric acid.[67] The 1,4-diiodo-2,5-dibromobenzene (**93**) is reacted in a selective Haghihara reaction to the 1,4-bis-trimethylsilylethynyl-2,5-dibromobenzene (**94**). The bromine atoms are lithiated by t-butyllithium and converted to the thiols by reacting with elemental sulfur. Upon treatment with ethanol, the thiols add to the triple bond forming two thiophene rings.[68] The trimethylsilyl groups are needed to allow lithiation, because ethynyl protons are more acidic than the phenyl protons. The protection groups are cleaved by fluoride ions to afford benzo[1,2-b;4,5-b']dithiophene (**96**).

Stannylation is achieved as before by double lithiation at -78 °C with t-butyllithium and subsequent treatment with trimethyltin-chloride to afford monomer **97**. The high symmetry of this molecule (D_{2h}) facilitates the crystallization process, so no reverse phase chromatography is needed as in the case of the ditin compound **83**.

A Stille polymerization is done under identical conditions as for polymer **88** utilizing dibromo-dialkyl-dithiophene (**87**) as the comonomer. During the polymerization, the polymer starts to precipitate with *o*-dichlorobenzene as solvent at 140°C. The high rigidity of a linear polymer thus lowers the solubility drastically. It can still be dissolved in warm *o*-dichlorobenzene, but not at such high concentrations as polymer **88**.

The field-effect characteristics of polymer **98** can be seen in Figure 5.19. The curves look relatively similar to those of polymer **88** (Figure 5.13 on page 146). The hystersis is a bit higher, but otherwise there are little differences. The mobility, however, is only $\mu_{sat} = 1.5 \cdot 10^{-2}$ $cm^2V^{-1}s^{-1}$, which means one order of magnitude

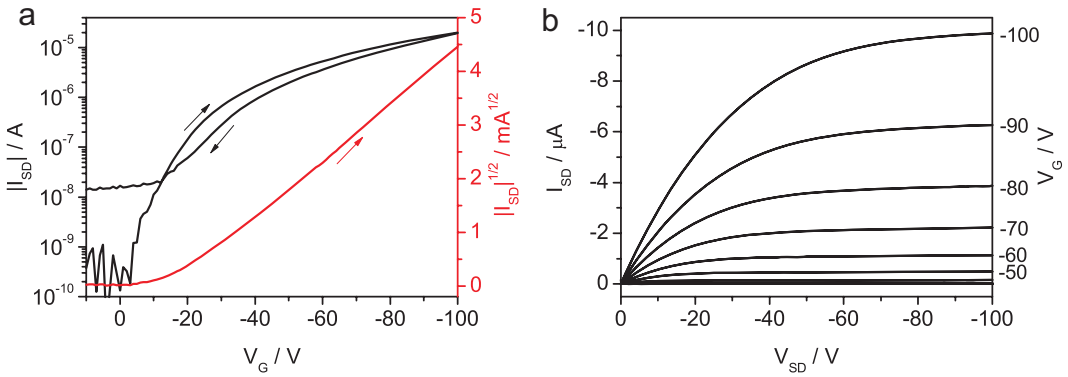

Figure 5.19: Field-effect transistor characteristics of polymer **98** on silicon wafer. **a.** transfer and **b.** output curve.

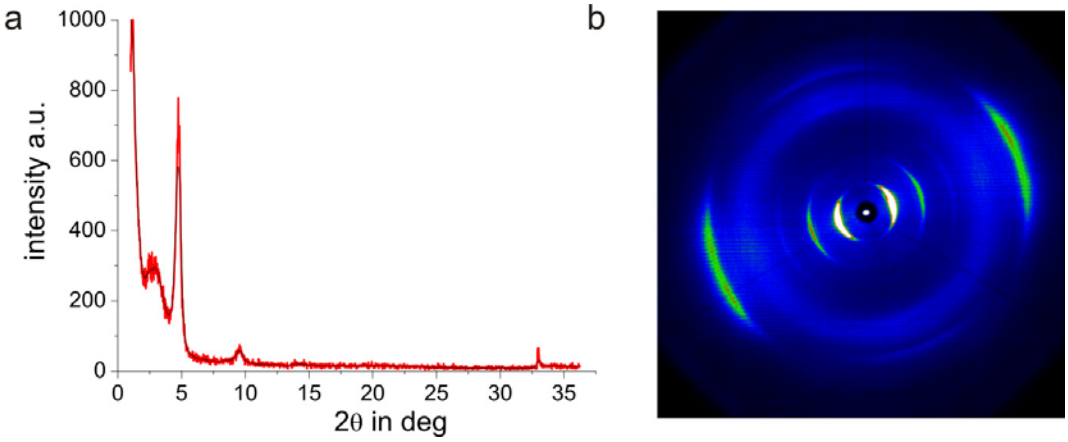

Figure 5.20: Morphology investigation of polymer **98**. **a.** film X-ray reflection diffraction, **b.** two-dimensional WAXD from an extruded fiber.

lower than that of polymer **88**. The on-off ratio has been determined to $I_{on}/I_{off} = 9.1 \cdot 10^4$, so roughly the same value as for polymer **88**.

At the first glance, this experimental result is unexpected. A similar polymer to **98** with the same backbone geometry has shown higher values.[18] There is, however, a report about polymer **98** with a mobility of $\mu_{sat} = 8 \cdot 10^{-5}$ $cm^2V^{-1}s^{-1}$, but this may be due to an ineffective device preparation.[69]

Morphological differences may be the reason for the lower performance of polymer **98** over polymer **88**.[70] X-ray diffraction experiments in film and on an extruded fiber have been performed. The results are depicted in Figure 5.20. The peaks in the film X-ray reflection pattern are almost identical to those of **88**. Sharp

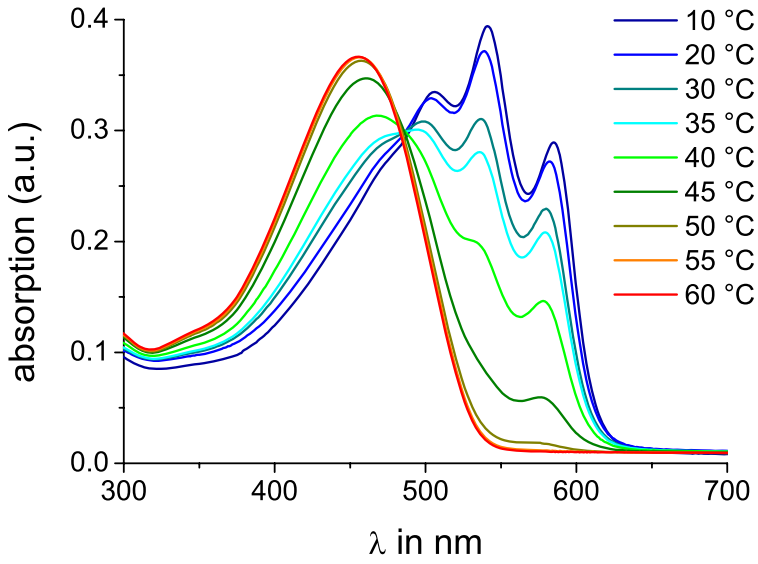

Figure 5.21: Temperature-dependent UV-vis absorption spectra of polymer **88** in *o*-dichlorobenzene.

reflections and up to third order peaks arising from lamellar packing are observed as for polymer **88** (see 5.14 on page 147), which means a comparable degree of order. The $\pi - \pi$ distance as determined from the wide-angle two-dimensional X-ray diffraction pattern from the extruded fiber is identical to polymer **88** (3.7 Å). It can, therefore, be concluded that both polymers form a very similar unit cell and crystallize to a comparable degree.

5.3.2 Optical Analysis

One difference between the two isomeric polymers **88** and **98** becomes obvious when heating dichlorobenzene solutions. The curved polymer **88** undergoes a strong color change from deep red at room temperature to light yellow at around 50 °C whereas the linear **98** is almost unaffected. This motivated to record temperature-dependent UV-vis absorption spectra of the polymer.

As shown in Figure 5.21, the absorption spectra of **88** change drastically upon heating. While there are three resolved bands between 500 and 600 nm visible at

low temperatures, these vanish upon heating and a broad band around 450 nm arises. A similar, but much weaker effect is observed for P3HT.[71] Such an absorption change has also been observed when a poor solvent such as methanol is added to the solution.[72, 73] It is proposed that J-aggregates of the molecules lead to this behavior. The polymer chains line up such that the transition moment of the single chains are oriented parallel and the angle between the transition moment and the polymer chain is zero. The strong coupling of several self-similar chains results in a coherent excitation at red-shifted wavelengths relative to the free chain.[74]

This thermochromic effect takes place in a very narrow temperature range for the transition between aggregated chains (20 °C) and free chains (50 °C). In P3HT, the transition takes place between 25 °C and 150 °C.[71] The photoluminescence intensity is measured at temperatures above and below the transition. At low temperatures the fluorescence intensity is about a fourth of that at high temperatures. Self-quenching of aggregated conjugated polymers is well known in the literature.[75, 76]

Good insight into aggregation phenomena can be obtained using light scattering techniques.[77, 78] Dynamic light scattering has been measured for polymer **88** in collaboration with Werner Steffen in this institute. For the excitation, a laser with a wave length of 831.5 nm is used as the polymer absorbs too strongly at shorter wavelengths which are normally used for light scattering. The polymer is dissolved at 2 mg/ml in *o*-dichlorobenzene, filtered at 70 °C through a PTFE filter to obtain dust-free samples.

The intensity-intensity autocorrelation functions are depicted in Figure 5.22. At low temperatures, the correlation function possesses a decay time of more than 1 ms which translates into particles of 100 nm to 5 μm in size. A single polymer coil with a molecular weight of 20 kg/mol is much smaller. Therefore, the polymer strongly aggregates which leads to the intensive red-shift of the UV-vis absorption spectrum (see Figure 5.21).

When the solution is heated to 60 °C, a temperature where the absorption bands

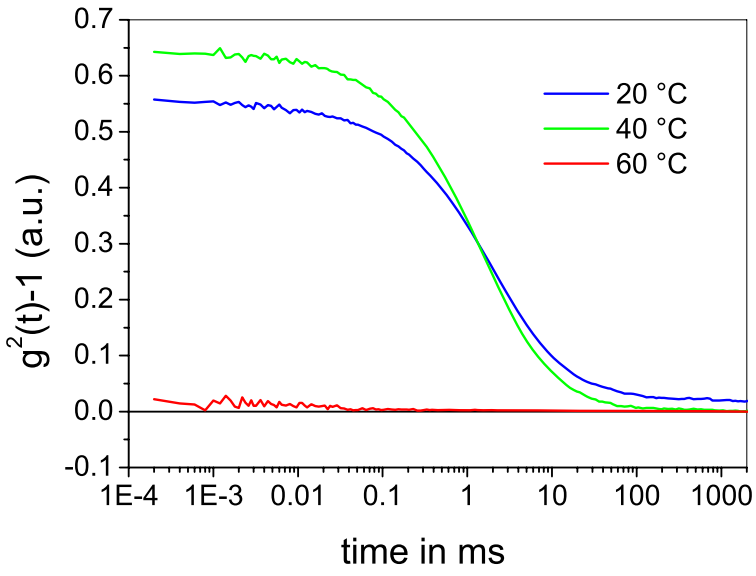

Figure 5.22: Intensity-intensity autocorrelation function from a light scattering experiment with polymer **88** in *o*-dichlorobenzene at various temperatures.

between 500 and 600 nm have completely vanished, the autocorrelation function is not detectable any more. The polymer chains no longer aggregate; they are solvated separately. The effect is completely reversible, so no permanent structural change occurs which is consistent with an aggregation phenomenon.

When cooling a solution of polymer **88** at a very high concentration ($>$ 10 mg/ml) to room temperature, the solution gelates. This is, again, evidence for a fine balance between strong interchain interaction and solubilization. This behavior stands in contrast to that of the linear isomer (**98**) which precipitates already at low concentrations with almost no change in the absorption spectrum. P3HT, for comparison, also gelates under certain conditions, but only in poor solvents at low concentrations.[79] The higher the regioregularity, the lower is its tendency to gelate. At very high regioregularities, it rather precipitates.

It can be concluded, that the curvature in polymer **88** increases the tendency to remain in solution but still allows efficient intermolecular interaction. During the fabrication process of the field-effect transistors, the polymer already organizes

itself in solution, so a good interfacial morphology can form. The linear polymer **98**, in contrast, interacts so strongly, that precipitation sets in quickly. Under the present processing conditions, no optimum interfacial morphology is formed because the mutual interactions of the polymer chains are too strong. If a precipitate settles on the silicon wafer, the bulk morphology shows high order in X-ray diffraction experiments, but no good contact to the dielectric is formed.

It can, furthermore, be assumed that the curved structure of polymer **88** introduces more flexibility to the material. Very short annealing times (five minutes) at low temperatures (100 °C) are sufficient to reach the maximum field-effect mobility. Often, longer annealing times at higher temperatures are needed to create high order and to reach the maximum field-effect mobility.[80, 81]

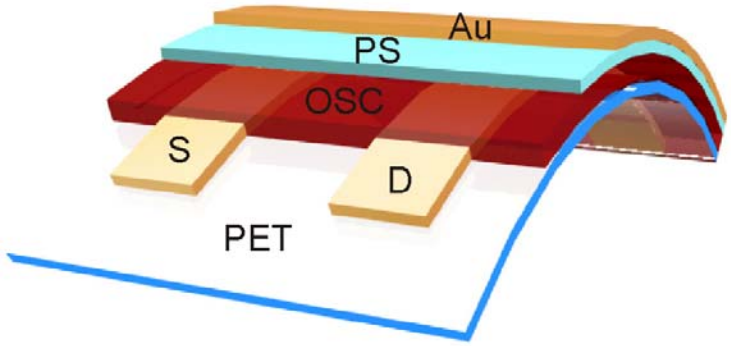

Figure 5.23: Transistor setup on flexible substrate, OSC: organic semiconductor (**88**), S: source electrode, D: drain electrode, Au: gold gate electrode.

5.4 Flexible Substrate

The great advantage of organic semiconductors over their inorganic counterparts is the mechanical flexibility which opens totally new possiblities for products.[82–85] It is obvious that silicon wafers, which are typically used as substrates to measure the mobility of organic materials, cannot be used. They are brittle, heavy, and expensive. Flexible polymeric substrates are essential to probe the potential of a material towards appliances.

Polyethylene terephthalate (PET) is the most promising material in this sense: it is cheap to produce, mechanically and chemically very stable, its fabrication is well established, and it is environmentally benign. Also, it has shown to be compatible with organic semiconductors.[86–89]

Testing polymer **88** on such substrates seemed most promising as it fulfils all requirements for potential applications: it is easily processed from solution, forming transistors with high reproducibility. Furthermore, it does not need annealing at high temperatures nor for long periods, it exhibits high charge-carrier mobility, and it is easily synthesized. The polymer is dissolved in chlorobenzene and spin coated on a PET film with prestructured gold source and drain electrodes. Polystyrene (PS) is spin cast on top as the dielectric. Finally, the gate contact is made by evaporating gold on the PS layer. The schematic setup can be seen in Figure 5.23.

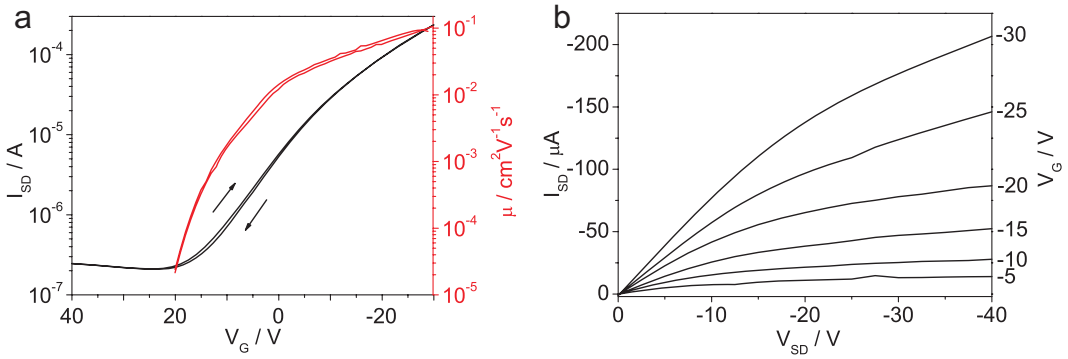

Figure 5.24: Field-effect transistor characteristics on flexible substrate **a.** transfer (V_{SD} = -30 V) and **b.** output curves.

The semiconductor is sandwiched in between polymer layers. This represents an encapsulation against air and moisture, albeit the protection is only weak. Many materials need much more drastic protection against environmental contact.[90, 91]

The measurements are done in collaboration with Marcel Kastler and the BASF Competence Center for Organic Electronics in Singapore. The results are depicted in Figure 5.24. The transfer curve shows practically absent hysteresis and good switching behavior. The field-effect mobility reaches $\mu_{sat} = 0.1$ $cm^2V^{-1}s^{-1}$already at a gate voltage of -30 V and a source-drain voltage of -40 V. This is very favorable with respect to applications in which the driving voltages should not be high. When reducing the layer thicknesses, even lower driving voltages are expected because the electric field is the effective parameter for the transistor performance.

The measurements are made at ambient conditions, which normally means high humidity in Singapore. The PET layer on the one hand and the PS layer on the other hand offer enough protection against oxygen and moisture that no changes can be observed after several days. This means that the polymer is sufficiently stable for the desired devices as was expected from the benzo annellation reducing the ionization potential.

When the source-drain voltage is increased to -60 V as is usually done for FET on silicon wafers, the mobility increases to $\mu_{sat} = 0.5$ $cm^2V^{-1}s^{-1}$. The corresponding transfer curve is depicted in Figure 5.25. It shows no hysteresis and good switch-

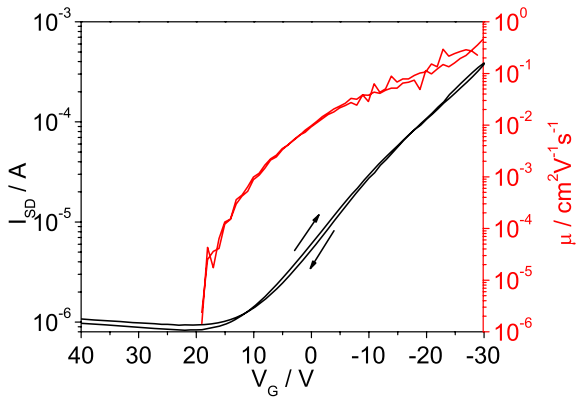

Figure 5.25: Transfer curve of an FET with polymer **88** on PET with source-drain voltage of -60 V.

Channel length in μm	μ_{sat}/ **cm^{2}V^{-1}s^{-1}**
10	0.104 ± 0.007
25	0.098 ± 0.003
50	0.103 ± 0.003
75	0.096 ± 0.010
100	0.095 ± 0.008

Table 5.3: Field-effect mobility of transistors on PET substrates at a source-drain voltage of -30 V, average value of 20 measurements.

ing behavior. There are some fluctuations in the curve which is most likely an artifact of the instrument as the current densities are relatively high. The reliability, however, is remarkable. For six different measurements a standard deviation of only 0.012 cm^{2}V^{-1}s^{-1}or 2.4 % is observed, a very good value for polymeric transistors.[7]

The on-off ratio is just above 100 between gate voltages of 0 V and -20 V. In all-polymer devices, however, higher values have not been reached so far. P3HT fabricated under identical conditions also shows an on-off ration of about 100. The transistor does not completely switch off at 0 V, a voltage of +20 V is needed instead. Further optimization of the device which are ongoing should improve the performance, but for low-cost applications such as radio-frequency identification tags, this value is sufficient.[92]

Another feature of the present material is the independence of the performance on the channel length. Table 5.3 shows the field-effect mobility at channel lengths between 10 and 100 μm. The transistor is operated at a source-drain voltage of -30 V and a gate voltage of -30 V. The mobility does not significantly deviate for the different device geometries. This is a very favorable fact for the built-up of complex circuitries.[93–95] Also, the material may be used for a variety of different devices regardless of their size. Again, the low standard deviations of the mobility in different measurements stress that this material is extremely reliable which is rarely found for the known materials so far.

5.5 Solar Cell

Thin-film solar cells from organic materials are expected to contribute to replace fossile energy supply in the future and open the market for new applications.[96–99] Polymers are attractive materials as they readily form films. In order to obtain a current out of a solar cell, the tightly bound excitons have to be separated after excitation.[100, 101] This is best achieved when preparing a bulk heterjunction with fullerenes.[102, 103] Efficiencies between 4 and 5 % have been realized with P3HT and phenyl-C_{61}butyric acid methyl ester (PCBM).[8, 104]

Polymer **88** is very promising towards a thin-film solar cell. It is easily processed with high reproducibility and has proven to be highly effective in an organic field-effect transistor (previous section). Furthermore, it is structurally similar to P3HT, but absorbs light at longer wavelengths, thus absorbing more photons of the solar spectrum. Its high aggregation tendency and crystallinity upon spin casting are expected to yield efficient solar cells. The following measurements are done by Miaoyin Liu and Chen Li in the institute.

The first issue to be resolved is choosing the appropriate acceptor. Fullerene derivatives have proven to be very effective. Several derivatives varying in size and substituent are available.[105] A good match of the electronic levels of donor and acceptor is essential for the solar cell to work and achieve a good performance.[106, 107]

To select the right acceptor, the energy levels of polymer **88** are determined by film cyclic voltammetry with an ITO working electrode and a platinum counter electrode with a silver quasi reference electrode. The HOMO level is calculated by the onset of the oxidation peak to be -5.2 eV. The LUMO level is determined by adding the optical band gap of 2.0 eV, giving -3.2 eV. Phenyl-C_{71}butyric acid methyl ester ([70]PCBM) fits well to these energy levels. Its LUMO level is determined to -4.3 eV and its HOMO level to -6.1 eV. This means that there is a 0.9 eV driving force to separate the exciton and a remaining 1.1 eV offset between the HOMO

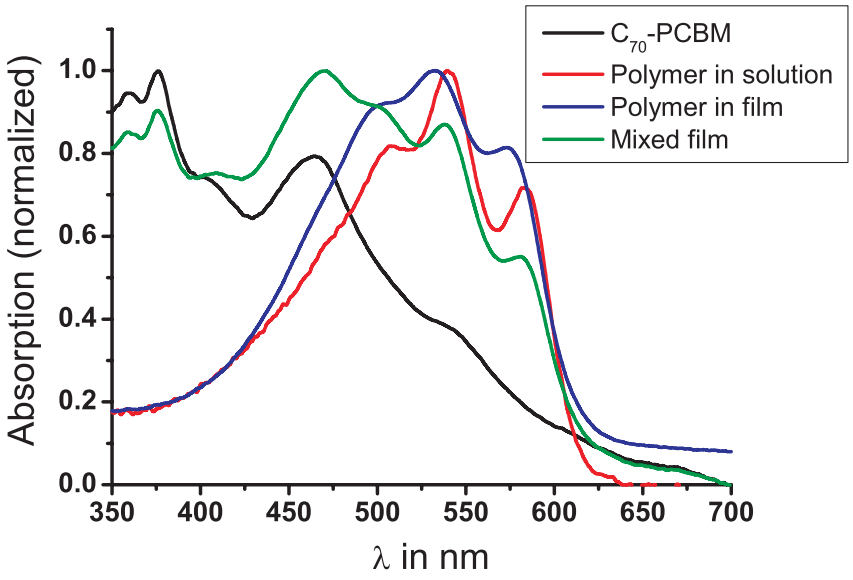

Figure 5.26: UV-vis absorption spectra of polymer **88** and [70]PCBM in a film.

level of the polymer and the LUMO level of the PCBM which determines the open circuit voltage.[100]

Figure 5.26 shows the UV-vis absorption spectra of polymer **88** and [70]PCBM in the film. For comparison, the solution spectrum of **88** is added. It can be seen that the absorption of **88** is almost identical in solution at room temperature to the film. This stresses, once again, the strong aggregation tendency of the polymer which does not lead to precipitation.

The film absorption of both [70]PCBM and polymer **88** span the whole region up to 600 nm, so harvesting of photons out of the solar spectrum is expected to be quite efficient. The absorption spectrum of the film of blended [70]PCBM and polymer **88** resembles the superposition of the separate film spectra. This indicates that the two compounds have separated into different phases as required for a bulk heterojunction.[108]

For the fabrication of photovoltaic cells, ITO substrates are first cleaned with acetone and isopropyl alcohol in an ultrasonic bath, followed by a cleaning treatment for 10 min with oxygen plasma. Subsequently, a 40 nm layer of PEDOT-PSS is spin-cast from an aqueous solution. On top, an *o*-dichlorobenzene solution containing

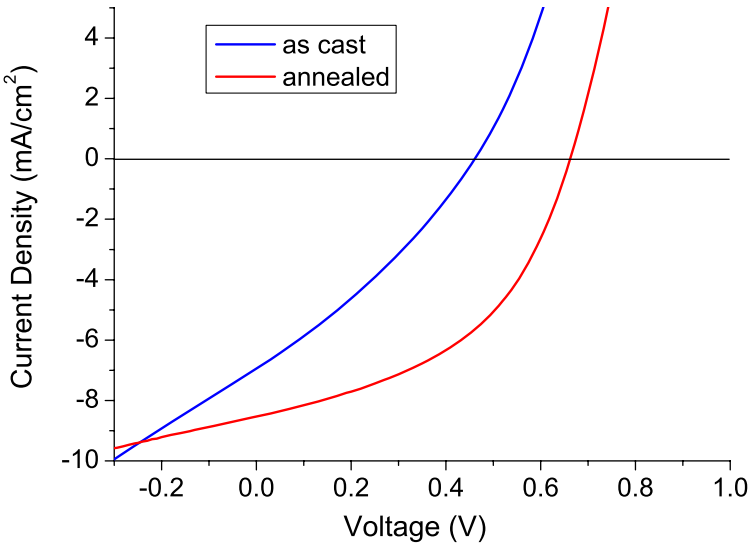

Figure 5.27: Current density-voltages curves of the photovoltaic cell with polymer **88** and [70]PCBM under AM1.5G illumination.

polymer **88** (8 mg/ml) and [70]PCBM (16 mg/ml) is spin cast. 1,8-Octanedithiol is used as a processing additive to enhance the phase separation process.[109] Another PEDOT-PSS layer is spin-cast on top followed by a silver layer (100 nm) deposited from the gas phase.

The cell is illuminated with 1000 W/m^2 of AM1.5G which resembles the solar spectrum.[110] The current density-voltage curve is shown in Figure 5.27. As cast, the cell reaches a power conversion efficiency of $\eta = 1\%$ with an open-circuit voltage of V_{OC} = 0.46 V and a short-circuit current density of J_{SC} = 6.94 mA/cm^2. The fill factor is determined to FF = 0.31.

The cell is annealed at 120 °C for two minutes, after which the performance increases significantly. Further annealing increases the performance only slightly, a plateau is reached after five minutes. After this period a power conversion efficiency of $\eta = 2.7\%$ is measured. The red curve in Figure 5.27 demonstrates the improvement in contrast to the blue one. The open-circuit voltage has increased to V_{OC} = 0.68 V, the short circuit current density to J_{SC} = 7.61 mA/cm^2. Also, the

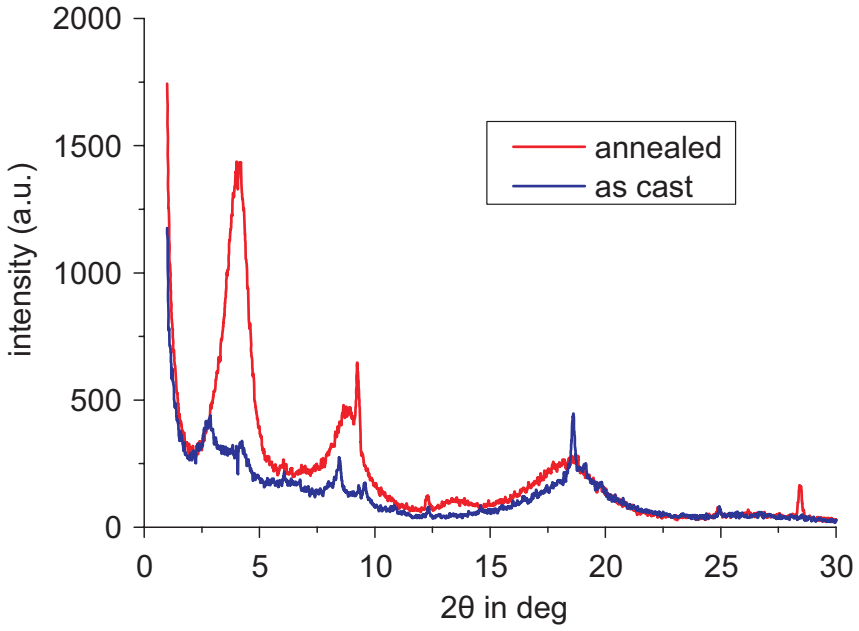

Figure 5.28: X-ray reflectometry of the blend of polymer **88** and [70]PCBM before and after annealing.

fill factor increases to FF = 0.43 as can be seen by the more strongly bent curve in Figure 5.27.

In comparison, a solar cell made of P3HT and PCBM shows about the same open-circuit voltage and short-circuit current.[111] Only the fill factor of the latter is higher (FF = 0.65) finally leading to 5 % power conversion efficiency. The annealing effect of the power conversion efficiency is classically explained by an improved phase separation of PCBM and the polymer leading to more percolation pathways.[112] Consequently, the short-circuit current density increases upon annealing while the open-circuit voltage and the fill factor remain essentially the same. In the present case, all values increase at the same time.

To get a better understanding of the annealing process, the films are subjected to X-ray reflectometry. The results are depicted in Figure 5.28. The film as cast only shows weak reflections with some crystalline domains of the [70]PCBM according to the broad peak around $2\theta = 18°$.[113] After annealing, intense peaks originating from the lamellar packing of the polymer arise at $2\theta = 4°$ and $2\theta = 8°$. It can,

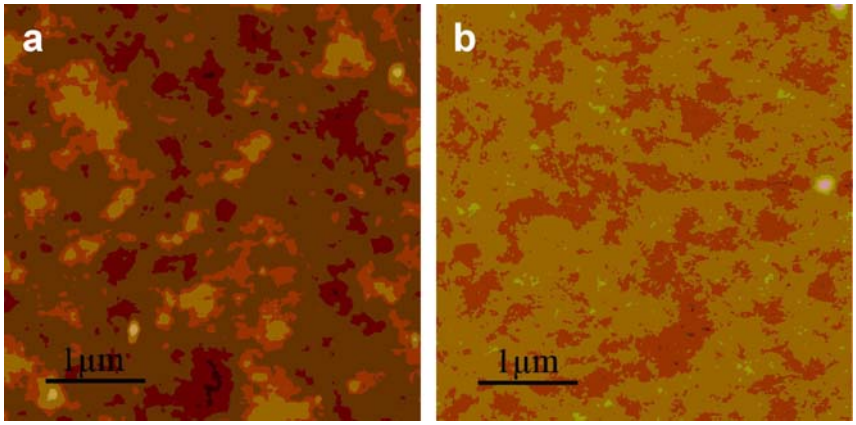

Figure 5.29: AFM images (tapping mode) of the blend film out of polymer **88** and [70]PCBM before and after annealing.

therefore, be assumed that the polymer and [70]PCBM do not phase separate effectively upon spin casting. Thermal motion is needed to drive the molecules apart allowing polymer **88** to crystallize. The lower degree of crystallinity and the contact to PCBM influences the energy level of polymer **88** thus explaining the shift of the open-circuit voltage.

Further insight into the film morphology is gained by AFM. Due to the softness of polymers, structural features can only be obtained in tapping mode. The images are depicted in Figure 5.29. Before annealing, a coarse two-phase system is seen. Only few percolation pathways through the two phases are present limiting the current flow by trapping the charges. Upon heating, a much finer structure is obtained increasing the heterojunction surface leading to a more efficient exciton separation. Also, more percolation pathways are created enabling the harvesting of the generated charges by the electrodes. This effect is well known for other polymer-PCBM systems.[114]

5.6 Varying the Degree of Curvature

In section 5.3 on page 154, it could be shown that the introduction of curvature into the polymer backbone is avery effective method to find a compromise between high order in the film but sufficient solubility in organic solvents. The latter is very important to fabricate devices from solution and to control the film formation process. In order to probe if the degree of curvature of polymer **88** is the optimum compromise or if other degrees of curvature are more advantageous, a series of structurally very similar polymers are synthesized. These shall all be isomers consisting of unsubstituted benzodithiophenes copolymerized with alkylated dithiophene units.

For the sake of stability and selectivity, only those benzodithiophenes are chosen with thiophenes fused at their b-side, leaving one α position as a connection site to the dithiophenes. C-fused thiophenes alter the electronic levels of the resulting polymers due to their partial quinoid structure.[115, 116] The latter would render less stable polymers which is undesirable.

Five benzodithiophene isomers are conceiveable in which both thiophenes are b-fused to the central benzene unit. As Figure 5.30 shows, the bond angles induced by these five building blocks differ significantly. Linear connectivity is found for benzo[1,2-b;4,5-b']dithiophene (**96**). A slight deviation from linearity is obtained by using benzo[2,1-b;4,5-b']dithiophene (**99**), *i.e.* an angle of 169.2°. Monomer **82** and polymers thereof have been described in section 5.2.4 on page 143. Its bonding angle of 127° is an intermediate value in the present series. Stronger angles are found for benzo[1,2-b;3,4-b']dithiophene (**100**) (113.0°) and even more for benzo[1,2-b;4,3-b']dithiophene (**101**) (105.9°). The bond angles are determined by a DFT structure optimization using the B3LYP method and the 6-31G basis. Monomer **100** is not symmetric and thus induces irregularities along the polymer backbone as the condensation reaction is not selective with regard to the orientation

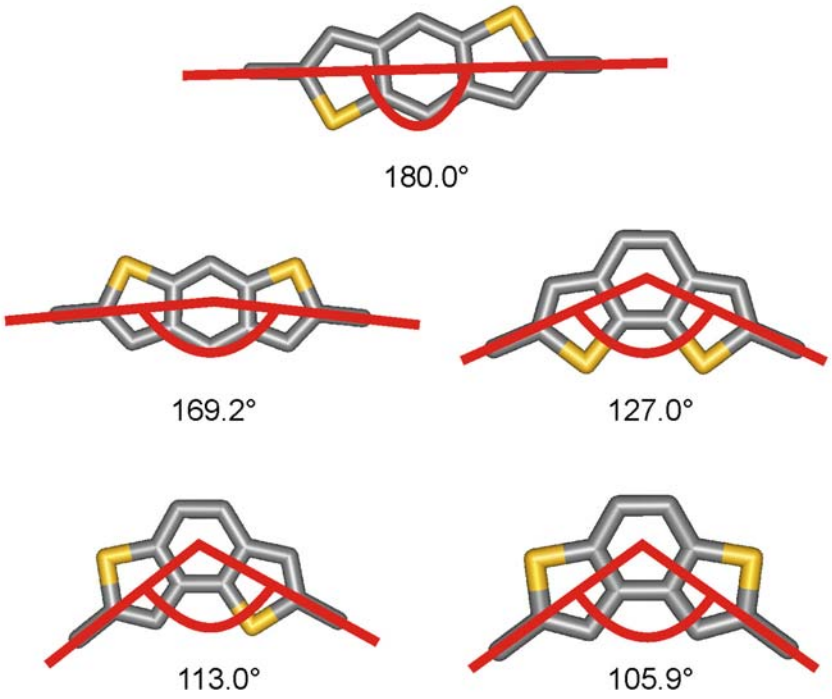

Figure 5.30: Bond angles of the five benzo[b]dithiophenes as determined by DFT calculation (B3LYP method, 6-31G basis).

Isomer	Bond Angle	Wavelength (nm)	Amplitude (Å)
96	180.0°	1.47	1.35
99	169.2°	2.82	2.86
82	127.0°	2.83	3.11
100	113.0°	2.75	5.89
101	105.9°	2.32	8.75

Table 5.4: Influence of the bonding angle of the benzodithiophene building block on the curvature of the polymer backbone.

of the monomer. The electronic impact should, however, be very low due to the very similar structure on both sides of the benzodithiophene.

The curvatures introduced to a polymer backbone consisting of the benzo[b]dithiophenes and dithiophene as comonomer are depicted in Figure 5.31. Following the trend of the bond angles, the curving amplitude increases and the wavelength decreases.

A quantitative analysis is given in Table 5.4. The structures are geometry optimized by the MMFF force-field method. The wavelength and amplitudes are de-

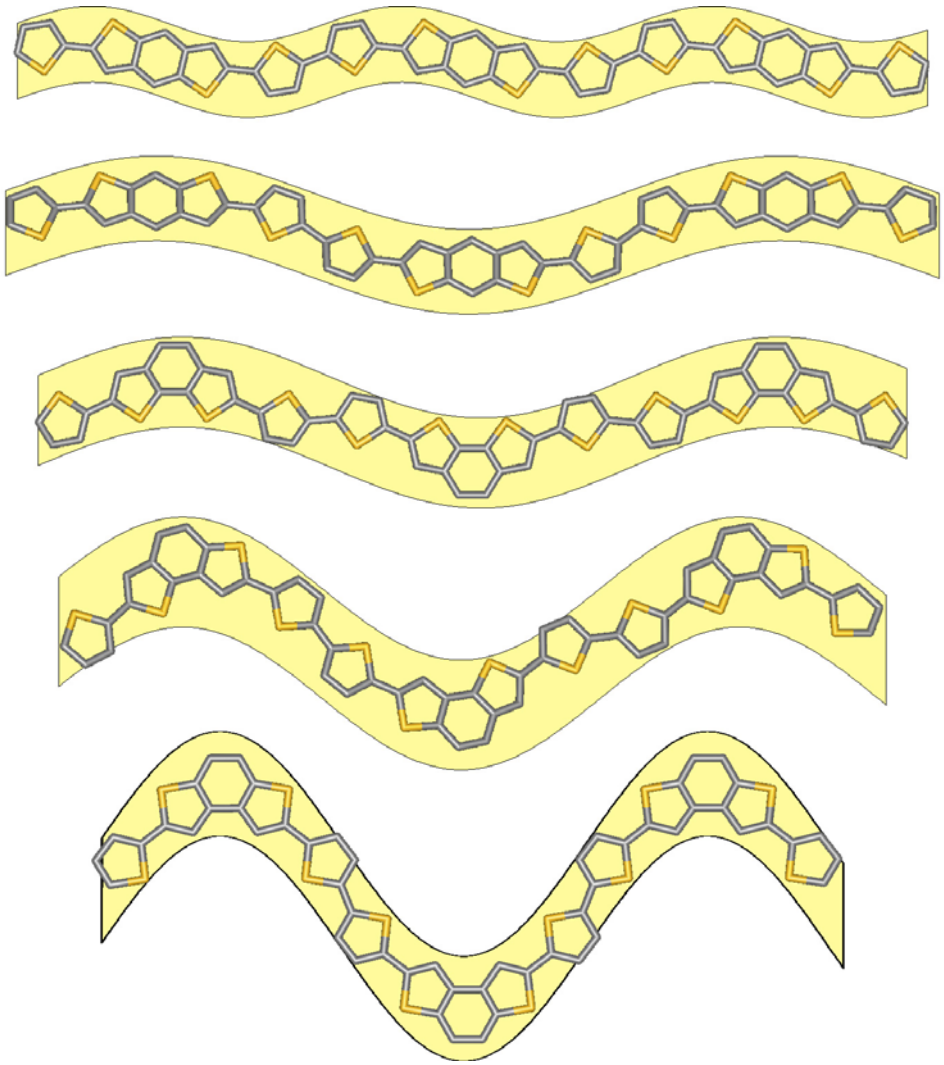

Figure 5.31: Curved polymer backbones resulting from the benzo[b]dithiophene series copolymerized with dithiophene.

termined by fitting sine functions to the contour line of the polymer structure. The "linear" isomer still leads a curved polymer backbone, but the amplitude is very low. The wavelength for this polymer is shorter than those for the other polymers because already half of the rings form a periodic element. If it was determined in analogy to the other polymers, double the value would result being the highest for all isomers.

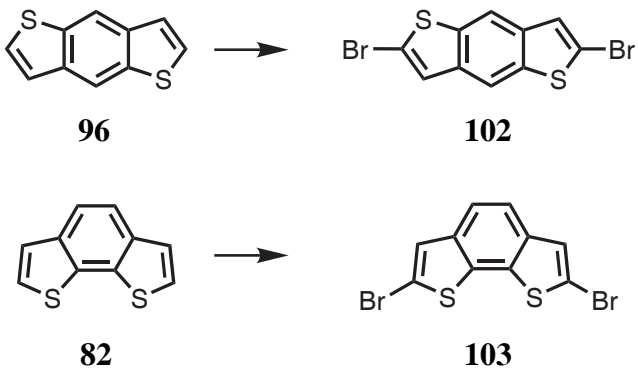

Figure 5.32: Synthesis of dibromobenzo[2,1-b;3,4-b']dithiophene (**103**) and dibromobenzo[1,2-b;4,5-b']dithiophene (**102**), conditions: N-bromosuccinimide, chloroform - DMF - acetic acid (5:5:1), RT, 50-60 %.

5.6.1 Synthesis

The preparation of all benzodithiophenes is described in the literature. It seemed straightforward to synthesize the missing three benzodithiophene molecules according to these procedures and stannylate them as it was done for **82** and **96** earlier in this chapter. Nevertheless, it turns out that the isomers with bond angles more strongly deviating from linearity do not crystallize from typical solvents. This means, that only non-pure monomer is obtained which cannot be used to make polymers of high molecular weight.

To anyway obtain the polymer series, a different strategy had to be followed. As described in section 5.2.2 on page 138, the benzodithiophenes can be coupled with two alkylated thiophenes first. These molecules can be polymerized in the presence of iron(III) chloride. For the sake of comparability, the two polymers already synthesized by Stille coupling (**88** and **98**) had to be made via this route as well. This opened the chance to also compare the influence of the polymerization process on the field-effect mobility of the resulting polymers.

For all benzodithiophenes, the α,α-dibromo derivatives are needed to later couple alkylated thiophenes. For dibromobenzo[2,1-b;3,4-b']dithiophene (**103**) and dibromobenzo[1,2-b;4,5-b']dithiophene (**102**), the route is straightforward as de-

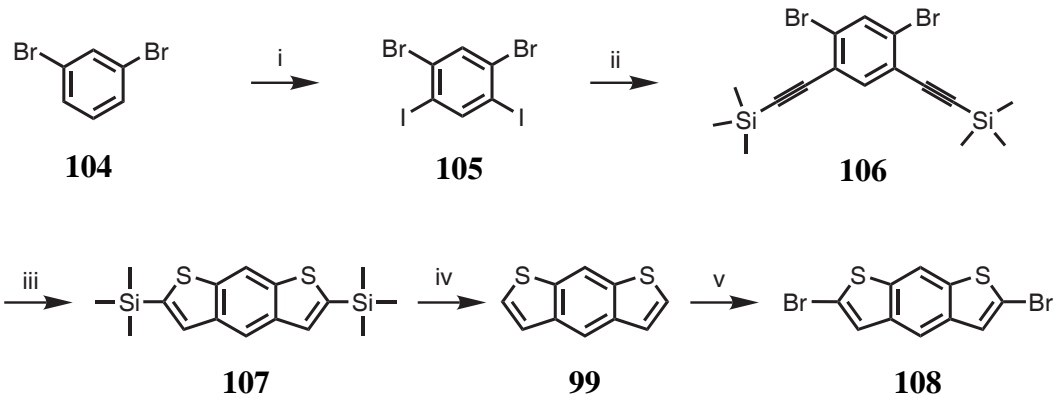

Figure 5.33: Synthesis of dibromobenzo[2,1-b;4,5-b']dithiophene (**108**), conditions: *i* I_2, $H_2SO_4 \cdot SO_3$, 120 °C, 35 %; *ii* trimethylsilylethyne, $Pd(PPh_3)_2Cl_2$, THF, diisopropylamine, RT, 71 %; *iii* 1. *t*-butyllithium, THF, -78 °C, 2. S_8, RT 3. ethanol, RT, 15 %; *iv* Bu_4NF, THF, RT, 81 %; *v* 1. *t*-butyllithium, THF, -78 °C, 2. CBr_4, -78 °C, 69 %.

picted in Figure 5.32. The already available reagents **82** and **96**, which have been previously stannylated, can be brominated by nucleophilic aromatic substitution using NBS and catalytic amounts of acetic acid. The products are obtained in high purity after crystallization. The solubility of the linear molecule (**102**) is much lower than that of the kinked one (**103**), a consequence of the higher symmetry and thus higher lattice energy in the crystal.

In the case of the other three benzodithiophenes, more synthetic work has to be done. Benzo[2,1-b;4,5-b']dithiophene (**108**) has been described in the literature using a long and tedious synthetic procedure.[117] Here, the method described for **96** is used (compare Figure 5.18 on page 154).[68]

As outlined in Figure 5.33, 1,3-dibromobenzene (**104**) is iodinated in oleum with iodine to afford 1,3-dibromo-4,6-diiodobenzene (**105**). A subsequent selective Sonogashira-Hagihara reaction with trimethylsilylethyne yields compound **106**. This molecule can be doubly lithiated with tert-butyllithium. Upon addition of elemental sulfur, the thiolate is formed. When protonated after the addition of ethanol, the thiol adds to the triple bond to form benzodithiophene with two trimethylsilyl groups (**107**).

A direct conversion of the trimethylsilyl group into a bromine group by aromatic ipso substitution is unsuccessful although described in the literature for a similar structure.[118] Instead, the bromine substitutes the β positions and leaves the trimethylsilyl groups unaffected.

The trimethylsilyl groups are cleaved with tetrabutylammonium fluoride, a highly effective method.[119] This gives the unsubstituted benzo[2,1-b;4,5-b']dithiophene (**99**), which cannot easily be converted to the dibromo compound (**108**) by nucleophilic bromination using N-bromosuccinimide or bromine. A complex mixture of regioisomers is obtained as evidenced by NMR spectroscopy. Both α and β positions seem to be of comparable reactivity towards electrophilic aromatic substitution. This can be understood when comparing similar systems. Benzo[b]thiophene is brominated selectively at the β position of the thiophene instead of the α which is the most reactive position in most thiophene derivatives.[120] Benzo[2,1-b;4,5-b']dithiophene (**99**) may be just the intermediate case with equal reactivity at both positions.

Dibromination of **99** is, instead, done by lithiation and subsequent treatment with tetrabromomethane. The lithiated species nucleophilically attacks a bromine atom of the tetrabromomethane leaving a tribromomethyl anion. At temperatures above -78 °C, it eleminates bromide and forms dibromocarbenes which decompose the product.[121] To avoid such decompositions, the reaction needs to be quenched at -78 °C. Tetrabromomethane as the bromination reagent is superior to other reagents, such as dibromoethane, because no reactions can occur other than bromine transfer.

Benzo[1,2-b;4,5-b']dithiophene (**101**) can be made photochemically.[122] For this reason, 2-carbonylthiophene (**109**) is reductively coupled in a McMurry reaction to yield E-dithienylethene (**110**).[123] This molecule is dibrominated by lithiation and treatment with tetrabromomethane as described above for **108**, the double bond does not tolerate electrophilic substitution with NBS or bromine. Compound **111**

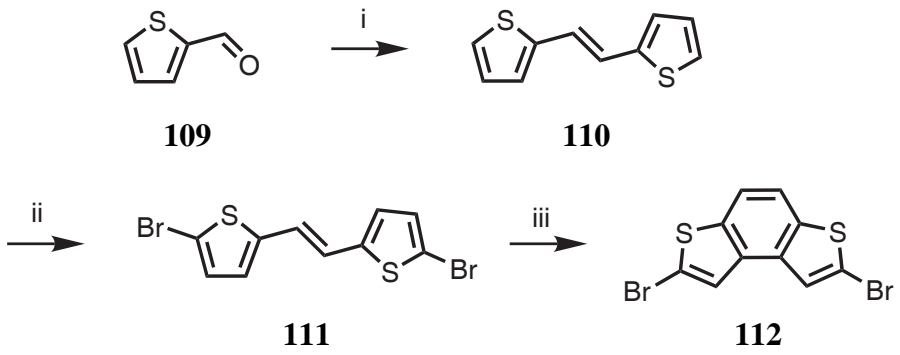

Figure 5.34: Synthesis of dibromobenzo[1,2-b;4,5-b']dithiophene (**112**), conditions: *i* $TiCl_4$, Zn, THF, reflux, 48 %; *ii* 1. *t*-butyllithium, THF, -78 °C, 2. CBr_4, -78 °C, 54 %; *iii* 350 nm irradiation (160 W), toluene, cat. I_2, RT, 86 %.

is relatively unstable; it has to be stored under argon at low temperatures. The dark color which develops on storage suggests cleavage of the C-Br bond.

Substance **111** is cyclodehydrogenated by UV irradiation at 350 nm in toluene. The double bond firstly isomerizes to the Z configuration from which it can undergo an intramolecular cycloaddition reaction. In the presence of oxygen, product **112** is formed. Catalytic amounts of iodine speed up this process significantly. Stoichiometric amounts, however, cannot be used because iodine adds to the double bond irreversibly under these conditions as evidenced by NMR spectroscopy. The isomerization reaction of the double bond is much faster than the cyclodehydrogenation as was discovered by NMR measurements of the reaction which had not gone to completion. Two days are needed for the reaction to complete, although lamps with a total power of 160 W are used. The low extinction coefficients of the Z intermediate may be responsible for this long reaction time. The use of 350 nm irradiation is, nevertheless, advantageous as the product does not absorb this irradiation and is thus hindered to undergo unwanted side reactions.

Benzo[1,2-b;3,4-b']dithiophene (**100**) is also accessible via photochemical cyclodehydrogenation. The required dithienylethene (**116**) needs a few additional steps in comparison to **110**. Firstly, thiophene is chlormethylated with formaldehyde in concentrated hydrochloric acid through which HCl gas is bubbled.[124] The

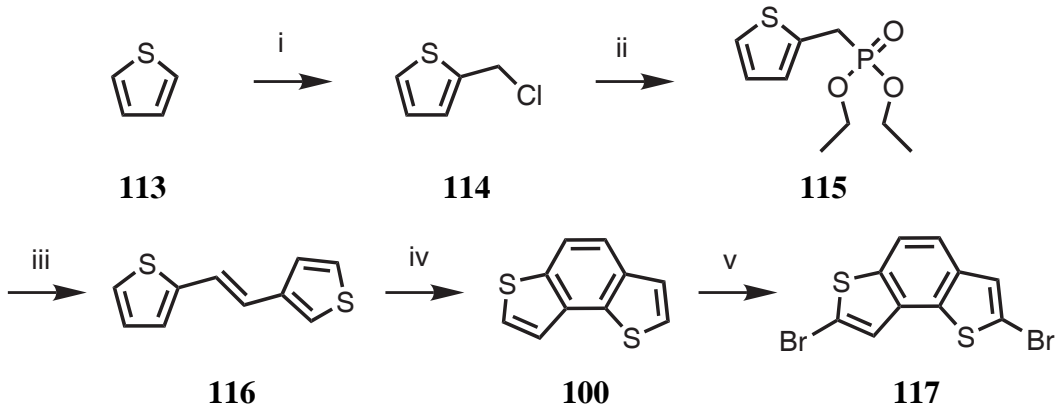

Figure 5.35: Synthesis of dibromobenzo[1,2-b;3,4-b']dithiophene (**117**), conditions: *i* HCHO, HCl, 0 °C, 23 %; *ii* $P(OEt)_3$, 150 °C, quantitative; *iii* KO-t-Bu, 3-carbonylthiophene (**59**), THF, 0 °C, 49 %; *iv* 350 nm irradiation (160 W), toluene, cat. I_2, RT, 28 %; *v* 1. *t*-butyllithium, THF, -78 °C, 2. CBr_4, -78 °C, 29 %.

product (**114**) is collected by distillation. Triethylphosphite reacts with it in an Arbusov reaction to give phosphonate **115**. Best results are obtained when both reagents are heated to 150 °C without solvent.[125] The product can be used without any purification.

A Wittig-Horner reaction of **115** with 3-carbonylthiophene (**59**) is run with potassium tert-butylate as base to afford E-dithienylethene (**116**). This reaction produces the E isomer in high selectivity enhancing purification and facilitating analysis.[126]

Photochemical cyclodehydrogenation is performed following the procedure for **101**. The yields in the present case are significantly lower than for **101**. The reason is given in the literatue and depicted in Figure 5.36.[127] After isomerization to the Z configuration, the dithienylethene (**118**) cyclizes to the dihydro adduct **119**. An oxidant like oxygen or iodine can abstract one of the two hydrogen atoms highlighted in Figure 5.36 to form either **120** or **121**. The former can gain aromaticity by homolytic cleavage of the C-S bond to form molecule **122**. This radical decomposes in an undefined way giving only intractable products.

Radical **121**, however, is stable enough until a second oxidant removes the adjacent hydrogen to form the final product (**100**). This means that a maximum yield of 50 % can be obtained given an equal first hydrogen radical abstraction. The higher

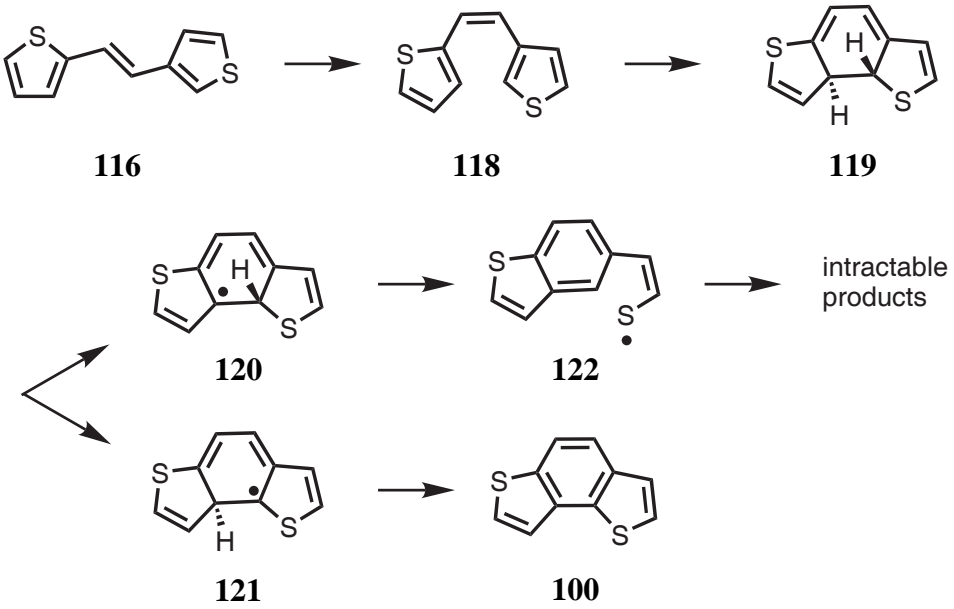

Figure 5.36: Mechanism of the photochemically induced cyclodehydrogenation to from benzo[1,2-b;3,4-b']dithiophene (**100**).

yield of **101** accounts for the fact that either hydrogen abstraction leads to a relatively stable radical, so no unwanted side reactions lower the yield. On the other hand, **82** cannot be synthesized photochemically from dithiophene-3-yl-ethene because exclusively unstable radicals are formed similar to **120**.

As the precursor for the cyclodehydrogenation reaction (**116**) can be made in large scale, it is possible to obtain reasonable amounts of benzodithiophene **100**. This compound is an oil which is not very stable towards air oxidation. It needs to be stored under argon in the fridge, otherwise it becomes dark brown after a few days. Bromination of the molecule is done by lithiation and treatment with tetrabromomethane, in analogy to **108**. Electrophilic aromatic substitution with NBS or bromine produces an isomeric mixture in this case as well. The brominated product (**117**) can be crystallized and exhibits much higher stability than the unsubstituted parent compound (**100**), most likely due to the inaccessability of the reactive α positions of the thiophene moieties.

The monomers needed for the oxidative polymerization are obtained in a Stille coupling from the dibromobenzodithiophenes. Figure 5.37 gives the overview

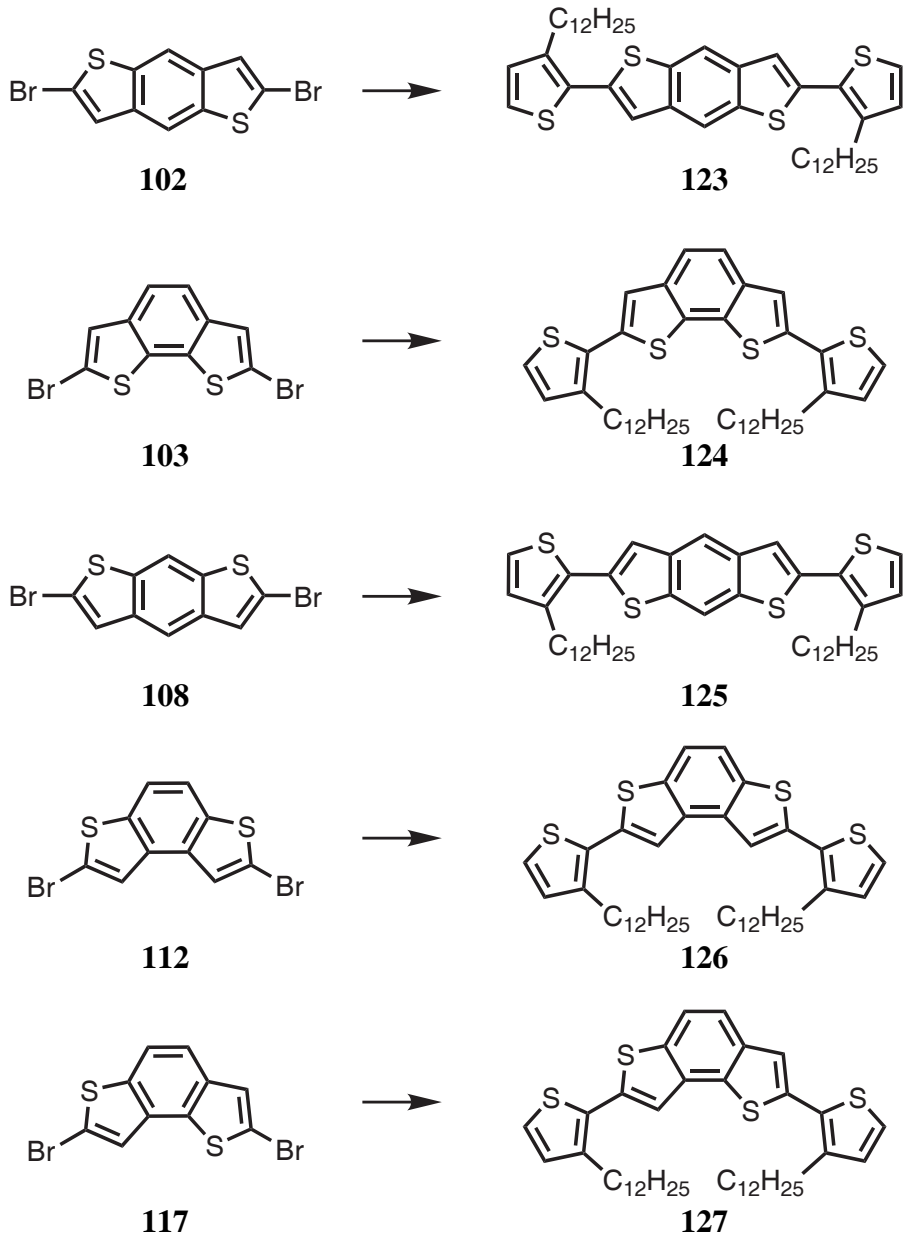

Figure 5.37: Synthesis of the dithienobenzodithiophene monomers, reaction conditions: 2-tributylstannyl-3-dodecylthiophene, $Pd(PPh_3)_4$, DMF, THF, 100 °C, 22-50 %.

of the synthesis. The dibromo compounds are reacted with 2-tributylstannyl-3-dodecylthiophene with the aid of $Pd(PPh_3)_4$ in DMF at 100 °C. As the tin reagent is not well soluble in DMF, it has firstly been dissolved in THF and added to the mixture.

The resulting dithienylbenzodithiophenes are purified by chromatography. Sub-

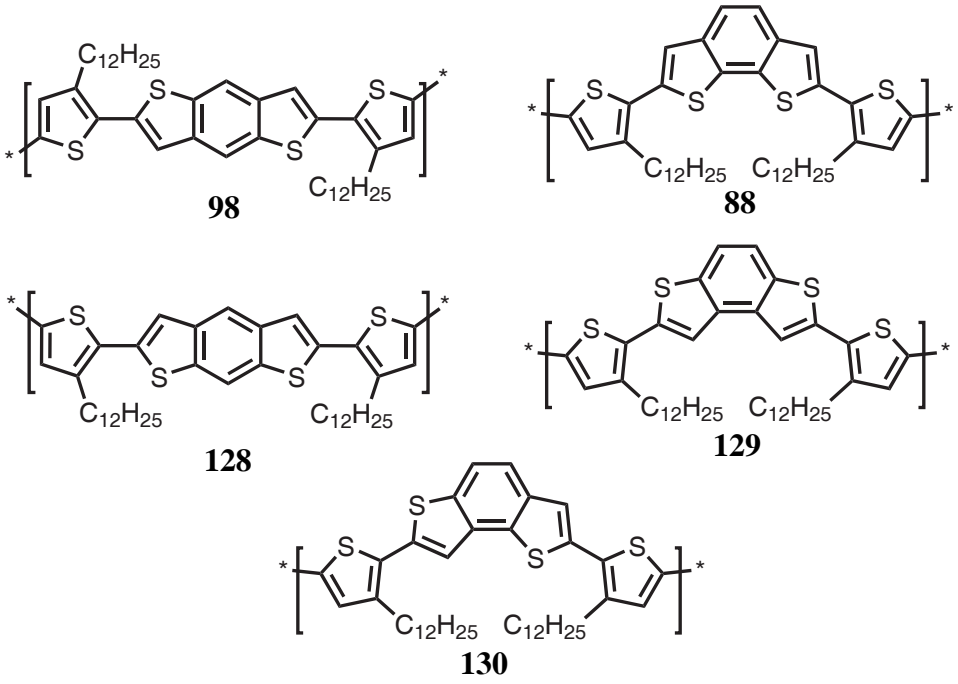

Figure 5.38: Overview of the isomeric polymers of benzodithiophene isomers copolymerized with alkylated dithiophenes.

sequent crystallization from ethyl acetate renders optimum purity for the polymerization reaction. Defects in the polymer chain shall be avoided in this way.

For the polyerization the monomer is dissolved at a high concentration in *o*-dichlorobenzene (50 mg/ml) and added to anhydrous iron(III) chloride. To avoid gelation, the mixture is heated to 60 °C. Figure 5.38 summarizes the thus obtained polymers. Polymers **88** and **98** are identical to the polymers obtained by Stille polymerization (see section 5.2.4 on page 143 and 5.3.1 on page 155).

To monitor the process of the polymerization reaction, samples of polymer **88** are taken after certain periods of time and analyzed by size exclusion chromatography in reference to polystyrene standards. The increase of molecular weight (M_w) is depicted in Figure 5.39. It follows a logarithmic increase, reaching a plateau after about one day at 30 kg/mol.

For the other structures, although chemically very similar, the polymerization rate is dramatically different. For the strongly curved polymer **129**, the molecular

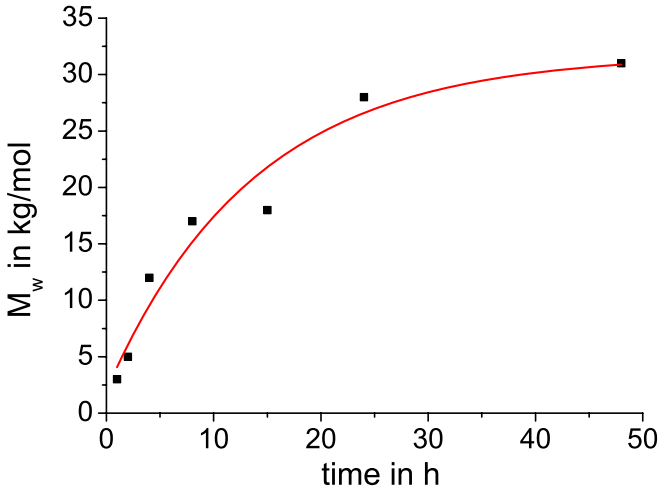

Figure 5.39: Molecular weight increase over time when monomer **124** is exposed to iron(III) chloride in dichlorobenzene at 60 °C.

weight goes up rapidly and reaches 70 kg/mol already after one day, and after two days the polymer is insoluble. The linear polymer **98** cannot be obtained in soluble form. Crosslinking seems to be responsible, because the polymer itself is soluble as shown in section 5.3.1 (page 155) where it is made by Stille coupling. Upon heating in dichlorobenzene for an extended period, the polymer forms gel-like flakes.

5.6.2 Optical Analysis

The absorption and photoluminescence spectra of the monomers **123**-**127** are recorded in order to investigate the electronic differences of the isomers among each other. If they are very similar, the differences of the polymers can be attributed to the curvature of the polymer backbone. The spectra are shown in Figure 5.40.

All spectra are relatively similar, one broad peak between 300 and 350 nm is the main absorption. Compounds **123**, **124**, and **126** show practically identical absorption and photoluminescence spectra. In these compounds, the two sulfur atoms on the benzodithiophene stand either in ortho or in para position to each other. In the other two isomers (**125** and **127**), the sulfur atoms are meta with

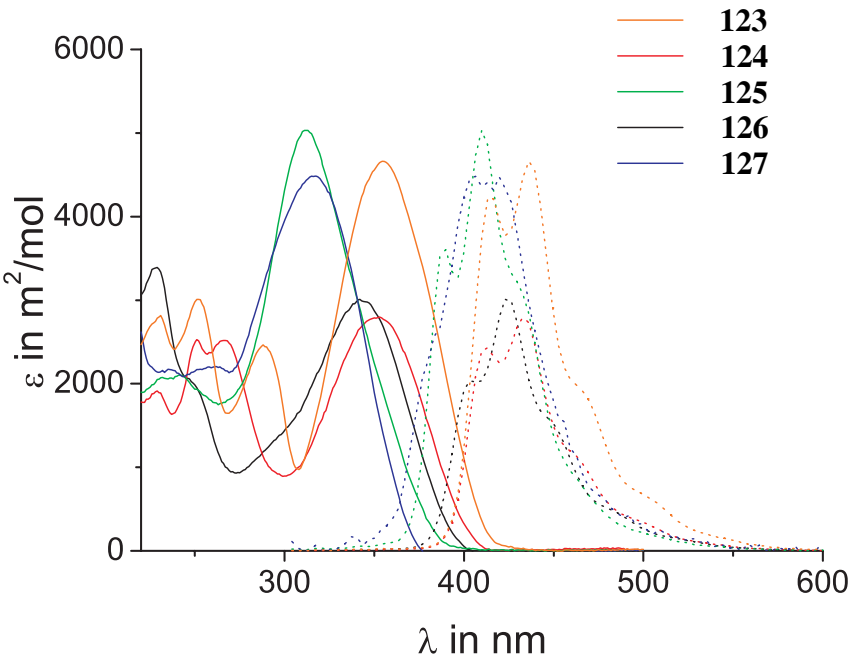

Figure 5.40: UV-vis absorption (solid lines) and photoluminescence (broken lines) of the alkylthienyl substituted benzodithiophene isomers.

respect to the central benzene ring. Their most intense absorption peak is shifted to a shorter wavelength by about 40 nm. Also their optical gaps as determined by the intersection of the absorption and photoluminescence spectra are shifted hypsochromic by about 40 nm.

The extinction coefficients also divide the monomers into two groups, three molecules (**123**,**125**,**127**) possess a value of ε = 5000 m^2/mol and two (**124**,**126**) of ε = 3000 m^2/mol. In this case, the difference does not arise from the meta position of the sulfur atoms. There does not seem to be an obvious reason for it.

Further insight into the electronic structure is gained by quantum mechanical calculations. Figure 5.41 shows the orbital surfaces of HOMO and LUMO of monomers **123**-**127**. There are only subtle differences visible between the isomers in agreement with the very similar absorption and photoluminescence spectra. The conjugation through the entire molecules is high, and there are no nodes either in the center or the ends which would locate the frontier orbitals on one monomer unit in a polymer. The orbital coefficients of the HOMO at the 5-position on the

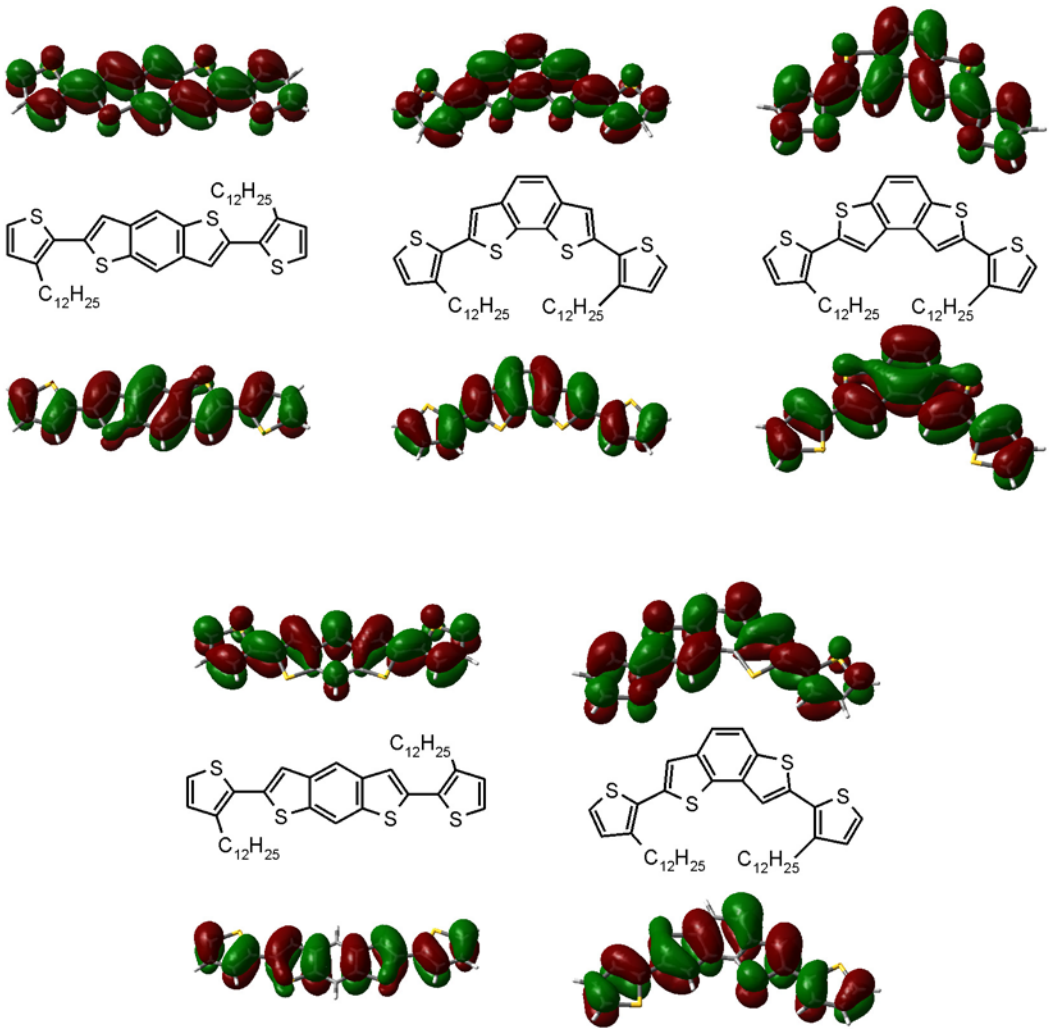

Figure 5.41: Orbital surfaces of the HOMO (below the formulae) and LUMO (above the formulae) of monomers **123**-**127** as determined by HF-SCF calculations (6-31G basis).

thiophene units where the bonds are formed during polymerization are big in all cases. Nevertheless, they are not equal. In molecule **124**, they are smaller than for the rest, explaining the lower polymerization rates leading to lower molecular weight upon iron(III) chlorid induced polymerization.

The UV-vis absorption and photoluminescence spectra of the five polymer isomers are depicted in Figure 5.42. The absorption spectra are recorded both at room temperature and at elevated temperatures to investigate the aggregation tendency (compare section 5.3.2 on page 157). The strong difference of the absorption spectra of polymer **88** between room temperature and higher temperatures have been dis-

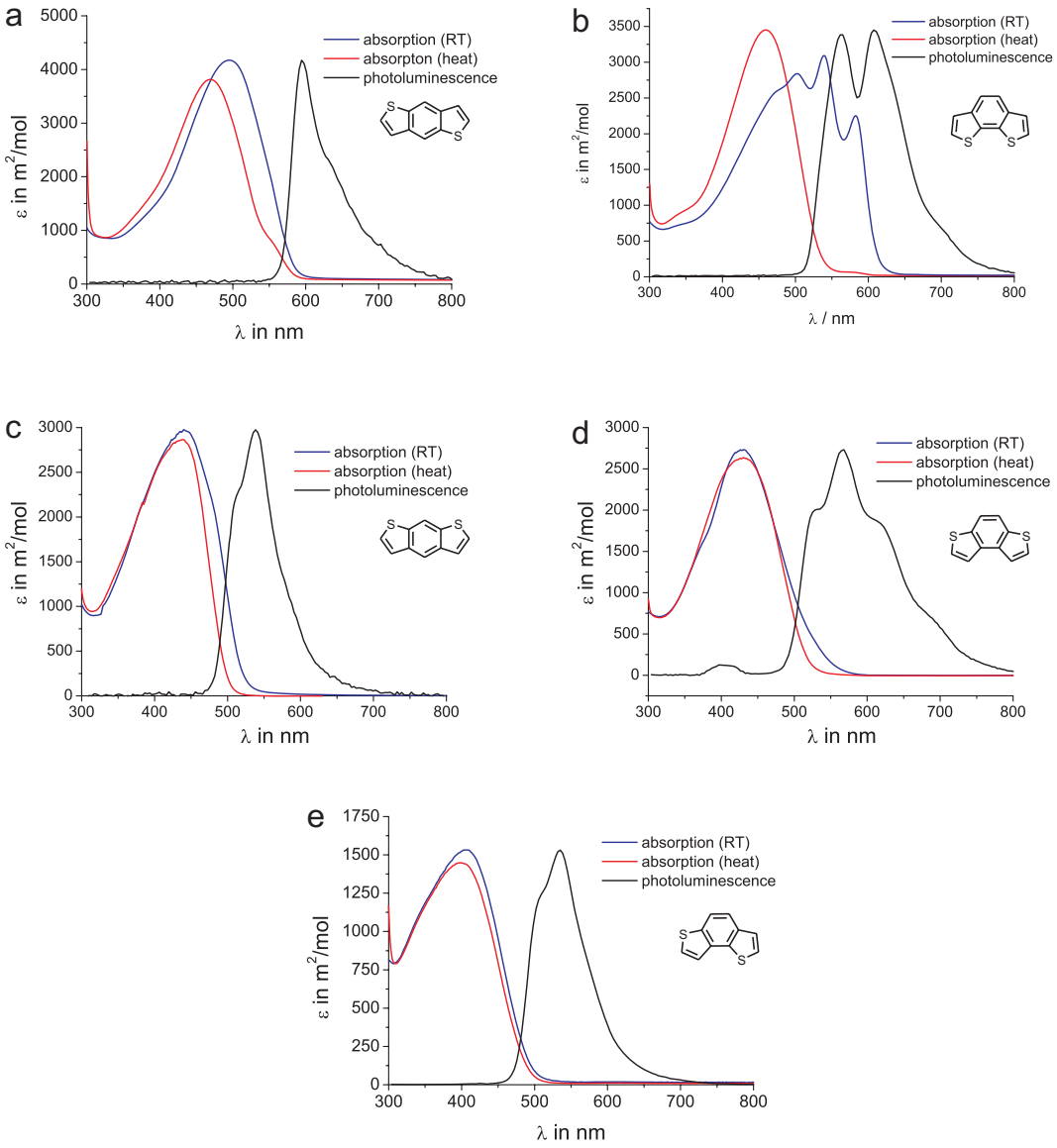

Figure 5.42: UV-vis absorption and photoluminescence spectra of the polymer isomers, the inset structures are the benzodithiophene core of the corresponding polymers.

cussed. The other polymers, in contrast, do not show any significant changes upon heating. No resolved bands are apparent at room temperature which means that only weak aggregation tendencies are present. For the strongly curved polymers **130** and **98**, this result is not surprising due to the dramatic entropy loss aggregation would induce.

The peak value of the absorption as well as the optical gap (intersection of the absorption and photoluminescence spectra) are almost equal for all polymers, only

the linear **98** is shifted bathochromically by 50 nm. This means that the curvature has very little influence on the effective conjugation length as one would expect. Intuitively, one would predict the chain to be less likely in a fully planar conformation the higher the amplitude of the backbone wave. This is obviously not the case as the conjugation along the backbone seems to overcompensate the entropic shortening of the effective conjugation length.

The extinction coefficients as calculated for the repeating unit decreases with increasing curvature. The corresponding monomer does not show the same trend. The transition dipoles may be effected by the kinks, because the antiparallel components of a curved segment cancel mutually. A detailed quantum mechanical treatment would be necessary to fully clarify this observation.

5.6.3 Transistor Characterization

Field-effect transistors for the polymer series are fabricated in the standard setup: highly doped silicon wafers with silicon dioxide dielectric are treated with HMDS to protect the hydroxy groups at the interface. The polymers are spin cast from a 5 mg/ml solution in dichlorobenzene to form a 30-50 nm thick film. Top-contact gold electrodes are deposited from the gas phase. The measurements are run in a nitrogen atmosphere with yellow light.

For polymer **88** oxidatively polymerized with iron(III) chloride, a field-effect mobility of $\mu_{sat} = 1.7 \cdot 10^{-3}$ $cm^2V^{-1}s^{-1}$with an on-off ratio of $I_{on}/I_{off}= 8.8 \cdot 10^3$ has been determined. This is two orders of magnitude lower than for the same polymer made in a Stille coupling reaction. Figure 5.43 shows the transfer and output curves of the transistor. Significant contact resistance is observed which is absent for the same polymer made by Stille coupling (compare Figure 5.13 on page 146). A gate voltage of -13 V is necessary before the current flow begins. As the energy alignment of the polymer and the gold electrode cannot be the reason

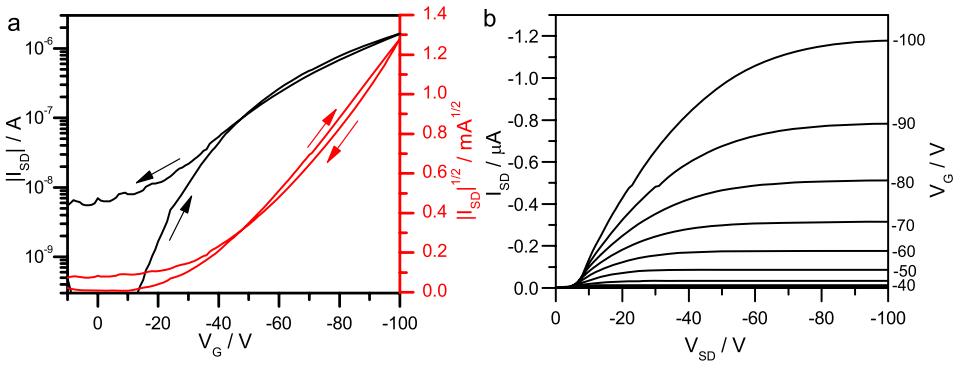

Figure 5.43: Field-effect measurements for polymer **88** polymerized by $FeCl_3$, **a.** transfer and **b.** output curves.

for this, trapping must be present. Crosslinking or defects due to chlorination of the aromatic polymer backbone are likely to be responsible. Furthermore, hysteresis is observed, when sweeping back the gate voltage, the source-drain current does not go back to the low value started from. The creation of permanent charges typically causes this effect. It can be concluded that in future studies, coupling reaction methods should be preferred.

Nevertheless, the lower results can be compared to each other. The slightly less curved polymer **128** exhibits a mobility of about the same order as **88**: $\mu_{sat} = 1.3 \cdot 10^{-3}$ $cm^2V^{-1}s^{-1}$and $I_{on}/I_{off} = 8.5 \cdot 10^3$.

The strongly curved polymer **126** shows a dramatically lower performance. The mobility only reaches $\mu_{sat} = 5.1 \cdot 10^{-6}$ $cm^2V^{-1}s^{-1}$with an on-off ratio of I_{on}/I_{off}=13. The low on-off ratio may arise from residual doping which cannot be completely removed by hydrazine treatment. The low mobility indicates a poor intermolecular interaction. The curving of this polymer is obviously too strong for good device performances.

No significant current flow can be measured for the polymer of intermediate curvature (**130**). As the monomer is not symmetric, and trapping due to irregularities may have occured. In combination with the relatively strong curvature which re-

duces the mobility due to inefficient interchain interactions, the mobility is so low that the current flow cannot be determined.

In conclusion, the moderate backbone curvature of polymer **88** turns out to be the optimum for benzodithiophene containing polymers. Lower curvatures render poorly soluble materials, higher curvature impede an efficient interchain interaction. In this respect, polymer **128** appears very promising in addition to **88** if it can be made via an alternative route without crosslinking. Future developments have to always find the optimal compromise of moderate curvature which gives enough solubility but does not hinder packing. A monomer bond angle around 127° as for polymer **88** should be a good target value.

5.7 Summary

In this chapter, polymers have been synthesized containing the curvature inducing benzo[2,1-b;3,4-b']dithiophene. After optimization of the polymer structure, *i.e.* finding the right place for the alkyl chains and the right comonomer, a polymer consisting of unsubstituted benzodithiophene copolymerized with alkylated dithiophenes is obtained which proves to be highly efficient in organic field-effect transistors. In a standard top-contact bottom-gate setup using a silicon wafer as substrate a field-effect mobility exceeding 0.1 $cm^2V^{-1}s^{-1}$can be measured without sophisticated device optimization. The polymer satifies all critical requirements for a transistor: (1) it possesses good solution processability, (2) it only needs short annealing times at low temperatures, (3) it is sufficiently stable under operation, (4) it exhibits high charge-carrier mobilities, and (5) it is easily synthesized.

The structural concept of introducing curvature to the polymer backbone is evidenced by comparison with the linear isomer. This polymer is poorly soluble and precipitates too quickly. In contrast, the bend polymer strongly aggregate as shown by UV-vis absorption spectroscopy and light scattering to form high order, but it does not precipitate.

On a flexible polymeric substrate, which is technically most relevant, even better performance can be obtained. Field-effect mobilities as high as 0.5 $cm^2V^{-1}s^{-1}$with high reproducibility are reached, probably due to a better interfacial morphology. The transistors show almost no dependency on the channel length, which indicates a very effective morphology between the driving electrodes of the FET.

This highly efficient polymer is also used to fabricate an organic solar cell. A bulk heterojunction is made with [70]PCBM and illuminated with AM1.5 standardized solar light. A power conversion efficiency of 2.7 % is reached without major optimization effort, even higher values are expected when the device parameters are optimized.

A comparative study of a series of isomeric polymers containing benzodithiophene copolymerized with alkylated dithiophene reveals that the degree of curvature in benzo[2,1-b;3,4-b']dithiophene is the ideal compromise between solubility and high structural order. The polymers are made by an oxidative polymerization with iron(III) chloride of the corresponding monomers. It turns out that this method is detrimental to the resulting polymers as it tends to crosslink the chains. Increased contact resistance and trapping is observed. Therefore, it is better to make new polymers via coupling reactions instead of oxidative polymerization. Nevertheless, the results suggest that the curving angle of around 127° is ideal for the optimal compromise between solubility and high order. Monomers of similar bond geometry are very promising for future developments.

5.8 Bibliography

[1] Allard, S.; Forster, M.; Souharce, B.; Thiem, H.; Scherf, U. *Angew. Chem. Int. Ed.* **2008**, *47*, 4070–4098.

[2] Facchetti, A. *Mater. Today* **2007**, *10*, 28–37.

[3] Singh, T. B.; Sariciftci, N. S. *Ann. Rev. Mater. Res.* **2006**, *36*, 199–230.

[4] de Boer, B.; Facchetti, A. *Polym. Rev.* **2008**, *48*, 423–431.

[5] Yan, H.; Chen, Z. H.; Zheng, Y.; Newman, C.; Quinn, J. R.; Dötz, F.; Kastler, M.; Facchetti, A. *Nature* **2009**, *457*, 679–688.

[6] Sirringhaus, H.; Ando, M. *MRS Bull.* **2008**, *33*, 676–682.

[7] Sirringhaus, H. *Adv. Mater.* **2005**, *17*, 2411–2425.

[8] Kim, Y.; Cook, S.; Tuladhar, S. M.; Choulis, S. A.; Nelson, J.; Durrant, J. R.; Bradley, D. D. C.; Giles, M.; McCulloch, I.; Ha, C. S.; Ree, M. *Nat. Mater.* **2006**, *5*, 197–203.

[9] Dimitrakopoulos, C. D.; Malenfant, P. R. L. *Adv. Mater.* **2002**, *14*, 99–117.

[10] Bao, Z.; J., L. *Organic Field-Effect Transistors*; CRC, 2007.

[11] Sirringhaus, H.; Brown, P. J.; Friend, R. H.; Nielsen, M. M.; Bechgaard, K.; Langeveld-Voss, B. M. W.; Spiering, A. J. H.; Janssen, R. A. J.; Meijer, E. W.; Herwig, P.; de Leeuw, D. M. *Nature* **1999**, *401*, 685–688.

[12] Chang, J. F.; Sun, B. Q.; Breiby, D. W.; Nielsen, M. M.; Solling, T. I.; Giles, M.; McCulloch, I.; Sirringhaus, H. *Chem. Mater.* **2004**, *16*, 4772–4776.

[13] Yang, H. C.; Shin, T. J.; Yang, L.; Cho, K.; Ryu, C. Y.; Bao, Z. N. *Adv. Funct. Mater.* **2005**, *15*, 671–676.

[14] Bao, Z.; Dodabalapur, A.; Lovinger, A. J. *App. Phys. Lett.* **1996**, *69*, 4108–4110.

[15] Chen, T. A.; Wu, X. M.; Rieke, R. D. *J. Am. Chem. Soc.* **1995**, *117*, 233–244.

[16] Ong, B. S.; Wu, Y. L.; Li, Y. N.; Liu, P.; Pan, H. L. *Chem. Eur. J.* **2008**, *14*, 4766–4778.

[17] Ong, B. S.; Wu, Y. L.; Liu, P.; Gardner, S. *J. Am. Chem. Soc.* **2004**, *126*, 3378–3379.

[18] Pan, H. L.; Li, Y. N.; Wu, Y. L.; Liu, P.; Ong, B. S.; Zhu, S. P.; Xu, G. *J. Am. Chem. Soc.* **2007**, *129*, 4112–4113.

[19] McCulloch, I.; Heeney, M.; Bailey, C.; Genevicius, K.; Macdonald, I.; Shkunov, M.; Sparrowe, D.; Tierney, S.; Wagner, R.; Zhang, W. M.; Chabinyc, M. L.; Kline, R. J.; McGehee, M. D.; Toney, M. F. *Nat. Mater.* **2006**, *5*, 328–333.

[20] McCulloch, I.; Bailey, C.; Giles, M.; Heeney, M.; Love, I.; Shkunov, M.; Sparrowe, D.; Tierney, S. *Chem. Mater.* **2005**, *17*, 1381–1385.

[21] Gallazzi, M. C.; Toscano, F.; Paganuzzi, D.; Bertarelli, C.; Farina, A.; Zotti, G. *Macromol. Chem. Phys.* **2001**, *202*, 2074–2085.

[22] Yoshida, S.; Fujii, M.; Aso, Y.; Otsubo, T.; Ogura, F. *J. Org. Chem.* **1994**, *59*, 3077–3081.

[23] Brzezinski, J. Z.; Reynolds, J. R. *Synthesis* **2002**, 1053–1056.

[24] Hu, X.; Xu, L. G. *Polymer* **2000**, *41*, 9147–9154.

[25] Abdou, M. S. A.; Lu, X. T.; Xie, Z. W.; Orfino, F.; Deen, M. J.; Holdcroft, S. *Chem. Mater.* **1995**, *7*, 631–641.

[26] Odian, G. *Principles of Polymerization*, 4th ed.; Wiley and Sons, 2004.

[27] Labadie, J. W.; Hedrick, J. L.; Ueda, M. *Step-Growth Polymers for High-Performance Materials - New Synthetic Methods* **1996**, *624*, 294–305.

[28] Kline, R. J.; McGehee, M. D.; Kadnikova, E. N.; Liu, J. S.; Frechet, J. M. J. *Adv. Mater.* **2003**, *15*, 1519–1522.

[29] Zen, A.; Pflaum, J.; Hirschmann, S.; Zhuang, W.; Jaiser, F.; Asawapirom, U.; Rabe, J. P.; Scherf, U.; Neher, D. *Adv. Funct. Mater.* **2004**, *14*, 757–764.

[30] Facchetti, A.; Yoon, M. H.; Marks, T. J. *Adv. Mater.* **2005**, *17*, 1705–1725.

[31] Rhee, S. W.; Yun, D. J. *J. Mater. Chem.* **2008**, *18*, 5437–5444.

[32] Horowitz, G.; Delannoy, P. *J. Appl. Phys.* **1991**, *70*, 469–475.

[33] Street, R. A.; Salleo, A. *Appl. Phys. Lett.* **2002**, *81*, 2887–2889.

[34] Shen, Y. L.; Hosseini, A. R.; Wong, M. H.; Malliaras, G. G. *ChemPhysChem* **2004**, *5*, 16–25.

[35] Prosa, T. J.; Winokur, M. J.; Moulton, J.; Smith, P.; Heeger, A. J. *Macromol.* **1992**, *25*, 4364–4372.

[36] Tsao, H. N.; Cho, D.; Andreasen, J. W.; Rouhanipour, A.; Breiby, D. W.; Pisula, W.; Müllen, K. *Adv. Mater.* **2009**, *21*, 209–212.

[37] Jaiswal, M.; Menon, R. *Polym. Int.* **2006**, *55*, 1371–1384.

[38] Cornil, J.; Beljonne, D.; Calbert, J. P.; Bredas, J. L. *Adv. Mater.* **2001**, *13*, 1053–1067.

[39] Li, J.; Qin, F.; Li, C. M.; Bao, Q.; Chan-Park, M. B.; Zhang, W.; Qin, J.; Ong, B. S. *Chem. Mater.* **2008**, *20*, 2057.

[40] Kline, R. J.; McGehee, M. D.; Kadnikova, E. N.; Liu, J. S.; Frechet, J. M. J.; Toney, M. F. *Macromol.* **2005**, *38*, 3312–3319.

[41] Pokrop, R.; Verilhac, J. M.; Gasior, A.; Wielgus, I.; Zagorska, M.; Travers, J. P.; Pron, A. *J. Mater. Chem.* **2006**, *16*, 3099–3106.

[42] Horowitz, G. *J. Mater. Res.* **2004**, *19*, 1946–1962.

[43] Burgi, L.; Richards, T. J.; Friend, R. H.; Sirringhaus, H. *J. Appl. Phys.* **2003**, *94*, 6129–6137.

[44] Klauk, H.; Schmid, G.; Radlik, W.; Weber, W.; Zhou, L. S.; Sheraw, C. D.; Nichols, J. A.; Jackson, T. N. *Solid-State Electron.* **2003**, *47*, 297–301.

[45] Fong, H. H.; Pozdin, V. A.; Amassian, A.; Malliaras, G. G.; Smilgies, D. M.; He, M. Q.; Gasper, S.; Zhang, F.; Sorensen, M. *J. Am. Chem. Soc.* **2008**, *130*, 13202–13203.

[46] Tierney, S.; Heeney, M.; McCulloch, L. *Synth. Met.* **2005**, *148*, 195–198.

[47] Wang, C. G.; Benz, M. E.; LeGoff, E.; Schindler, J. L.; Allbritton-Thomas, J.; Kannewurf, C. R.; Kanatzidis, M. G. *Chem. Mater.* **1994**, *6*, 401–411.

[48] Yoon, M. H.; DiBenedetto, S. A.; Russell, M. T.; Facchetti, A.; Marks, T. J. *Chem. Mater.* **2007**, *19*, 4864–4881.

[49] Schlüter, A. D. *J. Polym. Sci., Part A: Polym. Chem.* **2001**, *39*, 1533–1556.

[50] Heeney, M.; Bailey, C.; Genevicius, K.; Shkunov, M.; Sparrowe, D.; Tierney, S.; McCulloch, I. *J. Am. Chem. Soc.* **2005**, *127*, 1078–1079.

[51] Pernstich, K. P.; Haas, S.; Oberhoff, D.; Goldmann, C.; Gundlach, D. J.; Batlogg, B.; Rashid, A. N.; Schitter, G. *J. Appl. Phys.* **2004**, *96*, 6431–6438.

[52] Chabinyc, M. L.; Jimison, L. H.; Rivnay, J.; Salleo, A. *MRS Bull.* **2008**, *33*, 683–689.

[53] Kline, R. J.; McGehee, M. D. *Polym. Rev.* **2006**, *46*, 27–45.

[54] Ebata, H.; Izawa, T.; Miyazaki, E.; Takimiya, K.; Ikeda, M.; Kuwabara, H.; Yui, T. *J. Am. Chem. Soc.* **2007**, *129*, 15732–15733.

[55] Garnier, F.; Yassar, A.; Hajlaoui, R.; Horowitz, G.; Deloffre, F.; Servet, B.; Ries, S.; Alnot, P. *J. Am. Chem. Soc.* **1993**, *115*, 8716–8721.

[56] Gao, P.; Beckmann, D.; Tsao, H. N.; Feng, X.; Enkelmann, V.; Baumgarten, M.; Pisula, W.; Müllen, K. *Adv. Mater.* **2008**, *21*, 213–216.

[57] Vissenberg, M.; Matters, M. *Phys. Rev. B* **1998**, *57*, 12964–12967.

[58] Yang, H. C.; Shin, T. J.; Yang, L.; Cho, K.; Ryu, C. Y.; Bao, Z. N. *Adv. Funct. Mater.* **2005**, *15*, 671–676.

[59] Kelley, T. W.; Frisbie, C. D. *J. Phys. Chem.* **2001**, *105*, 4538–4540.

[60] Hanna, R.; Leclerc, M. *Macromol. Chem. Phys* **1997**, *198*, 1035–1049.

[61] Pal, S.; Nandi, A. K. *J. Appl. Polym. Sci.* **2006**, *101*, 3811–3820.

[62] Kaneto, K.; Lim, W. Y.; Takashima, W.; Endo, T.; Rikukawa, M. *Jpn. J. Appl. Phys.* **2000**, *39*, L872–L874.

[63] Kuo, C. T.; Weng, S. Z.; Huang, R. L. *Synth. Met.* **1997**, *88*, 101–107.

[64] Torsi, L.; Tanese, M. C.; Cioffi, N.; Gallazzi, M. C.; Sabbatini, L.; Zambonin, P. G.; Raos, G.; Meille, S. V.; Giangregorio, M. M. *J. Phys. Chem. B* **2003**, *107*, 7589–7594.

[65] Tashiro, K.; Ono, K.; Minagawa, Y.; Kobayashi, M.; Kawai, T.; Yoshino, K. *J. Polym. Sci. B* **1991**, *29*, 1223–1233.

[66] Takimiya, K.; Konda, Y.; Ebata, H.; Niihara, N.; Otsubo, T. *J. Org. Chem* **2005**, *70*, 10569–10571.

[67] Hart, H.; Harada, K.; Du, C. J. F. *J. Org. Chem* **1985**, *50*, 3104–3110.

[68] Sashida, H.; Sadamori, K.; Tsuchiya, T. *Synth. Comm.* **1998**, *28*, 713–727.

[69] Dang, T. T. M.; Park, S. J.; Park, J. W.; Chung, D. S.; Park, C. E.; Kim, Y. H.; Kwon, S. K. *J. Polym. Sci. Pol. Chem.* **2007**, *45*, 5277–5284.

[70] Surin, M.; Leclere, P.; Lazzaroni, R.; Yuen, J. D.; Wang, G.; Moses, D.; Heeger, A. J.; Cho, S.; Lee, K. *J. Appl. Phys.* **2006**, *100*, 33712.

[71] Roux, C.; Leclerc, M. *Macromolecules* **1992**, *25*, 2141–2144.

[72] Yamamoto, T.; Komarudin, D.; Arai, M.; Lee, B. L.; Suganuma, H.; Asakawa, N.; Inoue, Y.; Kubota, K.; Sasaki, S.; Fukuda, T.; Matsuda, H. *J. Am. Chem. Soc.* **1998**, *120*, 2047–2058.

[73] Leclerc, M.; Frechette, M.; Bergeron, J. Y.; Ranger, M.; Levesque, I.; Faid, K. *Macromol. Chem. Phys.* **1996**, *197*, 2077–2087.

[74] Maiti, N. C.; Mazumdar, S.; Periasamy, N. *J. Phys. Chem. B* **1998**, *102*, 1528–1538.

[75] Jenekhe, S. A.; Osaheni, J. A. *Science* **1994**, *265*, 765–768.

[76] Stampfl, J.; Tasch, S.; Leising, G.; Scherf, U. *Synth. Met.* **1995**, *71*, 2125–2128.

[77] Chu, B. *Laser Light Scattering: Basic Principles and Practice*, 2nd ed.; Dover Publishing Inc., 2007.

[78] Wyatt, P. J. *Anal. Chim. Acta* **1993**, *272*, 1–40.

[79] Malik, S.; Nandi, A. K. *J. Appl. Polym. Sci.* **2007**, *103*, 2528–2537.

[80] Kinder, L.; Kanicki, J.; Petroff, P. *Synth. Met.* **2004**, *146*, 181–185.

[81] Scheinert, S.; Schliefke, W. *Synth. Met.* **2003**, *139*, 501–509.

[82] Forrest, S. R. *Nature* **2004**, *428*, 911–918.

[83] Ju, S. Y.; Facchetti, A.; Xuan, Y.; Liu, J.; Ishikawa, F.; Ye, P. D.; Zhou, C. W.; Marks, T. J.; Janes, D. B. *Nat. Nanotechnol.* **2007**, *2*, 378–384.

[84] Reichmanis, E.; Katz, H.; Kloc, C.; Maliakal, A. *Bell Labs Tech. J.* **2005**, *10*, 87–105.

[85] Gelinck, G. H. et al. *Nat. Mater.* **2004**, *3*, 106–110.

[86] Sirringhaus, H.; Kawase, T.; Friend, R. H.; Shimoda, T.; Inbasekaran, M.; Wu, W.; Woo, E. P. *Science* **2000**, *290*, 2123–2126.

[87] Garnier, F.; Hajlaoui, R.; Yassar, A.; Srivastava, P. *Science* **1994**, *265*, 1684–1686.

[88] Backlund, T. G.; Sandberg, H. G. O.; Osterbacka, R.; Stubb, H.; Makela, T.; Jussila, S. *Synth. Met.* **2005**, *148*, 87–91.

[89] Noh, Y. Y.; Zhao, N.; Caironi, M.; Sirringhaus, H. *Nat. Nanotechnol.* **2007**, *2*, 784–789.

[90] Chwang, A. B.; Rothman, M. A.; Mao, S. Y.; Hewitt, R. H.; Weaver, M. S.; Silvernail, J. A.; Rajan, K.; Hack, M.; Brown, J. J.; Chu, X.; Moro, L.; Krajewski, T.; Rutherford, N. *Appl. Phys. Lett.* **2003**, *83*, 413–415.

[91] Ghosh, A. P.; Gerenser, L. J.; Jarman, C. M.; Fornalik, J. E. *Appl. Phys. Lett.* **2005**, *86*, 223503.

[92] Bao, Z. N. *Adv. Mater.* **2000**, *12*, 227–230.

[93] Crone, B.; Dodabalapur, A.; Lin, Y. Y.; Filas, R. W.; Bao, Z.; LaDuca, A.; Sarpeshkar, R.; Katz, H. E.; Li, W. *Nature* **2000**, *403*, 521–523.

[94] Melzer, C.; von Seggern, H. *IT-Inf. Technol.* **2008**, *50*, 158–166.

[95] Dimitrakopoulos, C. D.; Purushothaman, S.; Kymissis, J.; Callegari, A.; Shaw, J. M. *Science* **1999**, *283*, 822–824.

[96] Coakley, K. M.; McGehee, M. D. *Chem. Mater.* **2004**, *16*, 4533–4542.

[97] Li, Y.; Zou, Y. *Adv. Mater.* **2008**, *20*, 2952–2958.

[98] Brabec, C. J.; Durrant, J. R. *MRS Bull.* **2008**, *33*, 670–675.

[99] Riede, M.; Mueller, T.; Tress, W.; Schueppel, R.; Leo, K. *Nanotechn.* **2008**, *19*, 424001.

[100] Scholes, G. D.; Rumbles, G. *Nat. Mater.* **2006**, *5*, 683–696.

[101] Campbell, I. H.; Hagler, T. W.; Smith, D. L.; Ferraris, J. P. *Phys. Rev. Lett.* **1996**, *76*, 1900–1903.

[102] Thompson, B. C.; Frechet, J. M. J. *Angew. Chem. Int. Ed.* **2008**, *47*, 58–77.

[103] Dennler, G.; Scharber, M. C.; Brabec, C. J. *Adv. Mater.* **2009**, *21*, 1323–1338.

[104] Green, M. A.; Emery, K.; Hishikawa, Y.; Warta, W. *Prog. Photovolt. Res. Appl.* **2009**, *17*, 85–94.

[105] Andersson, L. M.; Inganas, O. *App. Phys. Lett.* **2006**, *88*, 82103.

[106] Blom, P. W. M.; Mihailetchi, V. D.; Koster, L. J. A.; Markov, D. E. *Adv. Mater.* **2007**, *19*, 1551–1566.

[107] Koster, L. J. A.; Mihailetchi, V. D.; Blom, P. W. M. *App. Phys. Lett.* **2006**, *88*, 93511.

[108] Hoppe, H.; Sariciftci, N. S. *J. Mater. Chem.* **2006**, *16*, 45–61.

[109] Peet, J.; Kim, J. Y.; Coates, N. E.; Ma, W. L.; Moses, D.; Heeger, A. J.; Bazan, G. C. *Nat. Mater.* **2007**, *6*, 497–500.

[110] Gueymard, C. A. *Sol. Energy* **2004**, *76*, 423–453.

[111] Li, G.; Shrotriya, V.; Huang, J. S.; Yao, Y.; Moriarty, T.; Emery, K.; Yang, Y. *Nat. Mater.* **2005**, *4*, 864–868.

[112] Campoy-Quiles, M.; Ferenczi, T.; Agostinelli, T.; Etchegoin, P. G.; Kim, Y.; Anthopoulos, T. D.; Stavrinou, P. N.; Bradley, D. D. C.; Nelson, J. *Nat. Mater.* **2008**, *7*, 158–164.

[113] Erb, T.; Zhokhavets, U.; Gobsch, G.; Raleva, S.; Stuhn, B.; Schilinsky, P.; Waldauf, C.; Brabec, C. J. *Adv. Funct. Mater.* **2005**, *15*, 1193–1196.

[114] Nguyen, L. H.; Hoppe, H.; Erb, T.; Gunes, S.; Gobsch, G.; Sariciftci, N. S. *Adv. Funct. Mater.* **2007**, *17*, 1071–1078.

[115] Cava, M. P.; Pollack, N. M.; Mamer, O. A.; Mitchell, M. J. *J. Org. Chem.* **1971**, *36*, 3932–3937.

[116] Meng, H.; Wudl, F. *Macromol.* **2001**, *34*, 1810–1816.

[117] Wynberg, H.; Wit, J. D.; Sinnige, H. J. M. *J. Org. Chem.* **1970**, *35*, 711–715.

[118] Licandro, E.; Rigamonti, C.; Ticozzelli, M. T.; Monteforte, M.; Baldoli, C.; Giannini, C.; Maioran, S. *Synthesis* **2006**, 3670–3678.

[119] Chuit, C.; Corriu, R. J. P.; Reye, C.; Young, J. C. *Chem. Rev.* **1993**, *93*, 1371–1448.

[120] Zajc, B.; Zupan, M. *Tetrahedron* **1989**, *45*, 7869–7878.

[121] Doering, W. V.; Hoffmann, A. K. *J. Am. Chem. Soc.* **1954**, *76*, 6162–6165.

[122] Kellogg, R. M.; Groen, M. B.; Wynberg, H. *J. Org. Chem.* **1967**, *32*, 3093–3100.

[123] Nakayama, J.; Murabayashi, S.; Hoshino, M. *Heterocycles* **1986**, *24*, 2639–2643.

[124] Hou, J. H.; Tan, Z. A.; Yan, Y.; He, Y. J.; Yang, C. H.; Li, Y. F. *J. Am. Chem. Soc.* **2006**, *128*, 4911–4916.

[125] Davis, M. C. *Synth. Comm.* **2005**, *35*, 2079–2083.

[126] Clayden, J.; Warren, S. *Angew. Chem. Int. Ed.* **1996**, *35*, 241–270.

[127] Mallory, F. B.; Mallory, C. W. *Org. React.* **1984**, *30*, 1–133.

6 Di(thienobenzo)thienothiophene Containing Polymers

6.1 Introduction

In the previous chapter the outstanding properties of benzo[2,1-b;3,4-b']dithiophene as a building block for polythiophenes and their use in organic eletronic devices have been demonstrated. This structural motif renders materials of excellent film formation properties and good device stability. To go one step further, the building block shall be extended to a rod-like molecule containing the successfull benzo[2,1-b;3,4-b']dithiophene.

Similar structures have been prepared as small molecules for field-effect transistors.[1–3] The rod-like shape enhances the propensity to crystallize on the surface to which they can line up in parrallel. Very high field-effect mobilities in excess of 1 $cm^2V^{-1}s^{-1}$have been reported for these materials.[3, 4] The excellent crystallization properties, high intermolecular interactions, and good compatibility to the dielectric interface lead to these performances.

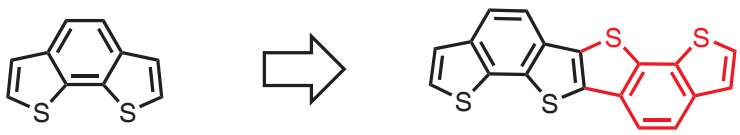

Figure 6.1: Extension of benzo[2,1-b;3,4-b']dithiophene to an extended rod-like π-system.

Figure 6.1 shows the strategy of the structure extension. Benzodithiophene is annellated by another benzodithiophene unit on the d-side of the thiophenes. A more or less linear, rod-like structure is the consequence. At the center, a thieno[3,2-b]thiophene unit is formed, a very successful building block for conjugated polymers.[5–7]

Polymers incorporating fused π-systems of this size are hitherto unknown. The polymer with the biggest fused π-system published so far incorporates four fused thiophene rings.[8] It shows good device characteristics and high charge-carrier mobility. A ladder-type polymer of fused thiophenes has been reported, but due to its insolubility, it could not be processed and thoroughly characterized.[9] Thus, sufficient alkyl chains have to be attached to the core to solubilize the polymer and direct the assembly into lamellar packing.

The structure optimization in the previous chapter has shown that it is unfavorable to attach two alkyl chains in ortho positions to a benzene moiety. The reduced degree of freedom for the alkyl chains do not solubilize the polymer chain effectively and hinder the formation of ordered lamellar packing. Similar effects are known in the literature.[10, 11]

To make sure that the alkyl chains possess maximum solubilization and can form good lamellar packing, only one chain shall be attached to the benzene unit. Figure 6.2 shows the packing of a potential polymer. The space between the alkyl chains is sufficient to allow interdigitation of the alkyl chains of neighboring polymer chains, potentially leading to small lamellar distances which are favorable with regard to charge-carrier transport.[7, 12, 13]

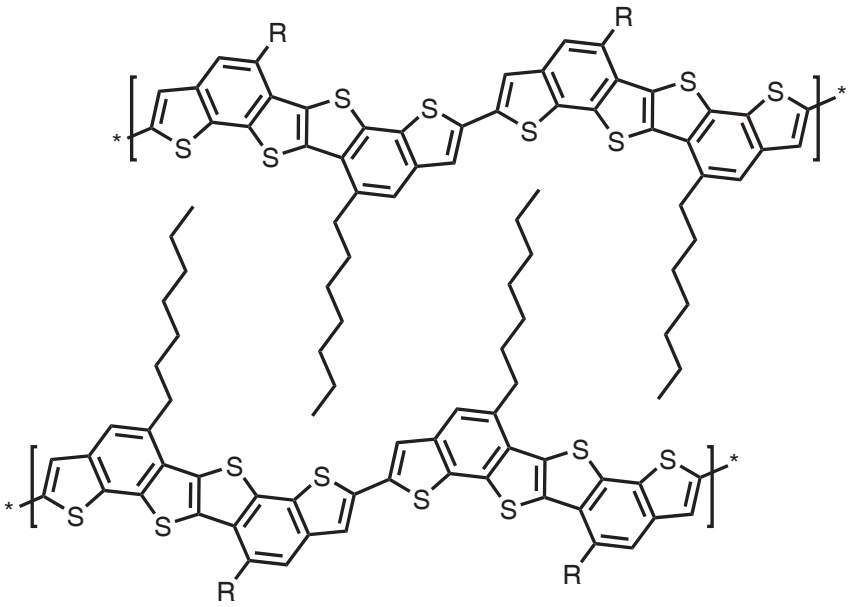

Figure 6.2: Interdigitation of alkyl chains of potential polymer for efficient lamellar packing.

6.2 Synthesis

6.2.1 Monomer

The strategy towards the double benzodithiophene molecule with two alkyl chains is outlined in Figure 6.3. The key step is the base induced cyclization of an alkynyl moiety to form a fused system.

The route starts with the regio-selective bromination of 3-iodothiophene (**131**) with NBS to afford 2-bromo-3-iodothiophene.[14] The iodine function can be selectively reacted in a Sonogashira-Hagihara reaction with diisopropylamine as base at room temperature.[15] Hexadecyne is coupled to the thiophene as it is the longest commercially available alkyne. This will lead to a C14 chain in the final product which should be sufficient for solubility.

The thus obtained 3-hexadecynyl-2-bromothiophene (**133**) is attached to thieno[1,2-b]thiophene (**134**) in a Stille coupling reaction. The required bis(trimethylstannyl)thienothiophene (**135**) is obtained by lithiation of thienothiophene and subsequent treatment with trimethyltin chloride.

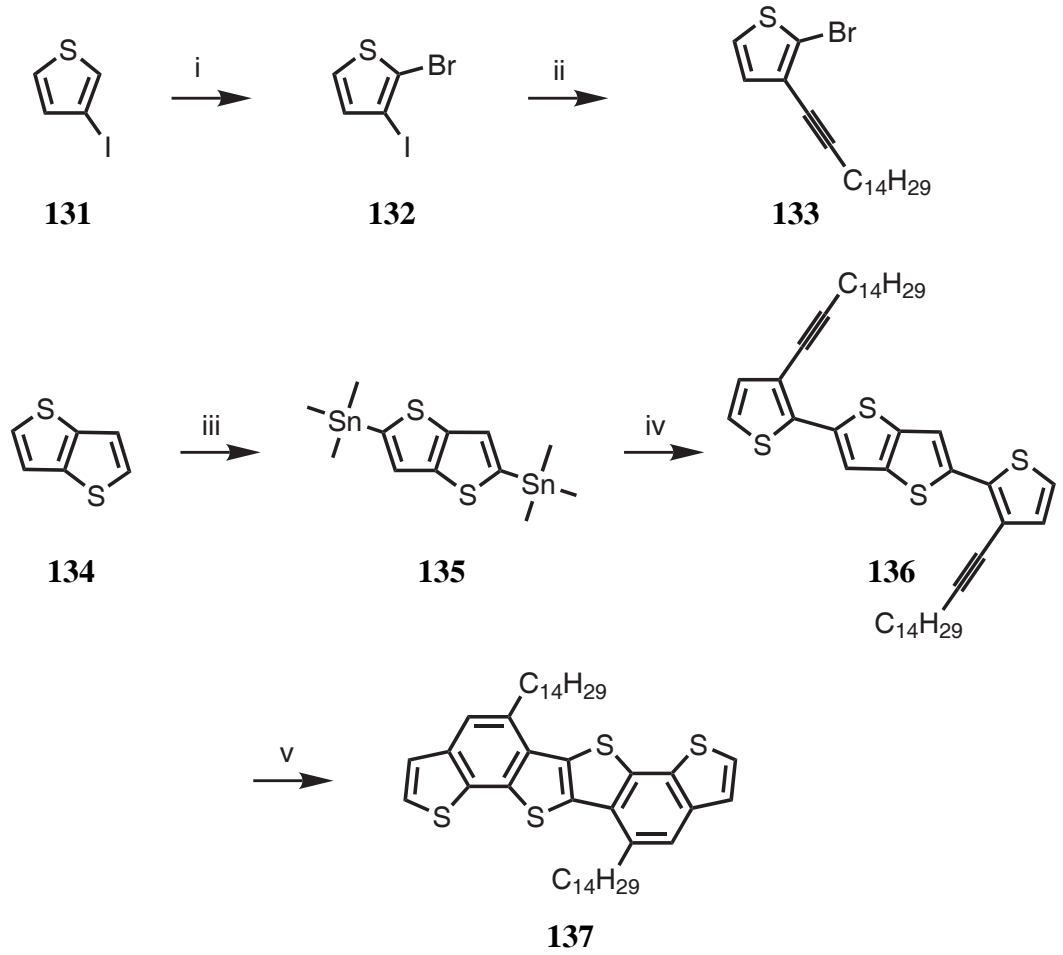

Figure 6.3: Synthesis of the double-benzodithiophene building block, conditions: *i* NBS, DMF, RT, 85 %; *ii* 1-hexyne, CuI, $Pd(PPh_3)_2Cl_2$, diisopropylamine, THF, RT, 98 %; *iii* 1. *t*-butyllithium, THF, -78 °C, 2. Me_3SnCl, 58 %; *iv* **133**, $Pd_2(dba)_3$, P(*o*-tol)$_3$, *o*-DCB, 140 °C, 64 %; *v* DBU, NMP, reflux, 78 %.

Thienothiophene has been synthesized in four steps according to the literature procedure.[16]

Compound **136**, obtained from the Stille coupling between stannylated thienothiophene **135** and the alkynylated bromothiophene **133**, needs to be cyclized to the target molecule **137**. Several methods are described in the literature. Transition metal catalyzed cyclization reactions have been tried using platinum.[17] The desired product is obtained in trace amounts, most likely due to decomposition of the product by the catalyst, because the longer the reaction is run the less product is obtained. Other metals such as ruthenium or gallium do not improve the yield

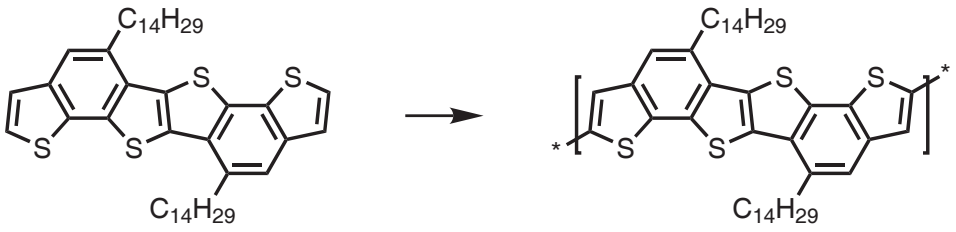

137 **138**

Figure 6.4: Attempted homopolymerization of the bisbenzodithiophene monomer **137** using $FeCl_3$ in *o*-dichlorobenzene at 60 °C.

significantly.[18, 19] The base-induced nucleophilic attack of the aromatic system on the alkyne moiety using 1,8-diazabicyclo[5.4.0]undec-7-ene (DBU) leads to **137** in good yield.[20] The reagent **136** is suspended in NMP, DBU is added, and the mixture is refluxed overnight. Upon cooling, the product crystallizes and can easily be collected by filtration. No additional purification is needed for the next step, the reaction proceeds almost quantitatively.

6.2.2 Homopolymer

Substance **137** is not well soluble at room temperature, but very well at slightly elevated temperatures (50 °C). A homopolymer has been attempted by oxidative polymerization in the presence of iron(III) chloride.[21, 22] For this reason, monomer **137** is dissolved in *o*-dichlorobenzene, a good solvent for polythiophenes. Anhydrous iron(III) chloride is added, the solution is heated to 60 °C for two days. No polymer is obtained, solely chlorinated and partially decomposed monomer is recovered after workup.

According to the mechanism of the iron(III) chloride induced polymerization of thiophene, terminal thiophenes of the growing chain are protonated. The thus formed cation electrophilically attacks a monomer or another chain.[23, 24] A possible explanation is that the monomer is not sufficiently protonated at the outer α positions of the thiophenes.

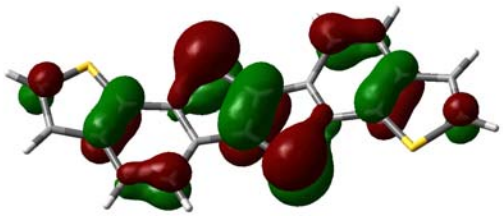

Figure 6.5: HOMO electron density surface of **137**.

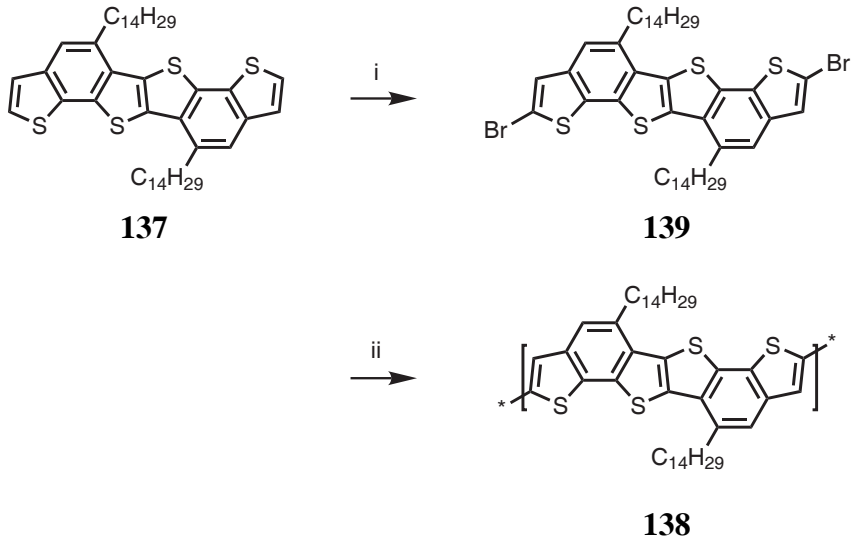

137 **139** **138**

Figure 6.6: Alternative route to homopolymer **138** via Yamamoto coupling, conditions: *i* NBS, chloroform, acetic acid, reflux, 89 %; *ii* $Ni(COD)_2$, 1,5-cyclooctadiene, bipyridine, toluene, DMF, 90 °C.

To get a clearer view, a DFT calculation has been run using the B3LYP method with the 6-31G basis set. The thus obtained electron surface of the HOMO is depicted in Figure 6.5. It is obvious that the orbital coefficient at the outer α positions is very small in comparison to those of the central part. This means that the electron density is low at these positions leading to a low basicity. It is very likely, that the molecule is not sufficiently protonated to initate an electrophilic attack on another molecule. Therefore, monomer **137** is not suitable for oxidative homopolymerization.

An alternative strategy is the reductive dehalogenation reaction, also known as Yamamoto polymerization.[25, 26] The route is depicted in Figure 6.6. Monomer **137** is brominated with NBS in a mixture of chloroform and acetic acid, a very effective

bromination procedure for thiophene.[27] Due to the poor solubility of **137** at room temperature, the solution is heated to reflux. The reaction time is crucial, because too long times produce a dark brown side product which is difficult to remove. Too short times leave singly brominated intermediate which can hardly be separated. A period of 45 minutes is the optimum compromise.

Monomer **139** is subject to reductive dehalogenation polymerization.[28] Dicyclooctadienenickel(0) is reacted with bipyridine in DMF and toluene to prepare the active catalyst. Compound **139** is added, the mixture is stirred at 90 °C for two days under careful exclusion of oxygen, moisture, and light.

The thus obtained polymer cannot be dissolved in any organic solvent. Even boiling 1,2,4-trichlorobenzene (214 °C) does not dissolve the material after an extended period. This means that the extended π system aggregates too strongly. Even two C14 alkyl chains per monomer unit are not able to render a soluble product.

6.2.3 Dithiophene Copolymer

Obviously, the homopolymer aggregates too stongly to get soluble material. Following the strategy of the previous chapter, alkylated dithiophene comonomers shall be introduced to make the backbone more flexible and thus solubilize the product.

Figure 6.7 shows the synthesis. Bisbenzodithiophene **137** is stannylated by lithiation and subsequent treatment with trimethyltin chloride. The lithiation reaction is remarkable, because both reagent (**137**) and lithiated species are not soluble to a reasonable extent in THF at -78 °C. Nevertheless, *t*-butyllithium is reactive enough to deprotonate the two α protons. The stannylated product is much more soluble than the reagent, the bulky tin moieties obviously hinder the tight packing. This enables crystallization from ethyl acetate to render the product in high purity. Chromatography cannot be applied to this molecules, because it decomposes on silica gel.

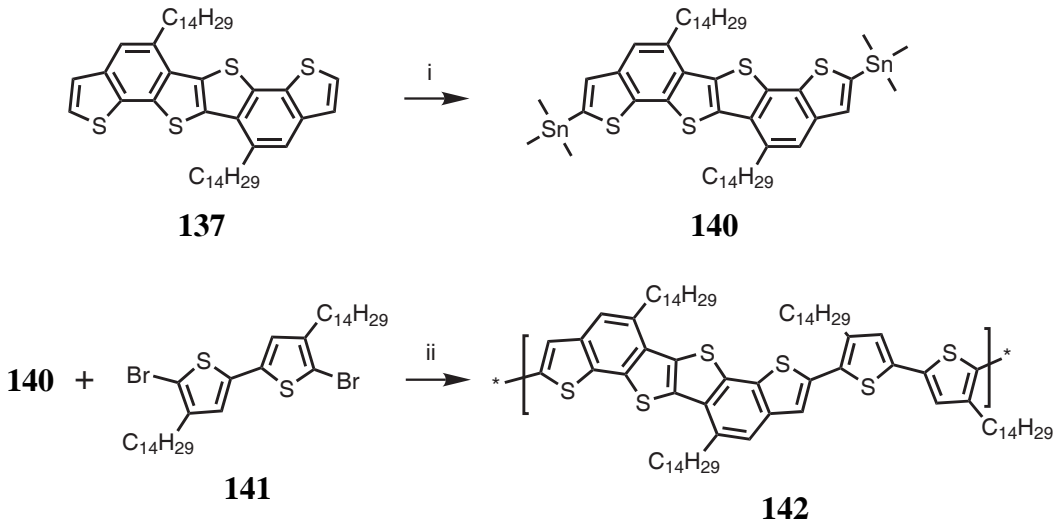

Figure 6.7: Synthetic route towards copolymer **142**, conditions: *i* 1. *t*-butyllithium, THF, -78 °C, 2. Me_3SnCl, 42 %; *ii* $Pd_2(dba)_3$, P(*o*-tol)$_3$, *o*-DCB, 140 °C, 80 %.

Ditetradecyl-dibromo-dithiophene (**141**) is made as the comonomer. The synthesis of the analogous C12 derivative is described in the previous chapter and can be found the literature.[29] C14 chains are selected to enhance lamellar formation due to a uniform chain length of both alkyl chains on the thiophenes as well as those attached to the bisbenzodithiophene. The polymerization procedure of the polymers in the previous chapter is followed, *i.e.* $Pd_2(dba_3)$ as palladium source, tri-*o*-tolylphosphine as ligand, and *o*-dichlorobenzene as solvent. The reaction mixture is heated to 140 °C for three days. No precipitation occurs during the polymerization process.

After precipitation in methanol, a red solid is obtained which dissolves in warm dichlorobenzene. This allows the determination of the molecular weight via size exclusion chromatography. A number average value of M_n = 8 kg/mol and a weight average molecular weight of M_w = 16 kg/mol have been determined in reference of polystyrene standards. These values are not very high to reveal the full potential of the material as has been shown for other polymers.[30–32] Nevertheless, it is enough for first investigations of the material properties. Later on, the polymerization procedure needs to be optimized to obtain higher molecular weights.

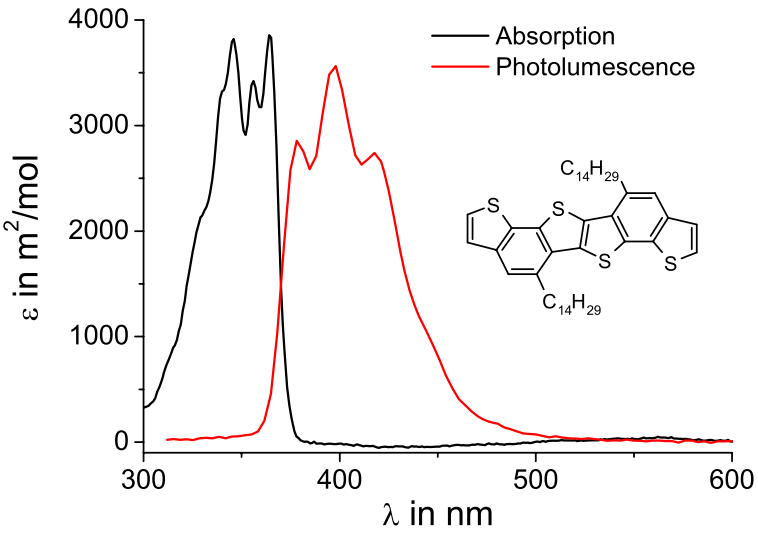

Figure 6.8: UV-vis absorption and photolumescence (λ_{ex} = 350 nm) of monomer **137** in *o*-dichlorobenzene at a concentration of 10^{-5} mol/l, the photoluminescence intensity is normalized to fit the absorption spectrum.

6.3 Optical Analysis

The optical properties of materials play a very important role towards applications such as solar cells. The analysis of absorption can yield a lot of information about the system, such as electronic levels, transition probability, or effective conjugation length.[33, 34] Additionally, the spectra are a good reference for quantum mechanical calculations.

6.3.1 Monomer

The absorption and photoluminescence of monomer **137** have been measured in *o*-dichlorobenzene at a concentration of 10^{-5} mol/l. This solvent is chosen to better compare the spectrum with that of the polymer, although the monomer is soluble in other solvents which allow recording at shorter wavelength. The corresponding spectra are depicted in Figure 6.9.

The highly resolved band with significant degree of fine structure indicates the

planarity of the fused π-system. Both absorption and photoluminescence show several peaks which are characteristic for polycyclic aromatic hydrocarbons. Symmetry forbidden transitions account for this phenomenon.[35, 36]

The optical gap of **137** is 370 nm as determined by the intersection of absorption and photoluminescence peak.[37] This is a bit more than the analogously fused hexathiophene which possesses an optical gap of 350 nm.[38] The benzo annellation, therefore, lowers the optical gap more strongly than a thiophene annellation.

The extinction coefficient is low for a polycyclic aromatic hydrocarbon ($<$ 4,000 m^2/mol). All-carbon PAHs exhibit extinction coefficients in excess of 20,000 m^2/mol.[39] The low values in the present case account for the low transition probabilities induced by the sulfur atom and is a typical trend for thiophene containing discs.[40]

6.3.2 Polymer

The absorption spectra of polymer **142** have been measured in a *o*-dichlorobenzene solution at a concentration of 10^{-5} mol/l with regard to the repeat unit. The extinction coefficient is calculated accordingly. For the film measurements, the extinction coefficient is normallized to the other values.

Figure 6.9 shows the spectra. At room temperature, three resolved bands are visible which vanish upon heating, very similar to the benzo[2,1-b;3,4-b']dithiophene containing polymer **88** in the previous chapter. Obviously, polymer **142** aggregates in solution at room temperature, but does not any more at elevated temperatures. The film absorption almost resembles the solution spectrum at room temperature which is consistent with the expectation of a highly aggregated polymer in solution.[41–43]

The onset of the absorption is at about 600 nm very similar to P3HT. The effective conjugation length is on the same order despite the stiffer backbone.[44] For P3HT

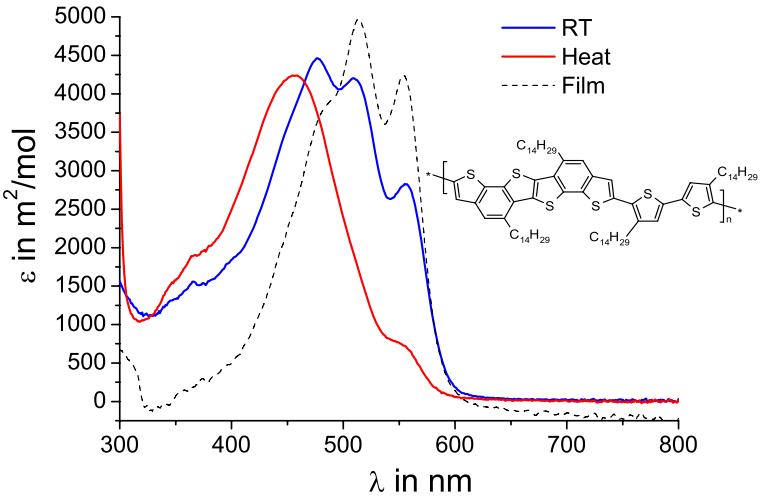

Figure 6.9: UV-vis absorption spectrum of polymer **142** in solution at roomtemperature and elevated temperature as well as film, the extinction coefficients are calculated with regard to the repeat unit of the polymer.

it has been estimated to be 15 thiophene rings at room temperature by comparing defined oligomer and polymer absorption spectra.[45] Given the optical gap shows the same length dependence as in P3HT, this means that the effective conjugation length is only about two repeat units. Comparing the absorption of the polymer (**142**) with the corresponding monomer (**137**) this seem to be reasonable. The absorption of the polymer is red-shifted by about 200 nm. Conjugation of two monomers with four thiophenes may be sufficient for this shift. The stiffness of the backbone obviously does not play a significant role for the effective conjugation length.

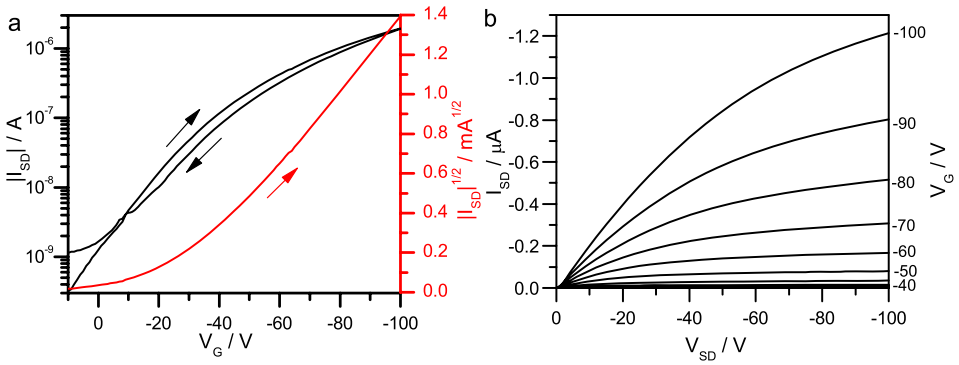

Figure 6.10: Field-effect transistor characteristics of polymer **142** on silicon wafer. **a.** transfer and **b.** output curve.

6.4 Transistor Characterization

Field-effect transistors with polymer **142** are fabricated on highly doped silicon wafers. The silicon dioxide dielectric is treated with HMDS to enhance the interface morphology and avoid trapping by protonation.[46–48] The polymer is dissolved in *o*-dichlorobenzene at elevated temperatures (60 °C) and spin cast at 3000 rpm. On top, gold electrodes are evaporated as source and drain contacts.

The transistor characteristics are depicted in Figure 6.10. The transfer curves show an almost linear dependence on the gate voltages at low values and quadratic dependence at high values. This means that the transistor operates in the space charge limited regime from -30 V on, no significant major injection barriers are observed.

However, the mobility is relatively low. A value of $\mu_{sat} = 1.8 \cdot 10^{-3}$ cm^{2}V^{-1}s^{-1}is determined in the saturated regime. An on-off ratio of $I_{on}/I_{off} = 1.3 \cdot 10^3$ is reasonable for the low mobility as the on currents are not particularly high.

The output curves seem to indicate minor injection problems, the current flow seems to begin at -2 V. When having a closer look (Figure 6.11), however, one can see that there is a positive charge flow at high gate voltages but no soure-drain

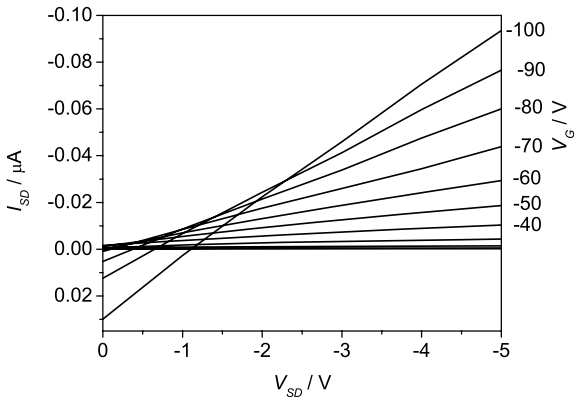

Figure 6.11: Zoom into the output curves of Figure 6.10 at low source-drain voltages.

voltage. This is a typical leakage current arising from an imperfect device, but it is of minor relevance as it is two orders of magnitude lower than the on voltage of the working transistor.

A switch-on voltage of about +10 V can be seen in the transfer curve. This suggests that the polymer is slightly doped. The reactive thiophene end groups may be oxidized in air creating doping sites. Higher molecular weights are expected to solve this problem.

Very low hysteresis is observed on the forward and back sweep of the gate voltage. The back scan of the transfer curve ends at about five times the value it has started from at zero gate voltage. Most likely, there is a small leakage current. This effect may also indicate some degree of doping upon transistor operation, due to reaction of the end groups. The molecular weight is relatively low, so the end groups play an important role. If the material can be made with higher molecular weight, a lower off current is expected.

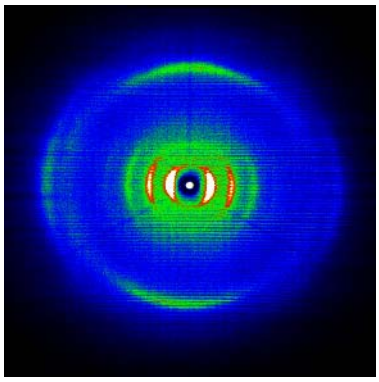

Figure 6.12: Two-dimensional wide-angle X-ray diffraction pattern of an extruded fiber of polymer **142**.

6.5 Morphology Investigation

The morphology of polymer **142** is investigated by two-dimensional X-ray diffraction in transmission mode. A fiber of the polymer is extruded and hit by an X-ray beam at room temperature. The diffraction pattern is shown in Figure 6.12.

Lamellar packing is observed as usual for polythiophenes.[12, 49, 50] The degree of order is high, comparable to **88** as can be seen from the sharp peaks and the appearance of up to the third order lamellar reflections. The molecular planes are oriented perpendicularly to the lamellar planes, a very typical assembly for polythiophenes.

The $\pi - \pi$ distance is determined from the peak on the meridional axis to be 3.7 Å, which is on the order of many other successful polymers. This low value should be very favorable for good field-effect mobility.

The lamellar distance, derived from the peaks on the equatorial axis, is determined to 2.38 nm. This value corresponds well to the length of a linear C14 alkyl chain plus the aromatic backbone. This means that the alkyl chains of the polymers interdigitate upon lamellae formation. High lattice energy is the consequence leading to a high degree of crystallinity and potentially large grains.[51, 52]

Based on the results of the X-ray diffraction measurements, a cartoon of the polymer assembly has been created (Figure 6.13). It can clearly be seen that the

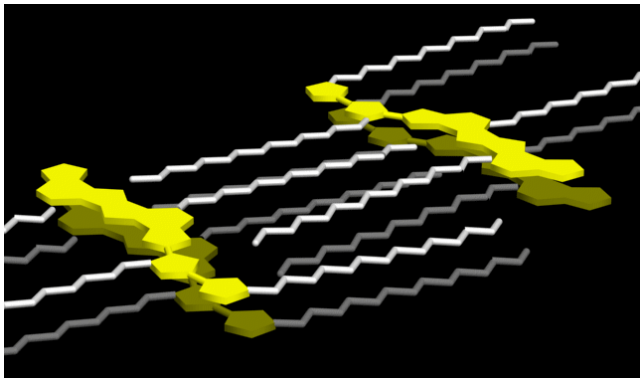

Figure 6.13: Cartoon of the polymer assembly based on the X-ray measurements of polymer **142**.

alkyl chains of adjacent polymer chains can interdigitate without steric clashes. As the lamellar distance measured by X-ray diffraction fits to the length of the alkyl chain plus the width of the aromatic backbone (about 2.4 Å), such an interdigitation is very likely. The space in between two chains of one polymer leaves enough space (11 Å) to fill in another alkyl chain. Derived from a P3HT model, the alkyl chains are 6 Åapart. This should give rise to crystallinity in the alkyl chain stabilizing the lamellar crystals of the polymer. The distance obtained from X-ray is in good agreement with force-field optimized molecular structures.

The alkyl chains of polymers stacked on top of each other have the possibility to avoid each other. They are attached to alternating sides of the polymer chain which allows a close π stacking favoring high charge-carrier mobility. The low value of 3.7 Å which has been determined by X-ray is obviously the result of the structural design concept.

In conclusion, the polymer shows good transistor characteristics arising from the favorable morphology. A high degree of order, a close $\pi - \pi$ distance, and dense lamellae show the high potential of this material. The charge-carrier mobility is presently not very high, *i.e.* in the low 10^{-3} $cm^2V^{-1}s^{-1}$regime. Considering the low molecular weight (M_n = 8 kg/mol; M_w = 16 kg/mol) there is plenty of room for improvements. It is well known that the field-effect mobility of polymers changes

several orders of magnitude with molecular weight.[53, 54] The catalytic system used for the polymer synthesis can be reconsidered, other catalysts may be more effective producing higher molecular weight. Also, the purity of the monomers may still be improved.

Furthermore, the device physics offer chances for further optimizations. The choice of dielectrics can have a strong influence on the transistor performance due to the surface morphology changes induced.[55] Also, the electrode materials play an important role which has impressively been demonstrated for a thienothiophene containing polymer.[6]

In summary, the benzodithiophene dimer with pending alkyl chains is a very promising building block for conjugated polymers. Copolymerized with dithiophene, good transistor characteristics have been recorded already at relatively low molecular weights. The high degree of order of the molecules exhibiting low $\pi - \pi$ distances and dense lamellar structures promise very good performances for this polymer when the molecular weight is increased and the device physics are optimized.

6.6 Bibliography

[1] Ebata, H.; Izawa, T.; Miyazaki, E.; Takimiya, K.; Ikeda, M.; Kuwabara, H.; Yui, T. *J. Am. Chem. Soc.* **2007**, *129*, 15732–15733.

[2] Takimiya, K.; Ebata, H.; Sakamoto, K.; Izawa, T.; Otsubo, T.; Kunugi, Y. *J. Am. Chem. Soc.* **2006**, *128*, 12604–12605.

[3] Gao, P.; Beckmann, D.; Tsao, H. N.; Feng, X.; Enkelmann, V.; Baumgarten, M.; Pisula, W.; Müllen, K. *Adv. Mater.* **2008**, *21*, 213–216.

[4] Takimiya, K.; Kunugi, Y.; Otsubo, T. *Chem. Lett.* **2007**, *36*, 578–583.

[5] McCulloch, I.; Heeney, M.; Bailey, C.; Genevicius, K.; Macdonald, I.; Shkunov, M.; Sparrowe, D.; Tierney, S.; Wagner, R.; Zhang, W. M.; Chabinyc, M. L.; Kline, R. J.; McGehee, M. D.; Toney, M. F. *Nat. Mater.* **2006**, *5*, 328–333.

[6] Hamadani, B. H.; Gundlach, D. J.; McCulloch, I.; Heeney, M. *App. Phys. Lett.* **2007**, *91*, 243512.

[7] Chabinyc, M. L.; Toney, M. F.; Kline, R. J.; McCulloch, I.; Heeney, M. *J. Am. Chem. Soc.* **2007**, *129*, 3226–3237.

[8] Fong, H. H.; Pozdin, V. A.; Amassian, A.; Malliaras, G. G.; Smilgies, D. M.; He, M. Q.; Gasper, S.; Zhang, F.; Sorensen, M. *J. Am. Chem. Soc.* **2008**, *130*, 13202–13203.

[9] Oyaizu, K.; Iwasaki, T.; Tsukahara, Y.; Tsuchida, E. *Macromol.* **2004**, *37*, 1257–1270.

[10] Wu, Y. L.; Liu, P.; Gardner, S.; Ong, B. S. *Chem. Mater.* **2005**, *17*, 221–223.

[11] Ong, B. S.; Wu, Y. L.; Li, Y. N.; Liu, P.; Pan, H. L. *Chem. Eur. J.* **2008**, *14*, 4766–4778.

[12] Prosa, T. J.; Winokur, M. J.; Moulton, J.; Smith, P.; Heeger, A. J. *Macromol.* **1992**, *25*, 4364–4372.

[13] Yamamoto, T.; Komarudin, D.; Arai, M.; Lee, B. L.; Suganuma, H.; Asakawa, N.; Inoue, Y.; Kubota, K.; Sasaki, S.; Fukuda, T.; Matsuda, H. *J. Am. Chem. Soc.* **1998**, *120*, 2047–2058.

[14] Gronowit.S,; Holm, B. *Acta Chem. Scand.* **1969**, *23*, 2207–2212.

[15] Chinchilla, R.; Najera, C. *Chem. Rev.* **2007**, *107*, 874–922.

[16] Leriche, P.; Raimundo, J. M.; Turbiez, M.; Monroche, V.; Allain, M.; Sauvage, F. X.; Roncali, J.; Frere, P.; Skabara, P. J. *J. Mater. Chem.* **2003**, *13*, 1324–1332.

[17] Mamane, V.; Hannen, P.; Furstner, A. *Chem. Eur. J.* **2004**, *10*, 4556–4575.

[18] Furstner, A.; Mamane, V. *J. Org. Chem.* **2002**, *67*, 6264–6267.

[19] Watanabe, M.; Mataka, S.; Thiemann, T. *Steroids* **2005**, *70*, 856–866.

[20] Wang, Y.; Burton, D. J. *J. Fluorine Chem.* **2007**, *128*, 1052–1057.

[21] Abdou, M. S. A.; Lu, X. T.; Xie, Z. W.; Orfino, F.; Deen, M. J.; Holdcroft, S. *Chem. Mater.* **1995**, *7*, 631–641.

[22] Sato, M. A.; Morii, H. *Macromol.* **1991**, *24*, 1196–1200.

[23] Andersson, M. R.; Selse, D.; Berggren, M.; Järvinen, H.; Hjertberg, T.; Inganäs, O.; Wennerstrom, O.; Osterholm, J. E. *Macromol* **1994**, *27*, 6503–6506.

[24] Amou, S.; Haba, O.; Shirato, K.; Hayakawa, T.; Ueda, M.; Takeuchi, K.; Asai, M. *J. Polym. Sci. Pol. Chem.* **1999**, *37*, 1943–1948.

[25] Yamamoto, T. *Prog. Polym. Sci.* **1992**, *17*, 1153–1205.

[26] Schlüter, A. D.; Wegner, G. *Acta Polym.* **1993**, *44*, 59–69.

[27] Kellogg, R. M.; Schaap, A. P.; Harper, E. T.; Wynberg, H. *J. Org. Chem.* **1968**, *33*, 2902–2909.

[28] Zhou, Z. H.; Yamamoto, T. *J. Organomet. Chem.* **1991**, *414*, 119–127.

[29] Heeney, M.; Bailey, C.; Genevicius, K.; Shkunov, M.; Sparrowe, D.; Tierney, S.; McCulloch, I. *J. Am. Chem. Soc.* **2005**, *127*, 1078–1079.

[30] Pokrop, R.; Verilhac, J. M.; Gasior, A.; Wielgus, I.; Zagorska, M.; Travers, J. P.; Pron, A. *J. Mater. Chem.* **2006**, *16*, 3099–3106.

[31] Kline, R. J.; McGehee, M. D.; Kadnikova, E. N.; Liu, J. S.; Frechet, J. M. J. *Adv. Mater.* **2003**, *15*, 1519–1522.

[32] Fumagalli, L.; Binda, M.; Natali, D.; Sampietro, M.; Salmoiraghi, E.; Di Gianvincenzo, P. *J. Appl. Phys.* **2008**, *104*, year.

[33] Gierschner, J.; Cornil, J.; Egelhaaf, H. J. *Adv. Mater.* **2007**, *19*, 173–191.

[34] de Melo, J. S.; Silva, L. M.; Arnaut, L. G.; Becker, R. S. *J. Chem. Phys.* **1999**, *111*, 5427–5433.

[35] Dierksen, M.; Grimme, S. *J. Chem. Phys.* **2004**, *120*, 3544–3554.

[36] Kastler, M.; Schmidt, J.; Pisula, W.; Sebastiani, D.; Müllen, K. *J. Am. Chem. Soc.* **2006**, *128*, 9526–9534.

[37] Muhlbacher, D.; Neugebauer, H.; Cravino, A.; Sariciftci, N. S. *Synth. Met.* **2003**, *137*, 1361–1362.

[38] Okamoto, T.; Kudoh, K.; Wakamiya, A.; Yamaguchi, S. *Chem. Eur. J.* **2007**, *13*, 548–556.

[39] Catalfo, A.; Serrentino, M. E.; Librando, V.; Perrini, G.; De Guidi, G. *Appl. Spectrosc.* **2008**, *62*, 1233–1237.

[40] Colditz, R.; Grebner, D.; Helbig, M.; Rentsch, S. *J. Inform. Rec.* **1996**, *22*, 457–463.

[41] Tashiro, K.; Ono, K.; Minagawa, Y.; Kobayashi, M.; Kawai, T.; Yoshino, K. *J. Polym. Sci. B* **1991**, *29*, 1223–1233.

[42] Leclerc, M.; Frechette, M.; Bergeron, J. Y.; Ranger, M.; Levesque, I.; Faid, K. *Macromol. Chem. Phys.* **1996**, *197*, 2077–2087.

[43] Ong, B. S.; Wu, Y. L.; Liu, P.; Gardner, S. *Adv. Mater.* **2005**, *17*, 1141–1142.

[44] Bjornholm, T.; Greve, D. R.; Geisler, T.; Petersen, J. C.; Jayaraman, M.; McCullough, R. D. *Adv. Mater.* **1996**, *8*, 920–923.

[45] Kobayashi, T.; Hamazaki, J.; Kunugita, H.; Ema, K.; Ochiai, K.; Rikukawa, M.; Sanui, K. *J. Nonlin. Opt. Phys. Mater.* **2000**, *9*, 55–61.

[46] Sirringhaus, H. *Adv. Mater.* **2005**, *17*, 2411–2425.

[47] Kline, R. J.; McGehee, M. D. *Polym. Rev.* **2006**, *46*, 27–45.

[48] Surin, M.; Leclere, P.; Lazzaroni, R.; Yuen, J. D.; Wang, G.; Moses, D.; Heeger, A. J.; Cho, S.; Lee, K. *J. Appl. Phys.* **2006**, *100*, 33712.

[49] Liu, J. Y.; Zhang, R.; Sauve, G.; Kowalewski, T.; McCullough, R. D. *J. Am. Chem. Soc* **2008**, *130*, 13167–13176.

[50] Sirringhaus, H.; Brown, P. J.; Friend, R. H.; Nielsen, M. M.; Bechgaard, K.; Langeveld-Voss, B. M. W.; Spiering, A. J. H.; Janssen, R. A. J.; Meijer, E. W.; Herwig, P.; de Leeuw, D. M. *Nature* **1999**, *401*, 685–688.

[51] DeLongchamp, D. M.; Kline, R. J.; Lin, E. K.; Fischer, D. A.; Richter, L. J.; Lucas, L. A.; Heeney, M.; McCulloch, I.; Northrup, J. E. *Adv. Mater.* **2007**, *19*, 833–837.

[52] Kim, D. H.; Park, Y. D.; Jang, Y. S.; Yang, H. C.; Kim, Y. H.; Han, J. I.; Moon, D. G.; Park, S. J.; Chang, T. Y.; Chang, C. W.; Joo, M. K.; Ryu, C. Y.; Cho, K. W. *Adv. Funct. Mater.* **2005**, *15*, 77–82.

[53] Zen, A.; Pflaum, J.; Hirschmann, S.; Zhuang, W.; Jaiser, F.; Asawapirom, U.; Rabe, J. P.; Scherf, U.; Neher, D. *Adv. Funct. Mater.* **2004**, *14*, 757–764.

[54] Kline, R. J.; McGehee, M. D.; Kadnikova, E. N.; Liu, J. S.; Frechet, J. M. J.; Toney, M. F. *Macromol.* **2005**, *38*, 3312–3319.

[55] Facchetti, A.; Yoon, M. H.; Marks, T. J. *Adv. Mater.* **2005**, *17*, 1705–1725.

7 Conclusion and Outlook

In this work electron rich and electron poor materials have been synthesized and characterized with respect to their potential use in organic electronic devices. The α-diketone moiety was focused on as electron withdrawing group, thiophene on the other hand as the electron donor.

The incorporation of three α-diketones into one extended flat molecule requires the development of a new coronene synthesis. The photochemical cyclodehydrogenation of substituted cyclophanes affords substituted coronenes with the option of choosing the symmetry. The reaction has been demonstrated with methoxy groups which can be cleaved leaving phenolic dialcohols easily undergoing oxidation to α-diketones. The thus obtained coronene-hexaone opens the way to a variety of important applications:

1. **Work function tuning of a metal.** The α-diketone proves to efficiently extract electrons out of a metal which creates a surface dipole increasing the work function of the metal. It can be shown by calculations that the α-diketones bend towards the metal strengthening the interaction with the metal.

2. **Charge-transfer complex formation.** The electron poor character of coronene-hexaone can extract partial charge out of a donor molecule forming a charge-transfer complex. The poor solubility of the molecule can be circumvented by cosublimation of the molecules. The charge-transfer

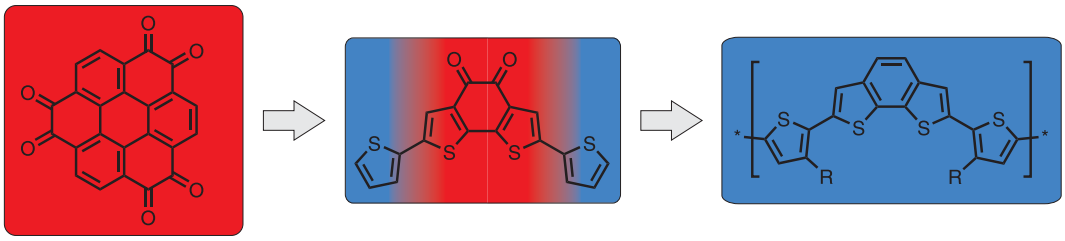

Figure 7.1: Donor and acceptor molecules under investigation in this thesis, electron acceptors are marked in red, donors in blue.

complex formation is monitored by UPS measurements which is unprecedented.

3. **Condensation reactions for larger π systems.** α-Diketones undergo condensation reactions very efficiently with diamines. A series of molecules with an extended aromatic core have been synthesized and characterized with regard to their bulk properties. It could be shown that liquid crystalline behavior is only obtained when peripheral phenyl groups are added, alkyl substitution alone leaves the molecule in the crystalline state. A high degree of control of the melting point is gained varying the length of the chain.

Using the route established in this thesis, a wide variety of substituted coronenes should be accessible if the corresponding cyclophanes can be made. Future developments could focus on extended discs incorporating sulfur in the periphery. The advantages of extended polycyclic aromatic hydrocarbons can thus be combined with the strong intermolecular interaction forces of sulfur. Even stronger acceptors may be obtained by attaching cyano groups or even twelve ketones to coronene.

In the second part, the α-diketone group has been attached to a thiophene containing system rendering another strong acceptor. This molecule has covalently been linked to electron rich thiophenes leading to donor-acceptor molecules. These resemble the repeat unit of a conjugated donor-acceptor polymer, a class of high importance towards organic electornic devices.

With this model system it could be shown that the assembly of conjugated donor-

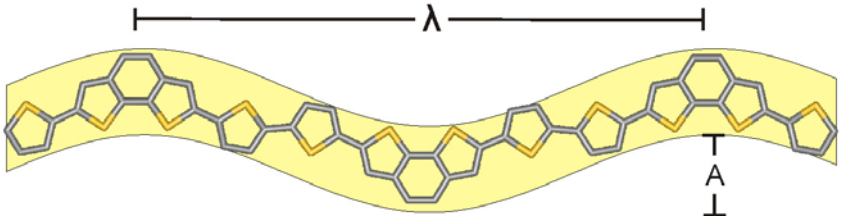

Figure 7.2: Curved polymer backbone with a characteristic wavelength (λ) and amplitude (A).

acceptor systems is dominated by intermolecular charge transfer interactions. A set of experimental data support this thesis: (1) the crystal adopts energetically unfavorable contacts and conformations, (2) a charge-transfer band is visible in the film UV-vis absorption spectrum, and (3) the interplanar distances are much shorter than in all-donor molecules.

This observation has important implications for the design of new donor-acceptor systems. The charge-transfer interactions bring the molecules in close contact which is good for high charge-carrier mobility, but significantly lower the solubility. Alkyl chains drive the molecular planes apart, thus increasing solubility. An optimum compromise has to be found for a high-performance material.

Purely donor molecules are important hole conductors for organic field-effect transistors. Benzo[2,1-b;3,4-b']dithiophene has been copolymerized with dithiophenes. After a rational optimization process for the position of the solubilizing alkyl chains, a polymer is obtained which satisfies all requirements for industrial applications: (1) it is well soluble and can thus be processed from solutions, (2) it is easily synthesized and can be scaled up for production, (3) it exhibits high charge-carrier mobility exceeding 0.1 $cm^2V^{-1}s^{-1}$, (4) it does not need long annealing at elevated temperatures for good performance, and (5) is stable enough against air and moisture for applications. On a flexible substrate, mobilities as high as 0.5 $cm^2V^{-1}s^{-1}$are measured which is among the best values for polymers reported so far.

The kink induced by the benzodithiophene creates a curved polymer backbone.

This geometry is very favorable as it represents a compromise between efficient packing and good solubility. UV-vis spectroscopy and light scattering reveal that the polymer is highly organized in solution, but does not precipitate. In contrast, the linear isomer can only be dissolved with difficulties. Lower field-effect mobilities are the result. Different benzodithiophene isomers have been incorporated in polymers to show that benzo[2,1-b;3,4-b']dithiophene consitutes the optimum compromise. Stronger curvatures reduce the interchain overlap, less curvature decreases the solubility hindering the device fabrication.

A solar cell based on the successful benzodithiophene copolymer has been made. In a bulk heterojunction with [70]PCBM a power conversion efficiency of 2.7 % has been measured without significant optimization effords.

Further developments in the field of polymeric materials for organic transistors should focus on other building blocks which induce a moderate curvature, for example dithienothiophene. This opens up a wide field of new materials with promising fabrication properties. Whenever possible, coupling reactions should be used to avoid crosslinking as shown in this thesis.

In the last part, the benzodithiophene building block has been doubled to yield an extended, rod-like monomer with pending alkyl chains. They can be copolymerized with alkylated dithiophene to afford a polymer with the largest fused π-system so far. The transistor characterization and especially the X-ray diffraction analysis reveal the high potential of this material. If polymerized with higher molecular weight, very good performance can be expected. These results suggest that similar rod-like thiophene containing structures which have successfully been tested in FETs should be copolymerized with dithiophene as well to explore this new polymer class. Improvements of field-effect mobility, processing, and light harvesting seem very realistic.

8 Experimental Part

8.1 General Methods

8.1.1 Chemicals and Solvents

All used chemicals and solvents were obtained from the companies ABCR, Acros, Aldrich, Alpha-Aesar, Fluka, Lancaster, Merck and Strem. Unless otherwise mentioned, they were used as obtained.

8.1.2 Chromatography

Preparative column chromatography was performed on silica gel from Merck with a grain size of 63 - 200 μm (silica gel) or 40 - 63 μm (flash silica gel, Geduran Si 60). For analytical thin layer chromatography (TLC), silica gel coated substrates "60 F254" from Merck were used. Compounds were detected by fluorescence quenching at 254 nm, self-fluorescence at 366 nm or staining in an iodine vapor chamber. For eluents, analytically pure solvents (p.a. or technical grade) were distilled prior to the use.

8.1.3 Inert Atmosphere

Oxygen or moisture sensitive reactions were carried out in an argon atmosphere (Westfalen AG). If not mentioned specifically, reactions were degassed by bubbling a stream of argon through the reaction mixture.

8.1.4 UV reactions

UV reactions were done in a Rayonet RPR-100 with up to eight lamps (20 W each) of either 300 or 350 nm as indicated. The lamps possess a half width wavelength distribution of 40 nm. The apparatus was cooled by a 15 W air fan. Quartz glassware was used as reaction vessel, the solution was stirred by a magnetic stir bar.

8.2 Analytical Techniques

8.2.1 Melting Points

Melting points were determined on a Büchi hot stage apparatus and were uncorrected.

8.2.2 Mass Spectrometry

Field-desorption mass spectra were obtained on a VG Instruments ZAB 2-SE-FPD spectrometer. MALDI-TOF spectrometry was conducted on a Bruker Reflex II-TOF spectrometer, utilizing a 337 nm nitrogen laser. If not specifically mentioned, tetracyanoquinodimethane (TCNQ) was used as the matrix substance for solid state prepared samples. Varying thicknesses of the prepared sample on the MALDI target reduced the resolution; therefore only integers of the molecular peaks were given. The most intense peak was compared to the calculated isotope of highest abundance.

8.2.3 NMR Spectroscopy

^{1}H-NMR, ^{13}C-NMR, H,H-COSY, C,H-COSY and NOESY experiments were recorded in the listed deuterated solvents on a Bruker DPX 250, Bruker AMX 300, Bruker DRX 500 or a Bruker DRX 700 spectrometer. The deuterated solvent was used as an internal standard, CD_2Cl_2 was set to δ_H = 5.32 ppm and δ_C = 54.00 ppm, THF to δ_H = 3.58 ppm and δ_C = 67.57 ppm, DMSO to δ_H = 2.50 ppm and δ_C = 39.51 ppm, $C_2D_2Cl_4$ to δ_H = 5.91 ppm and δ_C = 74.20 ppm.[1]

8.2.4 Elemental Analysis

Elemental analysis of solid samples was carried out on a Foss Heraeus Vario EL as a service of the Institute for Organic Chemistry, Johannes Gutenberg-Universität of Mainz. Liquid compounds or oils were not analyzed because of the difficulties to remove residual solvents and atmospheric gases like CO_2. The coroneneketones could not be analyzed due to the strong interaction of diktones and DMSO. The latter was crucial for the oxidation process, but cannot be removed completely . Halogen containing molecules evolve hydrohalogenic acids on burning such that for each halogen atom one hydrogen atom escapes the measurement. The theoretical values were corrected accordingly, a note was given when doing so.

8.2.5 UV-vis Spectroscopy

Solution UV-vis spectra were recorded at room temperature on a Perkin-Elmer Lambda 100 spectrophotometer. The molar extinctions were given in the unit m^2mol^{-1} which was consistent with the SI standard. Unless otherwise noted, a concentration of 10^{-5} mol/l was used. Solvents of spectroscopic grade were employed. The baseline was corrected by substracting a measurement of the cuvette filled with pure solvent used for the measurement.

Solution photoluminescence spectra were recorded on a SPEX-Fluorolog II

(212) spectrometer. Quantum yields of selected compounds were calculated by comparing to the known standard 5,10-diphenylanthracene (three different concentrations).[2] Unless otherwise stated, the measurement was performed at room temperature.

8.2.6 Infrared Spectroscopy

Infrared spectroscopy was measured on a Nicolet 730 FT-IR spectrometer in the evanscence field of a diamond. The sample was deposited as pristine material on the diamond crystal and pressed on it with a stamp. 64 measurements were recorded for each sample, the background was substracted.

8.2.7 Cyclic Voltammetry

Cyclic volatammetry was measured on a Princeton Applied Research Parstat 2273 instrument with anhydrous solvents under argon atmosphere. Tetrabutylammoniumperchlorate was used as conductive salt at a concentration of 0.1 mol/l. Ferrocen was added as internal standard (1 mM). A platinum working electrode (0.5 mm diameter), a platinum wire as counter electrode, and a silver wire as quasi-reference electrode were used. The peaks were calibrated according to the oxidation peak of ferrocene. Half-step potentials were used for the evaluation.[3]

8.2.8 Field-Effect Transistors

Standard procedure for transistors on silicon substrates: Heavily doped silicon wafers with a 200 nm thick thermally grown silicon dioxide layer were used as substrates. Hexamethyldisilazane was deposited out of the gas phase at 120 °C. The semiconductor polymeric film was prepared by spin-coating (3000 rpm, 60 s) a 5 mg/ml 1,2-dichlorobenzene solution (roughly 47.5 nm thick). After annealing the substrate at 100 °C for 5 min and slow cooling (1 °C/min), source and drain elec-

trodes were fabricated by vapor-depositing gold ($3 \cdot 10^{-6}$ mbar, 1 Å/s, $\sim$ 100 nm thick) onto the semiconductor thin films through a shadow mask to obtain devices with channel lengths of between 25-75 μm and of widths about 0.5 to 1.5 mm (W/L = 20). All preparations and electrical measurements using a Keithley 4200 semiconductor parameter analyzer were performed under nitrogen atmosphere in yellow light.

The charge carrier mobility was calculated in saturation from the equation

$$\mu_{\text{sat}} = \frac{2I_{SD}L}{WC_i\left(V_{SG} - V_{th}\right)^2}$$

PET substrates: Gold electrodes were evaporated onto an FET foil (roughly 35 nm thick). A solution (2 mg/ml) of the polymer in chlorobenzene was spin-cast at 90 °C onto the substrate and dried for 30 seconds at 100 °C. Polystyrene (MW = 820 kg/mol, BASF) was spin-cast on top from a 5.5 weight-percent solution in ethyl acetate. The gate contact was made by evaporating a layer of about 50 nm of gold on top by the aid of a shadow mask. Measurements were performed using a Keithley 4200 machine under ambient conditions in the absence of light. Gate-dependent mobility was calculated according to

$$\frac{dI_{SD}}{dV_G} = \frac{W}{L}\mu_{\text{sat}}C_iV_{SD}$$

8.2.9 X-ray scattering

The two-dimensional wide-angle X-ray diffraction experiments were performed by means of a rotating anode (Rigaku 18 kW) X-ray beam with a pinhole collimation and a 2D Siemens detector with a beam diameter of ca 1 mm. A double graphite monochromator for the Cu-Kα radiation (λ = 0.154 nm) was used.

Film X-ray diffraction was performed on a theta-theta Philips PW 1820 Kristalloflex diffractometer with a graphite-monochromized Cu-Kα X-ray beam

hitting a drop-cast film on a silicon wafer. The diffraction patterns were recorded in the 2 θ range from 1° to 32°.

8.2.10 Polarized Optical Microscopy

A Zeiss microscope equipped with polarizing filters and equipped with a Hitachi KPD50 Colour digital CCD camera was used in order to investigate the optical textures of the compounds. The samples were sandwiched between two glass slides and then thermally treated on a Linkam hotstage fitted with a Linkam TMS 91 temperature controller.

8.2.11 Differential Scanning Calorimetry

Differential scanning calorimetry (DSC) was measured on a Mettler DSC 30 with heating and cooling rates of 10 K/min.

8.2.12 Atomic force microscopy

Atomic force microscopy was performed by using a Nanoscope IIIa MultiMode scanning probe microscope; Digital Instruments, Santa Barbara, CA.

8.3 Coronene Chemistry

8.3.1 3,6-Dihydroxymethylveratrol

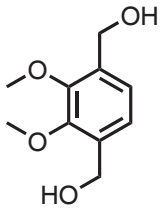

6

1 g (5.1 mmol) 2,3-Dimethoxyterephthalicdialdehyde was dissolved in 50 ml isopropanol and 200 mg (5.3 mmol) sodium borohydride were added. The suspension was stirred overnight. 20 ml 1M hydrochloric acid was added, and isopropanol was removed under reduced pressure. The remaining solution was extracted with dichloromethane. The organic phase was dried and the solvent removed in vaccum. 850 mg (84 %) of 3,6-dihydroxymethylveratrol was obtained as colorless crystals (mp: 82 °C); MS (FD, 8 kV) m/z = 198.3 g/mol - calculated: 198.1 g/mol for $C_{10}H_{14}O_4$; ^{1}H-NMR (250 MHz, CD_2Cl_2, RT, δ in ppm) 7.03 (s, 2 H), 4.62 (s, 4 H), 3.85 (s, 6 H); 2.46 (s, 2 H); ^{13}C-NMR (62.5 MHz, CD_2Cl_2, RT, δ in ppm) 151.2, 135.4, 124.0, 61.2; EA found: 60.59 % C, 7.09 % H - calculated for $C_{10}H_{14}O_4$: 60.59 % C, 7.12 % H, 32.29 % O

8.3.2 3,6-Di(triphenylposphoniumbromide)methylveratrol

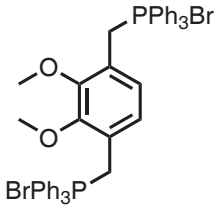

8

500 mg (2.6 mmol) 3,6-Dihydroxymethylveratrol were dissolved in 2 ml dichloromethane. 2 ml hydrobromic acid (48 %) were added and stirred overnight at room temperature. The solution was extracted with dichloromethane, neutralized with 1M aqueous sodium carbonate solution and dried. To the resulting solution 1.36 g (5.2 mmol) triphenylphosphine was added and stirred for 30 minutes. The solution was poured into toluene (30 ml), the precipitate was filtered off, washed with toluene and dried in vacuum. 2.2 g (quantitative) of a yellow powder was obtained (mp: 230 °C); ^{1}H-NMR (700 MHz, CD_2Cl_2, RT, δ in ppm) 7.78 (t, 6 H, J = 7.2 Hz), 7.71 (dd, 12 H, J = 12.4 Hz, 8.1 Hz), 7.64 (td, 12 H, J = 7.8 Hz, 3.3 Hz), 6.80 (s, 2 H), 5.23 (d, 4 H, J = 13.4 Hz), 3.35 (s, 6 H); ^{13}C-NMR (175 MHz, CD_2Cl_2, RT, δ in ppm) 152.1, 135.5, 134.8 (t, J = 4.8 Hz), 130.6 (t, J = 6.1 Hz), 127.3, 123.7, 118.5 (d, J = 86.9 Hz), 60.6, 26.3 (d, J = 49.8 Hz); ^{31}P-NMR (202 MHz, CD_2Cl_2, RT, δ in ppm) 22.2 (s); EA found: 65.22 % C, 5.16 % H - calculated for $C_{46}H_{42}Br_2O_2P_2$: 65.11 % C, 4.99 % H

8.3.3 Z,Z-1,4-Bis(4-carbonylstyryl)veratrol

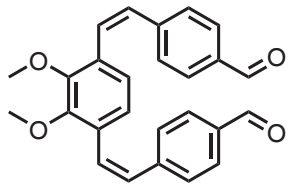

10

3.0 g (3.5 mmol) 3,6-Di(triphenylposphoniumbromide)methylveratrol and 1.15 g (8.5 mmol) terephthalic dialdehyde were dissolved in 50 ml dichloromethane and cooled to -40 °C. A mixture of 20 ml ethanol and 4.6 ml (7.4 mmol) *n*-butyllithium (1.6 M in hexanes) were slowly added. The mixture was kept at -40 °C for another 10 hours and then slowly warmed to room temperature. The solvents were removed in vacuum. The residue was dissolved in dichloromethane and extracted with 1 M

HCl. The organic phase was dried and the solvent removed under reduced pressure. The residue was purified by chromatography (petroleum ether - diethyl ether 1:1 v/v as eluent) to yield 340 mg (24 %) of a yellow oil; MS (FD, 8 kV) m/z = 398.7 g/mol - calculated: 398.2 g/mol for $C_{26}H_{22}O_4$; ^{1}H-NMR (250 MHz, CD_2Cl_2, RT, δ in ppm) 9.92 (s, 2 H), 7.70 (d, 4 H, J = 8.2 Hz), 7.38 (d, 4 H, J = 8.2 Hz), 6.84 (d, 2 H, J = 12.2 Hz), 6.69 (d, 2 H, J = 12.2 Hz), 6.60 (s, 2 H), 3.88 (s, 6 H); ^{13}C-NMR (62.5 MHz, CD_2Cl_2, RT, δ in ppm) 192.1, 152.1, 144.1, 135.7, 131.8, 130.4, 130.0, 129.9, 128.7, 125.1, 61.4

8.3.4 Dimethoxy-[2.2.2]paracyclophan-triene

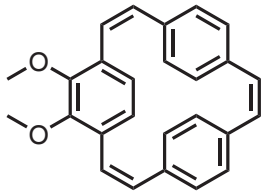

11

2.2 ml (20 mmol) Titanium(IV)-chloride were dissolved to 75 ml THF at 0 °C, 2.6 g (40 mmol) zinc dust and 1 ml pyridine were added and heated to reflux for one hour. 320 mg (0.8 mmol) Z,Z-1,4-Bis(4-carbonylstyryl)veratrol were dissolved in 50 ml THF and added dropwise over a period of 3 hours. The solution was kept at reflux for another hour, then cooled down to room temperature, 30 ml of 1 M HCl was added, the solution was decanted, most of the THF evaporated in vacuum. The residue was extracted with dichloromethane, dried, and the solvent removed. The residue was purified by chromatography (petroleum ether - dichloromethane 6:4 v/v as eluent) to yield 80 mg (27 %) of a yellow oil which solidifies after five days (mp: 70°C); MS (FD, 8 kV) m/z = 366.6 g/mol - calculated: 366.2 g/mol for $C_{26}H_{22}O_2$; ^{1}H-NMR (250 MHz, CD_2Cl_2, RT, δ in ppm) 6.89 (d, 2 H, J = 11.4 Hz), 6.83 (s, 2 H), 6.80 (d, 4 H, J = 8.3 Hz) 6.78 (d, 2 H, J = 11.3 Hz), 6.68 (d, 4 H, J =

8.3 Hz), 6.36 (s, 2 H); ^{13}C-NMR (62.5 MHz, CD_2Cl_2, RT, δ in ppm) 151.4, 137.2, 136.5, 133.6, 133.3, 131.9, 129.6, 129.0, 128.6, 126.3, 60.7; EA found 85.29 % C, 5.91 % H - calculated: 85.22 % C, 6.05 % H, 8.73 % O

8.3.5 1,2-Dimethoxycoronene

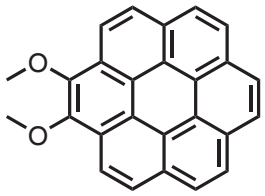

17

100 mg (0.27 mmol) Dimethoxy-[2.2.2]paracyclophan-triene were dissolved in 100 ml cyclohexane, 300 mg (0.86 mmol, 3.15 eq) iodine were added. After degassing three drops of propylene oxide was added. The solution was irradiated with 300 nm (40 W) overnight. The solution was diluted with 10 ml dichloromethane and extracted with aqueous sodium sulfite. After drying and evaporation of the solvent, the substance was purified crystallization from hexane to yield 15 mg (76 %) as yellow needles (mp: 213 °C); MS (FD, 8 kV) m/z = 360.6 g/mol - calculated: 360.1 g/mol for $C_{26}H_{16}O_2$; ^{1}H-NMR (250 MHz, CD_2Cl_2, RT, δ in ppm) 9.17 (d, 2 H, J = 8.7 Hz), 8.90 (d, 2 H, J = 8.8 Hz), 8.86 (d, 2 H, J = 8.7 Hz), 8.84 (s, 2 H), 8.81 (d, 2 H, J = 8.6 Hz), 4.45 (s, 6 H); ^{13}C-NMR (62.5 MHz, CD_2Cl_2, RT, δ in ppm) 156.4, 129.3, 128.7, 126.8, 126.7, 126.6, 126.4, 125.5, 122.9, 122.7, 120.7 (two peaks), 62.4; UV-vis ($CHCl_3$, λ in nm) 294 (rel 0.66), 304 (rel 1.00), 324 (rel 0.25), 341 (rel 0.27), 404 (rel 0.068), 429 (rel 0.065)

8.3.6 1,2-Coronene-dione

50 mg (0.14 mmol) 1,2-Dimethoxycoronene were dissolved in 10 ml dichloromethane and added to 10 ml 1 M BBr_3 solution in dichloromethane. The

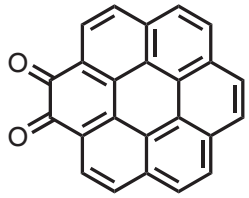

23

suspension was stirred overnight. The volatile substances were removed under high vacuum at room temperature. To the residue 5 ml concentrated nitric acid was added, after 1 minute, the solution was diluted with 20 ml water and centrifuged. The solid was refluxed in THF for 30 minutes and filtered to yield 30 mg (65 %) of a dark violet solid (mp: dec.); MS (FD, 8 kV) m/z = 330.7 g/mol - calculated: 330.1 g/mol for $C_{24}H_{10}O_2$; ^{1}H-NMR (250 MHz, CD_2Cl_2, RT, δ in ppm) (coronene added) 8.04 (d, 2 H, J = 8.0 Hz), 8.10 (s, 2 H), 7.78 (d, 2 H, J = 8.9 Hz), 7.66 (d, 2 H, J = 8.0 Hz), 7.56 (d, 2 H, J = 9.1 Hz), 7.35 (s, 2 H); IR (neat, $1/\lambda$ in cm^{-1}) 1664, 1651, 1606, 1510, 1300, 995, 850, 795, 563

8.3.7 Z,Z-1,4-Bis(4-carbonyl-2,3-dimethoxystyryl)benzene

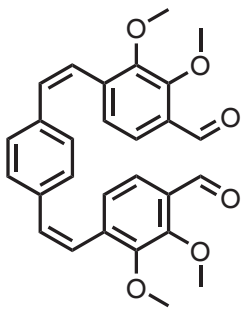

13

1.7 g (2.2 mmol) 1,4-Xylene-bis-triphenylphosphoniumbromide and 1.0 g (5.1 mmol) 2,3-dimethoxyterephthalic dialdehyde were dissolved in 40 ml DMF and cooled to -40 °C. A mixture of 15 ml ethanol and 2.2 ml (3.5 mmol) *n*-butyllithium (1.6 M in hexanes) were slowly added. The mixture was kept at -40 °C for another 10 hours and then slowly warmed to room temperature. The

solvents were removed in vacuum. The residue was dissolved in dichloromethane and extracted with 1 M HCl. The organic phase was dried and the solvent removed under reduced pressure. The residue was purified by chromatography (hexane - ethylacetate 3:1 v/v as eluent) to yield 210 mg (21 %) of a yellow powder (mp = 157-159 °C); MS (FD, 8 kV) m/z = 459.2 g/mol - calculated: 458.2 g/mol for $C_{28}H_{26}O_6$; ^{1}H-NMR (250 MHz, CD_2Cl_2, RT, δ in ppm) 10.32 (s, 2 H), 7.30 (d, 2 H, J = 8.2 Hz), 7.08 (s, 4 H), 7.30 (d, 2 H, J = 8.2 Hz), 6.69 (s, 2 H), 6.68 (s, 2 H), 3.99 (s, 6 H), 3.86 (s, 6 H); ^{13}C-NMR (62.5 MHz, CD_2Cl_2, RT, δ in ppm) 189.7, 157.1, 152.0, 139.6, 136.5, 132.8, 130.0, 129.8, 129.4, 125.7, 125.5, 122.5, 62.6, 61.3

8.3.8 Tetramethoxy-[2.2.2]paracyclophan-triene

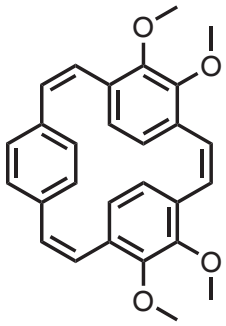

14

l0.2 ml (2 mmol) titanium(IV)-chloride were dissolved to 15 ml THF at 0 °C, 260 mg (4 mmol) zinc dust and 0.1 ml pyridine were added and heated to reflux for one hour. 100 mg (0.22 mmol) Z,Z-bis(4-carbonyl-2,3-dimethoxyphenyl)-divinylbenzene were dissolved in 20 ml THF and added dropwise over a period of 3 hours. The solution was kept at reflux for another hour, then cooled down to room temperature, 5 ml of 1M HCl was added, the solution was decanted, most of the THF evaporated in vacuum. The residue was extracted with dichloromethane, dried, and the solvent removed. The residue was purified by chromatography

(dichloromethane as eluent) to yield 34 mg (36 %) of a yellow oil which solidifies after five days (mp: 85 °C); MS (FD, 8 kV) m/z = 427.0 g/mol - calculated: 426.2 g/mol for $C_{28}H_{26}O_4$; ^{1}H-NMR (700 MHz, $C_2D_2Cl_4$, 100 °C, δ in ppm) 6.82 (d, 2 H, J = 11.2 Hz), 6.78 (s, 2 H), 6.75 (d, 2 H, J = 11.3 Hz), 6.29 (d, 2 H, J = 7.8 Hz), 6.15 (d, 2 H, J = 8.0 Hz), 3.78 (s, 6 H), 3.73 (s, 6 H); ^{13}C-NMR (175 MHz, $C_2D_2Cl_4$, 100 °C, δ in ppm) 151.0, 136.7, 133.2, 131.4, 131.4, 129.6, 129.5, 128.4, 126.5, 125.4, 60.5, 60.4; EA found 78.75 % C, 6.12 % H - calculated: 78.85 % C, 6.14 % H, 15.00 % O

8.3.9 1,2,5,6-Tetramethoxycoronene

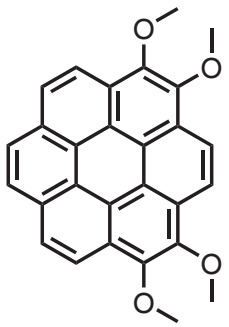

18

120 mg (0.47 mmol) Tetramethoxy-[2.2.2]paracyclophan-triene were dissolved in 200 ml cyclohexane, 530 mg (1.48 mmol; 3,15 eq) iodine were added. After degassing 0.1 ml of propylene oxide was added. The solution was irradiated with 300 nm (40 W) overnight. After extraction with aqueous sodium sulfite, drying, and evaporation of the solvent, the substance was purified by chromatography (dichloromethane - acetone 100:1 v/v) to yield 160 mg (80 %) of a yellow crystalline substance (mp: 195 °C); ^{1}H-NMR (500 MHz, CD_2Cl_2, RT, δ in ppm) 9.21 (s, 2 H), 9.17 (d, 2 H, J = 8.7 Hz), 8.91 (d, 2 H, J = 8.7 Hz), 8.84 (s, 2 H), 3.78 (s, 6 H), 3.73 (s, 6 H); ^{13}C-NMR (125 MHz, CD_2Cl_2, RT, δ in ppm) 146.5, 146.2, 129.0, 126.9, 125.8, 125.2, 123.0, 121.0, (two peaks), 120.9, 120.8, 62.4 (two peaks); MALDI-

TOF (TCNQ as matrix) m/z = 420.0 g/mol - calculated: 420.1 g/mol for $C_{28}H_{20}O_4$; EA found 79.87 % C, 4.84 % H - calculated: 79.98 % C, 4.79 % H, 15.22 % O; UV-vis ($CHCl_3$, λ in nm) 311 (rel 1.00), 323 (0.64), 353 (0.34), 391 (0.007), 414 (0.011), 430 (0.012), 438 (0.013); IR (neat, $1/\lambda$ in cm^{-1}) 3076, 1660, 1595, 1338, 1327, 1275, 1115, 1037, 991, 860, 758, 571

8.3.10 1,2,5,6-Coronene-tetraone

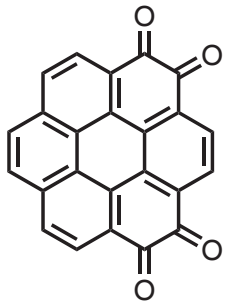

24

50 mg (0.12 mmol) 1,2,5,6-Tetramethoxycoronene were dissolved in 5 ml dichloromethane and added to 5 ml 1 M BBr_3 solution in dichloromethane. The suspension was stirred overnight. The volatile substances were removed under high vacuum at room temperature. To the residue 5 ml concentrated nitric acid were added, after 1 minute, the solution was diluted with 20 ml water and centrifuged. The solid was refluxed in THF for 30 minutes and filtered to yield 32 mg (74 %) of a reddish solid (mp: dec.); MS (FD, 8 kV) m/z = 360.8 g/mol - calculated: 360.0 g/mol for $C_{24}H_8O_4$; ^{1}H-NMR (250 MHz, DMSO$-d_6$, RT, δ in ppm) 8.69 (d, 2 H, J = 7.7 Hz), 8.55 (d, 2 H, J = 8.0 Hz), 8.51 (s, 2 H), 8.47 (s, 2 H)

8.3.11 Z,Z-3,6-Bis(4-carbonyl-2,3-dimethoxystyryl)veratrol

8.5 g (10 mmol) 3,6-Di(triphenylposphoniumbromide)methylveratrol and 4.3 g (22 mmol) of 2,3-dimethoxyterephthalic dialdehyde were dissolved in 150 ml

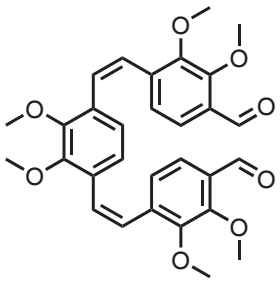

15

dichloromethane. The solution was cooled to -40 °C. A mixture of 13 ml (21 mmol) butyllithium (1.6 M in hexanes) and 60 ml ethanol were slowly added. The reaction mixture was kept at -40 °C for 6 hours and slowly warmed to room temperature overnight. 10 ml of 1 M hydrochloric acid was added and extracted with dichloromethane. After drying, the solvent was removed in vacuum. The residue was purified by chromatography (diethylether - petroleum ether 5.5:4.5 v/v as eluent). 2.4 g of a yellow oil was obtained. MS (FD, 8 kV) m/z = 518.1 g/mol - calculated: 518.2 g/mol for $C_{30}H_{30}O_8$; ^{1}H-NMR (250 MHz, CD_2Cl_2, RT, δ in ppm) 10.28 (s, 2 H), 7.25 (d, J = 8.2 Hz, 2 H), 6.92 (d, J = 8.2 Hz, 2 H), 6.87 (d, J = 12.2 Hz, 2 H), 6.74 (d, J = 12.3 Hz, 2 H), 6.57 (s, 2 H), 3.97 (s, 6 H), 3.86 (s, 6 H), 3.85 (s, 6 H); ^{13}C-NMR (62.5 MHz, CD_2Cl_2, RT, δ in ppm) 189.7, 157.0, 152.1, 152.0, 139.5, 131.6, 129.7, 128.4, 125.8, 125.5, 124.8, 122.3, 62.7, 61.4, 61.3

8.3.12 Hexamethoxy[2.2.2]paracyclophane-triene

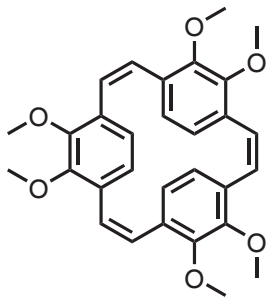

16

5 ml (50 mmol) Titanium(IV)-chloride was dropped at 0° C into 250 ml anhydrous THF. 6.5 g (100 mmol) zinc powder and 2.5 ml pyridine were added. The mixture was refluxed for one hour. 2.5 g (4.8 mmol) 3,6-Bis(4-carbonyl-2,3-dimethoxystyryl)veratrol in 500 ml anhydrous THF were added dropwise to the boiling solution over a period of about 2 hours. The mixture was refluxed for one additional hour. After cooling to room temperature, 50 ml 1 M hydrochoric acid was added. The solution was separated from the solid by decanting. Most of the THF was removed under reduced pressure. The remaining solution was extracted with dichloromethane, and dried. After removal of the solvent, the residue was purified by column chromatography (dichloromethane - acetone 100:1 v/v as eluent) to yield 1.13 g (48 %) of a yellow oil which becomes solid after several days (mp: 145 °C); MS (FD, 8 kV) m/z = 486.3 g/mol - calculated: 486.2 g/mol for $C_{30}H_{30}O_6$; ^{1}H-NMR (500 MHz, $C_2D_2Cl_4$, 120 °C, δ in ppm) 6.78 (s, 6 H), 6.23 (s, 6 H), 3.77 (s, 18 H); ^{13}C-NMR (125 MHz, $C_2D_2Cl_4$, 120 °C, δ in ppm) 150.9, 131.5, 129.5, 125.6, 60.4; EA found 73.97 % C, 6.24 % H - calculated: 74.06 % C, 6.21 % H

8.3.13 1,2,5,6,9,10-Hexamethoxycoronene

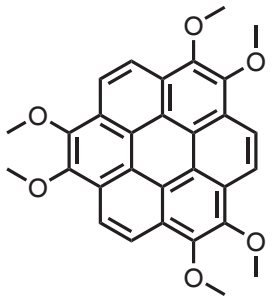

19

200 mg (0.4 mmol) Hexamethoxy[2.2.2]paracyclophane-triene and 420 mg (1.6 mmol) iodine were dissolved in 200 ml cyclohexane. The solution was purged with argon for 10 minutes, then 1 ml of propylene oxide was added. The solution was irradiated for 10 hours with UV irradiation (300 nm, 40 W). Excess iodine was removed by extraction with aqueous 2 M sodium sulfite solution. After drying and evaporation of the cyclohexane, the residue was purified by chromatography yielding 146 mg (73 %) of a yellow crystalline substance (mp: 218 °C); MS (FD, 8 kV) m/z = 479.9 g/mol - calculated: 480.2 g/mol for $C_{30}H_{24}O_6$; ^{1}H-NMR (300 MHz, CD_2Cl_2, RT, δ in ppm) 9.20 (s, 6 H), 4.43 (s, 18 H); ^{13}C-NMR (75 MHz, CD_2Cl_2, RT, δ in ppm) 146.0, 125.2, 102.9, 120.6, 62.3; EA found: 74.91 % C, 5.09 % H - calculated: 74.99 % C, 5.03 % H; UV-vis ($CHCl_3$, λ in nm) 306 (rel 0.99), 328 (1.00), 358 (0.47), 395 (0.006), 417 (0.013), 443 (0.013)

8.3.14 1,2,5,6,9,10-Coronene-hexaone

50 mg (0.12 mmol) 1,2,5,6,9,10-Hexamethoxycoronene were dissolved in 5 ml dichloromethane and added to 5 ml 1 M BBr_3 solution in dichloromethane. The suspension was stirred for two hours. The volatile substances were removed under high vacuum at room temperature. To the residue 5 ml concentrated nitric acid was added, after 1 minute, the solution was diluted with 20 ml water and centrifuged.

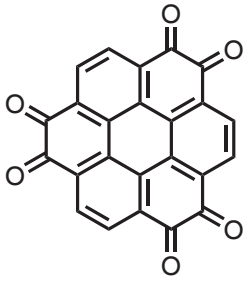

25

The solid was dissolved in 5 ml DMSO and heated for 30 min to 80°C while air was bubbled through the solution. After evaporation of DMSO, 34 mg (85 %) of a reddish solid was obtained (mp: dec.); MS (FD, 8 kV) m/z = 390.7 g/mol - calculated: 390.0 g/mol for $C_{24}H_6O_6$; ^{1}H-NMR (250 MHz, DMSO−d_6, RT, δ in ppm) 8.57 (s, 6 H); IR (neat, 1/λ in cm^{-1}) 1676, 1599, 1574, 1469, 1327, 1313, 1277, 1207, 1022, 985, 864, 588

8.3.15 1,2-Diamino-4,5-dialkylbenzenes

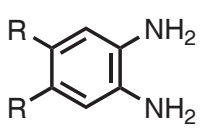

R = C_8H_{17} **43**
R = $C_{12}H_{25}$ **44**
R = $C_{16}H_{33}$ **45**

1,2-Diamino-4,5-dialkylbenzenes were prepared in analogy to the literature[4]

Octyl derivative **43**

^{1}H-NMR (250 MHz, CD_2Cl_2, RT, δ in ppm) 6.47 (s, 2H), 3.27 (br, 4H), 2.46 (t, J = 7.7 Hz, 4H), 1.52 (m, 4H), 1.32 (m, 20H), 0.92 (t, J = 6.5 Hz, 6H); ^{13}C-NMR (62.5 MHz, CD_2Cl_2, RT, δ in ppm) 133.1, 132.6, 118.0, 32.64, 32.55, 32.46, 30.4, 30.2, 30.0, 23.3, 14.5; MS (FD, 8 kV) m/z 332.1 g/mol - calculated for $C_{22}H_{40}N_2$: 332.3 g/mol

Dodecyl derivative **44**

^{1}H-NMR (250 MHz, CD_2Cl_2, RT, δ in ppm) 6.46 (s, 2H), 3.26 (br, 4H), 2.43 (t, J = 7.7 Hz, 4H), 1.49 (m, 4H), 1.27 (m, 36H), 0.89 (t, J = 6.5 Hz, 6H); ^{13}C-NMR

(62.5 MHz, CD_2Cl_2, RT, δ in ppm) 133.1, 132.6, 118.0, 32.60, 32.52, 32.42, 30.3-30.2 multiple peaks unresolved, 30.0, 23.3, 14.5; MS (FD, 8 kV) m/z = 444.5 g/mol - calculated for $C_{30}H_{56}N_2$: 444.4 g/mol

Hexadecyl derivative **45**

^{1}H-NMR (250 MHz, CD_2Cl_2, RT, δ in ppm) 6.46 (s, 2H), 3.24 (br, 4H), 2.42 (t, J = 7.8 Hz, 4H), 1.48 (quin, J = 7.3 Hz, 4H), 1.4-1.2 (m, 52H), 0.88 (t, J = 6.5 Hz, 6H); ^{13}C-NMR (62.5 MHz, CD_2Cl_2, RT, δ in ppm) 133.1, 132.5, 118.0, 32.60, 32.55, 32.44, 30.3-30.2 multiple peaks unresolved, 30.1, 23.3, 14.4; MS (FD, 8 kV) m/z = 556.4 g/mol - calculated for $C_{38}H_{72}N_2$: 556.6 g/mol

8.3.16 a,g,m-Tris(1,4-diaza-6,7-dialkylnaphtho)coronene

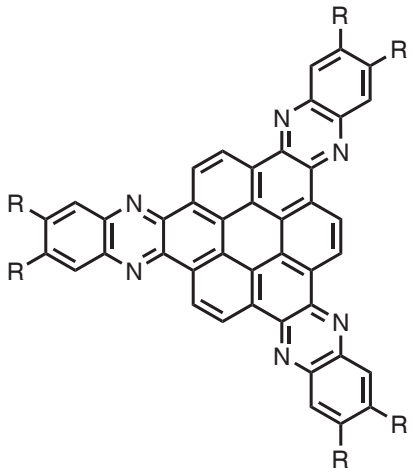

50 mg (0.13 mmol) 1,2,5,6,9,10-Coronene-hexaone and 0.57 mmol 1,2-diamino-4,5-dialkylbenzene were suspended in 5 ml o-dichlorobenzene and 5 ml acetic acid. The mixture was heated to reflux for two hours. The solution was cooled to room temperature and precipitated in methanol. After filtration the solid was dissolved in warm chlorobenzene and precipated in methanol, filtered and dried in vaccum.

Octyl derivative **46**

Yield: 83 %; Mp: 198 °C; ^{1}H-NMR (500 MHz, $C_2D_2Cl_4$, 100 °C, δ in ppm) (10 mg/ml) 9.48 (s, 6H), 7.94 (s, 6H), 2.85 (t, J = 7.6 Hz, 12H), 1.88 (quin, J = 7.4 Hz,

12H), 1.61 (quin, J = 6.7 Hz, 12H), 1.52 (quin, J = 7.0 Hz, 12H), 1.50-1.35 (m, 36H), 0.98 (t, J = 6.7 Hz, 18H); ^{13}C-NMR (125 MHz, $C_2D_2Cl_4$, 100 °C, δ in ppm) (10 mg/ml) 144.6, 141.4, 141.1, 129.7, 127.7, 124.0, 123.7, 33.3, 32.2, 30.7, 30.3, 29.9, 29.6, 23.0, 14.2; MS (MALDI, TCNQ matrix) m/z = 1280.1 g/mol - calculated for $C_{114}H_{162}N_6$: 1279.9 g/mol

Dodecyl derivative **47**

Yield: 82 %; Mp: 116 °C; ^{1}H-NMR (700 MHz, $C_2D_2Cl_4$, 100 °C, δ in ppm) (10 mg/ml) 9.38 (s, 6H), 7.88 (s, 6H), 2.82 (t, J = 6.8 Hz, 12H), 1.85 (quin, J = 7.0 Hz, 12H), 1.59 (quin, J = 6.8 Hz, 12 H), 1.51 (quin, J = 7.0 Hz, 12H), 1.45-1.30 (m, 84H), 0.90 (t, J = 6.6 Hz, 18H); ^{13}C-NMR (175 MHz, $C_2D_2Cl_4$, 100 °C, δ in ppm) (10 mg/ml) 145.0, 141.6, 141.3, 123.0, 127.9, 124.3, 123.9, 33.4, 32.1, 30.8, 30.3, 30.0 (multiple peaks), 29.9, 29.5, 22.8, 14.2; MS (MALDI, TCNQ matrix) m/z = 1616.1 g/mol - calculated for $C_{114}H_{162}N_6$: 1616.3 g/mol

Hexadecyl derivative **48**

Yield: 81 %; Mp: 85 °C; 1H-NMR ^{1}H-NMR (700 MHz, $C_2D_2Cl_4$, 100 °C, δ in ppm) (10 mg/ml) 9.27 (s, 6H), 7.74 (s, 6H), 2.68 (t, J = 6.9 Hz, 12H), 1.75 (quin, J = 7.1 Hz, 12H), 1.52 (quin, J = 6.6 Hz, 12H), 1.44 (quin, J = 6.9 Hz, 12H), 1.40-1.20 (m, 156H), 0.84 (t, J = 7.0 Hz, 18H); MS (FD, 8 kV) m/z = 1952.4 g/mol - calculated for $C_{138}H_{210}N_6$: 1952.7 g/mol

8.3.17 4-Trimethylsilyldodecylbenzene

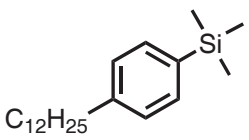

143

1.7 ml (8.6 mmol) 4-Trimethylsilybromobenzene were dissolved in 20 ml anhydrous THF under an argon atmosphere. 10 ml of a 1 M dodecylmagnesium bromide

solution in diethylether were added followed by 200 mg (0.25 mmol) Pd(dppf)Cl_2. The solution was heated to reflux for two hours. The solution was cooled to room temperature and poured into 1 M HCl, extracted with diethylether, dried and evacuated. The residue was chromatographed on silica gel with petroleum ether as eluent to yield 2.4 g (88 %) of a colorless oil. ^{1}H-NMR (250 MHz, CD_2Cl_2, RT, δ in ppm) 7.43 (d, J = 7.8 Hz, 2H), 7.17 (d, J = 7.8 Hz, 2H), 2.59 (t, J = 7.7 Hz, 2H), 1.60 (quin, J = 7.1 Hz, 2H), 1.4-1.2 (m, 18H), 0.89 (t, J = 6.5 Hz, 3H), 0.25 (s, 9H); ^{13}C-NMR (62.5 MHz, CD_2Cl_2, RT, δ in ppm) 144.3, 137.6, 133.9, 128.4, 36.5, 32.5, 32.2, 30.3-30.2 multiple peaks, 30.1, 30.02, 29.98, 23.3, 14.5, -0.8; MS (FD, 8 kV) m/z = 317.8 g/mol - calculated for $C_{21}H_{38}Si$: 318.3 g/mol

8.3.18 4,5-Bis-(4'-dodecylphenyl)-1,2-dinitrobenzene

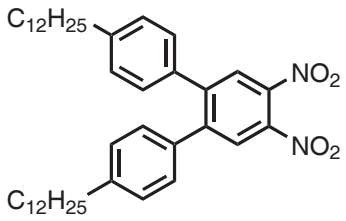

50

540 mg (1.7 mmol) 4-Trimethylsilyldodecylbenzene were dissolved in 20 ml anhydrous dichloromethane, 2.5 ml of a 1 M BBr_3 solution in dichloromethane were added and stirred for three hours. Water was added, and the organic phase was separated. The water phase was extracted with dichloromethane. The combined extracts were dried with anhydrous magnesium sulphate and evaporated. The remaining colorless solid was dissolved in 5 ml toluene. 2 ml Ethanol and 240 mg (0.57 mmol) 4,5-dinitro-1,2-diiodobenzene were added. After addition of 2 ml of a 2 M potassium carbonate solution, the solution was degassed and 33 mg (28 μmol) tetrakis(triphenylphosphine)palladium(0) were added. The mixture was heated to 100 °C over night. After cooling down, the solution was extracted with

toluene, dried and evaporated. The residue was chromatographed on silica gel with petroleum ether - dichloromethane 3:1 v/v as eluent to yield 245 mg of a yellow oil (65 % with regard to diiodobenzene). ^{1}H-NMR (250 MHz, CD_2Cl_2, RT, δ in ppm) 7.96 (s, 2H), 7.11 (d, J = 8.4 Hz, 4H), 7.06 (d, J = 8.4 Hz, 4H), 2.59 (t, J = 7.6 Hz, 4H), 1.58 (quin, J = 6.7 Hz, 4H), 1.3-1.2 (m, 36H), 0.88 (t, J = 6.5 Hz, 6H); ^{13}C-NMR (62.5 MHz, CD_2Cl_2, RT, δ in ppm) 146.8, 144.4, 141.7, 135.4, 129.8, 129.1, 127.6, 36.1, 32.5, 31.8, 30.2 (multiple peaks), 30.0, 29.9, 29.7, 23.3, 14.5; MS (FD, 8 kV) m/z = 656.8 g/mol - calculated for $C_{30}H_{56}N_2$: 656.5 g/mol

8.3.19 4,5-Bis-(4'-dodecylphenyl)-1,2-diaminobenzene

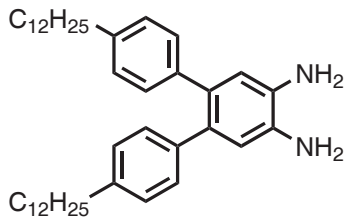

51

In a flask 1 g (1.5 mmol) 4,5-bis-(4-dodecylphenyl)-1,2-dinitrobenzene were combined with 10 ml methanol and 300 mg palladium on charcoal (10 %). The solution was degassed and put into a water cooling bath. 5 ml (30 mmol) Triethylsilane were added slowly such that the gas evolution remains moderate. After complete addition, the solution was stirred for 10 min, filtered through celite and evaporated. The residue was chromatographed on silica gel with hexane - ethyl acetate (1:1 v/v) as eluent to afford 730 mg (82 %) of an orange waxy solid; ^{1}H-NMR (250 MHz, CD_2Cl_2, RT, δ in ppm) 6.99 (s, 8H), 6.73 (s, 2H), 3.50 (br, 4H), 2.55 (t, J = 7.7 Hz, 4H), 1.58 (quin, J = 6.8 Hz, 4H), 1.4-1.2 (m, 36H), 0.89 (t, J = 6.5 Hz); ^{13}C-NMR (62.5 MHz, CD_2Cl_2, RT, δ in ppm) 141.0, 139.8, 134.8, 130.2, 128.2, 119.1, 36.0, 32.5, 32.1, 30.3 (multiple peaks), 30.1, 30.0, 29.9, 23.3, 14.5; MS (FD, 8 kV) m/z = 596.1 g/mol - calculated for $C_{30}H_{56}N_2$: 596.5 g/mol

8.3.20 a,g,m-Tris(1,4-diaza-6,7-(4'-didodecylphenyl)-naphtho)coronene

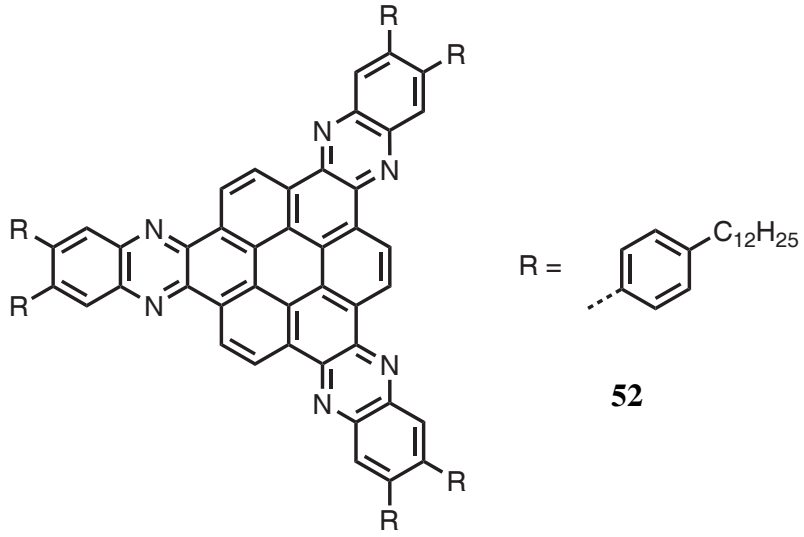

52

50 mg (0.13 mmol) 1,2,5,6,9,10-Coronene-hexaone and 345 mg (0.58 mmol) 4,5-bis-(4'-dodecylphenyl)-1,2-diaminobenzene were suspended in 5 ml o-dichlorobenzene and 5 ml acetic acid. The mixture was heated to reflux for two hours. The solution was cooled to room temperature and precipitated in methanol. After filtration the solid was dissolved in warm chlorobenzene and precipated in methanol, filtered and dried in vaccum. 210 mg of an orange sticky solid were obtained (85 %). Mp: ¿ 350 °C (dec.); ^{1}H-NMR (500 MHz, $C_2D_2Cl_4$, 100 °C, δ in ppm) (10 mg/ml) 8.97 (s, 6H), 8.04 (s, 6H), 7.17 (d, J = 7.3 Hz, 12H), 7.07 (d, J = 7.5 Hz, 12H), 2.67 (t, J = 7.2 Hz, 12H), 1.72 (quin, J = 6.5 Hz, 12H), 1.45-1.30 (m, 108H), 0.92 (t, J = 7.2 Hz, 18H); ^{13}C-NMR (125 MHz, $C_2D_2Cl_4$, 100 °C, δ in ppm) (10 mg/ml) 143.8, 141.9, 141.8, 138.2, 130.4, 129.5, 128.1, 123.8, 123.7, 36.0, 32.1, 31.5, 30.0 (multiple peaks), 29.9, 29.8, 29.7, 29.5, 22.8, 14.2; MS (MALDI, TCNQ matrix) m/z = 2072.8 g/mol - calculated for $C_{150}H_{186}N_6$: 2072.5 g/mol

8.4 Donor-Acceptor Model Systems for Polythiophenes

8.4.1 5,5'-Dibromobenzo[2,1-b;3,4-b']dithiophene-4,5-ethyleneoxolane

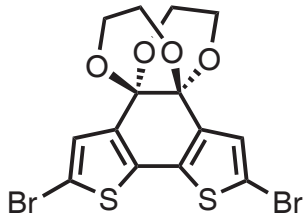

64

154 mg (0.5 mmol) Benzo[2,1-b;3,4-b']dithiophene-4,5-ethyleneoxolane[5] were dissolved in 5 ml DMF. 178 mg (1 mmol) N-bromosuccinimid were added. The mixture was stirred at room temperature for two hours, diluted with diethylether, extracted three times with water, and dried. After evaporation of the solvent, the residue was chromatographed on silica gel with dichloromethane as eluent. The obtained solid was recystallized from ethyl acetate to afford 130 mg (56 %) of slightly yellow needles. Mp = 130 °C; MS (FD, 8 kV) m/z = 465.9 g/mol - calculated: 465.8 g/mol for $C_{14}H_{10}Br_2O_4S_2$; ^{1}H-NMR (250 MHz, CD_2Cl_2, RT, δ in ppm) 7.14 (s, 2H), 4.1 (m, 4H), 3.6 (m, 4H); ^{13}C-NMR (62.5 MHz, CD_2Cl_2, RT, δ in ppm) 137.1, 133.9, 129.0, 111.8, 93.4, 67.2, 62.1; elemental analysis: found 35.76 % C, 1.83 % H, 13.45 % S - calculated: 36.07 % C, 2.16 % H, 13.76 % S

8.4.2 5,5'-(5-hexylthiophene-2-yl-)benzo[2,1-b;3,4-b']dithiophene-4,5-ethyleneoxolane

92 mg (0.2 mmol) 5,5'-Dibromobenzo[2,1-b;3,4-b']dithiophene-4,5-ehyleneoxolane and 228 mg (0.5 mmol) 5-hexyl-2-tributylstannylsthiophene were dissolved in 5 ml anhydrous DMF and degassed. 10 mg (1 μmol) Tetrakis(triphenylphsophine)-palladium was added. The resulting mixture was stirred for two hours under an argon atmosphere. After cooling, the solvent was

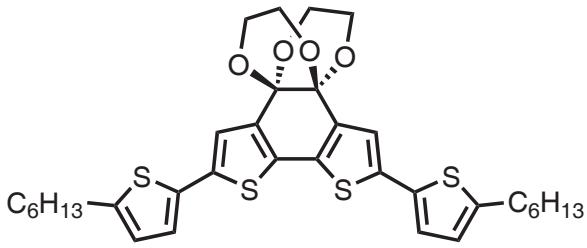

65

evaporated in high vacuum. The residue was chromatographed on silica gel with dichloromethane as eluent. 110 mg of a yellow substance were obtained (86 %). Mp = 148 °C; MS (FD, 8 kV) m/z = 640.5 g/mol - calculated: 640.2 g/mol for $C_{34}H_{40}O_4S_4$; ^{1}H-NMR (300 MHz, CD_2Cl_2, RT, δ in ppm) 7.16 (s, 2H), 7.02 (d, J = 3.6 Hz, 2H), 6.72 (d, J = 3.6 Hz, 2H), 4.2 (m, 4H), 3.7 (m, 4H), 2.81 (t, J = 7.5 Hz, 4H), 1.69 (quin, J = 7.1 Hz, 4H), 1.4-1.3 (m, 12H), 0.93 (t, J = 6.5 Hz); ^{13}C-NMR (75 MHz, CD_2Cl_2, RT, δ in ppm) 146.9, 137.4, 137.0, 134.6, 131.2, 125.6, 124.3, 121.7, 93.9, 62.2, 32.2, 32.1, 30.7, 29.3, 23.2, 14.4; elemental analysis: found 63.40 % C, 6.03 % H, 19.64 % S - calculated: 63.71 % C, 6.29 % H, 20.01 % S

8.4.3 5,5'-Di(5-hexylthiophene-2-yl-)benzo[2,1-b;3,4-b']dithiophene-4,5-diketone

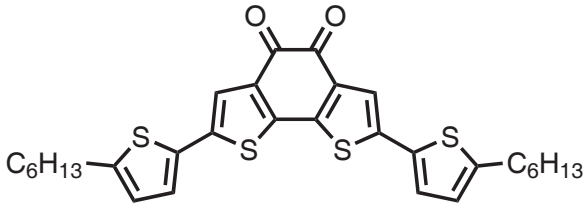

66

64 mg (0.1 mmol) 5,5'-(5-Hexylthiophene-2-yl-)benzo[2,1-b;3,4-b']dithiophene-4,5-ehyleneoxolane were dissolved in 5 ml dichloromethane/THF (2:1) and degassed. 2 ml tetrafluoroboronic acid (50 % in water) were added. The

mixture was intensively stirred for two days, extracted with dichloromethane and chromatographed on silica gel with dichloromethane as eluent. 45 mg of a blue solid were obtained (82 %). Mp = 150 °C; MS (FD, 8 kV) m/z = 552.2 g/mol - calculated: 552.1 g/mol for $C_{30}H_{32}O_2S_4$; ^{1}H-NMR (250 MHz, CD_2Cl_2, RT, δ in ppm) 7.30 (s, 2H), 7.03 (d, J = 3.6 Hz, 2H), 6.71 (d, J = 3.6 Hz, 2H), 2.79 (t, J = 7.5 Hz, 4H), 1.67 (quin, J = 7.0 Hz, 4H), 1.4-1.2 (m, 12H), 0.90 (t, J = 6.6 Hz); ^{13}C-NMR (62.5 MHz, CD_2Cl_2, RT, δ in ppm) 174.6, 148.6, 141.5, 139.0, 136.2, 132.8, 125.8, 125.7, 122.1, 32.1, 32.0, 30.7, 29.3, 23.2, 14.4; elemental analysis: found 64.90 % C, 5.76 % H, 23.22 % S - calculated: 65.18 % C, 5.83 % H, 23.20 % S

8.4.4 5,5'-Dithien-2-ylbenzo[2,1-b;3,4-b']dithiophene-4,5-ethyleneoxolane

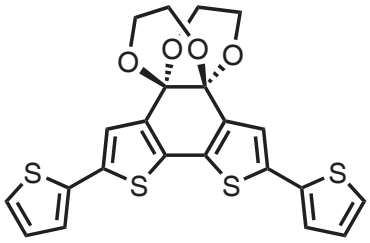

69

47 mg (0.1 mmol) 5,5'-Dibromobenzo[2,1-b;3,4-b']dithiophene-4,5-ehyleneoxolane were dissolved in 2 ml anhydrous DMF under argon. 93 mg (0.25 mmol) 2-Tributylstannylthiophene were added, followed by 5 mg (5 µmol) $Pd(PPh_3)_4$. The mixture was heated for two hours to 100 °C, diluted with diethylether, extracted with water three times, and dried. The solvents were evaporated, the residue was purified by preparative chromatography on silica gel with a gradient of petroleum ether - dichloromethane (9:11 v/v) to pure dichloromethane. After crystallization from ethyl acetate at -20 °C, 28 mg of a yellow crystalline substance were obtained (59 %). Mp = 262 °C, MS (FD, 8 kV) m/z = 471.8 g/mol - calculated: 472.0 g/mol for $C_{22}H_{16}O_4S_4$; ^{1}H-NMR

(250 MHz, CD_2Cl_2, RT, δ in ppm) 7.28 (dd, J_1 = 5.1 Hz, J_2 = 1.1 Hz, 2H), 7.26 (s, 2H), 7.23 (dd, J_1 = 3.6 Hz, J_2 = 1.1 Hz, 2H), 7.05 (dd, J_1 = 5.1 Hz, J_2 = 3.6 Hz, 2H), 4.15 (m, 4H), 3.70 (m, 4H); ^{13}C-NMR (62.5 MHz, CD_2Cl_2, RT, δ in ppm) 137.7, 137.2, 136.6, 131.7, 128.6, 125.6, 124.6, 122.5, 93.8, 62.2

8.4.5 5,5'-Dithiophene-2-yl-benzo[2,1-b;3,4-b']dithiophene-4,5-diketone

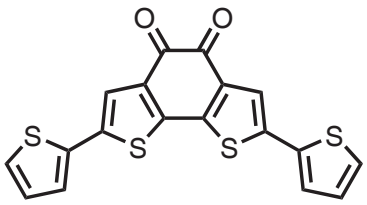

70

150 mg (0.32 mmol) 5,5'-Thiophene-2-yl-benzo[2,1-b;3,4-b']dithiophene-4,5-ehyleneoxolane were dissolved in a mixture of 5 ml dichloromethane and 2.5 ml THF. After degassing, 3 ml tetrafluoroboronic acid (50 % in water) were added. The mixture was intensively stirred overnight, extracted with dichloromethane and chromatographed on silica gel with dichloromethane as eluent. 100 mg of a blue solid were obtained (81 %). Mp = 292 °C; MS (FD, 8 kV) m/z = 383.7 g/mol - calculated: 383.9 g/mol for $C_{18}H_8O_2S_4$; ^{1}H-NMR (300 MHz, THF$-d_8$, RT, δ in ppm) 7.57 (s, 2H), 7.47 (dd, J_1 = 5.1 Hz, J_2 = 1.1 Hz, 2H), 7.40 (dd, J_1 = 3.6 Hz, J_2 = 1.1 Hz, 2H), 7.09 (dd, J_1 = 5.1 Hz, J_2 = 3.6 Hz, 2H); ^{13}C-NMR (175 MHz, THF$-d_8$, RT, δ in ppm) 172.3, 138.9, 136.5, 136.1, 134.3, 127.2, 125.5, 124.5, 121.5

8.5 Benzo[2,1-b;3,4-b']dithiophene Containing Polymers

8.5.1 3-Heptanoylthiophene

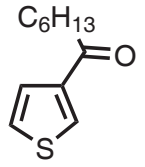

72

7.8 ml (89 mmol) Thiophene-3-carbaldehyde were dissolved in 45 ml anhydrous THF under argon, cooled in an ice bath to 0 °C. Then, 45 ml (90 mmol) of a 2 M solution of hexylmagnesium bromide in diethylether was added slowly. After complete addition, the solution was warmed to room temperature and stirred for two hours. The solution was diluted with 100 ml diethylether, extracted with ammonium chloride solution, dried, and evaporated. The residue is dissolved in 200 ml methylene chloride, and cooled to 0 °C in an ice bath. 20 g of celite and 21.5 g (100 mmol) pydridinium chlorochromate were added in small portions after which the suspension was stirred for one hour at room temperature. The suspension was filtered over celite, the solvent was evaporated, and the residue was purified by column chromatography with petroleum ether as eluent. 11.7 g of a light yellow oil were obtained (67 %). ^{1}H-NMR (250 MHz, CD_2Cl_2, RT, δ in ppm) 8.05 (dd, J_1 = 2.9 Hz, J_2 = 1.2 Hz, 1H), 7.53 (dd, J_1 = 5.1 Hz, J_2 = 1.6 Hz, 2H), 7.34 (dd, J_1 = 5.1 Hz, J_2 = 2.9 Hz, 1H), 2.87 (t, J = 7.4 Hz, 2H), 1.70 (quin, J = 7.2 Hz, 2H), 1.34 (m, 6H), 0.90 (t, J = 6.5 Hz, 3H); ^{13}C-NMR (62.5 MHz, CD_2Cl_2, RT, δ in ppm) 195.1, 143.1, 132.1, 127.4, 126.8, 40.4, 32.3, 29.6, 24.8, 23.1, 14.4

8.5.2 2-(Thiophen-3-yl)-2-hexyl-1,3-dioxolan

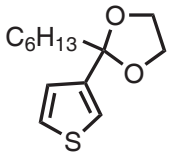

73

10 g (51 mmol) 3-Heptanoylthiophene were dissolved in 100 ml benzene. 10 ml (180 mmol) Ethylene glycol and 20 mg (0.12 mmol) toluenesulfonic acid were added. The mixture was heated with a dean stark trap for 24 hours after which the solution was extracted with sodium carbonate solution, dried and evaporated. 12.2 g of a slightly yellow oil was obtained (99 %). ^{1}H-NMR (250 MHz, CD_2Cl_2, RT, δ in ppm) 7.37 (s, 1H), 7.27 (d, J = 4.4 Hz, 1H), 7.03 (dd, J_1 = 4.5 Hz, J_2 = 1.7 Hz, 1H), 3.98 (m, 2H), 3.82 (m, 2H), 1.91 (t, J = 7.8 Hz, 2H), 1.26 (m, 8H), 0.88 (t, J = 6.9 Hz, 3H); ^{13}C-NMR (62.5 MHz, CD_2Cl_2, RT, δ in ppm) 145.5, 128.9, 126.7, 126.1, 122.3, 109.8, 65.3, 40.6, 32.4, 30.0, 24.2, 23.2, 14.4

8.5.3 3,3'-Diheptanoyl-2,2'-dithiophene

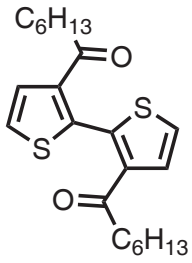

74

100 ml Anhydrous THF was cooled to 0 °C under argon. 3 ml (21 mmol) anhydrous diisopropylamine and subsequently 13 ml (21 mmol) *n*-butyllithium (1.6 M in hexanes) were added. The mixture was stirred for 30 minutes, then 5 g (21 mmol) of 2-(thiophene-3-yl)-2-hexyl-1,3-dioxolan were added and stirred for one hour. The mixture was cooled to -78 °C and 10.6 g (3 mmol) iron(III)-acetylacetonate were

added in small portions. The resulting suspension was warmed to room temperature over night. The reaction mixture was poured into 50 ml 6 M HCl, extracted with dichloromethane and dried. After evaporation of the solvent, the residue was purified by column chromatography on silica gel with petroleum ether as eluent to yield 2.6 g of a colorless oil (63 %). MS (FD, 8 kV) m/z = 390.8 g/mol - calculated: 390.2 g/mol for $C_{22}H_{30}O_2S_2$; ^{1}H-NMR (250 MHz, CD_2Cl_2, RT, δ in ppm) 7.47 (d, J = 5.4 Hz, 2H), 7.41 (d, J = 5.4 Hz, 2H) 2.60 (t, J = 7.3 Hz, 4H), 1.54 (m, 4H), 1.21 (m, 12H), 0.85 (t, J = 6.7 Hz, 6H); ^{13}C-NMR (62.5 MHz, CD_2Cl_2, RT, δ in ppm) 196.0, 140.6, 138.8, 128.9, 126.7, 41.7, 32.3, 29.9, 24.3, 23.1, 14.3

8.5.4 5,6-Dihexylbenzo[2,1-b;3,4-b']dithiophene

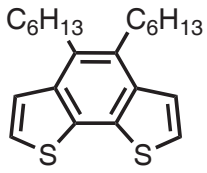

75

5 ml Titanium(IV)-chloride (50 mmol) were slowly dropped into 250 ml ice-cooled anhydrous THF. 6.5 g (100 mmol) zinc powder and 2.5 ml pyridine were added. The solution was heated to reflux for one hour. 3.5 g (9.0 mmol) 3,3'-diheptanoyl-2,2'-dithiophene were dissolved in 500 ml anhydrous THF and added to the boiling titanium solution dropwise over 2 hours. The solution was refluxed for another two hours, cooled to room temperature. After addition of 100 ml 1 M HCl the solution was decanted and most of the THF was evaporated. The residue was extracted with dichloromethane, dried and evaporated. The product was purified by column chromatography on silica gel with petroleum ether as eluent. 1.2 g of a colorless oil were obtained (37 %). MS (FD, 8 kV) m/z = 358.9 g/mol - calculated: 390.2 g/mol for $C_{22}H_{30}O_2S_2$; ^{1}H-NMR (250 MHz, CD_2Cl_2, RT, δ in ppm) 7.50 (d, J = 5.4 Hz, 2H), 7.40 (d, J = 5.4 Hz, 2H) 3.03 (t, J = 8.0 Hz, 4H), 1.65 (m, 4H), 1.51

(m, 4H), 1.38 (m, 8H), 0.93 (t, J = 6.9 Hz, 6H); ^{13}C-NMR (62.5 MHz, CD_2Cl_2, RT, δ in ppm) 138.2, 132.4, 131.7, 124.3, 124.0, 32.4, 32.1, 31.0, 30.7, 23.3, 14.5

8.5.5 5,6-Didodecylbenzo[2,1-b;3,4-b']dithiophene

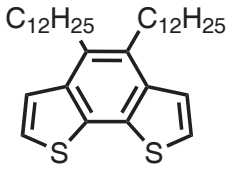

75

5,6-Didodecylbenzo[2,1-b;3,4-b']dithiophene was prepared like 5,6-dihexylbenzo[2,1-b;3,4-b']dithiophene.

MS (FD, 8 kV) m/z = 527.1 g/mol - calculated: 526.4 g/mol for $C_{34}H_{54}O_2S_2$; ^{1}H-NMR (250 MHz, CD_2Cl_2, RT, δ in ppm) 7.50 (d, J = 5.4 Hz, 2H), 7.40 (d, J = 5.4 Hz, 2H) 3.03 (t, J = 7.9 Hz, 4H), 1.66 (m, 4H), 1.51 (m, 4H), 1.30 (m, 32H), 0.90 (t, J = 6.8 Hz, 6H); ^{13}C-NMR (62.5 MHz, CD_2Cl_2, RT, δ in ppm) 138.2, 132.4, 131.7, 124.3, 124.0, 32.5, 32.1, 31.0, 30.7, 30.3 (four signals, not resolved), 30.1, 30.0, 23.3, 14.5

8.5.6 Poly(5,6-didodecylbenzo[2,1-b;3,4-b']dithiophene)

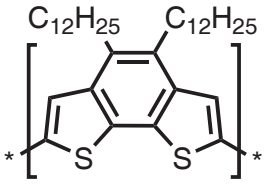

76

100 mg of (5,6-Didodecylbenzo)-2,2'-dithiophene were dissolved in 1 ml anhydrous o-dichlorobenzene and added to a suspension of 123 mg (0.76 mmol) iron(III)-chloride in dry o-dichlorobenzene under argon. The resulting mixture was stirred at 60 °C for one day. After this period 2 ml o-dichlorobenzene were added.

The solution was precipitated into methanol. After filtration, the polymer was dissolved in o-dichlorobenzene, 1 ml 65 % hydrazine in water was added, and stirred over night at room temperature. The mixture was poured into methanol, filtered and reprecipitated in methanol. 85 mg of a orange-red solid were obtained (85 %) GPC (1,2,4-trichlorobenzene, 135 °C) analysis gives M_n = 18 kg/mol and M_w = 124 kg/mol against polystyrene standard. ^{1}H-NMR (500 MHz, $C_6D_4Cl_2$, 80 °C, δ in ppm) 7.88 (s, 2H), 3.24 (br, 4H), 1.94 (br, 4H), 1.73 (br, 4H), 1.58 (br, 4H), 1.5-1.3 (br, 28H), 0.99 (br, 6H)

8.5.7 5,5'-Dibromo-(5,6-dihexylbenzo[2,1-b;3,4-b']dithiophene)

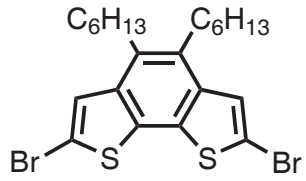

77

770 mg (2.2 mmol) (5,6-Dihexylbenzo)-2,2'-dithiophene were dissolved in a mixture of 5 ml chloroform and 5 ml acetic acid. 806 mg (4.5 mmol) N-bromosuccinic imide were added at room temperature. The resulting mixture was stirred for two hours. The solution is poured onto a 2 M sodium carbonate solution and extracted with chloroform. The organic phase was dried with anhydrous magnesium sulphate, the solvent was removed in vacuum and the residue was chromatographed on silica gel with petroleum ether as eluent. 790 mg of a colorless solid were obtained (71 %). Mp: 77 °C; MS (FD, 8 kV) m/z = 515.3 g/mol - calculated: 516.0 g/mol for $C_{22}H_{28}S_2Br_2$; ^{1}H-NMR (250 MHz, CD_2Cl_2, RT, δ in ppm) 7.45 (s, 2H), 2.90 (t, J = 8.0 Hz, 4H), 1.57 (m, 4H), 1.50 (m, 4H), 1.34 (m, 8H), 0.92 (t, J = 6.9 Hz, 6H); ^{13}C-NMR (62.5 MHz, CD_2Cl_2, RT, δ in ppm) 138.0, 132.4, 131.8, 127.1, 112.9, 32.3, 32.0, 30.9, 30.3, 23.3, 14.4; elemental analysis: found 50.76 % C, 5.28 % H, 12.37 % S - calculated: 51.17 % C, 5.47 % H, 12.42 % S

8.5.8 5,5'-Di(3-dodecyl-thiophene-2-yl)-(5,6-dihexylbenzo[2,1-b;3,4-b']dithiophene)

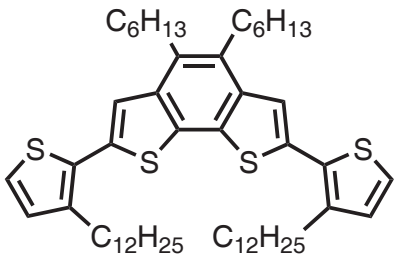

78

50 mg (0.1 mmol) 5,5'-Dibromo-(5,6-dihexylbenzo)-2,2'-dithiophene and 216 mg (0.4 mmol) 3-dodecyl-2-tributylstannylthiophene were dissolved in 5 ml anhydrous DMF by the aid of gentle heating. The solution was degassed, and 6 mg (5 μmol) tetrakis(triphenylphosphine)palladium(0) were added. The solution was heated to 100 °C for one hour. After being cooled to room temperature, 50 ml diethylether were added. The solution was extracted four times with water, dried and evaporated. The residue was purified by column chromatography on silica gel with hexane as eluent. 60 mg of a slightly yellow oil were obtained (70 %). MS (FD, 8 kV) m/z = 859.7 g/mol - calculated: 858.5 g/mol for $C_{54}H_{82}S_4$; ^{1}H-NMR (250 MHz, CD_2Cl_2, RT, δ in ppm) 7.46 (s, 2H), 7.27 (d, J = 5.2 Hz, 2H), 7.01 (d, J = 5.2 Hz, 2H), 3.03 (t, J = 7.9 Hz, 4H), 2.87 (t, J = 7.7 Hz, 4H), 1.7 - 1.2 (m, 56H), 0.93 (t, J = 6.7 Hz, 6H), 0.88 (t, J = 6.8 Hz, 6H); ^{13}C-NMR (62.5 MHz, CD_2Cl_2, RT, δ in ppm) 141.4, 138.5, 134.5, 132.7, 131.2 (two peaks), 130.9, 125.2, 122.6, 32.6, 32.4, 32.1, 31.4, 31.0, 30.5, 30.3 (multiple peaks), 30.2, 30.1, 30.0, 29.9, 23.3, 14.5

8.5.9 Poly(5,5'-Di(3-dodecyl-thiophene-2-yl)-(5,6-dihexylbenzo[2,1-b;3,4-b']dithiophene)

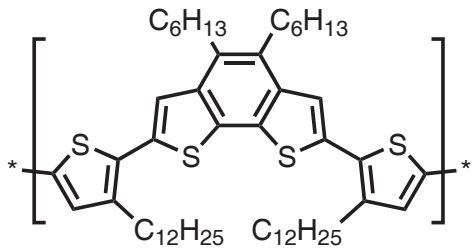

79

100 mg (0.12 mmol) 5,5'-Di(3-dodecyl-thiophene-2-yl)-(5,6-dihexylbenzo)-2,2'-dithiophene were dissolved in 1.5 ml anhydrous o-dichlorobenzene and added to a suspension of 75 mg (0.46 mmol) iron(III)-chloride in anhydrous o-dichlorobenzene under argon. The solution was stirred for 24 hours at 60 °C. After that period, 5 ml o-dichlorobenzene were added. The polymer was precipitated in methanol, filtered, redissolved in o-dichlorobenzene and added to methanol. Upon addition of a few droplets of hydrazine hydrate, a red precipitate was formed which was filtered off, dissolved in o-dichlorobenzene and stirred vigorously over night in the presence of hydrazine (65 % in water). The polymer was precipitated in methanol and reprecipitated from o-dichlorobenzene/methanol to yield 80 mg of a red solid (80 %). GPC (1,2,4-trichlorobenzene, 135 °C) analysis gives M_n = 22 kg/mol and M_w = 104 kg/mol against polystyrene standard. ^{1}H-NMR (250 MHz, $C_2D_2Cl_4$, RT, δ in ppm) (10 mg/ml) 7.38 (s, 2H), 7.03 (s, 2H), 2.93 (br, 4H), 2.78 (br, 4H), 1.7-1.0 (m, 56H), 0.87 (br, 6H), 0.79 (br, 6H)

8.5.10 5,5'-Dibromo-(5,6-dihexadecylbenzo[2,1-b;3,4-b']dithiophene)

5,5'-Dibromo-(5,6-dihexadecylbenzo[2,1-b;3,4-b']dithiophene) was prepared in analogy to 5,5'-dibromo-(5,6-dihexylbenzo)-2,2'-dithiophene.

Mp: 79 °C; MS (FD, 8 kV) m/z = 797.7 g/mol - calculated: 796.3 g/mol for

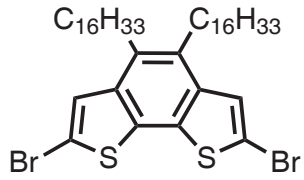

77

$C_{42}H_{68}Br_2S_2$; ^{1}H-NMR (250 MHz, CD_2Cl_2, RT, δ in ppm) 7.45 (s, 2H), 2.91 (t, J = 8.0 Hz, 4H), 1.59 (m, 4H), 1.51 (m, 4H), 1.34 (m, 48H), 0.89 (t, J = 6.5 Hz, 6H); ^{13}C-NMR (62.5 MHz, CD_2Cl_2, RT, δ in ppm) 138.0, 132.4, 131.8, 127.2, 113.0, 32.5, 32.0, 30.9, 30.6, 30.2 (multiple peaks) 30.1, 29.9, 23.3, 14.5; elemental analysis: found 62.78 % C, 8.04 % H, 7.93 % S - calculated: 63.30 % C, 8.60 % H, 8.05 % S

8.5.11 5,5'-Bis(trimethylstannyl)-2,2'-dithiophene

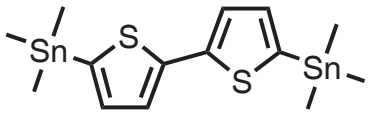

80

1 g (6 mmol) 2,2'-Dithiophene were dissolved in 50 ml anhydrous THF and cooled to -0 °C. 10 ml (16 mmol) *n*-butyllithium (1.6 M in hexanes) were slowly added which causes a white precipitate. After two hours at 0 °C the mixture was cooled to -78 °C and 4 g (20 mmol) solid trimethyltin chloride were added. The solution was warmed to room temperature, and stirred for two hours. Most of the THF was evaporated, the rest dissolved in diethylether, extracted with aqueous sodium bicarbonate, washed with water, dried and evaporated. The residue was crystallized three times from acetonitrile at 4 °C to obtain 1.56 g (53 %) of colorless platelets. Mp = 98-99 °C; MS (FD, 8 kV) m/z = 491.3 g/mol - calculated: 490.9 g/mol for $C_{14}H_{22}S_2Sn_2$; ^{1}H-NMR (250 MHz, CD_2Cl_2, RT, δ in ppm) 7.30 (d, 2H, J = 3.4 Hz), 7.12 (d, 2H, J = 3.4 Hz), 0.41 (s, 18H); ^{13}C-NMR (62.5 MHz, CD_2Cl_2, RT, δ in

ppm) 143.4, 137.9, 136.5, 125.3, 8.0; elemental analysis: found 34.16 % C, 4.37 % H, 13.04 % S - calculated: 34.19 % C, 4.51 % H, 13.04 % S

8.5.12 Poly(5,5'-dithieno-2-yl-(5,6-dihexylbenzo[2,1-b;3,4-b']dithiophene))

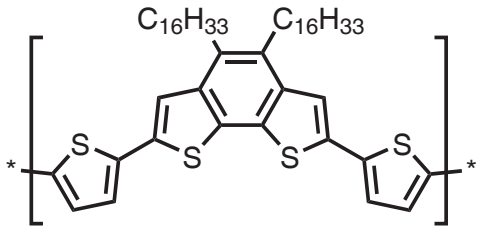

81

79.70 mg (0.1 mmol) 5,5'-Dibromo-(5,6-dihexadecylbenzo)-2,2'-dithiophene and 49.18 mg (0.1 mmol) 5,5'-bis(trimethylstannyl)-2,2'-dithiophene were dissolved in 2 ml anhydrous 1,2-dichlorobenzene under argon. 2.4 mg (8 μmol) tri-*o*-tolylphosphine and 1.8 mg (2 mmol) $Pd_2(dba)_3$ were added. The resulting mixture was heated to 140 °C for three days. The solution was diluted with 1,2-dichlorobenzene and precipitated in methanol. After filtration the polymer was reprecipitated twice in methanol and dried. 74 mg of a red solid was obtained (92 %). GPC (1,2,4-trichlorobenzene, 135 °C) analysis gives M_n = 21 kg/mol and M_w = 49 kg/mol against polystyrene standard. ^{1}H-NMR (500 MHz, CD_4Cl_2, 140 °C, δ in ppm) 7.68 (br, 2H), 7.16 (br, 2H), 7.11 (br, 2H), 3.20 (br, 4H), 1.91 (br, 4H), 1.70 (br, 4H), 1.58 (br, 4H), 1.5-1.3 (m, 44H), 0.93 (br, 6H)

8.5.13 5,5'-Dibromo-4,4'-didodecyl-2,2'-dithiophene

5,5'-Dibromo-4,4'-didodecyl-2,2'-dithiophene was prepared in analogy to the literature.[6]

Mp = 57 °C; MS (FD, 8 kV) m/z = 660.5 g/mol - calculated: 660.2 g/mol for $C_{32}H_{52}Br_2S_2$; ^{1}H-NMR (250 MHz, CD_2Cl_2, RT, δ in ppm) 6.82 (s, 2H), 2.53 (t, J =

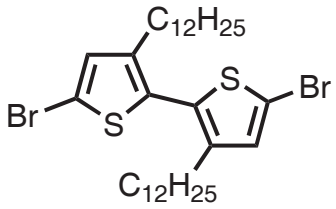

87

7.5 Hz, 4H), 1.58 (quin, J = 7.1 Hz, 4H), 1.4-1.2 (m, 36H), 0.88 (t, J = 6.5 Hz, 6H); ^{13}C-NMR (62.5 MHz, CD_2Cl_2, RT, δ in ppm) 143.8, 136.7, 125.1, 108.3, 32.2, 30.3-30.2 (multiple peaks), 30.1, 30.0, 29.8, 23.3, 14.5; elemental analysis: found 57.86 % C, 8.03 % H, 9.58 % S - calculated: 58.17 % C, 7.93 % H, 9.71 % S

8.5.14 5,5'-Bis(trimethylstannyl)-benzo[2,1-b;3,4-b']dithiophene

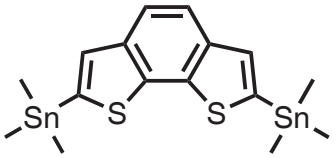

83

250 mg (1.3 mmol) Benzo[2,1-b;3,4-b']dithiophene[7] were dissolved in 10 ml anhydrous THF under argon. The solution was cooled to -78 °C, then 2.3 ml *n*-butyllithium (3.9 mmol, 3 eq) were added upon which a white precipitated was formed. The suspension was stirred for another 2 hours at -78 °C, 900 mg (4.5 mmol) trimethyltin chloride were added as solid. The solution was slowly warmed to room temperature over night. 30 ml Methylene chloride were added to the solution, extracted with sodium bicarbonate, dried and the solvent was evaporated. The residue was crystallized three times from acetonitrile at 4 °C to yield colorless needles (300 mg, 44 %). Mp = 87 °C; MS (FD, 8 kV) m/z = 516.1 g/mol - calculated: 515.9 g/mol for $C_{16}H_{22}S_2Sn_2$ hnmr250CD2Cl2RT 7.74 (s, 2H), 7.53 (s, 2H), 0.45 (s, 18H); ^{13}C-NMR (62.5 MHz, CD_2Cl_2, RT, δ in ppm) 138.9, 138.8,

138.3, 133.3, 120.1, -8.0; elemental analysis: found 37.08 % C, 4.31 % H, 12.32 % S - calculated: 37.25 % C, 4.30 % H, 12.43 % S

8.5.15 Poly(5,5'-bis(3-dodecylthiophene-2-yl)-benzo[2,1-b;3,4-b']dithiophene)

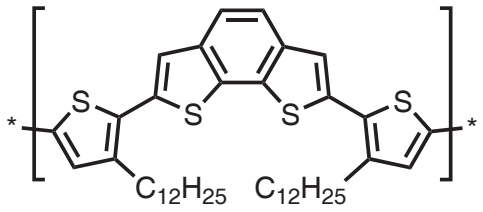

88

103.17 mg (0.2 mmol) 5,5'-Bis(trimethylstannyl)benzo-2,2'-dithiophene and 132.14 mg (0.2 mmol) 4,4'-didodecyl-5,5'-dibromo-2,2'-dithiophene were dissolved in 2 ml anhydrous 1,2-dichlorobenzene under argon. 5 mg (16 μmol) Tri-*o*-tolylphosphine and 4 mg (4 μmol) $Pd_2(dba)_3$ were added. The resulting mixture was heated to 140 °C for three days. The solution was diluted with 1,2-dichlorobenzene and precipitated in methanol. After filtration the polymer was reprecipitated twice in methanol and dried. 120 mg of a red solid was obtained (87 %). GPC (1,2,4-trichlorobenzene, 135 °C) analysis gives M_n = 21 kg/mol and M_w = 54 kg/mol against polystyrene standard. ^{1}H-NMR (500 MHz, $C_6D_3Cl_3$, 80 °C, δ in ppm) 7.79 (s, 2H), 7.59 (s, 2H), 7.29 (s, 2H), 3.09 (t, J = 6.8 Hz, 4H), 1.96 (quin, J = 6.7 Hz, 4H), 1.65 (quin, J = 6.9 Hz, 4H), 1.54 (quin, J = 6.7 Hz, 4H), 1.5-1.3 (m, 28H), 1.01 (t, J = 6.8 Hz, 6H)

8.5.16 5,5'-Bis(trimethylstannyl)benzo[1,2-b:4,5-b']dithiophene

500 mg (2.6 mmol) Benzo[1,2-b:4,5-b']dithiophene[8] were dissolved in 20 ml anhydrous THF under argon. The mixture was cooled to -78 °C, 4.1 ml (6.6 mmol) of *n*-butyllithium (1.6 M in pentane) were added whereupon a white precipitate

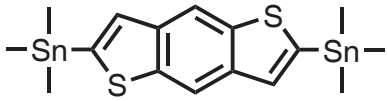

97

was formed. After 2 hours at -78 °C 1.55 g (7.8 mmol) trimethyltin chloride were added as solid. The solution was left in the cold bath to warm up over night. 50 ml diethylether were added to the solution which was then extracted with sodium bicarbonate solution and water, the solvent was evaporated, and the residue was crystallized from acetonitrile three times to yield 790 mg (59 %) of colorless platelets. Mp = 166 °C; MS (FD, 8 kV) m/z = 515.1 g/mol - calculated: 515.9 g/mol for $C_{16}H_{22}S_2Sn_2$; ^{1}H-NMR (250 MHz, CD_2Cl_2, RT, δ in ppm) 8.30 (s, 2H), 7.46 (s, 2H), 0.46 (s, 18H); ^{13}C-NMR (62.5 MHz, CD_2Cl_2, RT, δ in ppm) 142.7, 141.9, 139.2, 131.5, 115.5, -8.1; elemental analysis: found 37.21 % C, 3.89 % H, 12.48 % S - calculated: 37.25 % C, 4.30 % H, 12.43 % S

8.5.17 Poly(5,5'-di(3-dodecyl-thiophene-2-yl)benzo[1,2-b:4,5-b']dithiophene)

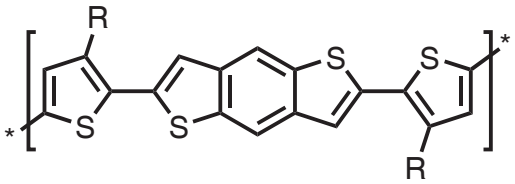

98

103.17 mg (0.2 mmol) 5,5'-Bis(trimethylstannyl)benzo[1,2-b:4,5-b']dithiophene and 132.14 mg (0.2 mmol) 4,4'-didodecyl-5,5'-dibromo-2,2'-dithiophene were dissolved in 2 ml anhydrous 1,2-dichlorobenzene under argon. 5 mg (16 μmol) Tri-*o*-tolylphosphine and 4 mg (4 μmol) $Pd_2(dba)_3$ were added. The resulting mixture was heated to 140 °C for three days. The solution was diluted with 1,2-dichlorobenzene and precipitated in methanol. After filtration the polymer was reprecipitated twice

in methanol and dried. 130 mg of a red solid was obtained (94 %). GPC (1,2,4-trichlorobenzene, 135 °C) analysis gives M_n = 17 kg/mol and M_w = 42 kg/mol against polystyrene standard. ^{1}H-NMR (500 MHz, CD_4Cl_2, 120 °C, δ in ppm) 8.27 (s, 2H), 7.61 (s, 2H), 7.40 (s, 2H), 3.17 (t, J = 7 Hz, 4H), 2.03 (quin, J = 7 Hz, 4H), 1.73 (quin, J = 7 Hz, 4H), 1.62 (quin, J = 7 Hz, 4H), 1.6-1.4 (m, 28H), 1.08 (t, J = 7 Hz, 6H)

8.5.18 5,5'-dibromobenzo[1,2-b;4,5-b']dithiophene

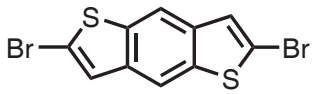

102

540 mg (2.8 mmol) Benzo[1,2-b;4,5-b']dithiophene were dissolved in 70 ml anhydrous THF under argon and cooled to -78 °C. 5.3 ml (8.5 mmol, 3 eq) *n*-butyllithium (1.6 M in pentane) were added. The solution was stirred for one hour in the cold bath. After this period, a solution of 2.8 g (8.5 mmol) tetrabromomethane in 5 ml anhydrous THF were added, stirred for 30 minutes in the cold bath. 10 ml of a concentrated sodium bicarbonate solution were added at -78 °C. After warming to room temperature, the solution was extracted with 100 ml dichloromethane, washed with water, dried, and the solvents were evaporated. The product was crystallized from chloroform to give 490 mg (50 %) of colorless platelets. Mp = 253 °C; MS (FD, 8 kV) m/z = 347.3 g/mol - calculated: 347.8 g/mol for $C_{10}H_4Br_2S_2$; ^{1}H-NMR (700 MHz, $C_2D_2Cl_4$, RT, δ in ppm) 7.97 (s, 2H), 7.27 (s, 2H); ^{13}C-NMR (125 MHz, $C_2D_2Cl_4$, 60 °C, δ in ppm) 138.8, 137.2, 126.1, 116.4, 115.5; elemental analysis: found 34.33 % C, 0.59 % H, 18.38 % S - calculated: 34.51 % C, 0.58 % H (HBr loss), 18.42 % S

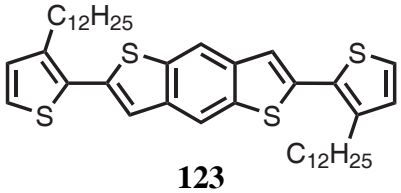

123

8.5.19 5,5'-di(3-dodecylthiophene-2-yl-)benzo[1,2-b;4,5-b']dithiophene

350 mg (1 mmol) 5,5'-Dibromobenzo[1,2-b;4,5-b']dithiophene and 1.6 g (3 mmol) 3-dodecyl-2-tributylstannylthiophene were dissolved in 15 ml anhydrous DMF under argon. 50 mg (50 μmol) tetrakis(triphenylphosphine)palladium(0) were added. The resulting solution was heated to 110 °C overnight. The solvents were removed in vacuum, the residue was crystallized twice from ethyl acetate to yield 340 mg (49 %) of a yellow powder. Mp = 111 °C; MS (FD, 8 kV) m/z = 690.5 g/mol - calculated: 690.3 g/mol for $C_{42}H_{58}S_4$; ^{1}H-NMR (300 MHz, THF$-d_8$, RT, δ in ppm) 8.25 (s, 2H), 7.42 (s, 2H), 7.36 (d, J = 5.2 Hz, 2H), 7.01 (d, J = 5.2 Hz, 2H), 2.91 (t, J = 7.7 Hz, 4H), 1.68 (quin, J = 7.8 Hz, 4H), 1.5-1.2 (m, 18H), 0.88 (t, J = 6.6 Hz, 6H); ^{13}C-NMR (75 MHz, THF$-d_8$, RT, δ in ppm) 141.9, 139.1, 138.6, 138.0, 131.7, 131.3, 126.1, 122.2, 117.1, 33.0, 31.8, 30.8 (multiple peaks) 30.6 (two peaks), 30.5, 30.3, 23.7, 14.6; elemental analysis: found 72.85 % C, 8.49 % H, 18.30 % S - calculated: 72.99 % C, 8.46 % H, 18.56 % S

8.5.20 Poly(5,5'-di(3-dodecylthiophene-2-yl-)benzo[1,2-b;4,5-b']dithiophene)

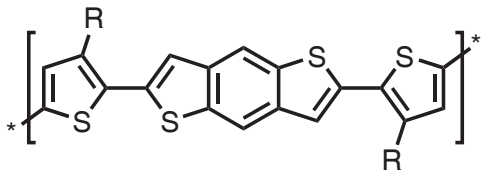

98

50 mg (0.7 mmol) 5,5'-Di(3-dodecylthiophene-2-yl-)benzo[1,2-b;4,5-b']dithiophene were dissolved in 1 ml anhydrous dichlorobenzene under argon and

added to of 47 mg (2.9 mmol) anhydrous iron(III) chloride in dichlorobenzene. The mixture was heated to 60 °C for 8 hours whereupon it was poured into methanol. The solid precipitate was filtered off, dissolved in dichlorobenzene, and added to methanol. The addition of a few drops of hydrazine (98 %) induces precipitation. The solid was obtained by filtration, dissolved in dichlorobenzene, hydrazine was added, and stirred for 24 hours at room temperature. The polymer was precipitated in methanol, filtered, and dried in vacuum to afford 41 mg of a red solid (82 %). GPC (1,2,4-trichlorobenzene, 135 °C, polystyrene standards): M_n = 17 kg/mol, M_w = 56 kg/mol; ^{1}H-NMR (500 MHz, o−dichlorobenzene−d_4, 120 °C, δ in ppm) 8.27 (s, 2H), 7.61 (s, 2H), 7.40 (s, 2H), 3.17 (t, J = 7 Hz, 4H), 2.03 (quin, J = 7 Hz, 4H), 1.73 (quin, J = 7 Hz, 4H), 1.62 (quin, J = 7 Hz, 4H), 1.6-1.4 (m, 28H), 1.08 (t, J = 7 Hz, 6H)

8.5.21 5,5'-Dibromobenzo[2,1-b;3,4-b']dithiophene

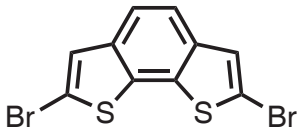

103

380 mg (2 mmol) Benzo[2,1-b;3,4-b']dithiophene were dissolved in 10 ml of a 9:1 mixture dichloromethane and acetic acid. After addition of 750 mg (4.2 mmol) N-bromosuccinimide the mixture was stirred at room temperature for three hours. The solvents were evaporated, the residue was adsorbed on silica gel and eluated with petroleum ether. Crystallization from ethanol yields 420 mg (60 %) of colorless needles. Mp = 147 °C; MS (FD, 8 kV) m/z = 348.3 g/mol - calculated: 347.8 g/mol for $C_{10}H_4Br_2S_2$; ^{1}H-NMR (300 MHz, CD_2Cl_2, RT, δ in ppm) 7.62 (s, 2H), 7.41 (s, 2H); ^{13}C-NMR (75 MHz, CD_2Cl_2, RT, δ in ppm) 137.7, 134.1,

128.2, 120.6, 113.8; elemental analysis: found 34.32 % C, 0.52 % H, 18.01 % S - calculated: 34.51 % C, 0.58 % H (HBr loss), 18.42 % S

8.5.22 5,5'-Di(3-dodecylthiophene-2-yl-)benzo[2,1-b;3,4-b']dithiophene

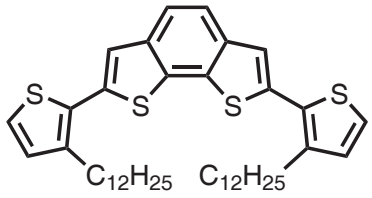

124

700 mg (2 mmol) 5,5'-Dibromobenzo[2,1-b;3,4-b']dithiophene were dissolved in 50 ml anhydrous DMF under argon. A solution of 2.38 g (4.4 mmol) 3-dodecyl-2-tributylstannylthiophene in 5 ml anhydrous THF and, finally, 50 mg (50 μmol) tetrakis(triphenylphosphine)palladium(0) were added. The resulting solution was heated to 100 °C overnight. DMF was removed in vacuum, the residue was adsorbed on silica gel and eluted with a mixture of petroleum ether and dichloromethane (20:1 v/v). Crystallization from ethyl acetate yields 680 mg (50 %) of a yellow powder. Mp = 72 °C; MS (FD, 8 kV) m/z = 690.3 g/mol - calculated: 690.3 g/mol for $C_{42}H_{58}S_4$; ^{1}H-NMR (300 MHz, CD_2Cl_2, RT, δ in ppm) 7.74 (s, 2H), 7.44 (s, 2H), 7.29 (d, J = 5.2 Hz, 2H), 7.01 (d, J = 5.2 Hz, 2H), 2.88 (t, J = 7.8 Hz, 4H), 1.69 (quin, J = 7.5 Hz, 4H), 1.4-1.2 (m, 36H), 0.87 (t, J = 6.7 Hz, 6H); ^{13}C-NMR (75 MHz, CD_2Cl_2, RT, δ in ppm) 141.6, 138.1, 135.5, 133.3, 130.9, 130.8, 125.4, 123.6, 121.2, 32.5, 31.3, 30.2 (multiple peaks), 30.18, 30.05, 30.02, 29.94, 29.85, 23.3, 14.5; elemental analysis: found 73.34 % C, 8.15 % H, 18.74 % S - calculated: 72.99 % C, 8.46 % H, 18.56 % S

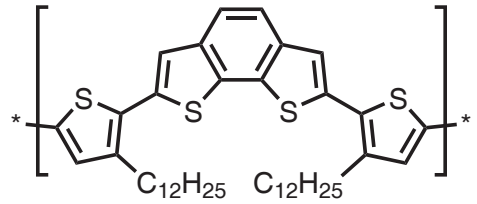

88

8.5.23 Poly(5,5'-di(3-dodecylthiophene-2-yl-)benzo[2,1-b;3,4-b']dithiophene)

50 mg (0.7 mmol) 5,5'-Di(3-dodecylthiophene-2-yl-)benzo[2,1-b;4,5-b']dithiophene were dissolved in 1 ml anhydrous dichlorobenzene under argon and added to of 47 mg (2.9 mmol) anhydrous iron(III) chloride in dichlorobenzene. The mixture was heated to 60 °C for 24 hours whereupon it was poured into methanol. The solid precipitate was filtered off, dissolved in dichlorobenzene, and added to methanol. The addition of a few drops of hydrazine (98 %) induces precipitation. The solid was obtained by filtration, dissolved in dichlorobenzene, hydrazine was added, and stirred for 24 hours at room temperature. The polymer was precipitated in methanol, filtered, and dried in vacuum to afford 45 mg of a yellow-red solid (90 %). GPC (1,2,4-trichlorobenzene, 135 °C, polystyrene standards): M_n = 7 kg/mol, M_w = 31 kg/mol, ^{1}H-NMR (500 MHz, $1,2,4-trichlorobenzene-d3$, 80 °C, δ in ppm) 7.79 (s, 2H), 7.59 (s, 2H), 7.29 (s, 2H), 3.09 (t, J = 6.8 Hz, 4H), 1.96 (quin, J = 6.7 Hz, 4H), 1.65 (quin, J = 6.9 Hz, 4H), 1.54 (quin, J = 6.7 Hz, 4H), 1.5-1.3 (m, 28H), 1.01 (t, J = 6.8 Hz, 6H)

8.5.24 1,5-Dibromo-2,4-bis(trimethylsilylethynyl)benzene

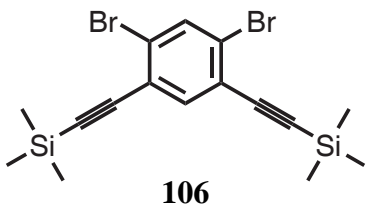

106

1.75 g (3.6 mmol) 1,5-Diiodo-2,4-dibromobenzene were dissolved in 20 ml anhydrous THF and 4 ml anhydrous diisopropylamine. 1.1 ml (7.8 mmol) trimethyethynylsilane were added, followed by 76 mg (0.4 mmol) and 56 mg (80 μmol) bis(triphenylphosophine)palladium(II)-dichloride. The mixture was stirred overnight at room temperature. The reaction mixture was poured onto 1M aqueous hydrochloric acid, extracted with dichloromethane, dried, and evaporated. The residue was adsorbed on silica gel and eluted with petroleum ether. 1.1 g of a colorless oil was obtained (71 %). MS (FD, 8 kV) m/z = 428.4 g/mol - calculated: 427.9 g/mol for $C_{16}H_{20}Br_2Si_2$; ^{1}H-NMR (300 MHz, CD_2Cl_2, RT, δ in ppm) 7.83 (s, 1H), 7.58 (s, 1H), 0.26 (s, 18H); ^{13}C-NMR (75 MHz, CD_2Cl_2, RT, δ in ppm) 137.9, 136.2, 126.1, 125.1, 102.1, 101.7, -0.1

8.5.25 5,5'-Bistrimethylsilylbenzo[2,1-b;4,5-b']dithiophene

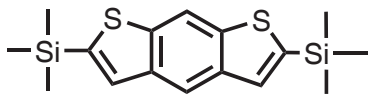

107

428 mg (1 mmol) 1,5-Dibromo-2,4-bis(trimethylsilylethynyl)benzene were dissolved in 15 ml anhydrous diethylether under argon. The solution was cooled to -78 °C, 2.5 ml (4 mmol) of a *n*-butyllithium solution (1.6M in pentane) were added and stirred for 15 minutes at that temperature. The mixture was warmed to room temperature, stirred for another 15 minutes. Then, 64 mg (2 mmol) sulfur were added, stirred for 15 minutes, whereupon 25 ml ethanol were poured into the reaction solution. After stirring for one hour, the product was extracted with diethyl ether, dried, and evaporated. The residue was adsorbed on silica gel, eluted with petroleum ether, and crystallized with ethanol to afford 51 mg (15 %) of colorless needles. Mp = 156 °C; MS (FD, 8 kV) m/z = 334.1 g/mol - calculated: 334.1 g/mol for $C_{16}H_{22}S_2Si_2$; ^{1}H-NMR (300 MHz, CD_2Cl_2, RT, δ in ppm) 8.35 (s, 1H), 8.24

(s, 1H), 7.55 (s, 2H), 0.41 (s, 18H); ^{13}C-NMR (75 MHz, CD_2Cl_2, RT, δ in ppm) 143.1, 141.5, 139.9, 131.3, 117.6, 115.4, -0.14; elemental analysis: found 57.33 % C, 6.72 % H, 18.65 % S - calculated: 57.43 % C, 6.63 % H, 19.16 % S

8.5.26 Benzo[2,1-b;4,5-b']dithiophene

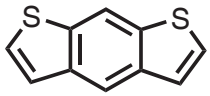

99

330 mg (1 mmol) 5,5'-Bistrimethylsilylbenzo[2,1-b;4,5-b']dithiophene were dissolved in 5 ml anhydrous THF under argon and cooled to 0 °C. 2 ml (2 mmol) of a 1M solution of tetrabutylammonium fluoride in THF were slowly added. The mixture was stirred for 10 minutes at 0 °C and poured onto an aqueous sodium bicarbonate solution. The product was extracted with dichloromethane, dried, evaporated, and chromatographed on silica gel with petroleum ether as eluent. 153 mg (81 %) of colorless crystals were obtained. Mp = 186 °C; MS (FD, 8 kV) m/z = 190.1 g/mol - calculated: 190.0 g/mol for $C_{10}H_6S_2$; ^{1}H-NMR (300 MHz, CD_2Cl_2, RT, δ in ppm) 8.38 (s, 1H), 8.28 (s, 1H), 7.47 (d, J = 5.6 Hz, 2H), 7.42 (d, J = 5.6 Hz, 2H); ^{13}C-NMR (75 MHz, CD_2Cl_2, RT, δ in ppm) 138.2, 137.8, 126.9, 124.2, 118.3, 116.2; elemental analysis: found 63.14 % C, 2.76 % H, 33.41 % S - calculated: 63.12 % C, 3.18 % H, 33.70 % S

8.5.27 5,5'-Dibromobenzo[2,1-b;4,5-b']dithiophene

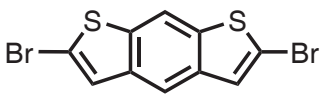

108

300 mg (1.58 mmol) Benzo[2,1-b;4,5-b']dithiophene were dissolved in 30 ml

anhydrous THF under argon and cooled to -78 °C. 3 ml (4.7 mmol, 3 eq) *n*-butyllithium (1.6 M in pentane) were added. The solution was stirred for one hour in the cold bath. After this period, a solution of 1.66 g (5 mmol) tetrabromomethane in 5 ml anhydrous THF were added, stirred for 30 minutes in the cold bath. 5 ml of a concentrated sodium bicarbonate solution were added at -78 °C. After warming to room temperature, the solution was extracted with 50 ml diethyl ether, washed with water, dried, and the solvents were evaporated. The crude product was dissolved in dichloromethane and filtered through a pad of silica gel. After evaporation of the solvent, the residue was crystallized from ethanol containing a bit of chloroform. 380 mg (69 %) of colorless platelets were obtained. Mp = 240 °C; MS (FD, 8 kV) m/z = 348.2 g/mol - calculated: 347.8 g/mol for $C_{10}H_4Br_2S_2$; ^{1}H-NMR (300 MHz, CD_2Cl_2, RT, δ in ppm) 8.10 (s, 2H), 8.03 (s, 2H), 7.41 (s, 2H); ^{13}C-NMR (75 MHz, CD_2Cl_2, RT, δ in ppm) 138.8, 138.0, 126.9, 116.7, 116.0, 114.7; elemental analysis: found 34.51 % C, 0.41 % H, 18.84 % S - calculated: 34.51 % C, 0.58 % H (HBr loss), 18.42 % S

8.5.28 5,5'-di(3-dodecylthiophene-2-yl-)benzo[2,1-b;4,5-b']dithiophene

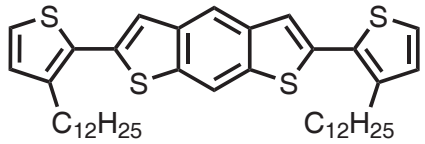

125

348 mg (1 mmol) 5,5'-Dibromobenzo[2,1-b;4,5-b']dithiophene were dissolved in 10 ml anhydrous DMF under argon. A solution of 1.35 g (2.5 mmol) 3-dodecyl-2-tributylstannylthiophene in 5 ml anhydrous THF and, finally, 50 mg (50 μmol) tetrakis(triphenylphosphine)palladium(0) were added. The resulting solution was heated to 100 °C overnight. After cooling to room temperature, diethylether was added, extracted three times with water, dried, adsorbed on silica gel and eluted with

a mixture of petroleum ether and dichloromethane (20:1 v/v). Crystallization from ethyl acetate yields 150 mg (22 %) of a yellow powder. Mp = 86 °C; MS (FD, 8 kV) m/z = 690.4 g/mol - calculated: 690.3 g/mol for $C_{42}H_{58}S_4$; ^{1}H-NMR (300 MHz, CD_2Cl_2, RT, δ in ppm) 8.23 (s, 2H), 8.16 (s, 2H), 7.40 (s, 2H), 7.29 (d, J = 5.2 Hz, 2H), 7.01 (d, J = 5.2 Hz, 2H), 2.88 (t, J = 7.8 Hz, 4H), 1.69 (quin, J = 7.6 Hz, 4H), 1.4-1.2 (m, 36H), 0.87 (t, J = 6.7 Hz, 6H); ^{13}C-NMR (75 MHz, CD_2Cl_2, RT, δ in ppm) 141.8, 138.8, 137.7, 136.9, 131.0, 125.5, 122.2, 117.9, 115.2, 32.5, 31.3, 30.2 (multiple peaks), 30.18, 30.08, 30.01, 29.94, 29.91, 23.3, 14.5 ; elemental analysis: found 73.51 % C, 8.25 % H, 18.08 % S - calculated: 72.99 % C, 8.46 % H, 18.56 % S

8.5.29 Poly(5,5'-di(3-dodecylthiophene-2-yl-)benzo[2,1-b;4,5-b']dithiophene)

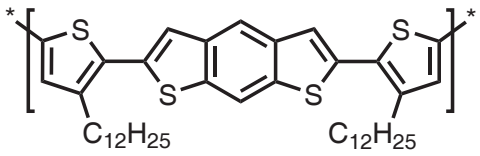

128

50 mg (0.7 mmol) 5,5'-Di(3-dodecylthiophene-2-yl-)benzo[2,1-b;4,5-b']dithiophene were dissolved in 1 ml anhydrous dichlorobenzene under argon and added to of 47 mg (2.9 mmol) anhydrous iron(III) chloride in dichlorobenzene. The mixture was heated to 60 °C for 12 hours whereupon it was poured into methanol. The solid precipitate was filtered off, dissolved in dichlorobenzene, and added to methanol. The addition of a few drops of hydrazine (98 %) induces precipitation. The solid was obtained by filtration, dissolved in dichlorobenzene, hydrazine was added, and stirred for 24 hours at room temperature. The polymer was precipitated in methanol, filtered, and dried in vacuum to afford 42 mg of a yellow-red solid (84 %). GPC (1, 2, 4-trichlorobenzene, 135 °C,

polystyrene standards): M_n = 8 kg/mol, M_w = 18 kg/mol; ^{1}H-NMR (500 MHz, 1 $_{24}$−trichlorobenzene−d_3, 100 °C, δ in ppm) 8.14 (br, 1H), 8.08 (br, 1H), 7.47 (br, 2H), 6.97 (br, 2H), 3.01 (br, 4H), 1.88 (br, 4H), 1.58 (br, 4H), 1.47 (br, 4H), 1.4-1.2 (m, 28H), 0.93 (t, J = 6 Hz, 6H)

8.5.30 5,5'-Dibromobenzo[1,2-b;4,3-b']dithiophene

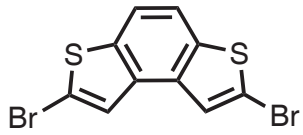

112

350 mg (1 mmol) Trans-di(5-bromthiophene-2-yl)ethene[9] were dissolved in 200 ml toluene. About 2 mg (∼ 10 μmol) iodine were added. The solution was irradiated with UV light (350 nm, 160 W) overnight while stirring rigorously in air. The solution was extracted with an aqueous solution of sodium sulfite, dried, and the solvent was evaporated. The residue was crystallized from ethanol to yield 300 mg (86 %) of colorless needles. Mp = 160 °C; MS (FD, 8 kV) m/z = 348.5 g/mol - calculated: 347.8 g/mol for $C_{10}H_4Br_2S_2$; ^{1}H-NMR (250 MHz, CD_2Cl_2, RT, δ in ppm) 7.65 (s, 2H), 7.61 (s, 2H); ^{13}C-NMR (62.5 MHz, CD_2Cl_2, RT, δ in ppm) 138.6, 133.9, 125.2, 118.6, 116.2; elemental analysis: found 34.59 % C, 0.50 % H, 18.41 % S - calculated: 34.51 % C, 0.58 % H (HBr loss), 18.42 % S

8.5.31 5,5'-Di(3-dodecylthiophene-2-yl-)benzo[1,2-b;4,3-b']dithiophene

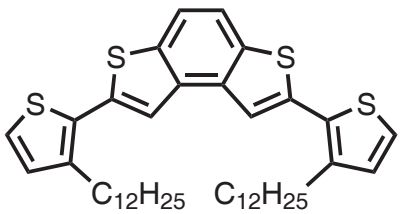

126

209 mg (0.6 mmol) 5,5'-Dibromobenzo[1,2-b;4,3-b']dithiophene were dissolved in 10 ml anhydrous DMF under argon. A solution of 810 mg (2.5 mmol) 3-dodecyl-2-tributylstannylthiophene in 5 ml anhydrous THF and, finally, 30 mg (30 µmol) tetrakis(triphenylphosphine)palladium(0) were added. The resulting solution was heated to 100 °C overnight. The solvents were removed in vacuum, the residue was adsorbed on silica gel and eluted with a mixture of petroleum ether and dichloromethane (20:1 v/v). Crystallization from ethyl acetate yields 155 mg (37 %) of a yellow powder. Mp = 84 °C; MS (FD, 8 kV) m/z = 690.6 g/mol - calculated: 690.3 g/mol for $C_{42}H_{58}S_4$; ^{1}H-NMR (300 MHz, CD_2Cl_2, RT, δ in ppm) 7.75 (s, 2H), 7.71 (s, 2H), 7.29 (d, J = 5.2 Hz, 2H), 7.02 (d, J = 5.2 Hz, 2H), 2.88 (t, J = 7.8 Hz, 4H), 1.69 (quin, J = 7.6 Hz, 4H), 1.4-1.2 (m, 36H), 0.87 (t, J = 6.7 Hz, 6H); ^{13}C-NMR (75 MHz, THF−d_8, RT, δ in ppm) 141.7, 138.0, 137.9, 135.9, 131.6 131.2, 126.0, 121.6, 119.3, 33.1, 31.9, 30.80, 30.76 (multiple peaks), 30.6, 30.5, 30.3, 23.7, 14.6 ; elemental analysis: found 73.10 % C, 8.27 % H, 18.50 % S - calculated: 72.99 % C, 8.46 % H, 18.56 % S

8.5.32 Poly(5,5'-di(3-dodecylthiophene-2-yl-)benzo[1,2-b;4,3-b']dithiophene)

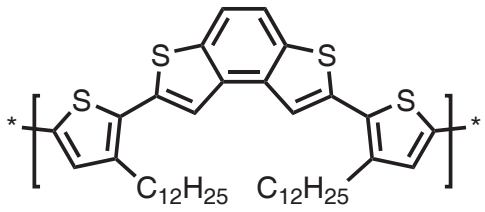

129

69 mg (1 mmol) 5,5'-Di(3-dodecylthiophene-2-yl-)benzo[1,2-b;4,3-b']dithiophene were dissolved in 1 ml anhydrous dichlorobenzene under argon and added to a suspension of 65 mg (4 mmol) anhydrous iron(III) chloride in dichlorobenzene. The mixture was heated to 60 °C for 24 hours whereupon

it was poured into methanol. The solid precipitate was filtered off, dissolved in dichlorobenzene, and added to methanol. The addition of a few drops of hydrazine (98 %) induces precipitation. The solid was obtained by filtration, dissolved in dichlorobenzene, hydrazine was added, and stirred for 24 hours at room temperature. The polymer was precipitated in methanol, filtered, and dried in vacuum to afford 62 mg of a yellow-red solid (90 %). GPC (1,2,4-trichlorobenzene, 135 °C, polystyrene standards): M_n = 26 kg/mol, M_w = 72 kg/mol; ^{1}H-NMR (500 MHz, o−dichlorobenzene−d_4, 100 °C, δ in ppm) 8.16 (s, 2H), 7.55 (s, 2H), 7.19 (s, 2H), 3.06 (br, 4H), 1.92 (br, 4H), 1.62 (br, 4H), 1.51 (br, 4H), 1.4-1.2 (m, 28H), 0.97 (br, 6H)

8.5.33 5,5'-Dibromobenzo[1,2-b;3,4-b']dithiophene

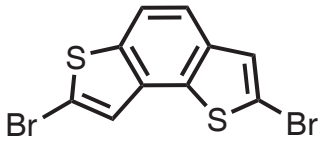

117

570 mg (3 mmol) Benzo[1,2-b;3,4-b']dithiophene were dissolved in 50 ml anhydrous THF under argon and cooled to -78 °C. 4.7 ml (7.5 mmol, 3 eq) *t*-butyllithium (1.6 M in pentane) were added. The solution was stirred for one hour in the cold bath. After this period, a solution of 2.49 g (7.5 mmol) tetrabromomethane in 5 ml anhydrous THF were added, and stirred for 30 minutes in the cold bath. 10 ml of a concentrated sodium bicarbonate solution were added at -78 °C. After warming to room temperature, the solution was extracted with 100 ml diethyl ether, washed with water, dried, and the solvents were evaporated. The crude product was adsorbed on silica gel and eluted with petroleum ether. The product was crystallized from ethanol to give 300 mg (29 %) of colorless needles. Mp = 128 °C; MS (FD, 8 kV) m/z = 348.2 g/mol - calculated: 347.8 g/mol for $C_{10}H_4Br_2S_2$; ^{1}H-NMR

(300 MHz, CD_2Cl_2, RT, δ in ppm) 8.70 (d, J = 7.6 Hz, 1H), 8.59 (d, J = 7.6 Hz, 1H), 7.46 (s, 1H), 7.43 (s, 1H); ^{13}C-NMR (75 MHz, CD_2Cl_2, RT, δ in ppm) 138.2, 137.6, 134.9, 133.1, 128.0, 124.7, 120.0, 119.1, 117.1, 114.0; elemental analysis: found 34.66 % C, 0.56 % H, 18.41 % S - calculated: 34.51 % C, 0.58 % H (HBr loss), 18.42 % S

8.5.34 5,5'-Di(3-dodecylthiophene-2-yl-)benzo[1,2-b;3,4-b']dithiophene

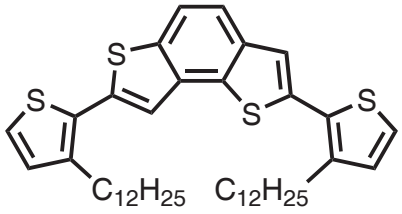

127

245 mg (0.7 mmol) 5,5'-Dibromobenzo[1,2-b;3,4-b']dithiophene and 1.1 g (2 mmol) 3-dodecyl-2-tributylstannylthiophene were dissolved in 10 ml anhydrous DMF under argon. 50 mg (50 μmol) Tetrakis(triphenylphosphine)palladium(0) were added. The resulting solution was heated to 110 °C overnight. The solvents were removed in vacuum, the residue was adsorbed on silica gel and eluted with a mixture of petroleum ether and dichloromethane (20:1 v/v). Crystallization from ethyl acetate yields 170 mg (35 %) of a beige powder. Mp = 54 °C; MS (FD, 8 kV) m/z = 690.5 g/mol - calculated: 690.3 g/mol for $C_{42}H_{58}S_4$; ^{1}H-NMR (300 MHz, CD_2Cl_2, RT, δ in ppm) 7.78 (d, J = 8.4 Hz, 1H), 7.71 (d, J = 8.5 Hz, 1H), 7.55 (s, 1H), 7.45 (s, 1H), 7.30 (d, J = 5.3 Hz, 1H), 7.28 (d, J = 5.3 Hz, 1H), 7.02 (d, J = 5.2 Hz, 2H), 2.89 (t, J = 7.8 Hz, 2H), 2.88 (t, J = 7.8 Hz, 2H), 1.69 (m, 4H), 1.4-1.2 (m, 36H), 0.87 (t, J = 6.9 Hz, 6H); ^{13}C-NMR (75 MHz, THF−d_8, RT, δ in ppm) 141.6, 141.3, 138.4, 138.3, 137.9, 137.7, 136.6, 135.3, 133.8, 130.8, 130.7, 130.6, 125.3, 125.0, 123.4, 120.4, 119.9, 119.2; elemental analysis: found 72.99 % C, 8.45 % H, 18.38 % S - calculated: 72.99 % C, 8.46 % H, 18.56 % S

8.5.35 Poly(5,5'-di(3-dodecylthiophene-2-yl-)benzo[1,2-b;3,4-b']dithiophene)

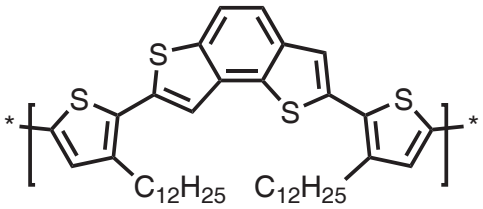

130

50 mg (0.7 mmol) 5,5'-Di(3-dodecylthiophene-2-yl-)benzo[1,2-b;3,4-b']dithiophene were dissolved in 1 ml anhydrous dichlorobenzene under argon and added to of 47 mg (2.9 mmol) anhydrous iron(III) chloride in dichlorobenzene. The mixture was heated to 60 °C for 8 hours whereupon it was poured into methanol. The solid precipitate was filtered off, dissolved in dichlorobenzene, and added to methanol. The addition of a few drops of hydrazine (98 %) induces precipitation. The solid was obtained by filtration, dissolved in dichlorobenzene, hydrazine was added, and stirred for 24 hours at room temperature. The polymer was precipitated in methanol, filtered, and dried in vacuum to afford 41 mg of a red solid (82 %). GPC (1,2,4-trichlorobenzene, 135 °C, polystyrene standards): M_n = 17 kg/mol, M_w = 88 kg/mol

8.6 Di(thienobenzo)thienothiophene Containing Polymers

8.6.1 1,3-Bis(trimethylstannyl)-thieno[3,2-b]thiophene

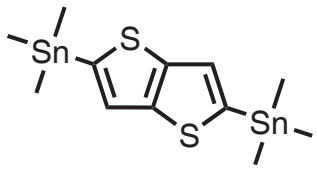

135

1 g (7.1 mmol) Thieno[3,2-b]thiophene was dissolved in 40 ml anhydrous THF under argon and cooled to -78 °C. 11 ml (17.6 mmol) of a 1.6M *t*-butyllithium solution in pentane were added slowly. The mixture was stirred for 2 hours at -78 °C, then 4 g (20 mmol) trimethyltin chloride were added as solid. The solution was warmed to room temperature, and stirred for one hour. The solution was diluted with 100 ml diethylether, extracted with aqueous sodium bicarbonate solution, dried, and evaporated. The residue was crystallized from acetonitrile at -20 °C to yield 1.9 g (58 %) of colorless crystals. Mp = 130 °C; MS (FD, 8 kV) m/z = 465.4 g/mol - calculated: 465.9 g/mol for $C_{12}H_{20}S_2Sn_2$; ^{1}H-NMR (300 MHz, CD_2Cl_2, RT, δ in ppm) 7.28 (s, 2H), 0.41 (s, 2H); ^{13}C-NMR (75 MHz, CD_2Cl_2, RT, δ in ppm) 148.0, 142.0, 16.6, -8.0; elemental analysis: found 30.91 % C, 4.48 % H, 13.61 % S - calculated: 30.94 % C, 4.33 % H, 13.77 % S

8.6.2 1,3-Bis(3-hexadecynylthiophene-2-yl)-thieno[3,2-b]thiophene

932 mg (2 mmol) 1,3-Bis(trimethylstannyl)-thieno[3,2-b]thiophene and 843 mg (2.2 mmol) 2-bromo-3-hexadecynylthiophene were dissolved in 20 ml anhydrous o-dichlorobenzene under argon. 61 mg (0.2 mmol) Tri-*o*-tolylphosphine and 47 mg (50 *upmu*mol) $Pd_2(dba)_3$ were added. The solution was heated to 120 °C for three hours. The solvent was removed in high vacuum. The residue was purified by column chromatography on silica gel with petroleum ether - dichloromethane

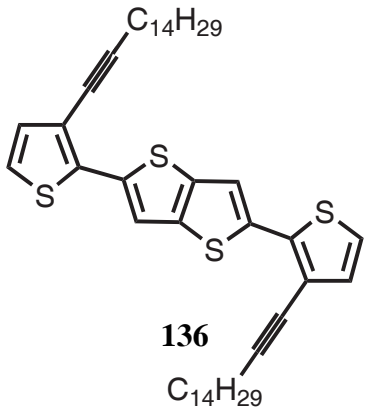

136

(17:3 v/v) as eluent. After crystallization from hexane at 0 °C, 950 mg (64 %) of an orange-yellow powder were obtained. Mp = 71 °C; MS (FD, 8 kV) m/z = 743.3 g/mol - calculated: 744.4 g/mol for $C_{46}H_{64}S_4$; ^{1}H-NMR (250 MHz, CD_2Cl_2, RT, δ in ppm) 7.68 (s, 2H), 7.14 (d, J = 5.3 Hz, 2H), 7.02 (d, J = 5.3 Hz, 2H) 2.54 (t, J = 7.0 Hz, 4H), 1.69 (quin, J = 7.4 Hz, 4H), 1.6-1.1 (m, 48H), 0.89 (t, J = 6.5 Hz, 6H); ^{13}C-NMR (62.5 MHz, CD_2Cl_2, RT, δ in ppm) 140.0, 138.99, 138.94, 132.3, 123.7, 119.2, 117.5, 97.4, 76.6, 32.6, 30.4-30.2 (multiple peaks), 30.0, 29.9, 29.7, 29.1, 23.3, 14.5; elemental analysis: found 74.00 % C, 8.62 % H, 17.30 % S - calculated: 74.14 % C, 8.66 % H, 17.21 % S

8.6.3 4,8-Bis(tetradecyl)-dithienobenzo- thieno[3,2-b]thiophene

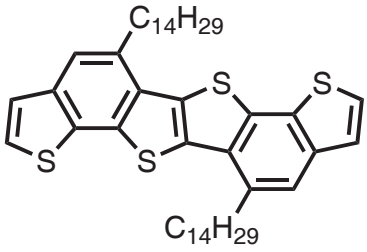

137

500 mg (0.67 mmol) 1,3-Bis(3-hexadecynylthiophene-2-yl)-thieno[3,2-b]thiophene were dissolved in 15 ml NMP. After degassing the solution, 0.11 ml (0.74 mmol) DBU were added. The resulting solution was refluxed over night,

cooled to room temperature, diluted with 20 ml methanol and filtered. The yellow solid was recrystallized from hexane to give 390 mg (78 %) slightly yellow fine needles. Mp: 118 °C, MS (FD, 8 kV) m/z = 743.5 g/mol - calculated: 744.4 g/mol for $C_{46}H_{64}S_4$; ^{1}H-NMR (500 MHz, $C_2D_2Cl_4$, 60 °C, δ in ppm) 7.65 (s, 2H), 7.40 (d, J = 5.2 Hz, 2H), 7.38 (d, J = 5.2 Hz, 2H), 3.20 (t, J = 7.9 Hz, 4H), 1.85 (quin, J = 7.7 Hz, 4H), 1.56 (quin, J = 7.6 Hz, 4H), 1.39 (quin, J = 7.5 Hz, 4H), 1.3-1.1 (m, 36H), 0.82 (t, J = 7.0 Hz, 6H); ^{13}C-NMR (125 MHz, $C_2D_2Cl_4$, 60 °C, δ in ppm) 138.3, 136.5, 134.2, 132.1, 131.8, 130.0, 125.1, 125.0, 120.8, 34.8, 32.2, 31.3, 29.9 (multiple peaks), 29.8, 29.6, 22.9, 14.4; elemental analysis: found 74.12 % C, 8.67 % H, 17.04 % S - calculated: 74.14 % C, 8.66 % H, 17.21 % S

8.6.4 2,8-Dibrom-5,12-bis(tetradecyl)-dithienobenzo-thieno[3,2-b]thiophene

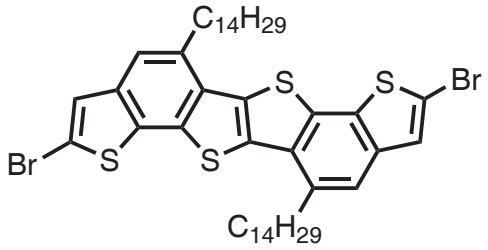

139

150 mg (0.2 mmol) 4,8-Bis(tetradecyl)-dithienobenzo-thieno[3,2-b]thiophene and 142 mg (0.8 mmol) N-bromosuccinimid were refluxed in 9 ml chloroform and 1 ml acetic acid for three hours. To the warm solution methanol was added, the precipitate was filtered off and crystallized from chloroform to yield 160 mg (89 %) of slightly reddish needles. Mp: 143 °C, MS (FD, 8 kV) m/z = 900.3 g/mol - calculated: 900.2 g/mol for $C_{46}H_{62}S_4Br_2$; ^{1}H-NMR (500 MHz, $C_2D_2Cl_4$, 60 °C, δ in ppm) 7.65 (s, 2H), 7.40 (d, J = 5.2 Hz, 2H), 7.38 (d, J = 5.2 Hz, 2H), 3.20 (t, J = 7.9 Hz, 4H), 1.85 (quin, J = 7.7 Hz, 4H), 1.56 (quin, J = 7.6 Hz, 4H), 1.39 (quin,

J = 7.5 Hz, 4H), 1.3-1.1 (m, 36H), 0.82 (t, J = 7.0 Hz, 6H); ^{13}C-NMR (125 MHz, $C_2D_2Cl_4$, 60 °C, δ in ppm) 138.3, 136.5, 134.2, 132.1, 131.8, 130.0, 125.1, 125.0, 120.8, 34.8, 32.2, 31.3, 29.9 (multiple peaks), 29.8, 29.6, 22.9, 14.4

8.6.5 2,8-Bistrimethylstannyl-5,12-bis(tetradecyl)-dithienobenzo-thieno[3,2-b]thiophene

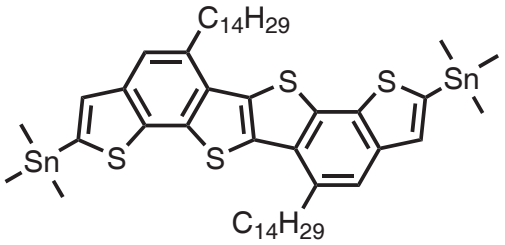

140

74.5 mg (0.1 mmol) 4,8-Bis(tetradecyl)-dithienobenzo-thieno[3,2-b]thiophene were suspended in 5 ml anhydrous THF under an argon atmosphere. The suspension was cooled to 0 °C, 0.16 ml (0.25 mmol) *t*-butyllithium (1.6M in pentane) were added slowly whereupon the suspension turns from light yellow to dark brown. The mixture was stirred for two hours at 0 °C while the color brightens up again. 50 mg (0.25 mmol) Trimethyltin chloride in 2 ml THF was added slowly, the mixture was warmed up to room temperature and stirred for one hour at that temperature. 20 ml Methanol were added, the precipitate was filtered off and recrystallized twice from ethyl acetate at 4 °C to obtain 45 mg of yellow needles (42 %). Mp: 67 °C, MS (FD, 8 kV) m/z = 1070.1 g/mol - calculated: 1070.3 g/mol for $C_{52}H_{80}S_4Sn_2$; ^{1}H-NMR (250 MHz, CD_2Cl_2, RT, δ in ppm) 7.67 (s, 2H), 7.51 (s, 2H), 3.23 (t, J = 7.7 Hz, 4H), 1.87 (quin, J = 7.6 Hz, 4H), 1.59 (quin, J = 7.4 Hz, 4H), 1.4-1.1 (m, 40H), 0.87 (t, J = 6.5 Hz, 6H), 0.48 (s, 18H); ^{13}C-NMR (75 MHz, CD_2Cl_2, RT, δ in ppm) 140.2, 139.6, 136.8, 136.2, 134.2, 133.2, 132.1, 129.5, 120.4, 35.2, 32.5, 31.7,

30.3 (multiple peaks), 30.2, 29.9, 23.3, 14.5; elemental analysis: found 58.84 % C, 7.66 % H, 11.38 % S - calculated: 58.33 % C, 7.53 % H, 11.98 % S

8.6.6 Poly(2,8-Bis-3-tetradecylthiophene-2-yl)-5,12-bis(tetradecyl)-dithienobenzo-thieno[3,2-b]thiophene

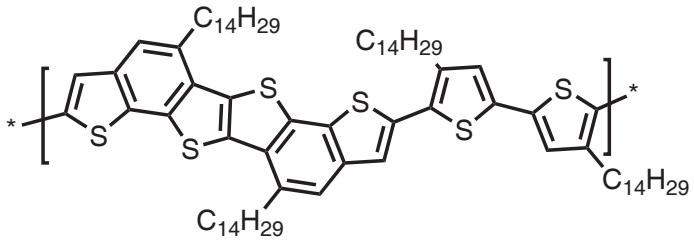

142

32.13 mg (30 μmol) 2,8-Bistrimethylstannyl-5,12-bis(tetradecyl)-dithienobenzo-thieno[3,2-b]thiophene and 21.50 mg (30 μmol) 5,5'-dibromo-4,4'-didodecyl-2,2'-dithiophene were dissolved in 2 ml anhydrous 1,2-dichlorobenzene under argon. 1.2 mg (4 μmol) Tri-*o*-tolylphosphine and 0.9 mg (1 μmol) $Pd_2(dba)_3$ were added. The resulting mixture was heated to 140 °C for three days. The solution was diluted with 1,2-dichlorobenzene and precipitated in methanol. After filtration the polymer was reprecipitated twice in methanol and dried. 31 mg of a red solid was obtained (80 %). GPC (1,2,4-trichlorobenzene, 135 °C) analysis gives M_n = 8 kg/mol and M_w = 16 kg/mol against polystyrene standard. ^{1}H-NMR (500 MHz, $C_2D_2Cl_4$, 120 °C, δ in ppm) 7.6 (br, 2H), 7.5 (br, 2H), 7.2 (br, 2H)

8.7 Crystal Structures

The single crystal analysis was performed on a Nonius-KCCD diffractometer with a Mo-K_α ($\lambda = 0.71923$ Å, graphite monochromatized) at a temperature of 150 K. The structures were solved by direct methods (Shelxs) and refined on F with anisotropic temperature factors for all non-hydrogen atoms. The H atoms were refined with fixed isotropic temperature factors in the riding mode.

8.7.1 Dimethoxycoronene (17)

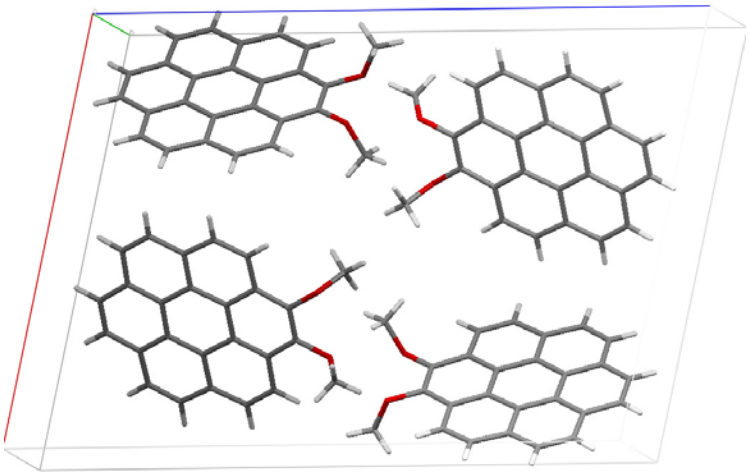

$C_{26}H_{16}O_2$, $M_r = 360.41$ g/mol, monoclinic, space group $P2_1/a$, a = 16.0660(6) Å, b = 4.5830(4) Å, c = 23.2180(7) Å, $\beta = 99.842(1)°$, V = 1684.39(17) $Å^3$, Z = 4, $\rho_{calcd} = 1.421$ g/cm^3, $\mu = 0.089$, $2\theta_{max} = 27.4968°$, 22586 reflections measured, 3817 unique, 1854 observed, $R_{int} = 0.087$, R = 0.0519, $R_w = 0.0432$

Cambridge Crystallographic Data Centre identifyer: CCDC-678259

8.7.2 Tetramethoxycoronene (18)

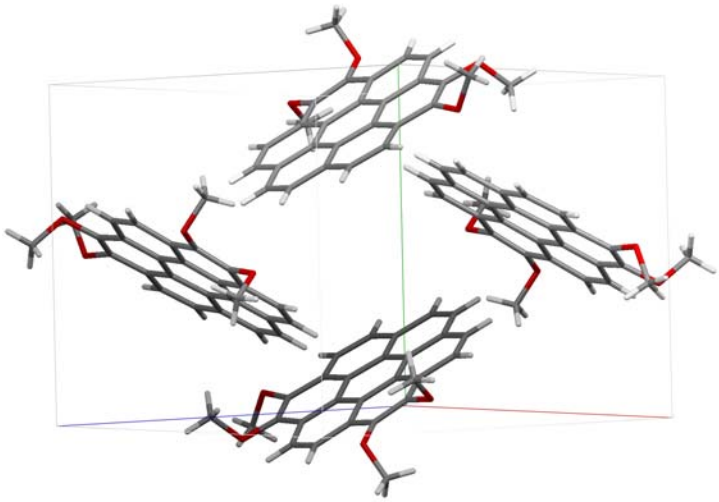

$C_{28}H_{20}O_4$, M_r = 420.46 g/mol, monoclinic, space group $P2_1/c$, a = 12.7901(6) Å, b = 11.7359(5) Å, c = 13.5211(6) Å, β = 107.344(1)°, V = 1937.29(15) $Å^3$, Z = 4, ρ_{calcd} = 1.442 g/cm^3, μ = 0.096, $2\theta_{max}$ = 30.000°, 21 479 reflections measured, 5540 unique, 2224 observed, R_{int} = 0.077, R = 0.0656, R_w = 0.0299

Cambridge Crystallographic Data Centre identifyer: CCDC-678260

8.7.3 Hexamethoxycoronene (19)

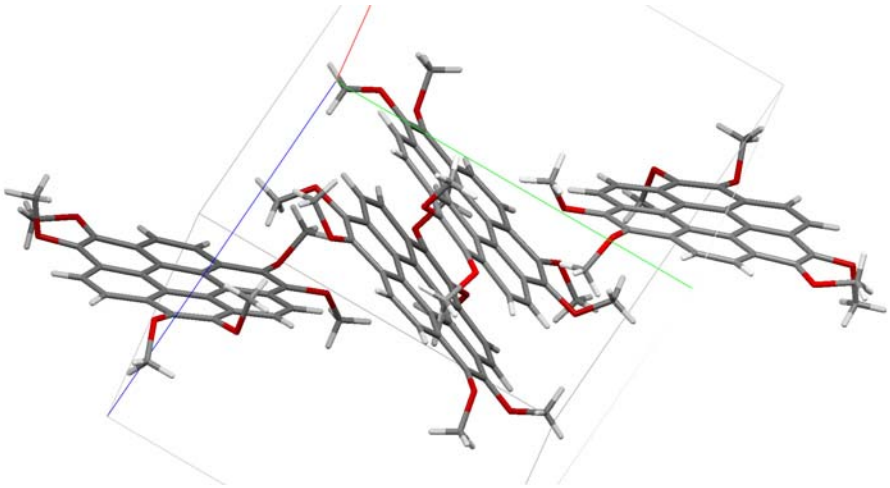

$C_{30}H_{24}O_6$, M_r = 480.52 g/mol, monoclinic, space group $P2_1/c$, a = 10.2336(5) Å, b = 13.6684(5) Å, c = 16.1664(6) Å, β = 101.541(1)°, V = 2215.58(16) $Å^3$, Z = 4,

ρ_{calcd} = 1.440 g/cm^3, μ = 0.100, $2\theta_{max}$ = 29.499°, 28868 reflections measured, 6095 unique, 1726 observed, R_{int} = 0.076, R = 0.0491, R_w = 0.0536

Cambridge Crystallographic Data Centre identifyer: CCDC-678261

8.7.4 Hexamethoxycoronene (19) - TCNQ

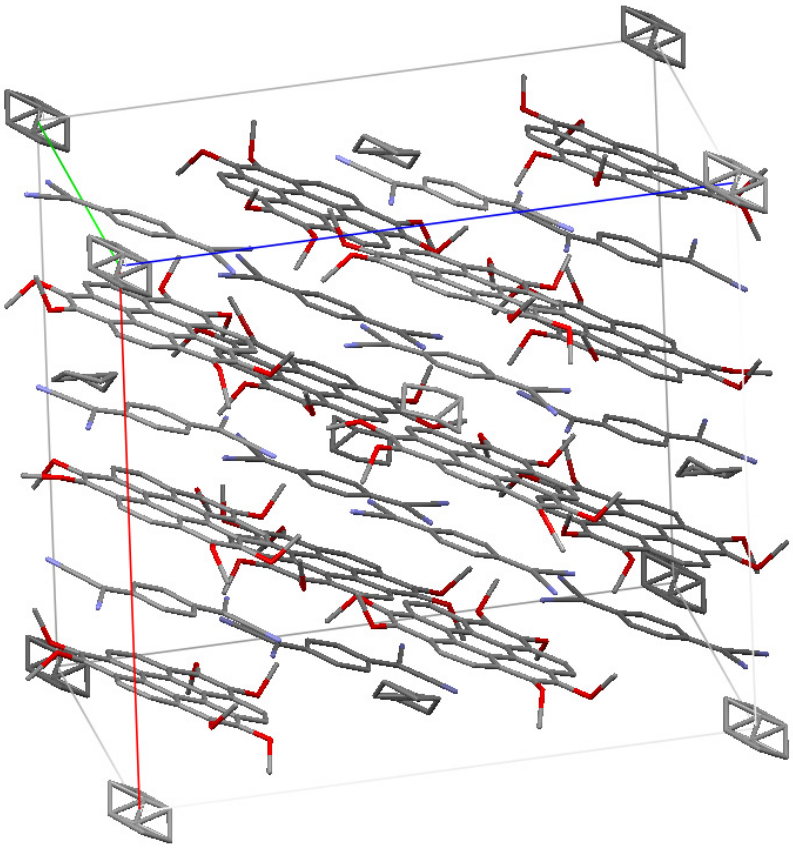

$C_{42}H_{28}N_4O_6$ - THF solvate, M_r = 648.69 g/mol, monoclinic, space group $P2_1/c$, a = 21.5570(6) Å, b = 20.1480(6) Å, c = 23.7650(7) Å, β = 93.3420(12)°, V = 10304.3(5) Å^3, Z = 12, ρ_{calcd} = 1.308 g/cm^3, μ = 0.090, $2\theta_{max}$ = 29.500°, 132298 reflections measured, 27898 unique, 7709 observed, R_{int} = 0.045, R = 0.1006, R_w = 0.1004

8.7.5 Benzo[2,1-b;3,4-b']dithiophene-5,6-dione (36)

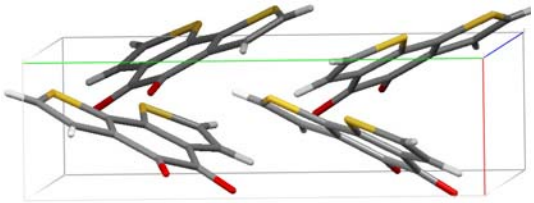

$C_{10}H_4O_2S_2$, M_r = 220.27 g/mol, orthorhombic, space group $P2_1nb$, a = 3.8339(2) Å, b = 12.8622(12) Å, c = 17.0125(16) Å, V = 838.93(12) Å^3, Z = 4, ρ_{calcd} = 1.744 g/cm^3, μ = 0.594, $2\theta_{max}$ = 29.563°, 6811 reflections measured, 2228 unique, 1874 observed, R_{int} = 0.051, R = 0.0335, R_w = 0.0375

Cambridge Crystallographic Data Centre identifyer: CCDC-740346

8.7.6 Benzo[2,1-b;3,4-b']dithiophene-5,6-bisdioxane (62)

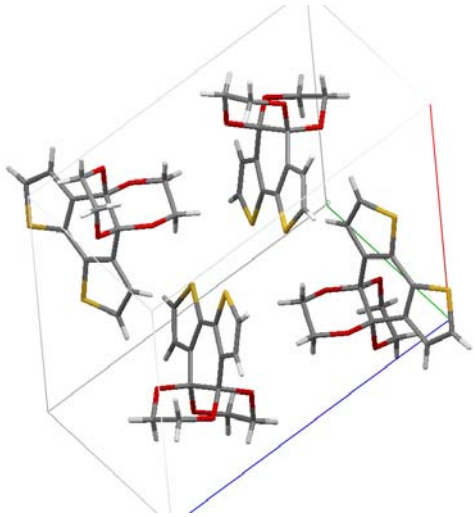

$C_{14}H_{12}O_4S_2$, M_r = 308.38 g/mol, monoclinic, space group P1 $2_1/c$, a = 11.4002(4) Å, b = 8.4816(2) Å, c = 13.8504(4) Å, β = 103.3233(12)°, V = 1303.18(7) Å^3, Z = 4, ρ_{calcd} = 1.572 g/cm^3, μ = 0.418, $2\theta_{max}$ = 29.586°, 12270 reflections measured, 3644 unique, 3073 observed, R_{int} = 0.050, R = 0.0325, R_w = 0.0382

Cambridge Crystallographic Data Centre identifyer: CCDC-740345

8.7.7 5,5'-Di(5-hexylthiophene-2-yl-)benzo[2,1-b;3,4-b']dithiophene-4,5-diketone (66)

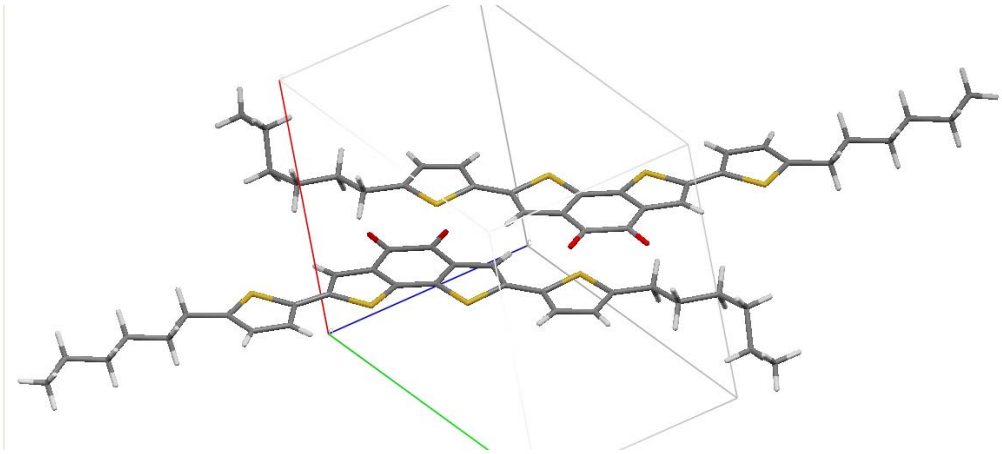

$C_{30}H_{32}O_2S_4$, M_r = 552.85 g/mol, triclinic, space group P -1, a = 10.7680(4) Å, b = 11.3767(4) Å, c = 12.2773(3) Å, α = 100.264(2)°, β = 105.346(2)°, γ = 103.265(2)°, V = 1365.21(8) Å^3, Z = 2, ρ_{calcd} = 1.345 g/cm^3, μ = 0.375, $2\theta_{max}$ = 29.569°, 19251 reflections measured, 7575 unique, 5403 observed, R_{int} = 0.066, R = 0.0394, R_w = 0.0478

Cambridge Crystallographic Data Centre identifyer: CCDC-740343

8.7.8 5,5'-Dithiophene-2-yl-benzo[2,1-b;3,4-b']dithiophene-4,5-diketone (70)

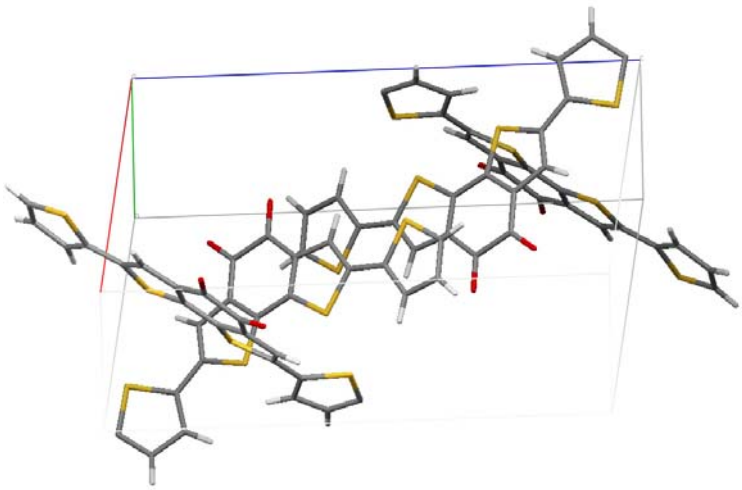

$C_{18}H_7O_2S_4$, M_r = 383.52 g/mol, monoclinic, space group P 1 2_1/n, a = 15.9180(6) Å, b = 5.47300(10) Å, c = 17.6830(6) Å, β = 96.4220(14)°, V = 1530.86(8) $Å^3$, Z = 4, ρ_{calcd} = 1.664 g/cm^3, μ = 0.628, $2\theta_{max}$ = 29.523°, 14386 reflections measured, 4276 unique, 3114 observed, R_{int} = 0.080, R = 0.0502, R_w = 0.0572

Cambridge Crystallographic Data Centre identifyer: CCDC-740344

8.8 Bibliography

[1] Gottlieb, H. E.; Kotlyar, V.; Nudelman, A. *J. Org. Chem.* **1997**, *62*, 7512–7515.

[2] Hamai, S.; Hirayama, F. *J. Phys. Chem.* **1983**, *87*, 83–89.

[3] Bard, A. J.; R., F. L. *Electrochemical Methods. Fundamentals and Applications*, 2nd ed.; Wiley and Sons, 2001.

[4] Zhang, H. C.; Huang, W. S.; Pu, L. *J. Org. Chem.* **2001**, *66*, 481–487.

[5] Kozaki, M.; Sugimura, K.; Ohnishi, H.; Okada, K. *Org. Lett.* **2006**, *8*, 5235–5238.

[6] Heeney, M.; Bailey, C.; Genevicius, K.; Shkunov, M.; Sparrowe, D.; Tierney, S.; McCulloch, I. *J. Am. Chem. Soc.* **2005**, *127*, 1078–1079.

[7] Yoshida, S.; Fujii, M.; Aso, Y.; Otsubo, T.; Ogura, F. *J. Org. Chem.* **1994**, *59*, 3077–3081.

[8] Takimiya, K.; Konda, Y.; Ebata, H.; Niihara, N.; Otsubo, T. *J. Org. Chem* **2005**, *70*, 10569–10571.

[9] Bouachrine, M.; Lere-Porte, J. P.; Moreau, J. J. E.; Torreilles, C. *J. Chim. Phys. Phys.-Chim. Biol.* **1998**, *95*, 1176–1179.

9 List of Publications

1. Rieger, R.; Kastler, M.; Enkelmann, V.; Müllen, K.: Entry to coronene chemistry - Making large electron donors and acceptors, *Chem. Eur. J.* **2008**, 14, (21), 6322-6325.

2. Glowatzki, H.; Bröker, B.; Blum, R. P.; Hofmann, O. T.; Vollmer, A.; Rieger, R.; Müllen, K.; Zojer, E.; Rabe, J. P.; Koch, N.: "Soft" Metallic Contact to Isolated C-60 Molecules, *Nano Lett.* **2008**, 8, (11), 3825-3829.

3. Bröker, B.; Blum, R. P.; Frisch, J.; Vollmer, A.; Hofmann, O. T.; Rieger, R.; Müllen, K.; Rabe, J. P.; Zojer, E.; Koch, N.: Gold work function reduction by 2.2 eV with an air-stable molecular donor layer, *App. Phys. Lett.* **2008**, 93, (24), 243303.

4. Frank, P.; Koch, N.; Koini, M.; Rieger, R.; Müllen, K.; Resel, R.; Winkler, A.: Layer growth and desorption kinetics of a discoid molecular acceptor on Au(111), *Chem. Phys. Lett.* **2009**, 473, (4-6), 321-325.

5. Cañas-Ventura, M. E.; Xiao, W.; Ruffieux, P.; Rieger, R.; Müllen, K.; Brune, H.; Fasel, R.: Stabilization of bimolecular islands on ultrathin NaCl films by a vicinal substrate, *Surf. Sci.* **2009**, 603, 2294-2299.

6. Rieger, R.; Beckmann, D.; Pisula, W.; Steffen, W.; Kastler, W.; Müllen, K: Rational Optimization of Benzo[1,2-b:3,4-b']dithiophene Containing

Polymers for Organic Transistors, *Adv. Mater.* **2009** early view, DOI: 10.1002/adma.200901286

7. Liu, M.; Rieger, R.; Li C.; Menges, H.; Kastler, M.; Baumgarten, M.; Müllen, K.: Polymer with Benzo[2,1-b;3,4-b']dithiophene Moiety for Photovoltaic Applications, *submitted*

8. Gonzalez-Lakunza, N.; Cañas-Ventura, M. E.; Ruffieux, P.; Rieger, R.; Müllen, K.; Fasel, R.; Arnau, A.: Hydrogen-Bonding Fingerprints in Electronic States of Two-Dimensional Supramolecular Assemblies, *submitted*

9. Bieri, M.; Treier, M.; Cai, J.; Aït-Mansour, K.; Ruffieux, P.; Gröning, O.; Gröning, P.; Kastler, M.; Rieger, R.; Feng, X.; Müllen, K.; Fasel, R.: Porous graphenes: Two-dimensional polymer synthesis with atomic precision, *submitted*

10. Aït-Mansour, K.; Cañas-Ventura, M. E.; Ruffieux, P.; Rieger, R.; Müllen, K.; Fasel, R.; Gröning, O.: Strain-Relief Pattern as Guide for the Formation of Surface-Supported Bimolecular Nanoribbons, *submitted*

Patent

Kastler, M.; Rieger, R.; Beckmann, D.; Liu, M.; Müllen, K.: Poly(5,5'-bis(thiophen-2-yl)-benzo[2,1-b;3,4-b']dithiophene) and its use as high performance solution processable semiconducting polymer, *filed 2008*